Finanziato dall'Unione europea
NextGenerationEU
Ministero dell'Università e della Ricerca
Italiadomani
PIANO NAZIONALE DI RIPRESA E RESILIENZA

DOTTORATO DI RICERCA IN

Ingegneria Industriale

CICLO XXXVIII - ex D.M. 352/2022

Offshore electricity and green hydrogen production in European Seas: A techno-economic assessment

Settore Scientifico Disciplinare

ING-IND / 09

Dottorando

Dott. Travaglini Riccardo

Supervisore

Prof. Bianchini Alessandro

Coordinatore

Prof. Governi Lapo

UNIVERSITÀ
DEGLI STUDI
FIRENZE

PhD in
Industrial Engineering

CYCLE XXXVIII

Offshore electricity and green hydrogen production in European Seas: A techno-economic assessment

Academic Discipline (SSD) ING-IND/09

Doctoral Candidate
Dr. Travaglini Riccardo

Supervisor
Prof. Bianchini Alessandro

Coordinator
Prof. Governi Lapo

Years 2022-2025

Per esser di Firenze vanto e gloria

Narciso Parigi, Canzone Viola

A mio fratello,
per la pazienza e l'affetto dimostrato in questi anni

DECLARATION

I hereby declare that this submission is my own work and, to the best of my knowledge and belief, it contains no material previously published or written by another person, nor material which to a substantial extent has been accepted for the award of any other degree or diploma at University of Florence or any other educational institution, except where due references are provided in the thesis itself.

Any contribution made to the research by others, with whom I have been working at the University of Florence or elsewhere, is explicitly acknowledged in the thesis.

Riccardo Travaglini
30/10/2025

ACKNOWLEDGEMENTS

Credo che per esprimere appieno un sentimento si debba usare la propria lingua, per cui sono costretto ad abbandonare l'inglese per qualche riga. Questa è davvero l'ultima tesi, i ringraziamenti saranno un po' corposi. Spero non me ne vogliate.

Grazie a mio fratello. Se penso a questi ultimi anni e alle cose successe, mi rendo conto di quanto abbia da imparare da te. So che non è facile starmi accanto, ma non per questo mi hai mai fatto sentire solo. Questa tesi è anche, in parte, merito tuo. Grazie, Lucignolo.

Grazie a mia mamma. Grazie per avermi insegnato ad apprezzare le cose belle della vita, piccole o grandi che fossero. Non credo che sarei così senza i tuoi: "Mi raccomando, fai una cosa bella!". Certo, spesso discutiamo, ma negli anni mi sono reso conto che è perché, sotto certi aspetti, siamo fatti con lo stampino.

Grazie a mio babbo. Grazie per avermi insegnato a lottare con il "sangue negli occhi" per quello che voglio. Ricordo bene momenti in cui mi hai messo l'argento vivo addosso per non essere secondo a nessuno.

Grazie ai miei nonni. Arrivato a questo punto, mi rendo conto che l'unico rimpianto che ho è non avervi conosciuti da "grande" e non aver condiviso con voi i traguardi che ho raggiunto. Spero siate fieri di me, di Gio e del lavoro fatto da babbo e mamma.

Grazie a Chiara. Grazie per avermi fatto capire quali sono le mie battaglie e che lottare "su tutti i palloni" spesso non porta da nessuna parte. Nonostante i chilometri che spesso ci hanno separato in questi tre anni, sei riuscita a farmi sentire a casa con la tua energia e il tuo sorriso. Grazie

Senza di voi non sarei arrivato dove sono adesso.

Grazie ad Alessandro, sotto la cui ala sono cresciuto.

Grazie ai ragazzi e ai senior del fu gruppo REASE, in particolare ai buoni vecchi Cocks e Sup, per i momenti di spensieratezza in ufficio e fuori. Auguro a tutti voi che leggete di trovare qualcuno con cui tirare l'amuchina sul ventilatore. Vi assicuro che ne vale la pena.

Infine, grazie a Laurens, Renske, Justin e Kenneth per avermi accolto (e riaccolto) a TU Delft, creando un ambiente stimolante e delle amicizie sincere.

ABSTRACT

Offshore wind energy has emerged as a key component of Europe's decarbonization, with significant advantages over onshore wind. Offshore sites often benefit from higher and more consistent wind speeds, resulting in higher capacity factors and energy harvesting. Furthermore, the reduced constraints on space occupation allow for the installation of larger-scale wind farms, avoiding the problems that onshore projects usually face. Their installation away from densely inhabited regions also mitigates concerns about visual and acoustic impacts, fostering public acceptance. The North Sea represents the European standard for large-scale offshore wind deployment due to its shallow waters, good wind conditions, and favourable legislative and infrastructure frameworks. These elements have facilitated the rapid construction of cost-effective offshore wind farms, which not only provide competitive power to the grid but also pave the way for sector coupling, particularly through the production of green hydrogen.

In contrast, despite being surrounded by major industrial and urban areas, the Mediterranean Sea remains far behind in terms of offshore wind deployment. This basin owes its strategic importance to its proximity to energy-intensive industries such as steel, cement, petrochemicals, and port operations, all of which are under increasing pressure to reduce carbon emissions. Developing offshore wind in the Mediterranean will thus not only provide clean power but also allow for the direct provision of energy vectors such as green hydrogen to local companies, reducing reliance on imported fossil fuels and improving regional energy self-sufficiency. Furthermore, the Mediterranean region contains extensive unexploited maritime areas close to key demand spots, which could overcome the issues related to land constraints that sometimes hinder large-scale renewable deployment onshore. However, the reasons behind the underexploitation of this basin are twofold. On the one hand, the deep seabed of most Mediterranean areas excludes the fixed-bottom solutions successfully adopted in the North Sea, making floating offshore wind turbines (FOWTs) the only viable option. Additionally, the moderate wind regimes result in lower capacity factors, which require tailored technological improvements to maximize energy yield. On the other hand, the integration of variable offshore generation into regional grids represents an additional challenge. Electrical networks of Mediterranean countries, in fact, often suffer from high congestion and curtailment rates, which make them unsuitable to accept large punctual installations. These issues underline the urgent need for dedicated research to adapt and optimize offshore wind development to Mediterranean conditions. Besides the strategic relevance of the Mediterranean Sea, the scientific literature on offshore wind in this basin remains scarce and fragmented.

Moving from this background, this thesis investigates three distinct techniques for ensuring the techno-economic viability of Mediterranean offshore wind farms. The first strategy emphasizes the employment of low-specific-power FOWTs. The reduced specific power resulting from increased rotor swept areas leads to the turbine's power curve shifting toward lower wind speeds. This approach enhances energy capture in sites with moderate wind speed and offers a competitive solution when the velocity distributions are pushed to the lower range of the Weibull

curve. The second option tackles grid integration issues by mitigating curtailment impact via energy storage and conversion systems. During the network congestion, the excess energy that would otherwise be lost is stored in batteries or converted into hydrogen. In the case of batteries, electricity can be reinjected into the grid after the curtailment phase, offering temporal flexibility and increasing overall system efficiency. In the hydrogen pathway, curtailed energy is used to power electrolyzers, which produce hydrogen that can be sold as a secondary product. Finally, the third scenario takes hydrogen as the main product of offshore wind farms. In this setup, all electricity output is employed in electrolyzers in a hydrogen-driven configuration. The green hydrogen produced is then used by energy-intensive industries. This approach not only provides a renewable option to decarbonize hard-to-abate sectors such as steel, cement, and chemicals, but it also overcomes the issue of grid congestion by requiring no direct connection to the electricity transmission system, since the electrolysis facility can be placed close to the electricity point of delivery. The results obtained have been compared to those of the North Sea scenario, revealing both the technological promise and the economic constraints unique to the Mediterranean setting.

To this end, the study combines a critical examination of the current state of the art with the creation of novel simulation and optimization tools. Python-based electrolyzer and battery detailed models have been developed to capture the dynamic interactions with fluctuating wind supply, while open-source tools such as PyWake and TopFarm have been used to optimize and simulate wind farms. The comparative examination of electrolysis technologies, such as alkaline, proton exchange membrane, and anion exchange membrane systems, enhances the techno-economic assessment by taking into account efficiency, scalability, and operational flexibility.

This thesis proposes a complete framework for offshore wind development in the Mediterranean Sea by combining novel design techniques with modelling tools. It seeks not only to close the gap with the consolidated North Sea case but also to identify specific initiatives that might unlock the region's latent potential, fostering Europe's offshore energy transition.

Keywords: Offshore wind, Hydrogen, Curtailments, Li-ion batteries, floating wind

PROPOSITIONS

Motivation (max 2)

- The decarbonization of the European energy system requires a massive expansion of offshore wind power, yet the Mediterranean basin remains underexploited due to resource, technological, and grid constraints.
- Unlocking the potential of floating offshore wind and sector coupling solutions in the Mediterranean is essential to ensure regional energy security, economic competitiveness, and alignment with EU climate targets.

Original contribution (max 4)

- Comprehensive comparative analysis between the North Sea and the Mediterranean offshore wind contexts, highlighting techno-economic drivers and bottlenecks for large-scale deployment.
- Novel assessment of low-specific-power turbine configurations for floating wind farms under moderate wind conditions, demonstrating improved energy capture and system performance.
- Integrated evaluation of curtailment mitigation strategies, combining advanced and second-life storage solutions with hydrogen production as a flexible demand-side option.
- Techno-economic comparison of leading electrolysis technologies (ALK, PEM, AEM) under realistic Mediterranean offshore wind profiles, providing design guidelines for optimal integration.

Open questions (max 4)

- How can the long-term reliability and lifecycle sustainability of second-life batteries be quantified and ensured in offshore energy applications?
- What is the most effective regulatory and market design framework to incentivize hydrogen production from offshore wind in regions with constrained grids?
- How can future multi-vector energy systems (electricity, hydrogen, storage) be optimally coordinated to maximize the value of offshore wind in the Mediterranean basin?

INDEX

1 Introduction 1

1.1 Offshore wind energy
1.2 Floating offshore wind turbines

2 Benchmark definition: the role of offshore wind in green hydrogen production in the Dutch North Sea 9

2.1 Introduction
2.1.1 Contribution
2.2 Literature review and knowledge gaps
2.3 Methodology
2.3.1 System components
2.3.2 Economic assessment
2.4 Case study
2.4.1 System configurations
2.4.2 Scenarios and databases
2.5 Results
2.5.1 Economic analysis of system configurations
2.5.2 Operational differences across configurations
2.6 Discussion
2.6.1 Comparison to literature
2.6.2 Implications for stakeholders
2.6.3 Limitations
2.7 Conclusions

3 The Mediterranean challenges: Unlocking Potential with Floating Wind 41

3.1 Challenges in floating offshore wind development: a review
3.1.1 Floating farm design: the need for tailored solutions
3.1.2 Objectives and structure of the study
3.2 Study cases
3.2.1 Turbines
3.2.2 Farm layout
3.2.3 Wind dataset
3.2.4 Installation sites
3.3 FOWT cost and scaling models: review and critical assessment
3.3.1 Rotor performance
3.3.2 Component mass and cost
3.3.3 OPEX increase
3.4 Optimization model
3.4.1 Power production assessment

3.4.2 IA cables layout
3.4.3 Objective function
3.4.4 Wind farm optimization algorithm
3.4.5 Constraints
3.5 Results
3.5.1 Technical results of the optimization
3.5.2 Environmental analysis
3.5.3 Economic results of the optimization
3.6 Discussion
3.7 Conclusions

4 Mitigating Grid Congestion in Offshore Wind: Comparative Modeling of Li-ion Batteries and Hydrogen 79

4.1 Introduction
4.1.1 Main scientific contributions and novelty
4.2 Second-life batteries
4.2.1 Existing SBESS projects
4.2.2 Battery passport
4.2.3 Techno-economic impact
4.3 Study cases
4.3.1 Wind turbines
4.3.2 Sicily: Wind farm layout and installation site
4.4 Methodology
4.4.1 Wind data
4.4.2 Power production calculations
4.4.3 Curtailments
4.4.4 Battery modelling
4.4.5 Electrolyzer modelling
4.4.6 Metrics for cost estimation
4.4.7 Component costs
4.5 Results
4.5.1 Wind farm layout optimization
4.5.2 mLCoE
4.5.3 LCoH
4.5.4 NPV
4.5.5 Preliminary environmental analysis
4.6 Discussion
4.7 Conclusions

5 From Wind to Hydrogen: Comparative Evaluation of Electrolyzer Technologies and Cost Reduction Pathways 107

5.1 Introduction
5.1.1 Contribution and novelty
5.2 Methods
5.2.1 Wind farm optimization model
5.2.2 Wind farm simulation model
5.2.3 Electrolyzer model
5.2.4 Techno-economic metrics and financial assumptions

5.3 Case study
5.3.1 Wind farm
5.3.2 Electrolysis facility
5.3.3 Installation sites
5.4 Results
5.4.1 Wind farm optimization
5.4.2 Hydrogen production
5.5 Discussion
5.6 Conclusions

6 Conclusions 141

LIST OF FIGURES

Figure 1.1: rendering of onshore vs offshore wind turbines. 1

Figure 1.2: Rendering of the most common foundations for bottom fixed wind turbines. 4

Figure 1.3: offshore wind energy projects classified by bathymetry and distance to shore [23]. 5

Figure 1.4: Rendering of the most common platforms for floating wind turbines. 6

Figure 2.1: Simulation model workflow. 14

Figure 2.2: Polarization curve of the PEM electrolyzer (a) [64] and ALK electrolyzer (b) [42]. 16

Figure 2.3: Available wind park sites in the Dutch North Sea. 19

Figure 2.4: Weibull distribution of the available wind sources. 20

Figure 2.5: Wind source in the chosen installation sites. 21

Figure 2.6: Wind farm layout and corresponding wind rose for the installation sites at 50 km (a) and 100/200 km (b) from the shore. 21

Figure 2.7: Schematic representation of the C-ON, C-OFF, and D-OFF system configuration. 24

Figure 2.8: Range of LCoH found for each system configuration for three wind park sites (characterized by their distance to shore). 25

Figure 2.9: LCoH breakdown for two scenarios (under expert validated cost and mean technology input data) for each system configuration: a 50 km offshore distance using an ALK electrolyzer, and a 200 km offshore distance using a PEM electrolyzer. 26

Figure 2.10: Annual hydrogen delivered to the backbone for C-ON, C-OFF, and DOFF for different distances to shores and electrolysis technologies in the mean technical scenario. 29

Figure 2.11: Mean overall system efficiency across all scenarios and configurations. 30

Figure 2.12: Losses due to electrolyzer constraints (a) (minimum load requirements, cold startups, and power electronics) and total losses (b) (including distance from shores) per system configuration. 30

Figure 2.13: Sankey diagrams for the ALK electrolyzer in the C-OFF system configuration. 31

Figure 2.14: Sankey diagrams for the PEM electrolyzer in the C-OFF system configuration. 32

Figure 2.15: Capacity factor (CF) per wind turbine in the D-OFF configuration for the mean technical scenario in the 100 km offshore site. 32

Figure 2.16: Comparison between the operational behavior of the offshore configurations with PEM and ALK. 33

Figure 2.17: Range of LCoH for each system configuration for five wind park sites, characterized by their distance to shore. 34

Figure 2.18: Overview of the operational behavior of the offshore configurations with PEM and ALK, with the inclusion of additional wind park sites HKZ (20 km) and IJV (60 km). 35

Figure 3.1: Workflow of the study. Review phases are highlighted with dashed boxes. 47

Figure 3.2: Comparison between the Weibull (a) of the considered installation sites (b) at 100 m asl. Wind speed map from Global Wind Atlas. 50

Figure 3.3: WT power curves in the laminar (a) and turbulent (b) free stream wind conditions.53

Figure 3.4: WT thrust curves without (a) and with (b) active pitch control. 54

Figure 3.5: WT power curves in the laminar (a) and turbulent (b) free stream wind conditions.54

Figure 3.6: M_T literature and proposed data relying on the introduced correlation. 56

Figure 3.7: (a) platform mass - literature and proposed data relying on the introduced correlation. (b) platform cost - literature and proposed data relying on the introduced correlation. Red markers indicate platform mass and cost of proposed designs without the adoption of peak shaving. 59

Figure 3.8: Comparison between the results and literature data for platform masses and costs. 61

Figure 3.9: WT CAPEX breakdown for the designed aerogenerators. 62

Figure 3.10: Optimal IA cable layout obtained with the TSP reimplementation (a) or Edwin (b). 65

Figure 3.11: Schematic representation of the optimization model. 66

Figure 3.12: Scheme for minimum IA distance between WTs. 67

Figure 3.13: Comparison between the AEP and the AEP variation in the different installation sites for the new aerogenerator designs. 68

Figure 3.14: Comparison between the AEP distribution in the French and Greek installation sites for the MED15MW_240 and MED15MW_330. 68

Figure 3.15: Comparison between the wake effects of the MED15MW_240 and the MED15MW_330 WTs. 69

Figure 3.16: Comparison between the optimal layout obtained in Sicily (a) and Cyprus (b) for the wind farms with the MED15MW_240 and the MED15MW_330 WTs. 70

Figure 3.17: Comparison between the optimal layout obtained in Sicily with two different IA cable costs for the MED15MW_240. 70

Figure 3.18: Comparison between the carbon emissions saved and the carbon PBT for the tested WTs in the different installation sites depending on the emission factor of each Country [207]. 71

Figure 3.19: Comparison between the LCoE and the LCoE variation in the different installation sites for the new aerogenerator designs. 72

Figure 3.20: Comparison between the LCoE in the different installation sites for the new WT designs with different IA cable costs. 73

Figure 4.1: Example of wind farm layout with wind rose of the specific site in terms of frequency [%]. 86

Figure 4.2: a) Comparison between Weibull curves of ERA5 and the reconstructed data at 100 m a.s.l: b) procedure to evaluate the wind variation of the measured data; c) evaluation of the ten-minute series at 100 m a.s.l. 87

Figure 4.3: Scheme of the overall process used to obtain 1-min wind power data starting from 1-hour wind speed data. 88

Figure 4.4: SOH decrease due to cyclic operation of the BESS for the two degradation fittings tested. 90

Figure 4.5: ALK electrolyzers CAPEX in 2020 and in 2030. 93

Figure 4.6: AEP (a) and mLCoE (b) in different curtailment scenarios for the discount rates analyzed. 94

Figure 4.7: Power production and curtailed power for the time-dependent and statistical approach, in all curtailment scenarios. 95

Figure 4.8: Power production and curtailed power for the time-dependent and statistical approach, the 15% AEP curtailment scenario. 96

Figure 4.9: LCoH and capacity factors in S1 and S2 in the 10 % curtailment scenario. 97

Figure 4.10: NPV of the wind farm in the 5 % curtailment scenario and a curtailed energy remuneration of 0 % (a), 25 % (b), and 50 % (c) of the LCoE with the adoption of the NBESS. 98

Figure 4.11: NPV of the wind farm in the 5 % curtailment scenario and a curtailed energy remuneration of 0 % (a, d), 25 % (b, e), and 50 % (c, d) of the LCoE for the NBESS (above) and SBESS (below). 99

Figure 4.12: NPV of the wind farm with an Ecost of 0 % of the LCoE and a BESS cost of 130 €/kWh for the NBESS (a) and 70 €/kWh for the SBESS (b). 100

Figure 4.13: NPV Variation in the configuration with the optimal BESS size varying battery cost for different curtailed energy remuneration and wind farm output reduction of 5 % (a), 10 % (b), and 15 % (c) of the AEP with the NBESS (above) and SBESS (below). 101

Figure 4.14: Comparison between the NPV of the electrolysis, the BESS and the base solution in S1 and S2 in the 10 %, LCoH low curtailment scenario. 102

Figure 4.15: Battery replacements and environmental impact of the storage after thirty years of operation of the plant. 103

Figure 5.1: Overview of the LCoH calculation procedure. 113

Figure 5.2: Schematic representation of the optimization model. 114

Figure 5.3: Polarization surfaces of the electrolysis technologies compared. 116

Figure 5.4: Power curves of the wind turbines adopted in this study [297,305]. 119

Figure 5.5: Centralized onshore configuration scheme. 121

Figure 5.6: Weibull curve of the wind source at 100 m asl for the installation site in Sicily and in Cyprus. 123

Figure 5.7: Wind rose distribution of the wind source at 100 m asl for the installation site in Sicily (a) and in Cyprus (b). 123

Figure 5.8: Comparison between the AEP and the ΔAEP in the two installation sites for the new aerogenerator designs. 125

Figure 5.9: LCoE and ΔLCoE in the two installation sites for the new aerogenerator designs. 125

Figure 5.10: Wind farm optimal layout comparison for the MED15MW_240 and MED15MW_330 for the installation site in Sicily (a) and in Cyprus (b). 126

Figure 5.11: Wind farm power production distribution for the installation site in Sicily (a) and in Cyprus (b) with the MED15_270 and MED15_330, respectively. 127

Figure 5.12: Gain in available energy for ALK electrolyzer between 240m and larger rotor diameter wind farms in Sicily (left) and Cyprus (right) considering the: a) shift of power curves and minimum power required by ALK electrolyzers, b) impact on available wind speeds from the point of view of wind resource characterizing the sites, c) gross AEP increment and gain in available energy for H2 production by ALK electrolyzers. 128

Figure 5.13: Wind Farm and Electrolyzer CF comparison in Sicily (a) and Cyprus (b). 130

Figure 5.14: Unexploited energy and Electrolyzer Utilization Factor comparison due to electrolyzer technical constraints in Sicily (a, c) and Cyprus (b, d). 131

Figure 5.15: Time-dependent behavior of the system in terms of produced and exploited power a), and hydrogen production b) during seven days of operation with the MED15_240 FOWT. PEM trends have been omitted due to similar behavior to AEM technology. 132

Figure 5.16: Hydrogen production comparison in Sicily (a) and Cyprus (b) varying the turbine diameter. 133

Figure 5.17: Time-dependent variation of the yearly average ϕ in Sicily comparing the three technologies with the MED15_240 (a), and the behavior of ALK with the MED15_240 and MED15_330 (b) in the optimal degradation scenario. 134

Figure 5.18: LCoH distribution across all the scenarios analyzed, considering uncertainty in efficiencies, degradation factors, and costs. 136

LIST OF TABLES

Table 1.1: Global offshore wind substructure capacity (MW) for various substructure types installed in 2022 and projects to 2030 [23]. 7

Table 2.1: State of the art of techno-economic simulation models of offshore wind-based electrolysis. 12

Table 2.2: Overview of the technical specifications of all components of the considered system configurations [67]. 23

Table 2.3: Electrolyzer lifetime per technology and technical scenario. 28

Table 3.1: Main design parameters for the IEA15MW RWT and the proposed FOWTs. 48

Table 3.2: Installation sites comparison. 49

Table 3.3: Existing and proposed FOWTs' M_T and H_T. 56

Table 3.4: Mass scaling equations for the main RNA components. 57

Table 3.5: Proposed FOWTs' MR, MTOT and HCOM. 57

Table 3.6: Steel consumption and CO_2 production increase for the single turbine-floater assembly due to higher swept areas. 72

Table 4.1: IEA 15 MW reference data. 85

Table 4.2: Wind farm layout spacing description. 85

Table 4.3: Curtailment description in terms of power reduction. 89

Table 4.4: Specific Expenditures for the case study. 92

Table 4.5: Wind farm AEP and LCoE for the analyzed layouts with different interest rates i. 94

Table 4.6: Optimal electrolyzer sizes and LCoH in the different curtailment scenarios. 98

Table 5.1: Summary of the existing literature on techno-economic simulation models of offshore wind-based electrolysis. 110

Table 5.2: Settings of the wind farm layout optimization. 114

Table 5.3: Settings of the wind farm layout optimization. 118

Table 5.4: Design parameters for the different wind turbines considered. 120

Table 5.5: Design parameters for the different wind turbines considered. 121

Table 5.6: Design parameters for the different wind turbines considered. 122

Table 5.7: Design parameters for the different wind turbines considered. 124

Table 5.8: Summary of the results obtained for the technical average scenario. 135

NOMENCLATURE

Acronyms

AEM	Anion exchange membrane electrolyzer
AEP	Annual energy production
ALK	Alkaline electrolyzer
a.s.l.	Above the sea level
AVG	average technical scenario
BESS	Battery energy storage system
CAPEX	Capital expenditure
CF	Capacity Factor
C-ON	Centralized onshore
C-OFF	Centralized offshore
COP	Coefficient of performance
C_P	Power coefficient
C_T	Thrust coefficient
D-OFF	Decentralized offshore
EOL	Endo of life
ESS	Energy storage system
FOWT	Floating offshore wind turbines
H_2	Hydrogen
HB	Higher bound
HKZ	Hollandse Kust Zuid
HVAC	High voltage alternating current
HVDC	High voltage direct current
IA	Inter array
IRENA	International Renewable Energy Agency
IJV	IJmuiden Ver
LB	Lower bound
LCA	Life cycle assessment
LCoE	Levelized cost of energy
LCOH	Levelized cost of Hydrogen
LSP	Low specific power
MED	Mediterranean Sea
NBESS	Brand-new battery
NED	Nederwiek
NMC	Nickel-Manganese-Cobalt
NPV	Net present value
OPEX	Operational expenditure
OPT	Optimistic technical scenario

PEM	Proton exchange membrane electrolyzer
PES	Pessimistic technical scenario
POD	Point of delivery
PV	Photovoltaic
REF	Reference technical scenario
RES	Renewable energy source
RWT	Reference wind turbine
S	Scenario
SBESS	Second-life battery
TI	Turbulence intensity
TLP	Tension-leg platform
TNW	Ten Noorden van de Waddeneilanden
TSR	Tip speed ratio
UF	Utilization factor
WS	Wind speed
WT	Wind Turbine

Greek symbols

Δ	variation of a magnitude	[-]
Φ	conversion factor	[kg/MWh]
ρ	air density	[kg/m^3]

Latin symbols

A	*rotor swept area*	*[m^2]*
C	*cost*	*[€]*
cf	*cash flow*	*[€]*
D	*diameter*	*[m]*
E	*energy*	*[MWh]*
h	*working hours*	*[h]*
I	*current*	*[A]*
i	current density	[A/cm^2]
L	height	[m]
mLCoE	market LCoE	[€/MWh]
M	mass	[kg]
n	cell number	[-]
P	*Power*	*[MW]*
Q	*Heat*	*[MWt]*
r	discount rate	[-]
R	*coefficient of determination*	*[-]*
SOC	*State of charge*	*[%]*
SOH	*State of health*	*[%]*
T	Temperature	[°C]
V	Voltage	[V]

Subscripts

actual

available	
avg	average
BP	bed plate
cells	stack cells
COM	center of mass
Cool	cooling
degr	degradation
DES	value in design condition
DISC	incentives
Diss	dissipated
EL	electrolyzer working value
F	floater
flow	mass flow
Gen	generated
HUB	hub value
id	ideal value
in	input
Max	maximum value
Min	minimum value
loss	loss
NAC	nacelle
NEW	brand-new
OP	operating value
PB	pitch bearing
PS	pitch system
R	rotor
rated	rated value
repl	replacement
REUSE	repurposing cost
SEC	secondary hub components
T	thermal
USED	second life

SYNOPSIS

Offshore wind energy represents a key component of Europe's decarbonization strategy, thanks to its higher capacity factors and steadier power outputs with respect to onshore alternatives. The less strict constraints on space occupation and distance from inhabited areas also foster the deployment of large-scale wind farms while mitigating concerns about landscape and noise, hence enhancing social acceptance. Among European seas, the North Sea has served as the benchmark for large-scale offshore wind deployment, combining favorable wind sources, shallow waters, and supportive regulatory frameworks that have enabled rapid development of cost-competitive farms. Moreover, the proximity to energy-intensive industries has enabled offshore wind in this region to create a strong link with sector coupling, especially through green hydrogen production.

On the other hand, the Mediterranean Sea, despite its closeness to industrial clusters and port operations, remains largely unexplored. This gap is of particular concern considering the strategic importance of this basin: offshore wind here could both provide clean power to local grids and directly supply renewable energy carriers such as hydrogen to industrial users, thereby reducing reliance on imported fossil fuels. At the same time, large maritime areas close to major demand centers offer opportunities to overcome onshore land-use conflicts. The reasons for the delayed uptake of offshore wind in the Mediterranean are, however, twofold. On the one hand, the deep seabed of most areas rules out the fixed-bottom technology successfully adopted in the North Sea, leaving floating offshore wind turbines (FOWTs) as the only viable alternative. Moderate wind regimes further exacerbate this technological challenge, as they reduce capacity factors. On the other hand, the integration of large offshore wind farms into Mediterranean grids is hindered by poor electricity grids, highlighting the need for complementary storage or conversion pathways to mitigate curtailments. Despite these pressing issues, the scientific literature on Mediterranean offshore wind development remains scarce and fragmented.

Moving from this background, the present thesis investigates different strategies to enhance the techno-economic viability of offshore wind deployment in the Mediterranean Sea. To this end, open-source libraries such as PyWake and TopFarm were employed for the simulation and optimization of wind farm layouts under Mediterranean conditions, coupled with dedicated Python-based dynamic models for electrolyzers and batteries to mimic the interactions with fluctuating wind power supply. Specifically, these tools were developed and employed in multi-fidelity analyses to address the three main issues currently associated with wind farm deployment in the Mediterranean Sea:

1. *Challenging bathymetry and moderate wind sources.* This thesis focused on the adoption of low-specific-power FOWTs to overcome the issues related to the unconventional characteristics of the Mediterranean Sea. First, an extensive review of existing scientific and industrial literature, aimed at collecting techno-economic data on both aerogenerators and floating platforms, has been conducted. Given the lack of relevant data, a set of cost and mass scaling functions has been derived, enabling the extrapolation

of turbine and floater characteristics depending on rotor diameters. The developed correlations have been subsequently implemented into the TopFarm optimization framework, allowing for the optimization of floating wind farm layouts specifically tailored to Mediterranean conditions. The results were then compared, providing insights into the techno-economic trade-offs of rotor upscaling. In particular, the analyses highlighted how larger rotors increase both energy capture in moderate wind regimes and the expenditures related to turbines and substructures. Through this approach, the thesis delivers a quantitative and generalizable framework for assessing the viability of low-specific-power FOWTs in the Mediterranean context. The methodology not only compensates for the lack of consolidated cost data in the literature but also establishes a set of design guidelines that can support the optimization of future floating wind farms in the region.

2. *Unsuitable electricity grid.* To address the issue of the limited capacity of regional electricity grids, two complementary strategies aimed at mitigating the impact of curtailment while enhancing the overall techno-economic performance of offshore wind farms have been implemented. The first approach considered the integration of large-scale battery energy storage systems (BESS). A dedicated Python-based dynamic model has been developed to simulate the interaction between fluctuating offshore wind generation, curtailment events, and Li-ion battery operation. The model enabled the quantification of benefits associated with shifting curtailed electricity to later reinjection into the grid, thereby providing temporal flexibility and reducing energy losses. Both brand-new and second-life storage have been compared in order to estimate the trade-offs between economic and environmental effectiveness. The second strategy focused on the conversion of curtailed electricity into green hydrogen. For this purpose, a dynamic electrolyzer model for alkaline technology has been implemented to capture transient performance under variable load conditions. Both approaches have been integrated into the simulation framework and evaluated under realistic Mediterranean grid conditions. The analyses enabled a techno-economic comparison of storage versus hydrogen-based pathways, highlighting the contexts in which each option proves advantageous.

3. *Green Hydrogen cost competitiveness.* In order to tackle this challenge, offshore wind dedicated electrolysis configurations have been explored, where the entire wind farm output is converted into green hydrogen through electrolyzers. By decoupling power production from the electricity grid, this approach fully circumvents the issue of network congestion and simultaneously enables the direct supply of green hydrogen to hard-to-abate sectors. Despite its potential, the main limitation of this configuration lies in the high cost of green hydrogen, which currently prevents large-scale competitiveness with fossil-based alternatives. To examine whether offshore wind in the Mediterranean could contribute to bridging this cost gap, the thesis analyzed the impact of low-specific-power turbines on hydrogen production economics. Given the enhanced energy capture under moderate wind regimes, their integration into hydrogen-driven plants has been assessed as a potential solution to reduce the production costs and to narrow the gap with benchmark projects in the North Sea. The analysis combined the wind farm optimization framework with detailed electrolyzer models for alkaline, proton, and anion exchange membrane technologies. Each system has been evaluated in terms of efficiency, scalability, and operational flexibility under variable wind power inputs. Finally, to deal

with the considerable uncertainties related to hydrogen supply chains, the thesis carried out an extensive uncertainty analysis on both electrolyzer performance and cost projections. By applying scenario-based projections up to 2030, a broad envelope of possible levelized costs of hydrogen outcomes has been established for Mediterranean hydrogen-driven farms.

Results from these studies have been benchmarked against the established North Sea scenario, highlighting both the opportunities and the constraints of Mediterranean offshore wind. In particular, the findings show how tailored turbine designs, combined with flexible storage and hydrogen production strategies, can significantly improve the competitiveness of Mediterranean projects despite less favorable wind conditions and grid limitations.

In conclusion, this thesis provides a comprehensive framework for adapting offshore wind development to the specific challenges of the Mediterranean Sea. By integrating innovative turbine design, energy conversion strategies, and advanced modelling tools, it identifies a set of pathways capable of unlocking the region's untapped potential, thereby contributing to Europe's broader offshore energy transition.

Thesis outline

- *Chapter 1* introduces offshore wind energy in comparison to onshore installations, highlighting the specific advantages of offshore sites in terms of capacity factors, scalability, and social acceptance. The chapter contrasts the well-established North Sea model with the current underdevelopment of the Mediterranean basin, providing the motivation for the research and framing the technological and infrastructural challenges to be addressed.
- *Chapter 2* defines the North Sea benchmark, with particular emphasis on the role of offshore wind in green hydrogen production. In this section, the implementation of the adopted model is reported in detail along with the obtained results. Different scenarios have been evaluated, varying distance from shores, electrolysis technologies, and economic parameters, in order to define the costs of hydrogen production that will be used for comparisons.
- *Chapter 3* presents the first approach to promote Mediterranean installations, focused on low-specific-power FOWTs. The chapter details the derivation of cost and mass scaling correlations for turbines and floating platforms based on an extensive literature review, their implementation into the TopFarm optimization framework, and the comparative analysis of different farm layouts under Mediterranean wind conditions.
- *Chapter 4* addresses the issue of grid congestion and curtailment, introducing two complementary mitigation strategies: battery energy storage systems and hydrogen conversion. The chapter describes the Python-based dynamic models adopted for both technologies, their integration with offshore wind simulations, and the comparative techno-economic evaluation of the two pathways.
- *Chapter 5* explores the hydrogen-driven configuration, in which all wind farm output is directly converted into hydrogen. The chapter discusses the techno-economic implications of this grid-independent approach, the role of low-specific-power

turbines in reducing the levelized cost of hydrogen, and the comparative performance of alkaline, PEM, and AEM electrolyzers. An extensive uncertainty analysis on cost and efficiency projections up to 2030 is presented to assess the future viability of Mediterranean hydrogen-driven offshore wind farms.

- *Chapter 6* concludes the thesis by summarizing the main contributions of the research, outlining the conditions under which offshore wind in the Mediterranean can achieve techno-economic viability, and identifying future research directions to further unlock the basin's renewable energy potential.

1 INTRODUCTION

1.1 Offshore wind energy

Figure 1.1: rendering of onshore vs offshore wind turbines.

Offshore wind energy has rapidly become crucial for global renewable energy strategies, emerging as a response to the limitations of onshore wind systems and the rising demand for low-carbon electricity. Onshore developments are constrained by limited land availability, difficulties in transporting and installing increasingly large turbines, and public concerns over visual and noise impacts. These issues have pointed the focus on offshore deployment, where the resource potential and site availability are significantly greater [1–3].

A major advantage of offshore wind lies in the higher average wind speeds available at sea. Offshore sites, in fact, benefit from stronger and more consistent wind sources, which not only increases the capacity factors (CF) but also improves the proficiency of the technology. The higher CF achieved by offshore wind farms compared to their onshore counterparts contributes to greater system reliability [4,5]. In addition, while photovoltaic (PV) plants or onshore wind projects compete with agricultural production, urban expansion, or terrestrial ecosystems, one of the offshore turbines' key benefits is the relative absence of land-use conflicts. Furthermore, locating installations at sea also reduces visual and acoustic disturbances, which are frequently cited as causes of local opposition to onshore projects [3].

Beyond technical benefits, offshore wind supports economic growth and job creation. According to the International Renewable Energy Agency (IRENA), the sector could provide nearly 900,000 jobs globally by 2030, spanning manufacturing, engineering, marine transport, construction, and long-term maintenance. For coastal regions, particularly those with histories of offshore oil and gas activity, the expansion of offshore wind presents new opportunities for skilled employment and industrial diversification [6,7]. By relying on domestic wind resources, countries can also reduce dependence on imported fossil fuels, thereby improving energy security and resilience to price volatility [5].

Nevertheless, the sector faces significant challenges. Offshore projects remain capital-intensive, with high costs related to site permitting, installation, operation, and maintenance. Harsh marine conditions demand corrosion-resistant materials, advanced foundation designs, and specialized vessels, all of which contribute to higher expenses compared with onshore wind. Additional concerns include potential undersea cable infrastructure requirements, and uncertainties surrounding substructure decommissioning and material recycling [8–10]. Environmental impacts also require careful management. Offshore wind farms may affect seabed habitats, bird migration, and marine fauna, but they can also provide ecological benefits by creating artificial reef structures and restricting certain types of commercial fishing [11,12].

In Europe, combining the expansion of offshore wind with marine protection objectives is an emerging priority. Spatial planning plays a critical role in balancing renewable energy development with conservation goals, fisheries, and maritime transport. The EU's Offshore Renewable Energy Strategy emphasises a flexible, ecosystem-based approach to maritime spatial planning to mitigate conflicts and ensure sustainability [5,13]. This includes not only scaling up production but also addressing cumulative environmental pressures, stakeholder engagement, and long-term circular economy considerations in turbine decommissioning [3,14].

The resource potential of offshore wind is considerable. Technological innovation, particularly in floating wind systems, is giving access to deeper waters and expanding the viable deployment area beyond the continental shelf [15,16]. This makes offshore wind a cornerstone technology in national and regional strategies for decarbonisation, including the EU's legally binding 2030 target of at least a 55% reduction in net greenhouse gas emissions [5,17]. To meet these goals, Europe is planning an expansion from 19.38 GW of installed offshore wind capacity in 2023 to 111 GW by 2030 and 317 GW by 2050 [18,19].

Globally, onshore wind remains the dominant form of wind power deployment, although offshore wind is growing much faster in relative terms. By 2022, total installed wind capacity reached around 900 GW, of which 93 % was onshore and only 7 % offshore [20]. In absolute terms, this corresponds to roughly 59 GW of offshore wind across 292 projects, after a record 8.4 GW was added that year, a 16.6 % increase from 2021 [21]. China led these new offshore installations with 5.7 GW, followed by the UK (1.4 GW), France (0.5 GW), Germany (0.3 GW), and Vietnam (0.3 GW). By the end of 2022, China accounted for 46 % of global offshore capacity, surpassing the UK's 23 %, while Germany, the Netherlands, and Denmark made up 13.5 %, 5.1 %, and 3.9 % respectively. Regionally, offshore wind capacity is still concentrated almost entirely in Europe (51 %) and Asia (49 %), with North America holding just 0.1 % [21].

While onshore wind continues to dominate due to its lower costs and easier deployment, offshore wind holds distinct advantages in terms of scale and efficiency. Capacity factors for offshore projects typically range between 45–50 %, compared with 25–35 % for onshore farms [20]. This means that each megawatt of offshore capacity delivers significantly more electricity than the same capacity installed onshore. In addition, offshore projects can often be developed at larger scales—such as the UK's 3.6 GW Dogger Bank project—whereas most onshore projects are smaller [20]. The International Energy Agency estimates that offshore wind could theoretically generate more than 18 times the world's current electricity demand if fully exploited [20], highlighting its long-term strategic role.

Europe provides a good illustration of the current dynamics. In 2024, the continent installed 16.4 GW of new wind capacity, of which 84 % (13.8 GW) was onshore and only 2.6 GW offshore [18]. Germany led the way with 4 GW of new capacity, followed by the UK (1.9 GW) and France (1.7 GW), each expanding both onshore and offshore. By the end of 2024, Europe's installed base reached 285 GW, made up of 248 GW onshore and 37 GW offshore—meaning offshore represented about 13 % of the total [18]. Looking forward, Europe is expected to install 187 GW of new capacity between 2025 and 2030, bringing the total to around 450 GW. If the current trend of roughly 15 % offshore share continues, offshore capacity would reach about 65 GW by 2030. However, stronger policies and auctions push could increase this share up to 19 % (84 GW) by the same date [18].

Extrapolations at the global scale emphasize these trends. According to DNV, total wind capacity is projected to grow from about 1.0 TW in 2023 to 1.8 TW in 2030 and 6.3 TW by mid-century [22]. Offshore wind is expected to gain momentum during this period. Today, onshore generation outpaces offshore by a ratio of about 9:1, but by 2050, DNV expects this to narrow to 3:1 [22]. Given offshore's higher CF, this would imply that offshore capacity will rise to around 17 % of the total by 2050, providing roughly one-quarter of total wind generation. Translated into installed capacity, that would correspond to about 1.0 TW of offshore wind and 5.2 TW of onshore by mid-century [22]. This implies offshore capacity could grow at an annual average rate of around 9 % from 2030 to 2050, compared with about 6 % for onshore.

Regional patterns show contrasting trajectories. China has established itself as the global leader in offshore deployment, aided by industrial scale, supportive policies, and lower cost inflation than in Europe and North America [21,22]. Europe remains the pioneer in offshore development and is expected to lead the emerging floating offshore segment, especially in the North Sea [22]. By contrast, North America is still starting from an almost negligible offshore base, though new policy incentives and supply-chain investments are beginning to shift momentum [21].

Cost dynamics are also shaping the pace of the onshore–offshore shift. Offshore projects remain significantly more expensive to build and finance than onshore farms. In 2023, the global levelized cost of electricity (LCoE) for fixed-bottom offshore wind averaged about 133 $/MWh, more than double onshore's 49 $/MWh [22]. Costs for offshore rose sharply post-2020 due to supply chain disruptions, higher capital costs, and inflationary pressures. However, by 2050, DNV expects offshore LCoE to decrease by about 7 $/MWh, while onshore declines further to around 8 $/MWh [22]. These projections suggest offshore will remain more costly per unit of energy but will become increasingly competitive given its higher output per turbine and proximity to coastal demand centers.

In short, onshore wind remains the backbone of current global wind deployment but offshore is growing much faster and will play an increasingly important role in the energy mix. By 2030, offshore wind is likely to account for around 10 % of global installed capacity and up to 19 % in Europe. By 2050, offshore is expected to represent about 17 % of global capacity but closer to 25 % of generation, reflecting its higher efficiency and larger project scale [18,20–22].

1.2 Floating offshore wind turbines

The evolution of offshore wind substructures reflects both the technological maturity of bottom-fixed foundations and the growing necessity to access deeper waters. Fixed-bottom foundations have historically dominated the offshore wind sector, benefiting from simpler design principles, established installation practices, and cost-effective manufacturing supported by standardized global supply chains [21]. According to the NREL reports [21], fixed-bottom technologies comprised the large majority of offshore projects in 2022, with monopiles alone accounting for 60.2 % of installations, followed by jackets (10.4 %), suction bucket (8.6 %), tripods (1.8 %), and gravity-based structures (1.4 %). This portfolio illustrates the maturity and reliability of fixed-bottom solutions in water depths up to 60 m.

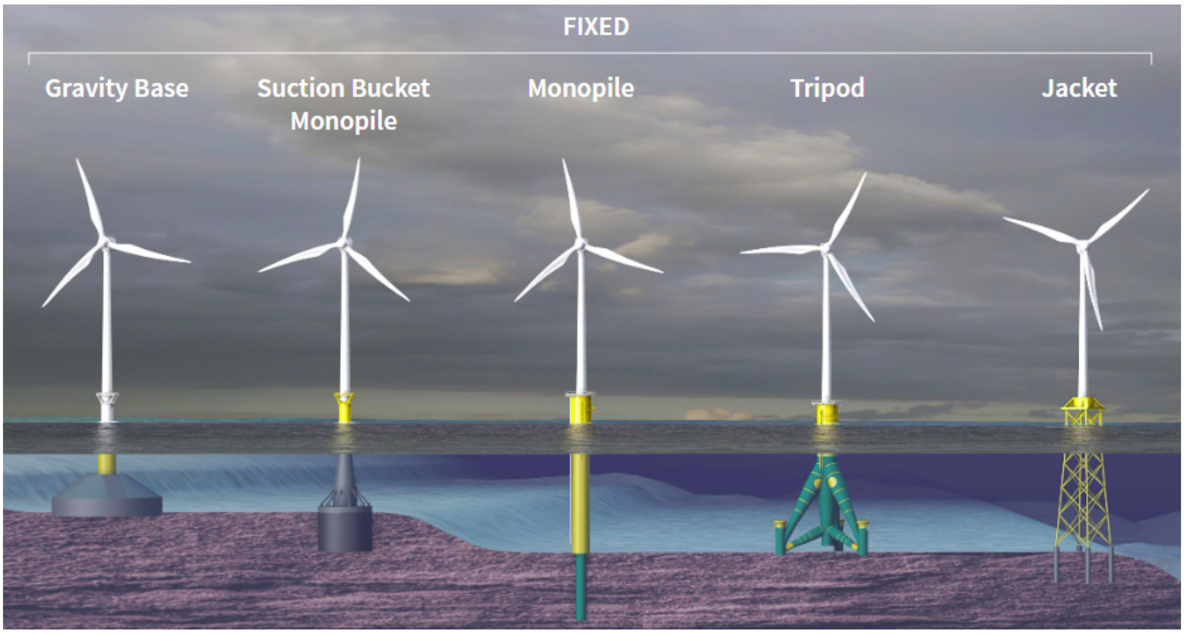

Figure 1.2: Rendering of the most common foundations for bottom fixed wind turbines.

Figure 1.2 illustrates the adaptability of fixed-bottom systems to varying seabed conditions and water depths, while also highlighting the limitations that motivate the development of floating alternatives. The main existing design can be described as follows:

- Gravity-based foundations transfer loads through self-weight and large base contact areas. They are generally constructed from reinforced concrete and require seabed preparation to ensure stability.
- Suction bucket consists of steel cylinders that penetrate the seabed under applied suction pressure, providing both vertical and lateral resistance.
- Monopiles are large-diameter steel piles driven into the seabed, offering a straightforward design and rapid installation.
- Tripods employ three-legged structures extending from a central shaft, distributing loads across multiple pile foundations and enhancing stability in intermediate water depths.
- Jackets are multi-leg frameworks anchored by piles at each corner. Their high stiffness makes them suitable for deeper waters and larger turbines, albeit at higher fabrication and installation costs.

Despite the dominance of fixed-bottom technologies, several constraints are expected to limit their long-term applicability. The continuous upscaling of wind turbines increases structural demands, while soil conditions and environmental restrictions can reduce the feasibility of pile-driven foundations. Furthermore, the scarcity of shallow-water sites has led to the expansion of project locations farther offshore and into deeper waters. To meet future decarbonization targets, the industry therefore requires access to larger offshore resource areas, a shift that cannot be achieved with fixed-bottom technologies alone [21]. This trend is highlighted by **Figure 1.3**, where the light blue dots show that projects are increasingly located further from shores and in installation sites with higher sea depths. This would enable access to larger wind farm capacities, as depicted by the larger dot sizes.

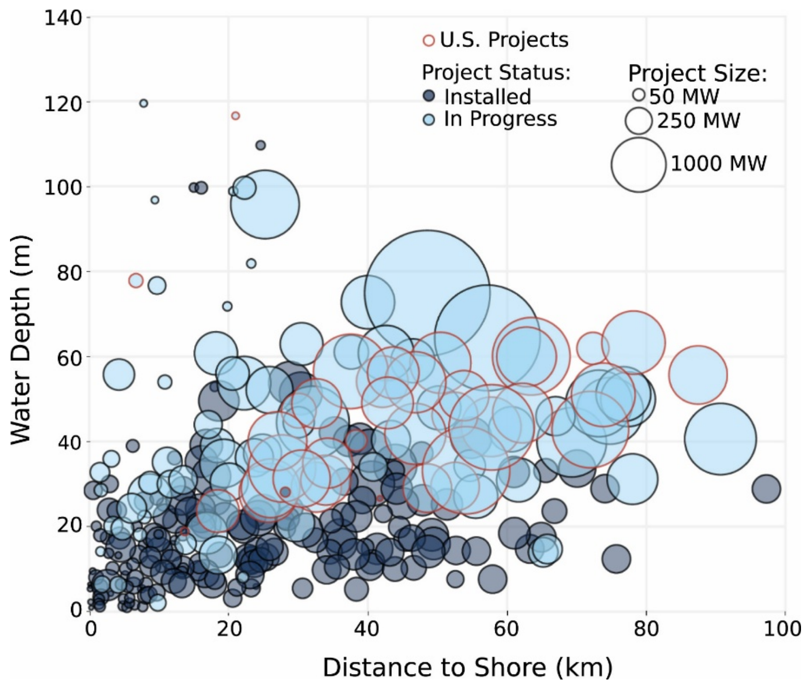

Figure 1.3: offshore wind energy projects classified by bathymetry and distance to shore [23].

In response, attention has increasingly shifted toward floating offshore wind technologies, which enable deployment in water depths far beyond the limits of bottom-fixed systems. Floating substructures, as depicted by **Figure 1.4** are typically categorized into four main types: semi-submersibles, spars, tension-leg platforms (TLPs), and barges. Current statistics indicate that semi-submersibles dominate the market, representing around 80 % of floating projects due to their favorable stability, shallow draft, and port-based assembly that eliminates the need for heavy-lift vessels [23]. Spar platforms, accounting for 9 % of projects, provide stability through deep ballasted cylinders but are restricted to sites with sufficient port depth [23]. TLPs (6 %) offer minimal seabed footprint and suitability for large-scale deployment, though their installation complexity remains a barrier. Barges, at 4 %, distribute buoyancy across a large platform but face hydrodynamic challenges that limit their competitiveness [23].

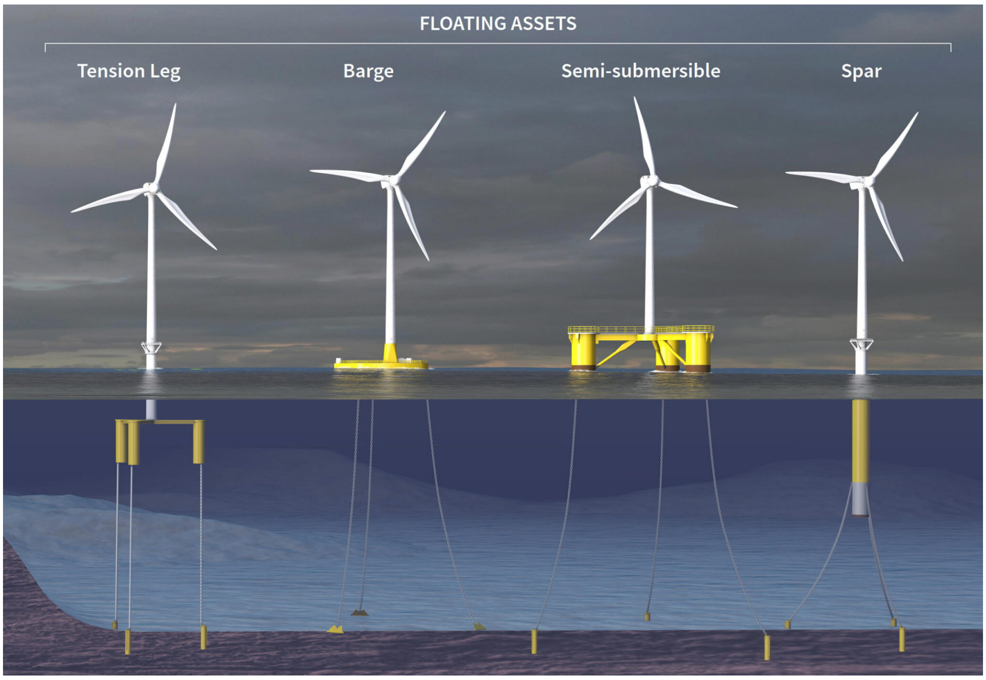

Figure 1.4: Rendering of the most common platforms for floating wind turbines.

The market trajectory underscores this transition: while floating platforms accounted for just 0.2 % of substructures in 2022, projections suggest they could represent more than 30 % of future installations [23]. Several international programs are accelerating this shift. Portugal's WindFloat Atlantic project, commissioned in 2020, marked the world's first semi-submersible floating wind farm [24]. In parallel, the U.S. government launched the Floating Offshore Wind Shot initiative in 2022, targeting a 70 % reduction in costs, down to 45 $/MWh, along with the deployment of 15 GW of floating capacity by 2035 [25]. Achieving these goals requires industrial-scale production, standardization of designs, and the transfer of knowledge from fixed-bottom offshore wind, which has already demonstrated steep cost reductions [21].

Looking forward, forecasts consistently highlight the critical role of floating technologies in scaling offshore wind. The DOE projects cumulative offshore wind capacity to surpass 182 GW by 2028, with floating wind reaching nearly 8 GW by the same year and expanding to 39 GW by 2030 [21]. Complementary estimates from BloombergNEF (BNEF) [26] and 4C Offshore [27] predict global offshore wind capacity between 379 and 394 GW by 2032, with Europe, China, and emerging Asian markets as key drivers. Within these scenarios, floating wind alone could grow from 10 GW in 2030 to 300 GW by 2050, supported by cost reductions, technological innovation, and supply-chain maturity [21]. Delving deeper into details on the installations per substructure type, **Table 1.1** gives an idea of the state of the art in offshore wind and the projections to 2030. It is apparent how, despite the dominance of bottom fixed technologies, floaters such as semisubmersibles will play a key role in the next decade.

Table 1.1: Global offshore wind substructure capacity (MW) for various substructure types installed in 2022 and projects to 2030 [23].

Column 1	2022 [MW]	Projections to 2030 [MW]
Monopile	35502.3	52659.7
Jacket	6152.2	16244.4
Tripod	1060.0	-
Gravity Base	815.5	5229.9
Suction Bucket	4.3	-
Semisubmersible	80.7	28216.4
Spar	37.9	3277.8
Tension Leg Platform	-	1972.7
Barge	5	1542.0

Regarding energy costs, floating offshore wind is expected to follow the cost trajectory of fixed-bottom technology, moving from early-stage demonstration toward competitive large-scale deployment. Current estimates place the LCoE for U.S. floating projects between 82 and 255 $/MWh in 2022, with reductions to 66–128 $/MWh expected by 2030. These improvements are anticipated through a combination of turbine scaling, wake management, component reliability, modular design, and advances in manufacturing methods such as additive production and automation [21,28].

Taken together, the literature emphasizes that fixed-bottom foundations will remain the most efficient option in shallow waters, but floating substructures are essential to unlock deep-water resources and expand global offshore capacity. Their accelerated deployment is central to achieving long-term decarbonization goals and diversifying the technological base of the offshore wind industry.

2 BENCHMARK DEFINITION: THE ROLE OF OFFSHORE WIND IN GREEN HYDROGEN PRODUCTION IN THE DUTCH NORTH SEA

2.1 Introduction

The North Sea region hosts a large wind energy potential. The European Union, Norway, and the UK have a combined 2050 target of nearly 500 GW of offshore wind in the North Sea [29]. The Netherlands alone aims to expand its offshore wind capacity to 50 GW by 2050 and to 70 GW by 2070 [30]. These ambitious targets for offshore wind energy may necessitate partially converting the produced electricity to hydrogen offshore to efficiently deliver this wind energy to onshore demand locations [31], although the desired ratio between offshore hydrogen and electricity remains the subject of debate [32,33].

Green hydrogen will be required to decarbonize hard-to-abate sectors and industries [34]. For the production of low-emission hydrogen, water electrolysis is the most anticipated and promising conversion method [35,36]. Key challenges arise in increasing the capacity of electrolyzers to GW-scale and developing the upstream supporting infrastructure. Moreover, there are difficulties in financing the projects [37].

Against this background, this study provides a comprehensive framework to explore the economic characteristics and operational dynamics of different offshore wind-based hydrogen production system configurations. The three analyzed configurations include:

1. Onshore centralized electrolysis (C-ON): Offshore wind-based hydrogen production occurs entirely onshore, with wind-generated electricity transported via high-voltage cables to shore.
2. Offshore centralized electrolysis (C-OFF): This approach involves offshore hydrogen production at a single centralized platform where electricity from nearby turbines is converted to hydrogen and piped to shore.

3. Offshore decentralized electrolysis (D-OFF): Each offshore wind turbine platform hosts an individual electrolysis system, producing hydrogen locally and eliminating the need for offshore electricity transmission infrastructure.

The D-OFF system configuration may have five major advantages over the two centralized alternatives. Firstly, Timmers et al. [38] conceptually showed that it is possible to modify wind turbine (WT) power systems to minimize the number of power conversion steps, i.e., by bypassing one conversion step (direct current (DC)-alternating current (AC)) and using less electric transmission infrastructure to reduce conversion losses. This approach may reduce power conversion losses since the WT and electrolyzer are at the same site [39,40] and may both operate on the same DC-voltage level. Secondly, offshore decentralized electrolysis replaces all electrical export infrastructure (inter-array (IA) cables, high voltage (HV)AC/DC cables, substations, and converter stations) with pipeline transmission infrastructure [39,40], which may result in lower costs and lower transmission losses. Thirdly, decentralized brine disposal has a lower environmental impact and lower costs [39]. Fourthly, the WT and electrolyzer can be integrated into a single modular system [39,40], rather than using two independent systems. Fifthly, Ibrahim et al. [39] state that D-OFF has more manageable failure events due to the modular system, and there is no need for additional support structures.

In this context, the aim is to answer the following research question: How do different offshore wind-based hydrogen production system configurations in the Dutch North Sea region affect the Levelized Cost of Hydrogen (LCoH), considering the effects of operational behavior, energy flows, and production rates under intermittent wind energy inputs?

An innovative modular simulation, time-dependent model based on a Python environment that allows analyzing the hydrogen production systems with multiple levels of detail has been introduced. It enables quasi-steady state modelling, analysis of operational dynamics, energy flows, material flows, and economic assessments. The model combines high-detail modules for the main system components (the wind farm (PyWake) [41] and electrolyzer (physically accurate electrolyzer model) [42]) and the lower-detail modules for the modelling of other system components. The higher detail level modules are required for conducting a detailed analysis of the D-OFF configuration, as it captures the unique dynamics driven by direct connections to individual wind turbines. As these results will illustrate, this is crucial for examining the impacts of wind energy fluctuations and intermittency on system performance, hydrogen production rates, and overall efficiency.

To feed this framework, at first, an extensive technoeconomic dataset, validated by industrial and scientific experts, has been compiled for the full upstream hydrogen system spanning from the wind farm to injection into the onshore Dutch hydrogen backbone, which is expected to be developed in the upcoming years [43]. Second, a comprehensive economic analysis has been performed by determining the LCoH for different scenarios across three system configurations. Third, the operational dynamics and time-dependent energy flows have been assessed and analyzed for each system configuration, including start-stop frequency, degradation rates, and minimum load thresholds, to provide critical insights into the lifetime and efficiency of electrolyzers under different conditions.

2.1.1 Contribution

First, a validated dataset incorporating projected costs and technological advancements from 2030 onward has been compiled, ensuring alignment with current knowledge. Expert validation of economic data for key components enhances the reliability and relevance of the cost modelling.

Second, this research presents a detailed analysis of the system costs for a range of scenarios for both centralized and decentralized offshore hydrogen production systems. A total of 432 scenarios based on lower, mean, and higher bounds for input parameters are included to address the wide range of potential future costs and technological developments. Typically, the literature relies on single-point estimates as input data, overlooking the inherent uncertainty in both economic and technological parameters, particularly for future systems. This comprehensive simulation tool has been used for extrapolating the behavior of auxiliary components, such as compressors and desalination units, in terms of weight on LCoH for the forks presented afterward.

Third, the presented framework is, to the best of the author's knowledge, the most comprehensive open-source framework to date. In contrast to many existing approaches in the literature [40,44,45], this study incorporates a detailed assessment of energy production at the individual wind turbine level, integrating the effects of wind speed variability, wake losses, and other spatiotemporal factors. This approach enables a more time and location-specific evaluation of wind energy generation, addressing limitations in prior studies that often rely on aggregated or simplified assumptions. Existing studies often exclude [40,44,46–48] or only partially incorporate [49–52] detailed electrolyzer operations. In contrast, this study fully considers operational dynamics and component interdependencies of the hydrogen production system. By providing outputs on interconnections, energy flows, and costs, along with flexibility in time steps from annual to 10-minute intervals, the model captures the effects of intermittent energy inputs.

2.2 Literature review and knowledge gaps

P1.

Table 2.1 presents an overview of the literature on system simulation models for offshore wind-powered hydrogen production, highlighting several omissions in the literature. In contrast, in this study, wake losses and per-turbine energy production, minimum load thresholds for electrolyzers, detailed component representation, and comprehensive modelling of component interactions are key aspects to analyze and compare the system configurations in cost and operational performance. To capture these key aspects, a detailed geographical and temporal resolution is required. In many existing studies [40,44,45,47,48], few of these aspects are incorporated or are not combined, as their primary aim is not to analyze the consequences of the operational-level interaction between the different components on the performance and cost of the systems.

Firstly, most studies utilize an hourly temporal resolution and incorporate either actual or empirical wind data [48–53] or data derived from existing models or datasets [40,44,47]. Despite the reliance on real-world wind data, few studies account for production per WT considering wake losses and other aspects [46,52]. This is crucial for D-OFF, given expected interactions with operational characteristics of the electrolyzer [39,45].

Table 2.1: State of the art of techno-economic simulation models of offshore wind-based electrolysis.

Source	Temporal resolution	Measured wind data input	Production per wind turbine	Detailed electrolyzer operation	Stack degradation	Economies of scale
This study	10 min	✓	✓	✓	✓	✓
Rogeau et al. [40]	Annual	x	x	x	x	x
Egeland and Sartori [49]	Hourly	✓	x	Partly	x	x
Komorowska et al. [44]	Annual	x	x	x	x	x
Vu Dinh et al. [46]	Hourly	✓	✓	x	x	x
Singlitico et al. [53]	Hourly	✓	x	✓	✓	✓
Hill et al. [50]	hourly	✓	x	Partly	x	x
Calado et al. [51]	Hourly	✓	x	Partly	x	x
Jang et al. [45]	Annual	x	x	✓	✓	✓
Song et al. [47]	Hourly	✓	x	x	x	x
Zhuang et al. [48]	Hourly	✓	x	x	x	x
Mehta et al. [52]	Hourly	✓	✓	Partly	x	x
Rezaei et al. [54]	Hourly	✓	✓	Partly	✓	✓

Secondly, some studies detail electrolyzer operations [45,53], while others partially address this by including minimum load requirements [49,52] or operating temperature considerations [50,51]. However, stack degradation is rarely included. Kojima et al. [55], Kuhnert et al. [56], and Nguyen et al. [57] have studied the effects of intermittent power input on electrolyzers, finding that degradation rates can drastically increase for both Alkaline (ALK) and Proton exchange membrane (PEM) types.

Thirdly, only Singlitico et al. [53], Jang et al.[45], and Rezaei et al. [54] consider the economies of scale for the electrolyzers, which refer to the cost benefits associated with centralized large-scale electrolytic hydrogen production over a decentralized approach, consisting of multiple facilities with smaller capacities.

The work by Singlitico et al. [53], Jang et al. [45], and Rogeau et al. [40] is closest to the analysis presented in this work. These authors analyze comparable system configurations and consider the North Sea region for hydrogen production. Here, is discussed how they address key modelling challenges central to this work: the dynamic behavior of wind farms and electrolyzers over time, the influence of geographic conditions, the role of economies of scale, and comprehensive cost estimation. Together, they provide a strong foundation for comparison and help clarify how the approach adopted advances the current state of the art.

The study by Singlitico et al. [53] provides a cost estimation of three system configurations in the North Sea region. Their analysis includes dynamic modelling of the wind farm and the electrolyzer. The study highlights the strong influence of economies of scale, particularly for small electrolyzer capacities that incur higher specific costs. However, the study employs two operating strategies: a ‘hydrogen-driven’ operation mode, where the electrolyzer is operated at a fixed power rating, and an ‘electricity-driven’ operation mode, where only excess electricity is used for hydrogen production. In contrast, the dedicated wind-based hydrogen production systems are herein addressed. Furthermore, the study relies on an hourly temporal resolution, which may be insufficient for capturing the operational dynamics of D-OFF. This work addresses this by using a finer temporal resolution (10-minute timesteps) to enhance modelling accuracy. In this study, a more advanced wind farm model is adopted, improving Singlitico et al.’s electrolyzer model [53] to represent the dynamic interaction between these key components. Singlitico et al. [53]

highlight the strong influence of economies of scale, i.e., small electrolyzer capacities exhibit higher specific costs.

Jang et al. [45] assess C-ON, C-OFF, and D-OFF configurations to estimate the LCoH and net present value (NPV). Their study includes a detailed cost breakdown that incorporates fixed operating cost assumptions and a predefined, static capacity factor. While this approach provides clear cost comparisons across system configurations, it limits the representation of operational dynamics by not accounting for temporal fluctuations in wind power generation or electrolyzer operations. As a result, system constraints on dynamic operations and real-time performance are underrepresented. Nonetheless, the study confirms that electrolyzers for D-OFF system configuration face higher specific costs, due to their smaller capacities at each turbine, which underscores the anticipated cost disadvantage associated with reduced economies of scale in decentralized configurations.

The North Sea region is also the focus of the study by Rogeau et al. [40], which presents a detailed techno-economic analysis of C-ON, COFF, and D-OFF configurations for the years 2020, 2040, and 2050. Their work offers an in-depth breakdown of the cost components across the entire value chain, including turbines, substations, pipelines, and infrastructure. However, the study does not apply the same level of detail to the operational side of hydrogen production adopted in the present analysis. Hydrogen yields are based on fixed conversion efficiencies and predefined loss factors, without considering the dynamic behavior of the electrolyzer or the variability in wind generation.

Across all three studies, only a single set of input data is used. While they include sensitivity analyses to illustrate the influence of individual components on overall cost estimates, they do not incorporate a broader range of data points that could better reflect the uncertainty surrounding future costs of key technologies such as wind turbines and electrolyzers. In contrast, this study integrates a wide set of input parameters drawn from both scientific literature and industry data. However, even with more comprehensive input data, there remain notable gaps in how these systems are modelled.

Several authors indicate knowledge gaps related to the modelling of the costs of these system configurations. Rogeau et al. [40] state that a harmonized comparison of onshore electrolysis considering HVAC and HVDC export and offshore electrolysis, including both centralized and decentralized configurations, is lacking. Komorowska et al. [44] highlight that a detailed consideration of geographical effects for offshore wind locations is (often) not (fully) included in the cost assessment. This is also acknowledged by Vu Dinh et al. [46], who emphasize that there is a gap in the literature for a technically rich, location-dependent cost model for green hydrogen production. Hill et al. [50] point out that there is limited consideration of dynamic electrolyzer operation and its impact on efficiency, as well as a lack of focus on offshore wind farms as a primary energy source for hydrogen production. Additionally, few studies examine the lack of reliable data on the cost of offshore renewable hydrogen production projects.

2.3 Methodology

This section outlines the modelling approach, the description of the main system components, the economic assessment framework, and the data collection process. The simulation framework presented in this work is available open-source on GitHub [58].

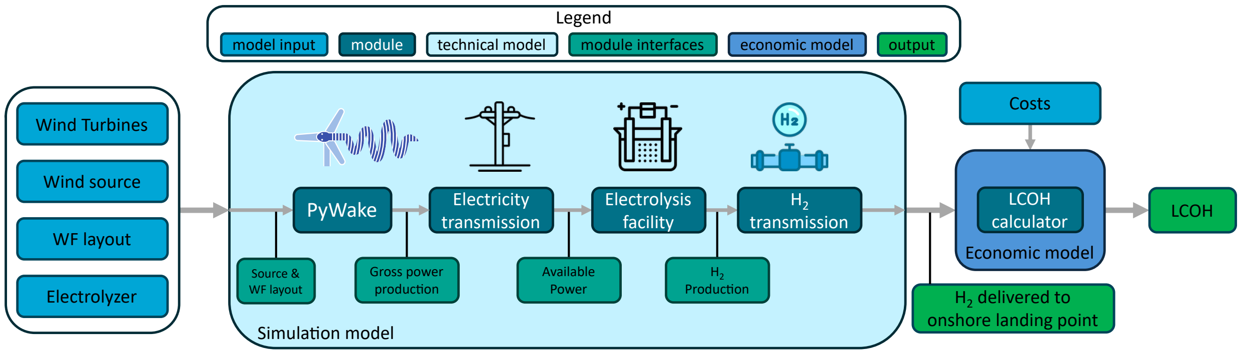

Figure 2.1: Simulation model workflow.

An engineering model to assess the performance and costs of electrolytic hydrogen production from dedicated wind farms is developed. This framework describes the operation of the different hydrogen production configurations, starting from components that comprise the system, focusing on energy and physical flows, such as hydrogen and water, resulting from an intermittent power input. This engineering model forms the heart of the model workflow (**Figure 2.1**). After the estimation of the energy and physical flows, the LCoH is calculated, considering the production of hydrogen and costs over the lifetime of the assets.

Delving deeper into details, the engineering model can be described as follows: after calculating the gross wind farm power production, the model estimates the electricity transmission losses to evaluate the power available to the electrolyzer per timestep. The hydrogen that can be fed into the hydrogen grid is then calculated through a detailed module of the electrolysis facility that reproduces the behavior of the stack and the auxiliary systems. For the wind farm and the electrolysis facility, detailed simulation models are utilized, but components such as pipelines, electric transmission infrastructure, and auxiliaries such as compressors and the desalination unit are handled with a simplified method. This assumption is justifiable based on the minor impact of these components on the system's behavior at the adopted time scales.

As shown in **Figure 2.1**, physical and energy flows represent the interconnections between the components. The output of each module is utilized as input for the next. Regarding the time resolution for the simulations, 10-minute-based wind speed and direction data have been selected. This resolution allows modelling the operation of the electrolyzer, including degradation and temperature effects, and variability of offshore wind energy. This time step size allows for analyzing the effects of cold startup time for the electrolyzers. Additionally, wind power curves provided by wind farm manufacturers are typically averaged over 10-minute intervals [59]. A coarser time resolution would have led to overestimating the production [60].

Each component is sized to the peak output of the upstream component. As such, the definition of the wind farm installed capacity determines the size of all the components of the electrolysis facility and the hydrogen production potential. The wind farm's characteristics, such as the layout and the WT type, and the component costs, are set as boundary conditions.

2.3.1 System components

This section describes the assumptions and the modelling approach adopted for each component.

2.3.1.1 Wind power production

PyWake [41] has been utilized to assess the wind farm's performance due to its large adoption in the design, development, and evaluation processes of wind projects. PyWake is an open-source and Python-based wind farm simulation tool that is capable of computing flow fields and the power production of a wind farm. The main potential of this tool is the ability to calculate the wake interactions within a wind farm for a range of steady-state conditions with a low computational cost. This enables the integration of different Python-based modules, such as the electrolysis facility and the transmission infrastructure, within the same numerical model using the wind power output to model the interfaces. Moreover, it allows for time-dependent analyses to evaluate the power production of the single wind turbines within the wind farm.

In PyWake's architecture, the primary object is the Wind Farm module, which includes two key components: a site and a wind turbine object. The site object defines local wind conditions based on given turbine positions, reference wind speed, and reference wind direction. The wind turbine object, defined for each turbine type and effective wind speed, provides the power curve, thrust coefficient curve, hub height, and rotor diameter of the wind turbines. Upon calculation, the Wind Farm module generates the results in terms of the calculated effective wind speed, power production, and thrust coefficient for each turbine.

Concerning the wake effects, the N.O.J. wake deficit model [61], based on the assumption of a linearly expanding wake diameter with a constant wake decay coefficient, has been adopted. In order to deal with the marine environment of the Dutch North Sea, the DTU guidelines for offshore installations have been adopted, neglecting factors such as surface roughness and orography due to the offshore site [62].

2.3.1.2 Electrolyzer

To account for the effects of intermittent power input, time-dependent hydrogen production requires a model that can provide a variable efficiency of the component depending on power inputs, temperature, and load hours for the different electrolyzer technologies considered in this study—ALK and PEM. The approach proposed in Superchi et al. [42] has been adopted and expanded to include PEM electrolysis. This module mimics the electrolyzer stack in terms of hydrogen production through the implementation of the polarization curve of the cell. This curve describes the relationship between the cell's voltage and current, depicting the efficiency of the component by including the system's irreversibilities. Specifically, the actual operating voltage of the cell consists of the thermoneutral voltage—the theoretical minimum voltage needed for water splitting—and additional overpotentials. These overpotentials arise from three types of losses: activation (due to reaction kinetics) that mostly affects the hydrogen production curve for low power inputs, ohmic (due to resistance in the electrolyte and other cell components) prevailing in the inner part, and, finally, concentration losses (due to mass transport limitations). Together, these factors influence the efficiency and power requirements of the electrolysis process [63]. Furthermore, this approach addresses the effects of the thermal variation of the stack thanks to the computation of the heat generation and dispersion to the environment based on the geometry of the electrolyzer itself.

Regarding the power source, this module enables addressing the impact of variable operation on system productivity when connected to non-dispatchable power sources. The modelling strategy mimics a management system that seeks to maximize the number of active modules within the electrolyzer by distributing the minimum required power across as many modules as possible.

Figure 2.2(a) and (b) show the link between the voltage and the current density (i) of the electrolyzer at different temperatures for the PEM [64] and ALK [42]. The control system of the ALK allows a minimum power input of 20 % of the nominal power. The low-voltage region of the operational curve is not modeled in the analysis, forcing the component to work in the linear part of the polarization curve. On the other hand, the PEM also enables the operation in the area affected mostly by activation overvoltages, which leads to strongly nonlinear behavior. To assess the impact of the temperature variation, the modelling of this initial portion of the curve requires a 3-D approach. While the ALK efficiency has been modeled with a linear curve—see **Figure 2.2**(b)-, the behavior of the PEM is reproduced with a surface, see **Figure 2.2**(a).

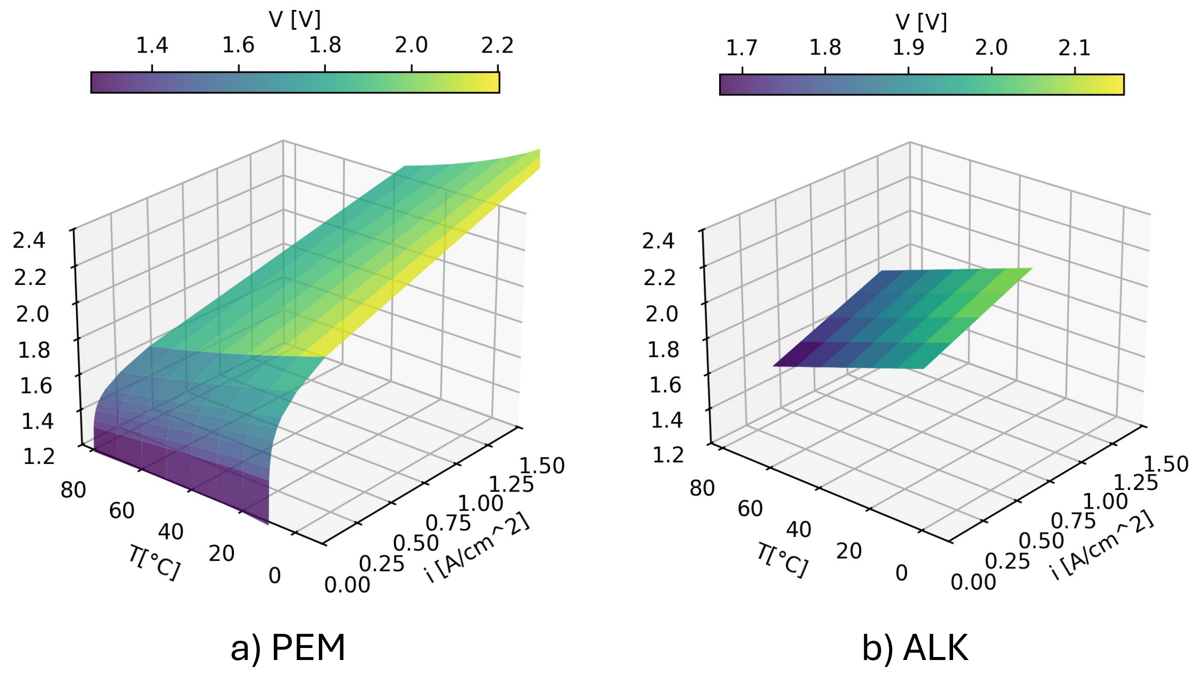

Figure 2.2: Polarization curve of the PEM electrolyzer (a) [64] and ALK electrolyzer (b) [42].

The impact of temperature on the stack efficiency can be observed in **Figure 2.2**. A decrease in temperature due to heat losses leads to a shift of the curve towards higher voltages of 0.5 mV [42] and 0.4 mV [64] per ◦ C for the ALK and PEM. This leads to a decrease in the efficiency of the component. Adopting this modelling strategy thus leads to the assumption that the hydrogen flow rate is proportional to the current density of the cell. An enhanced working voltage at the same current density results in a higher power input needed to produce the same amount of hydrogen. Finally, an efficiency degradation mechanism that accounts for the operating hours is considered. A linear relationship between degradation and operating hours has been considered, setting a constant increase in the overvoltage per working hour for both technologies. However, although the intermittent operation of the electrolyzer strongly affects the lifetime of the component itself [56,57,65], incorporating this aspect into a parametric model remains an unresolved gap in the literature. To address this challenge, several degradation factors have been tested, as extensively depicted in Section 2.4, to reproduce the mimic of a lower electrolyzer lifetime on the revenues of the plant.

To quantify the variation of the voltage, Eq. 2.1 is employed per time step. Here, V_{OP} represents the operating voltage, V_{id} the voltage of the new electrolyzer working at design temperature, ΔV_{time} the time degradation overvoltage, h the cumulative number of operating hours, ΔV_T the thermal overvoltage, and T_{rated} and T_{el} the design and working temperatures.

$$V_{OP} = V_{id} + \Delta \mathrm{V_{time}} * \mathrm{h} + \Delta V_T * (T_{rated} - \mathrm{T_{el}}) \qquad 2.1$$

As described in Superchi et al. [42], the operating voltage leads to the estimation of the conversion factor (Ω) and the heat generated by the component. Ω represents the link between the power input to the component and hydrogen production. This coefficient is evaluated per time-step through the ratio between the maximum hydrogen production ($H_{2,id}$) and the product of the number of cells (n_{cell}), the operating voltage, and the ideal current (I_{id}), as shown in Eq. 2.2.

$$\Omega = \frac{H_{2,id}}{n_{cell} * V_{OP} * I_{id}} \qquad 2.2$$

Hydrogen production is estimated by multiplying Ω and the electrolyzer input power provided by the renewable source. The definition of the correct working temperature is required to match the correct operating point on the polarization curve. Heat generation (Q_{Gen}) and dissipation (Q_{Diss}) are estimated following the approach mentioned in the reference model [42], adapting the geometries to the ones described in Tiktak [64] for PEM.

Regarding the electrolysis facility, a few assumptions have been made. Considering the thermal model reproduces the heat exchange between the gas-liquid separator and the environment (ALK), and between the whole stack and the environment (PEM), a realistic thermal capacity should be set. For both electrolyzers, a reference size of 1 MW has been set for the stack. This leads to the possibility of scaling up the whole electrolysis facility by adding 1 MW modules, resulting in homogeneous heat generation and loss for each stack. Moreover, considering a control strategy that keeps the temperature at a maximum value equal to the nominal one to avoid overheating, the cooling required (Q_{Cool}) is evaluated as shown in Eq. 2.3:

$$Q_{Cool} = \mathrm{Q_{Gen}} - \mathrm{Q_{Diss}} \qquad 2.3$$

This cooling requirement is then converted into the power required by the chiller by adopting a coefficient of performance (COP), set to 3.5 [66].

Extended periods of no power input result in an electrolyzer temperature drop due to heat dissipation, leading to reduced efficiency as indicated by the upward shift of the polarization curve. 30 ◦ C has been set as the target value at which the shutdown of the component occurs. To restore the operation of the electrolyzer, an approach similar to Singlitico et al. [53] has been adopted, considering a cold startup time of five and twenty minutes for the PEM and ALK, where the power input to the electrolyzer is used to increase the temperature, and no hydrogen is produced.

Thesimulation of the whole lifespan of the plant leads to the possibility of assessing the real replacement time for the electrolyzer stacks. According to manufacturers, the component replacement should occur when the cell voltage at nominal temperature exceeds 2.3 V for the ALK stack [42]. Starting from this assumption, also for the PEM, a maximum voltage of 2.23 V, equivalent to an increase of 21 % at rated temperature and current density, has been assumed.

Therefore, by monitoring the increase in overvoltage induced by degradation, it is possible to evaluate the component's end of life.

2.3.1.3 Auxiliaries

Adopting a time-dependent approach allows for the evaluation of the energy availability of the electrolysis facility powered by a specific wind farm. This is key for assessing the physical flows, such as oxygen, brine, and heat production, or water feed. Auxiliary components such as compressors and reverse osmosis units have been included in the analyses. However, due to the minor role of these technologies, a simplified approach has been adopted, as described in [67].

2.3.2 Economic assessment

Hydrogen production cost assessments are typically conducted through techno-economic assessments utilizing the LCoH as the main cost metric. This metric evaluates the annualized cost of hydrogen produced at a specific installation site over its economic lifetime. The LCoH considers the capital expenditures ($CAPEX$) of each component, the operational and maintenance costs ($OPEX$), discount rates, and inflation. The LCoH is calculated following the approach shown in Singlitico et al. [53] and Rogeau et al. [40]and depicted in the equation below.

$$LCOH = \frac{\sum_{y=1}^{n} \frac{\mathrm{CAPEX}_{\mathrm{y}}^{Total} + \mathrm{OPEX}_{\mathrm{y}}^{Total}}{(1+r)^{y}}}{\sum_{y=1}^{n} \frac{H_{2,production}}{(1+r)^{y}}} \tag{2.4}$$

The n in Eq. 2.4 represents the economic lifetime, y is the year, $\mathrm{CAPEX}_{y}^{\mathrm{Total}}$ and $\mathrm{OPEX}_{y}^{\mathrm{Total}}$ represent the total system capital and operational expenditures for each y, and r is the discount rate.

Economies of scale and scale factor. In the studies by Singlitico et al. [53] and Jang et al. [53], the economies of scale benefit centralized configurations more than decentralized ones. Even though electrolyzer stacks are modular, centralized system configurations consolidate all electrolysis components at a single location. As Cooper et al. [68] highlight, larger electrolyzer plants allow for a cheaper balance of plant—which is part of the CAPEX of the electrolyzer—which reduces the specific cost as system size increases. A scale factor of 0.69 is introduced in Travaglini et al. [60] based on scientific literature [69] and correspondence with industrial experts, resulting in cost benefits for electrolysis, as shown by Eq. 2.5. Conversely, due to its decentralized setup, the D-OFF configuration, which employs smaller electrolyzers distributed across multiple wind turbines, does not realize the same cost advantages.

$$CAPEX_{electrolyzer} = \mathrm{C}_0 * \left(\frac{\mathrm{X}}{\mathrm{X}_0}\right)^{0.69} \tag{2.5}$$

This equation shows how, taking a reference cost (C_0) and size (X_0), the $CAPEX$ of the electrolyzer can be scaled according to the actual size of the component (X). In this work, while C_0 depends on the economic scenario, X_0 has been set to 15 MW.

2.4 Case study

For each combination of system configuration and selected wind farm location in the North Sea, different scenarios have been simulated. Both economic and technical data are gathered to develop a large dataset. This is done by executing a desktop study on the existing literature from academia and industry. The analysis focused on data for 2030 and beyond. The most recent data were selected when projections were available for this period.

Based on interviews and communications with experts in the fields of wind energy, electrolysis, hydrogen infrastructure, and electricity infrastructure, the data are validated for the core components. For confidentiality reasons, most of the references are excluded. Together, these values make up the benchmark scenarios for the combination of each system configuration and the predefined location of the offshore wind farm.

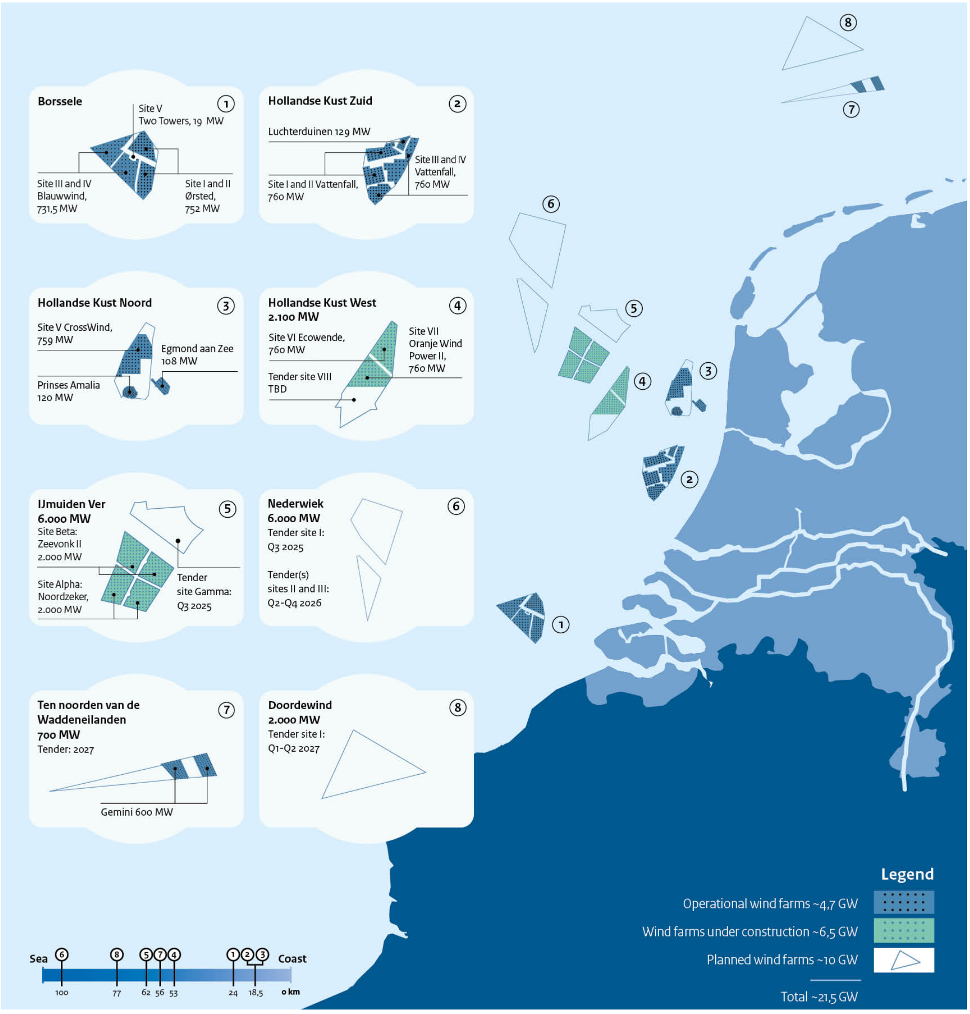

Figure 2.3: Available wind park sites in the Dutch North Sea.

Measured wind data are obtained for the Dutch North Sea region, more particularly for the Nederwiek [70] and Ten Noorden van de Waddeneilanden (TNW) [71], located 100 and 50 km from the assumed landing area. Additionally, to assess the robustness of the findings, the wind resources in two additional sites have been included: Hollandse Kust Zuid (HKZ) and IJmuiden Ver (IJV) [71]. These offshore sites are located 20 km and 60 km from the assumed landing area.

Data provided by the RVO are obtained with LIDAR measurements in different experimental campaigns. The database provides the wind speed, wind direction, and air temperature at different heights, completely defining the source in the area of interest. **Figure 2.3** shows the available installation sites in the Dutch North Sea.

The choice of the installation sites relied on two selection criteria: the distance from the shore and the statistical wind speed distribution. While the "Hollandse Kust Zuid" (HKZ) is the closest to the shores (n.2 in **Figure 2.3**), TNW, Nederwiek (NED), and IJmuiden Ver (IJV) provide a comprehensive representation of the wind source in the site. **Figure 2.4** shows the Weibull distribution of the available wind sources. It is apparent that, while TNW experiences a low average wind speed, the probability of having wind velocities higher than 20m/s is relevant. On the other hand, NED experiences one of the highest average wind speeds in the selected sea region. Finally, IJV represents the site with the lowest source, despite its export distance comparable to the TNW site. While for the analyses a time-dependent approach has been adopted, to compare the wind sources, a strategy based on the statistical distribution and wind roses has been introduced.

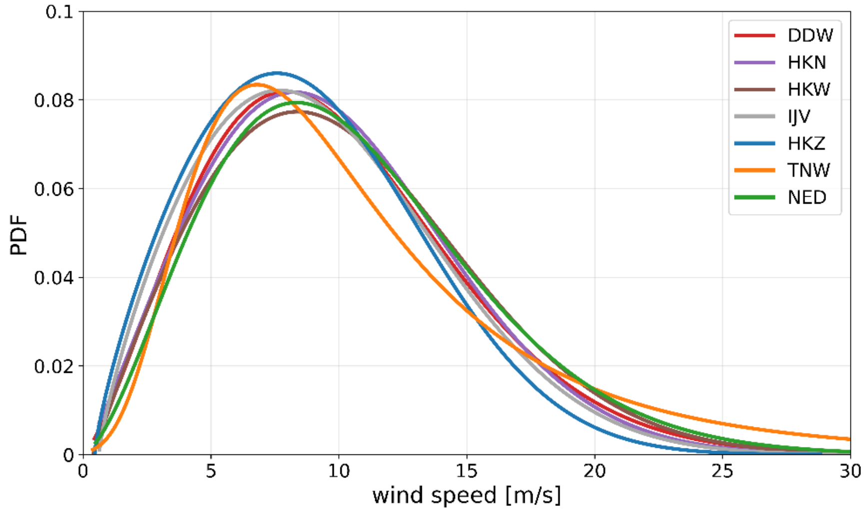

Figure 2.4: Weibull distribution of the available wind sources.

The Weibull curves shown in **Figure 2.5** highlight a high shape parameter for the Nederwiek farm that shifts the curve to higher average speed values. This is consistent with an enhanced distance from the shores, which is associated with a lower impact of terrain orography and morphology on the source and thus a higher average wind speed. The distributions shown in **Figure 2.5** represent the wind source at rotor height; therefore, no additional empirical models, such as scalers based on wind shear, are needed. Finally, given the need to conduct analyses over time horizons longer than the two years provided by measurements, with periods of interest spanning twenty-five years in order to calculate a reasonable replacement time for the electrolyzer, the estimated power dataset at ten-minute intervals is extended to achieve a length equal to the plant lifetime. In detail, considering the peculiar behavior of wind in certain months of the year, it was chosen to reconstruct the missing months by randomly shuffling the days from those same months available in previous years. With respect to a simple repetition of the available years to reach the required ten-year time span, this randomization allows for increased variability in the repeated periods, while statistically respecting the seasonal variability of the wind resource [72]. The evaluation of the operational degradation of the electrolyzer, by means of the increased overvoltage, leads to the assessment of the end of life of the stack, avoiding the assumption of the 7-10 years usually adopted [42].

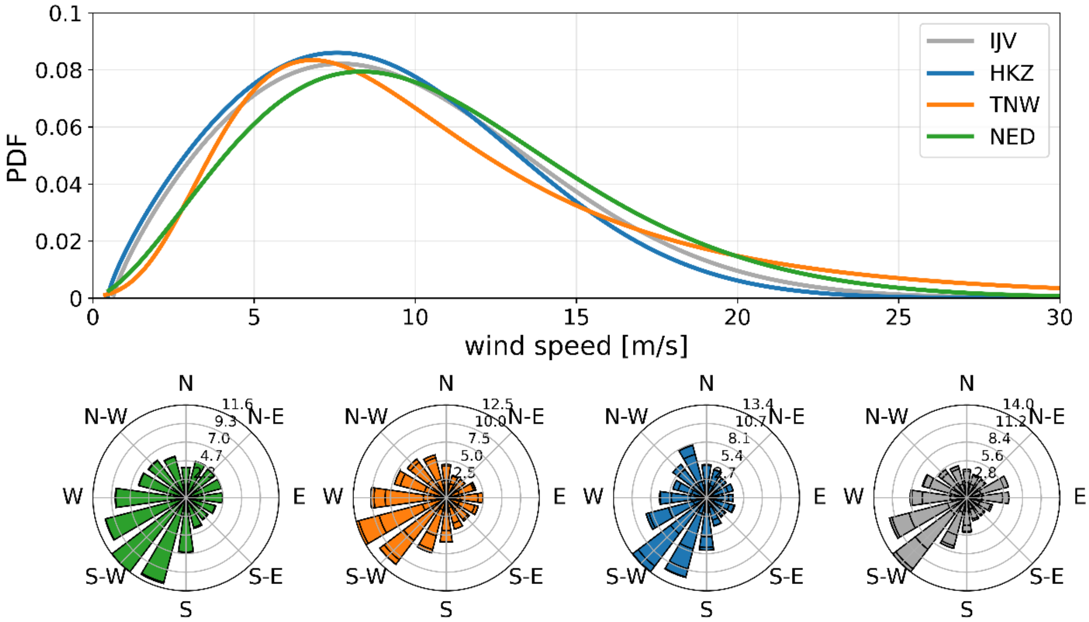

Figure 2.5: Wind source in the chosen installation sites.

Real-life data with the required 10-minute timestep resolution for locations at 200 km from shore are currently unavailable. Considering the reduced variation in the wind source for distances from shores higher than 80 km, as depicted by the online database Global Wind Atlas[73], the same wind speed and direction series as the 100 km case have been adopted.

Two different wind farms have been designed. As depicted in **Figure 2.6**, both wind farms show a similar layout, obtained by the trade-off between wake losses and cable cost reduction, characterized by IA turbine distances of 14 and 5 wind turbine diameters in along-wind and crosswind directions. The dots in the plot represent the wind turbines, and the lines represent the IA cables (centralized system configurations) or pipelines (decentralized system configuration).

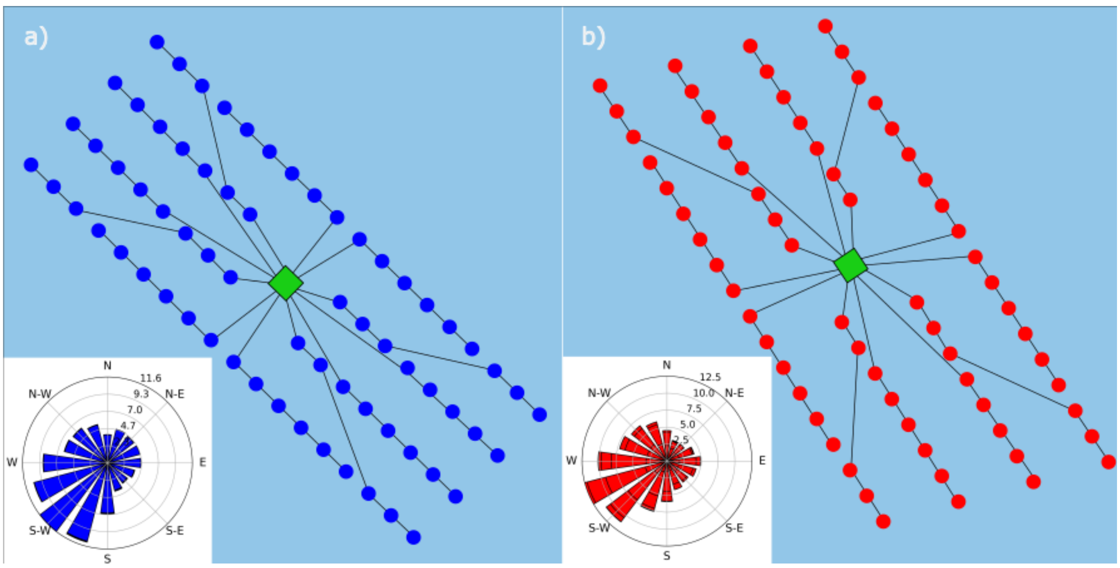

Figure 2.6: Wind farm layout and corresponding wind rose for the installation sites at 50 km (a) and 100/200 km (b) from the shore.

The green square in the middle represents the centralized substation for electrical or hydrogen transmission to shore.

Upon examination of the wind rose (**Figure 2.6**a and b), the prevalent wind direction at the installation site is South-West for Nederwiek (a) and West-Southwest for TNW (b), considering both wind frequency and energy. These directions have been adopted to define the wind farm orientations to maximize the parks' energy production. As HKZ and IJV experience a wind rose similar to Nederwiek, as shown in detail in Supplementary Appendix C, the same wind farm layout has been adopted. **Figure 2.6**a and b depict the relative positions between wind turbines and the electrical scheme for the wind farms located at 50 and 20/60/100 /200 km from shore.

2.4.1 System configurations

For each system configuration, the offshore wind farm is composed of sixty-seven 15 MW wind turbines, for a cumulative installed capacity of 1.005 GW. Is assumed that the electricity produced is dedicated to hydrogen production and the auxiliary processes. The produced hydrogen is transported via an onshore pipeline to an onshore hydrogen backbone network, which is assumed to be situated 10 km inland. It is assumed that the backbone can accommodate fluctuating hydrogen input, allowing this analysis to focus on the production aspect of the hydrogen chain while excluding storage facilities.

The system configurations—C-ON, C-OFF, and D-OFF—differ in the electrolysis facility location, resulting in different energy requirements, hydrogen production rates, and associated costs. Several operational aspects of the electrolyzer, such as start-stop frequency, degradation rates, and minimum load thresholds, affect each system configuration.

C-ON. This is the conventional system configuration, considering that the components in the system have the highest TRLs and most are already commercially available on a larger scale or are expected to be in the near future (**Figure 2.7** top). The offshore wind farm is connected through IA cables that lead to an HVAC or HVDC export infrastructure, depending on the distance to the onshore landing area. At the landing area, the electrolyzer is located together with the desalination unit and compressors, and it is connected to the national hydrogen grid. The onshore compressor is assumed to be powered by the grid, and a cost of 100€/MWh is assumed for the electricity.

C-OFF. Individual WTs are connected through IA cables (**Figure 2.7** center). The IA cables are connected to an offshore structure or platform where a centralized electrolysis plant is stationed, including a seawater desalination system and a compressor. The hydrogen export infrastructure requires offshore and onshore hydrogen compression. The onshore and offshore compressors are connected to the power grid, assuming a cost of 100€/MWh and an additional cost per km/MW for the offshore cables required to transmit the power to the compressor.

D-OFF. D-OFF is the most innovative configuration with the lowest TRL. Each WT powers an on-site electrolyzer plant that is scaled to the WT power output (**Figure 2.7** bottom). The D-OFF configuration utilizes DC output at the turbine, reducing half of the conversion steps [38]. A direct coupling between the wind turbine and the electrolyzer located on its foundation has been considered, neglecting any potential interaction between other wind-electrolyzer configurations. In this configuration, half of the losses are prevented, resulting in losses at the rectifier by 1 % compared to the centralized system configurations [74]. A co-located desalination unit is present, but it is assumed that an additional compressor per turbine is not required. IA pipelines connected to a large export hydrogen pipeline deliver hydrogen to shore. Due to the simplified modelling approach adopted for the pipelines, no mass flow interactions have been accounted for between the electrolyzers, which operate independently within the wind farm. Both offshore and onshore compressors are required to increase the hydrogen pressure for hydrogen transmission. The compressors are powered in a similar way to the C-OFF configuration.

2.4.2 Scenarios and databases

This study evaluates three system configurations across 432 scenarios. The scenarios consist of the combination of data for economic and technical parameters. For each economic and technical parameter, a lower, average, and upper bound are defined upon examination of the literature. An additional value incorporates expert-validated economic data. Experts from industry and academia provided validated economic data on the key system components. This provides an extra economic scenario, resulting in a total of four economic configurations.

Key variables include electrolyzer type, pipeline options—new vs. repurposed—and distances to shore. Each scenario was constructed as follows: One of the three different system configurations is the basis: C-ON, C-OFF, and D-OFF. Each system configuration is evaluated for three distances to shore (50 km, 100 km, and 200 km) and two types of electrolyzers (ALK and PEM). For each combination, both economic and technical parameters are systematically considered by applying three different scenarios (lower bound, average, and upper bound) for cost and performance parameters. The economic data refer to projections for the year 2030 and beyond [67]. An overview of the technical data for 2030 and beyond is presented in **Table 2.2**.

Table 2.2: Overview of the technical specifications of all components of the considered system configurations [67].

Component	Specification	Unit	Lower bound	Average	Higher bound
HVAC cables	Transmission losses	[%/1000km]	6.7	6.7	6.7
HVAC substation	Conversion losses	[%]	1	1	1
HVDC cables	Transmission losses	[%/1000km]	3.5	3.5	3.5
HVDC substation	Conversion losses	[%]	1	1.67	2
ALK plant	Energy Requirement	[kWh/kg]	47	51.8	55.6
	Degradation	[V/h]	4.00e-6	5.04E-06	6.85e-6
PEM plant	Energy Requirement	[kWh/kg]	49	52.6	58.1
	Degradation	[V/h]	4.29e-6	4.85E-06	6.60e-6
Desalination unit	Energy requirement	[kWh/m^3]	3	3	3
H_2 pipelines	Transmission losses	[%/1000km]	0	0.03	0.05

2.5 Results

This section compares different system configurations in terms of cost and operational performance. The economic analysis results in LCoHs spanning from 3.0 to 10.5€/kgH_2 with C-OFF obtaining the lowest outputs and D-OFF the highest, as presented in Section 2.5.1. In this case, technical results such as hydrogen production and energy efficiency have not been included to evaluate the best configuration. The expert-validated scenarios show smaller ranges from 4.1 to 5.5€/kgH_2. Additionally, offshore electrolysis offers lower costs due to the use of hydrogen transmission infrastructure, centralized system configurations benefit from economies of scale, and PEM outperforms ALK electrolyzers as presented in Section 2.5.1.

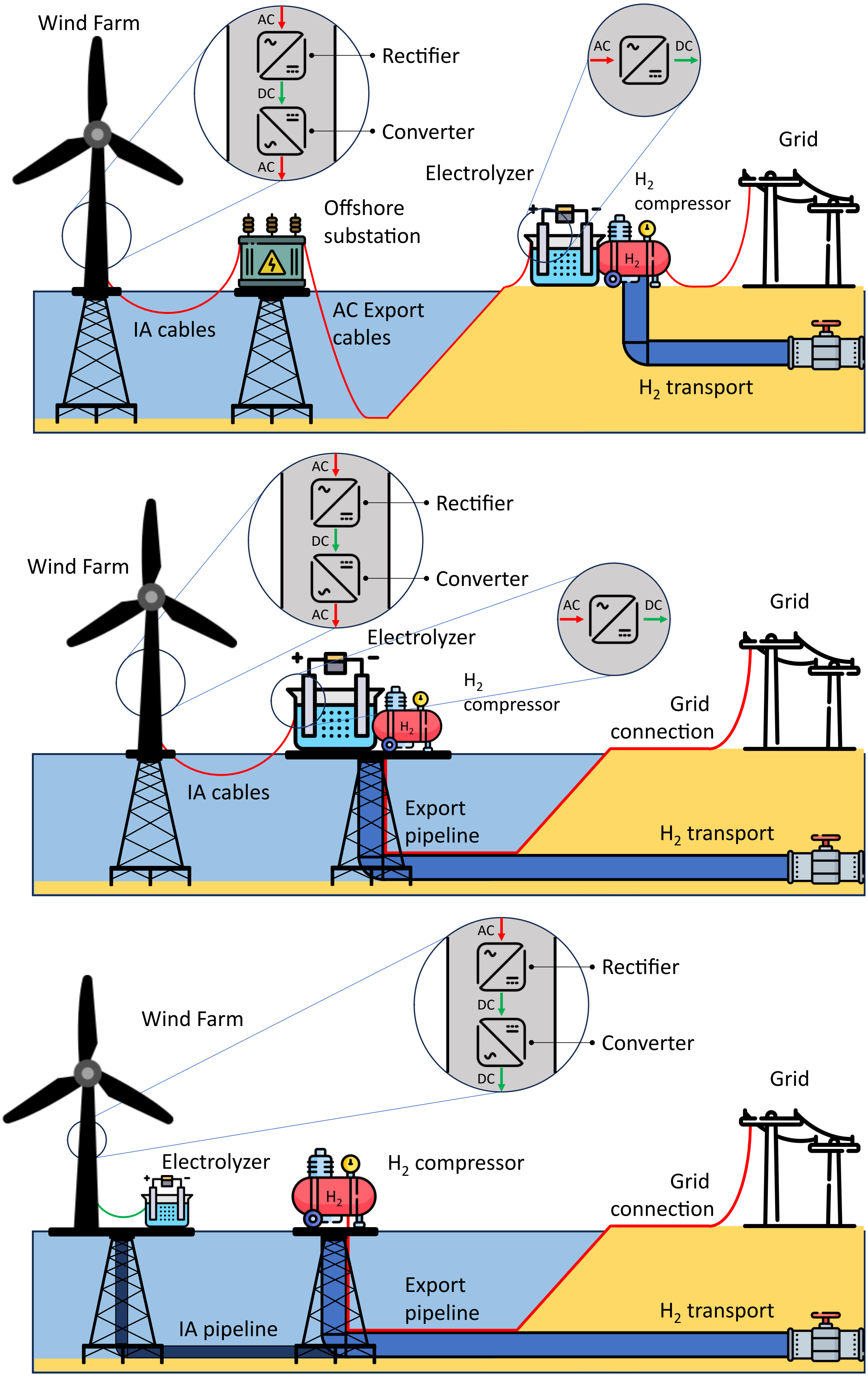

Figure 2.7: Schematic representation of the C-ON, C-OFF, and D-OFF system configuration.

On the other hand, although D-OFF has the highest LCoH for the different scenarios, it has the highest annual production rate and system efficiency (Section 2.5.2.1). Therefore, when the focus is on the technical performance, the decentralized configuration benefits from the lower power losses. Additionally, the time-dependent analysis in Section 2.5.2.2 shows that PEM electrolyzers benefit from a wider power range in comparison to ALK electrolyzers, resulting in more hydrogen production.

2.5.1 Economic analysis of system configurations

For the C-ON configuration, a wide LCoH range is found (**Figure 2.8**): from 3.3€/kgH_2 —for PEM electrolysis at 50 km, assuming lower bound economic costs, upper bound technological input data, and repurposed onshore pipelines—to 10.1€/kgH_2, which represents ALK electrolysis at 200 km with upper bound economic costs, more conservative technological assumptions, and new onshore pipelines.

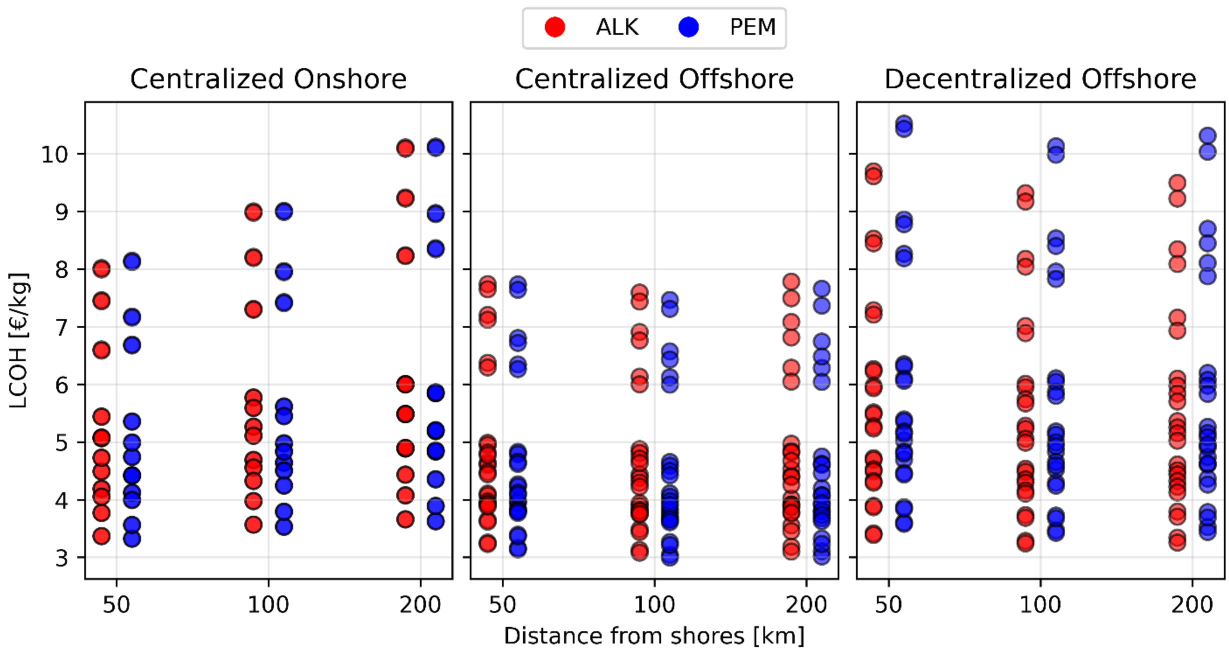

Figure 2.8: Range of LCoH found for each system configuration for three wind park sites (characterized by their distance to shore).

The LCoH outcomes for C-OFF configurations span from 3.0€/kgH_2 —for PEM electrolysis at 100 km under lower bound economic costs, upper bound technology input, and repurposed onshore pipelines—to 7.8€/kgH_2 for ALK electrolysis at 200 km, incorporating higher economic costs, more conservative technological assumptions, and new pipelines.

The LCoH for D-OFF configurations ranges from 3.2€/kgH_2 —achieved with PEM electrolysis at 100 km using lower bound economic conditions, advanced technology assumptions, and repurposed pipelines—to 10.5€/kgH_2, for the scenario with PEM electrolysis at 50 km with upper bound economic cost inputs, conservative technology assumptions, and new offshore and onshore pipelines.

Figure 2.9 presents the LCoH breakdown for two benchmark scenarios—with expert-validated costs and mean technology input data—for each system configuration: a 50 km offshore distance using an ALK electrolyzer, and a 200 km offshore distance using a PEM electrolyzer. Across all system configurations, the largest contributor to the LCoH is consistently the wind farm, accounting for ≈60 to ≈80 % of the LCoH. Other components include the electrical transmission infrastructure—notably in the C-ON configuration (~15–30 %)—and the electrolyzers (~9 % for centralized configurations and up to ≈35 % for D-OFF). In contrast, the hydrogen transmission infrastructure, both onshore and offshore, accounts for less than 1 % of the LCoH for 50 km and around 3 % for distances up to 200 km.

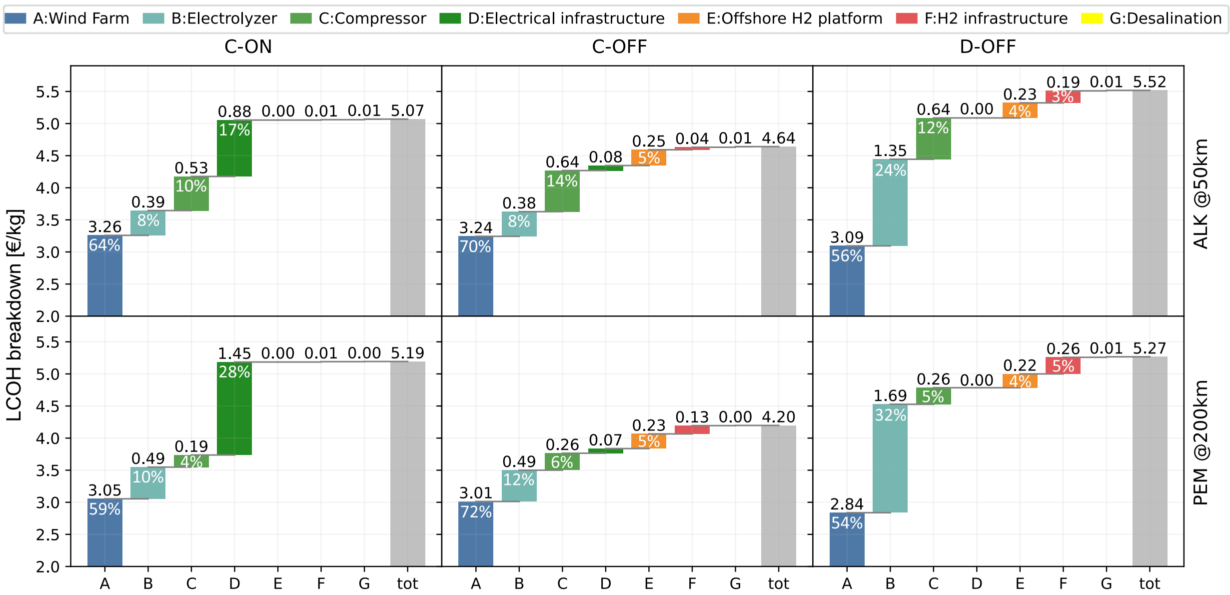

Figure 2.9: LCoH breakdown for two scenarios (under expert validated cost and mean technology input data) for each system configuration: a 50 km offshore distance using an ALK electrolyzer, and a 200 km offshore distance using a PEM electrolyzer.

Onshore vs. offshore electrolysis. C-OFF shows lower LCoH values than C-ON configurations, especially for distances farther from shore, indicating that offshore systems may be more cost-effective. This cost advantage is largely due to differences in transmission infrastructure costs. The analyzed data reveal that the 36-inch hydrogen export infrastructure—which can transmit 15 GW of hydrogen—CAPEX ranges from 3.6 M€/km to 5.8 M€/km or about 0.24 to 0.39 M€/km/GW [75] for new pipelines and 0.36 M€/km to 1.09 M€/km [76] for repurposed pipelines. In contrast, electricity export infrastructure costs are higher, with HVAC cable costs ranging from 3.0 M€/GW/km [77] to 6.8 M€/GW/km [78], HVDC cable costs from 0.8 M€/GW/km [77] to 6.8 M€/GW/km [79]. These values differ greatly, but the sources lack detailed explanations for their selected cable costs. Additionally, expenses for substations and platforms contribute to the overall cost. For C-ON, the increasing distance affects the LCoH linearly, resulting from the cost per km of the HVAC or HVDC transmission infrastructure. This increase ranges from 3 % per 100 km to 10 % per 100 km.

This effect is less pronounced for C-OFF and D-OFF due to the low cost of the hydrogen transmission infrastructure. Moreover, a decrease in LCoH is observed between 50 and 100 km for all offshore system configurations of ≈4 %, attributed to higher wind speeds that boost hydrogen production rates. This advantage, however, does not persist at distances of 200 km, as the modeled wind speeds reach their maximum beyond 100 km offshore [71,71]. Beyond 100 km, the LCoH increases by 2 to 3 % for both C-OFF and D-OFF configurations across all scenarios.

Centralized vs. decentralized. Across all distances and for both electrolyzer types, the C-OFF configuration consistently demonstrates the lowest LCoH. Notably, it achieves the lowest LCoH not only in the most lower-bound cost and upper-bound technology scenarios −3.0€/kgH_2 versus 3.5€/kgH_2 for both C-ON and D-OFF with PEM electrolysis at 100 km, but also in the mean and upper-cost bound cases −7.4€/kgH_2 versus 9.0€/kgH_2 for C-ON and 10.1€/kgH_2 for D-OFF with PEM electrolysis at 100 km. This is attributed to two major advantages: economies of scale and minimal reliance on external electrical transmission infrastructure. Using the LCoH metric, C-OFF outperforms other system configurations for dedicated hydrogen production.

In summary, the centralized configurations are likely the most cost-effective option. In the conducted simulations, D-OFF is the least cost-effective system configuration in most scenarios. While it benefits from fewer losses in transmission due to hydrogen production directly at the turbine, it is more affected by minimum load requirements, particularly for ALK electrolysis, as discussed in Section 2.5.2. The primary driver of its higher LCoH is the lack of economies of scale [60].

To assess the effects of economies of scale, the same specific cost per unit size has been assumed across all configurations, setting the scaling factor equal to one. This leads to LCoHs of 4.0€/kgH_2 for CON, 3.5€/kgH_2 for C-OFF, and a lowest of 3.3€/kgH_2 for D-OFF in the lower bound cost and upper bound technology scenario (ALK, 200 km offshore). In worst-case scenarios, LCoHs increase to 13.7€/kgH_2 for C-ON, 12.6€/kgH_2 for C-OFF, and 10.8€/kgH_2 for D-OFF. For D-OFF configurations, the inability to exploit the benefits of scaling results in electrolyzer plant costs three to four times higher compared to centralized systems under similar production rates for both ALK and PEM electrolyzers. In other words, D-OFF can become the most cost-effective solution for all scenarios, distances, and electrolyzer types only if cost scaling effects were not available. However, as Cooper et al. [68] have pointed out, the balance of plant for the electrolyzer facilities benefits from centralized setups for large-scale electrolytic hydrogen production, resulting in a higher specific cost for decentralized over centralized configurations.

ALK vs. PEM. PEM electrolyzers consistently outperform ALK electrolyzers in terms of cost-efficiency across all configurations and distances. For example, for the mean cost and technology performance scenario at 50 km, the LCoH for C-ON PEM is 4.4€/kgH_2, making it 6 % cheaper than C-ON with ALK at 4.7€/kgH_2.

While PEM electrolyzers have a higher CAPEX than ALK electrolyzers, they demonstrate superior performance under intermittent operating conditions. This enhanced performance results in lower degradation rates in most scenarios, subsequently reducing replacement costs. Additionally, the wider operational load range of PEM electrolyzers facilitates increased hydrogen production across all system configurations.

However, there is still a lot unknown about the degradation rate of electrolyzer stacks under dynamic operational conditions, potentially leading to a higher degradation rate in comparison to that under a stable power input [55–57]. To analyze the impact of the degradation of the stacks, additional simulations were run for both PEM and ALK electrolyzers with degradation rates twice as high as for scenarios visualized in **Figure 2.8**. At multiple distances, the LCoH increases by 2–4 % for ALK electrolyzers under the lower bound and mean cost and technology scenarios. For PEM electrolyzers, the LCoH rises more, with a 5–7 % increase, primarily due to higher stack degradation rates. In higher bound cost and lower bound technology scenarios, the cost differences are more pronounced: ALK electrolyzers experience a 4–8 % increase in LCoH, while PEM electrolyzers face a rise of 10–15 %. This difference arises from the higher CAPEX of PEM electrolyzers, meaning more frequent replacements have a greater impact on overall costs than ALK electrolyzers. However, these analyses mimic the degradation of the electrolyzer per hour of operation, disregarding the impact of dynamic loading.

Table 2.3 shows the average lifetime for each system configuration and technical scenario. The higher bound cost and lower bound technology scenarios lead to a higher number of replacements. The D-OFF configuration experiences a reduced lifetime compared to the centralized setups if the ALK technology is deployed. This is due to the higher average capacity factor of the electrolyzer, which is related to a higher number of hours of operation.

For all scenarios, PEM stacks require more frequent replacement than ALK stacks. This is due to two reasons. First, as shown in **Table 2.2**, in the lower-bound technology scenarios, ALK has a lower degradation rate (4.00e-6 V/h) than PEM (4.29e-6 V/h). However, this difference does not hold in the mean and higher bound scenarios. The main reason for the higher replacement rate of PEM is its higher number of load hours, resulting from its wider operational range (0–100 %) compared to ALK (20–100 %). Consequently, the PEM stacks experience more degradation per year due to the modelling approach adopted and must be replaced more often.

Table 2.3: Electrolyzer lifetime per technology and technical scenario.

Component	C-ON		C-OFF		D-OFF		Unit
Electrolyzer	ALK	PEM	ALK	PEM	ALK	PEM	
Upper-bound scenario	15	10	15	10	14	10	Years
Mean scenario	12	9	12	9	11	9	Years
Lower-bound scenario	9	7	9	7	8	7	Years

The salvage value of the stacks has been excluded from the analysis. However, the residual value of the stacks at the end of their operational life could contribute to lowering the LCoH. For D-OFF employing ALK electrolyzers, the remaining lifetime extends at most to seven years, representing 88 % of the total operational life. Accounting for its salvage value can lower the LCoH by over €0.5/kg, bringing it to approximately 9€/kgH_2. For C-ON and C-OFF systems using ALK electrolysis, the remaining operational lifetime of the stacks is at most 11 years, exceeding 90 % of their total lifetime. When these salvage values are incorporated, the LCoH for C-OFF systems decreases from 4.3–4.5€/kgH_2 to 4.2–4.4€/kgH_2, and for C-ON systems from 4.7–5.5€/kgH_2 to 4.7–5.4€/kgH_2. The inclusion of salvage values can have a measurable effect on reducing LCoH but does not change the relative order of the configurations.

2.5.2 Operational differences across configurations

Firstly, annual hydrogen production, efficiency, and the impact of wake effects is discussed (Section 2.5.2.1). Secondly, the work describes how system configurations interact with the operational limitations of electrolyzer technologies (Section 2.5.2.1).

2.5.2.1 Hydrogen production and system efficiency

Depending on the selected scenario, the yearly production ranges between 76.2 and 95.8 kton for C-ON, between 76.4 and 96.2 kton for C-OFF, and between 80.3 and 99.9 kton for D-

OFF. **Figure 2.10** shows the comparison between the different system configurations in the mean technical scenario. PEM electrolyzers always result in higher hydrogen production, regardless of distance from shore. This results in lower LCoH values for PEM compared to ALK (Section 2.5.1).

Focusing on the impact of the length of electrical and hydrogen transmission infrastructure, **Figure 2.10** shows how the increased distance from shore leads to more hydrogen delivered to the backbone due to more favorable wind conditions, despite the losses related to energy and hydrogen transmission. Note that this effect does not persist beyond 100 km offshore due to the assumption of an unchanged wind source. The electricity transmission losses that affect the C-ON result in a decreased energy input to the onshore electrolyzer, and thus less hydrogen production. PEM electrolysis enables higher production rates. This is due to the higher efficiency and large operating range of this technology, which allow for the exploitation of almost all the available wind energy. The D-OFF experiences the highest production due to the higher overall conversion efficiency compared to the other configurations.

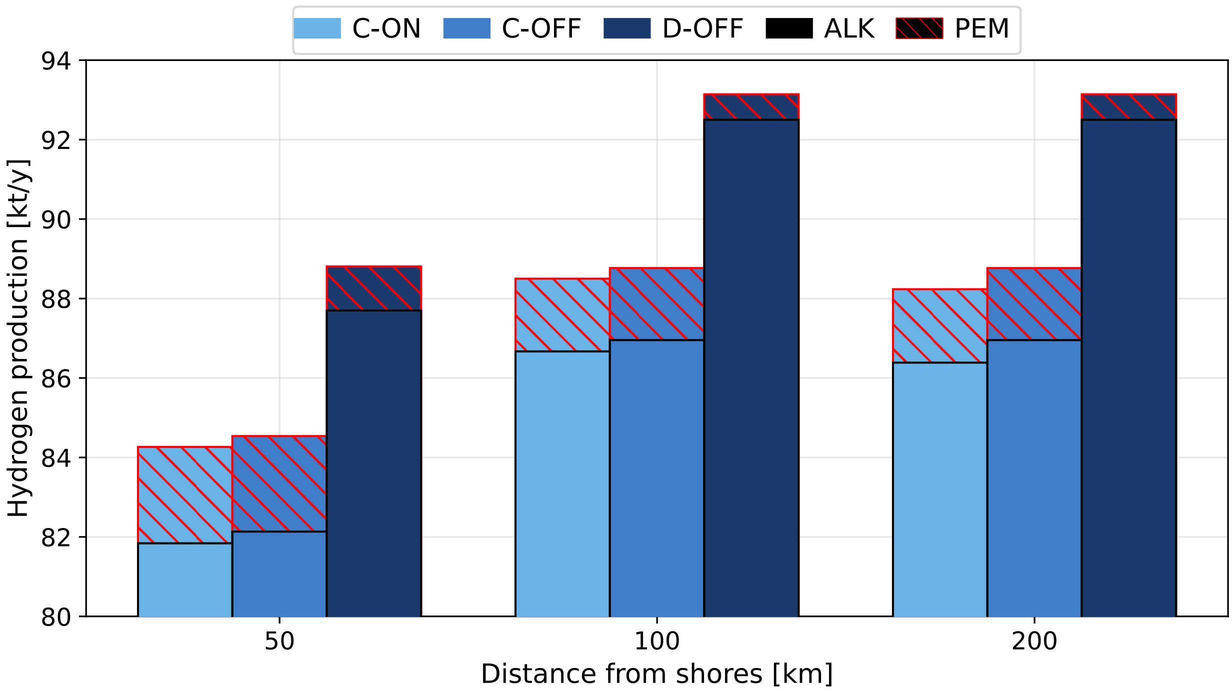

Figure 2.10: Annual hydrogen delivered to the backbone for C-ON, C-OFF, and DOFF for different distances to shores and electrolysis technologies in the mean technical scenario.

The overall system conversion efficiency can be estimated as the energy content of the produced hydrogen over by all the input energy (**Figure 2.11**). D-OFF experiences the highest system efficiency—resulting from the lowest losses—while C-ON has the lowest production and system efficiency. PEM is less affected by fluctuations in the wind energy source than ALK, as highlighted by the light green bars in **Figure 2.12**(a). Finally, accounting also for the impact of distance to shore on the conversion efficiency (**Figure 2.12**(b)), it is apparent how it adds at most 1 p.p. and does not affect the relative performance of configurations. Despite the higher amount of produced hydrogen, an increase in the length of the cables or pipelines results in lower efficiency due to the reduced exploitation of the available source. This effect is particularly evident for the C-ON, which experiences the highest energy transmission losses, as depicted by the comparison between **Figure 2.12**(a) and (b).

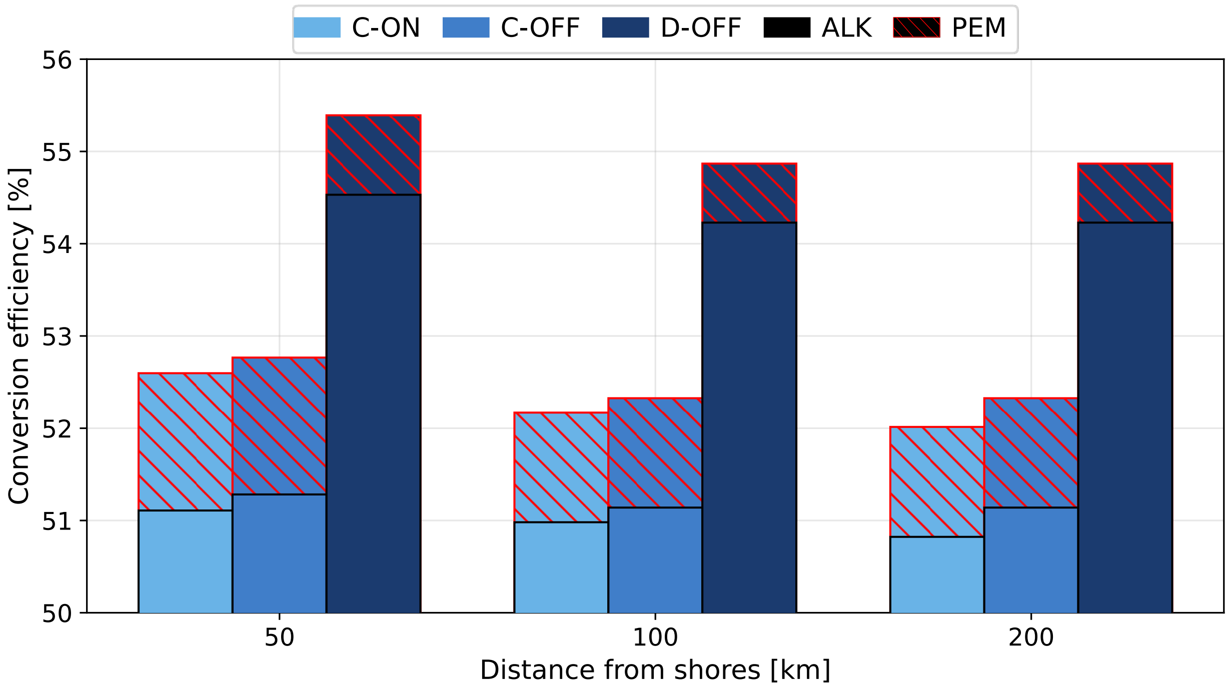

Figure 2.11: Mean overall system efficiency across all scenarios and configurations.

Figure 2.12 shows the aggregated impact of the electrolyzer constraints, namely minimum stable loads, cold startups, and power electronics on losses. These losses are estimated as the ratio between the energy available to the electrolyzer and the energy converted to hydrogen. While the D-OFF configuration has the highest curtailments due to the technical constraints of the electrolyzer, it has the highest overall system efficiency (Fig. 8).

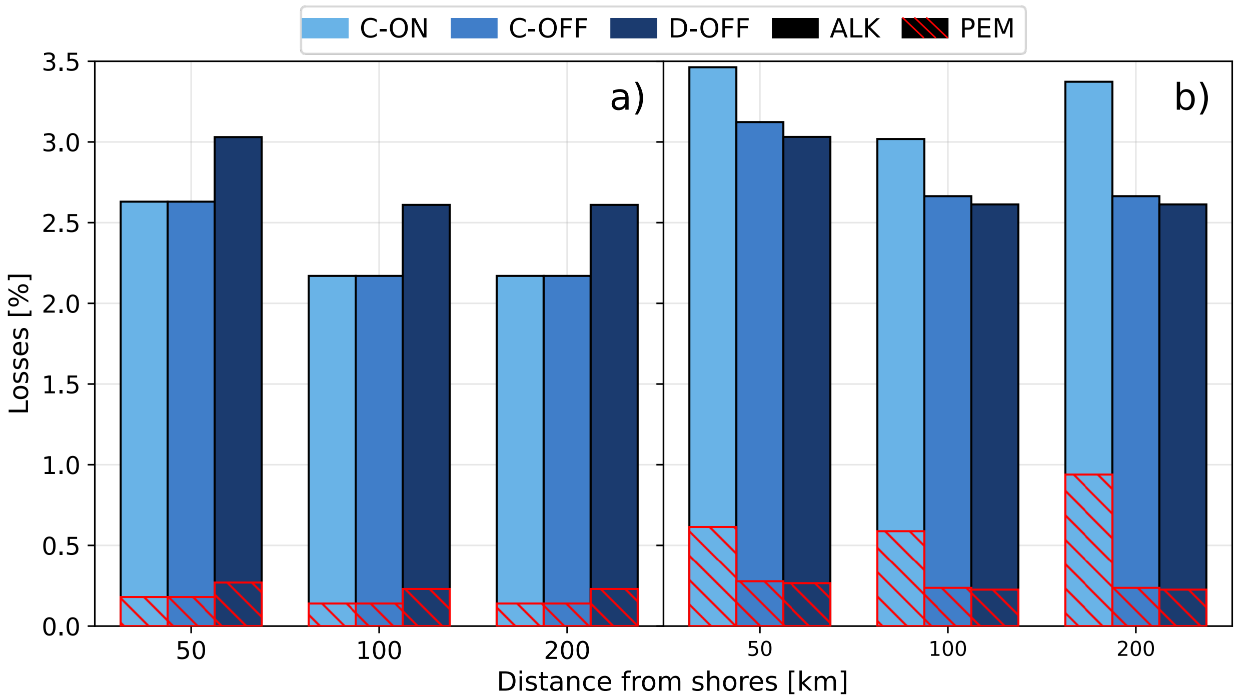

Figure 2.12: Losses due to electrolyzer constraints (a) (minimum load requirements, cold startups, and power electronics) and total losses (b) (including distance from shores) per system configuration.

The centralized configurations experience lower system efficiencies due to losses in electricity transmission and conversion. Increasing the distance to shore reduces the effects of minimum loads and cold startups due to the improved wind resources. Finally, looking at the comparison between electrolyzer technologies, PEM shows losses below 1 % compared to up to 3.5 % for ALK, which is consistent with the higher hydrogen production shown in **Figure 2.10**.

To provide an overview of the system operation, the links between the components can be depicted as energy flows in a Sankey diagram (**Figure 2.13** and **Figure 2.14**). These two plots show the differences in the operation of the system for the C-OFF configuration with the two electrolyzer technologies, in terms of total yearly energy. Starting from the same wind farm power production, the PEM offers a more efficient solution.

Fewer curtailments occur due to the component constraints, leading to about 447 GWh per year of additional energy available to the electrolyzer. Furthermore, despite the higher stack conversion efficiency of the ALK—testified by the ratio between produced hydrogen and losses of the stack—the scenario with PEM provides a higher amount of hydrogen and, hence, an increased system efficiency. In the D-OFF configuration, the loading of each electrolyzer varies based on its position in the wind farm due to wake effects. This is illustrated via the electrolyzers' capacity factors (CF), estimated as the ratio between the produced hydrogen and the nominal capacity of the electrolyzer.

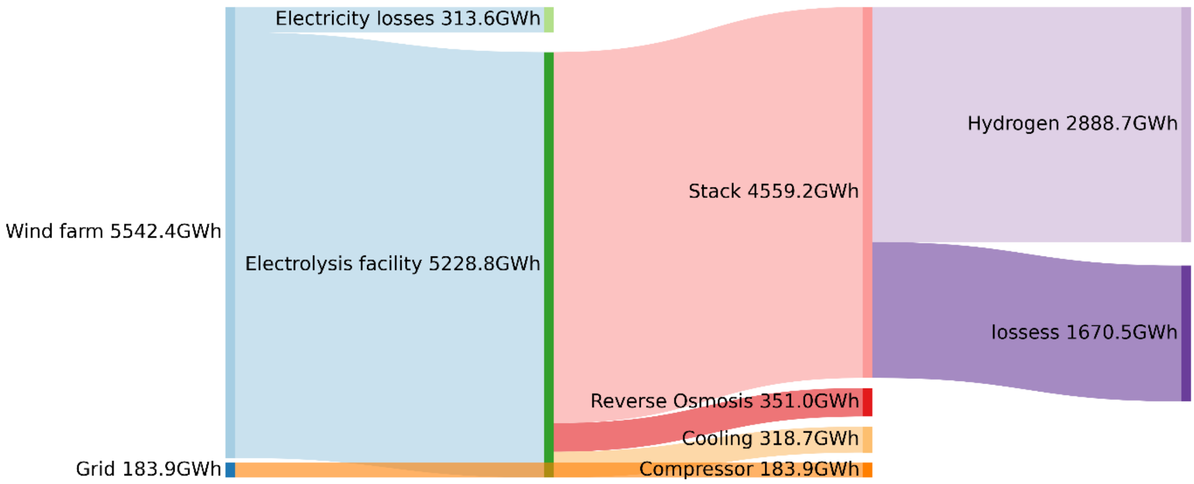

Figure 2.13: Sankey diagrams for the ALK electrolyzer in the C-OFF system configuration.

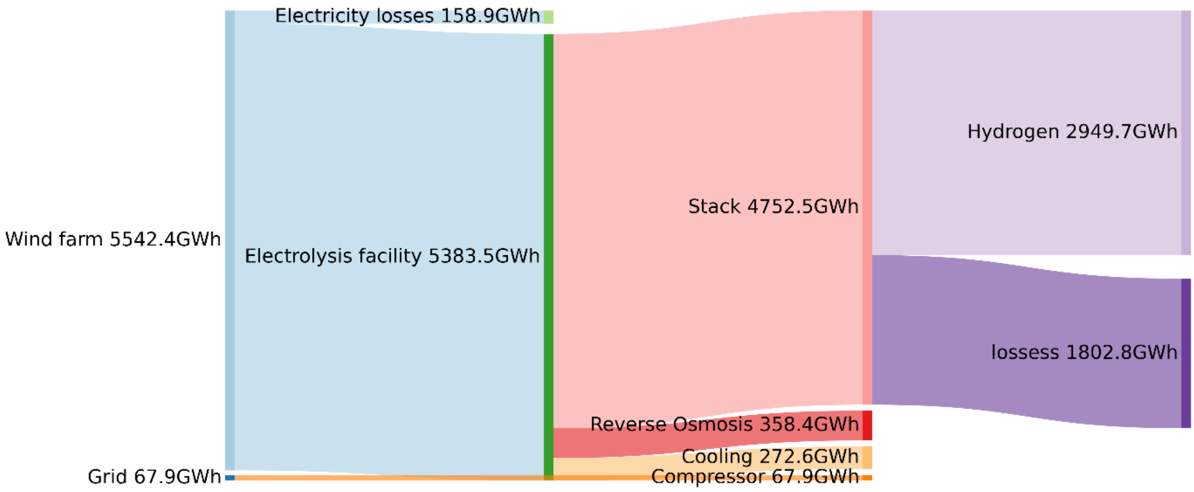

Figure 2.14: Sankey diagrams for the PEM electrolyzer in the C-OFF system configuration.

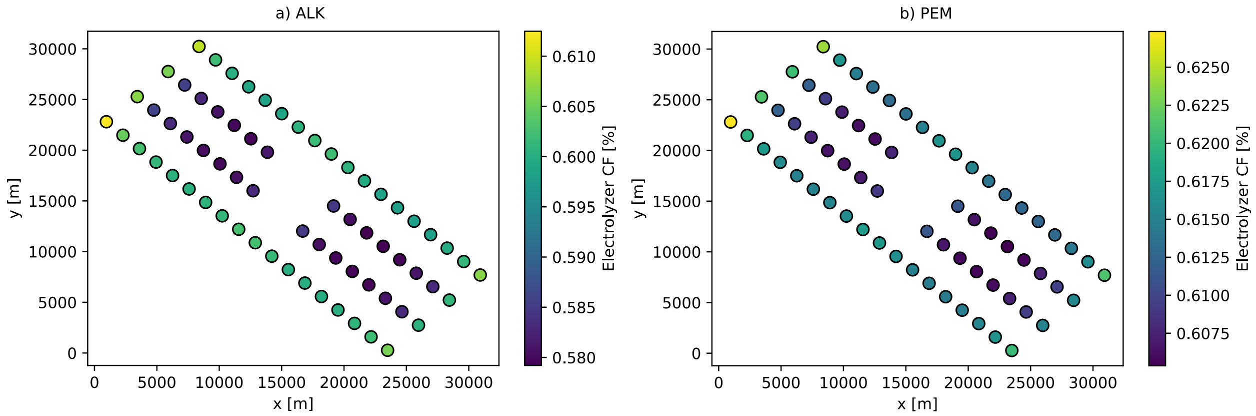

Figure 2.15: Capacity factor (CF) per wind turbine in the D-OFF configuration for the mean technical scenario in the 100 km offshore site.

Figure 2.15 illustrates the variation of the CF throughout the wind farm in the mean technical scenario. As a point of reference, the centralized configurations offer the worst CFs, ranging from 55 % to 58 % for ALK and PEM. In D-OFF, PEM outperforms ALK, which is affected by higher losses and, thus, shows lower CFs. On average, CFs range from 61 % for PEM and 59 % for ALK. The inner arrays of the wind farm face wake effects; hence, the outer electrolyzers show better performance and higher CFs. Furthermore, the comparison between the two plots depicts how inner electrolyzers are more disadvantaged with ALK technology due to the stricter technical constraints. The higher difference between the electrolyzer CFs—shown by the colors of the single wind turbines—observed between outer and inner WTs in **Figure 2.15** highlights a larger impact of the wake effect for this technology.

2.5.2.2 Operational behavior

Figure 2.16 shows the hydrogen production of the offshore configurations with both electrolysis technologies for one day, with a 10-minute resolution in the mean technical scenario at 100 km from shore. The variability in the wind power input results in periods of low and high hydrogen production within the same day, represented by the magnifications in the lower and upper right of the image.

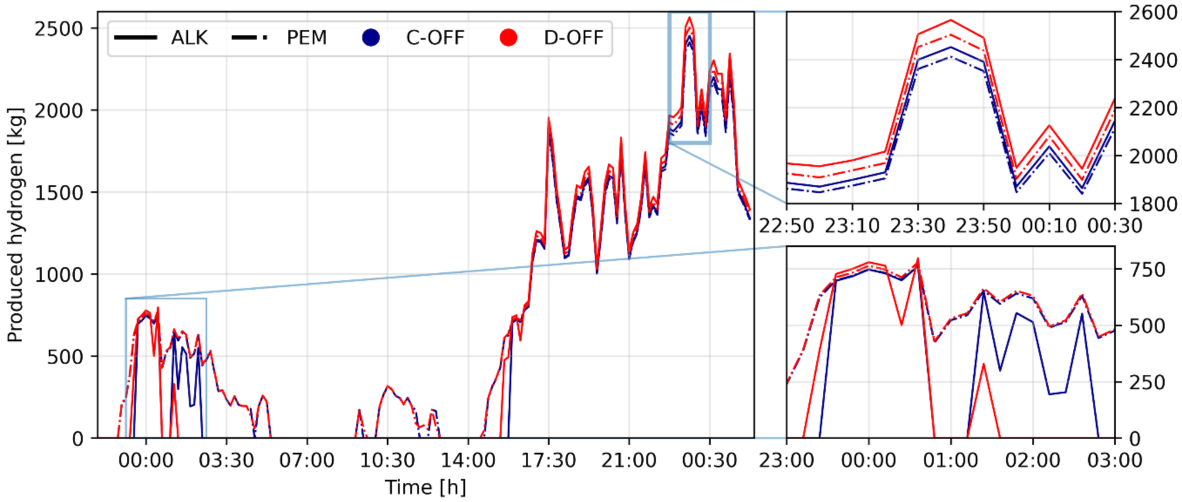

Figure 2.16: Comparison between the operational behavior of the offshore configurations with PEM and ALK.

Focusing on the comparison between the system configurations during periods of low wind power output, several differences can be observed. PEM's wider operating range is beneficial for hydrogen production (dashed lines). The minimum power input of ALK—set at 20 % of the nominal power— results in higher losses due to the constraints of the electrolysis facility, as illustrated in the aggregated results shown in **Figure 2.12**.While C-OFF experiences a higher hydrogen production with ALK during low wind periods, as shown in the first hours of the selected day, when the power input to the electrolysis facility is higher than the minimum allowed, D-OFF experiences improved performance. The wake losses affect the available power for the electrolyzers located on the inner WTs, triggering the minimum load constraint more often compared to centralized configurations. This is again consistent with **Figure 2.12** due to the lower conversion and transportation electricity losses.

The close-up of the last hours of the day depicts the system's behavior during operation far from the minimum load. D-OFF outperforms C-OFF for both electrolyzer technologies. Close to the nominal input, the ALK shows a higher hydrogen production. However, this is representative of the behavior of a new electrolyzer when degradation has not yet set in.

2.5.2.3 Impact of the selected site in the Dutch North Sea

Two additional offshore wind sites have been analysed to provide better insight into the performance of the hydrogen production configurations. One of these sites is situated closer to shore, approximately 20 km from the landing area (HKZ), and is characterized by lower wind speeds. The other is located at a distance of 60 km (IJV), between the primary test sites (NED and TNW). These supplementary analyses capture the influence of site-specific factors such as wind availability and distance from shore on both technical performance and economic viability. From a cost perspective, as shown in **Figure 2.17**, the outcomes from these additional sites are generally less favorable than those of the primary reference case.

Despite experiencing poorer wind conditions, the HKZ site (20 km from shore) achieves lower LCoHs compared to the IJV site (60 km from shore) for C-ON configurations.

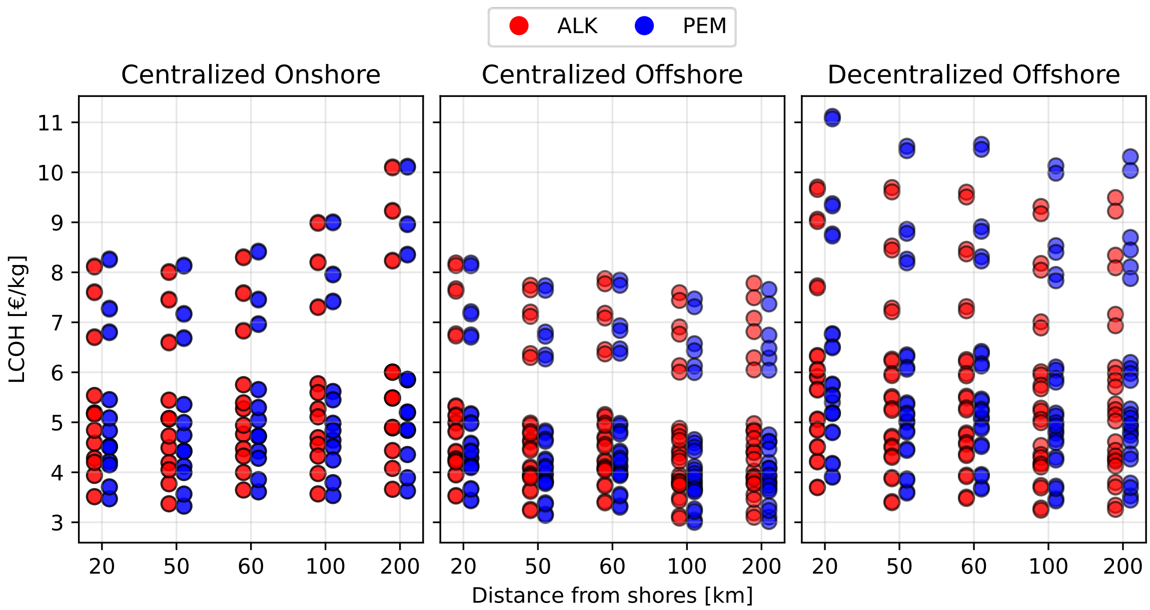

Figure 2.17: Range of LCoH for each system configuration for five wind park sites, characterized by their distance to shore.

This is primarily due to the shorter distance for energy transmission, which reduces transmission infrastructure-related costs and losses, compensating for the reduced energy yield.

On the other hand, the IJV site results in improved economic performance for the offshore configurations. This is attributed to the technical and economic advantages of deploying pipelines at longer distances offshore over cables. Therefore, the cost increase due to the larger transmission distance is balanced by the increased hydrogen production due to the beneficial wind source.

As shown in **Figure 2.18**, the findings for the two additional sites show that increasing the distance from shore, resulting in better wind sources, can reduce conversion losses due to operational constraints of the electrolyzer systems. This confirms the findings presented in Section 2.5.2. PEM consistently demonstrates higher efficiency compared to ALK, reinforcing earlier conclusions on the superiority of PEM technology in applications with fluctuating power input. The total system losses in the C-OFF configuration are affected by electricity transmission losses, which increase with distance and can outweigh gains in conversion efficiency, particularly for configurations relying on power transmission rather than direct hydrogen transport.

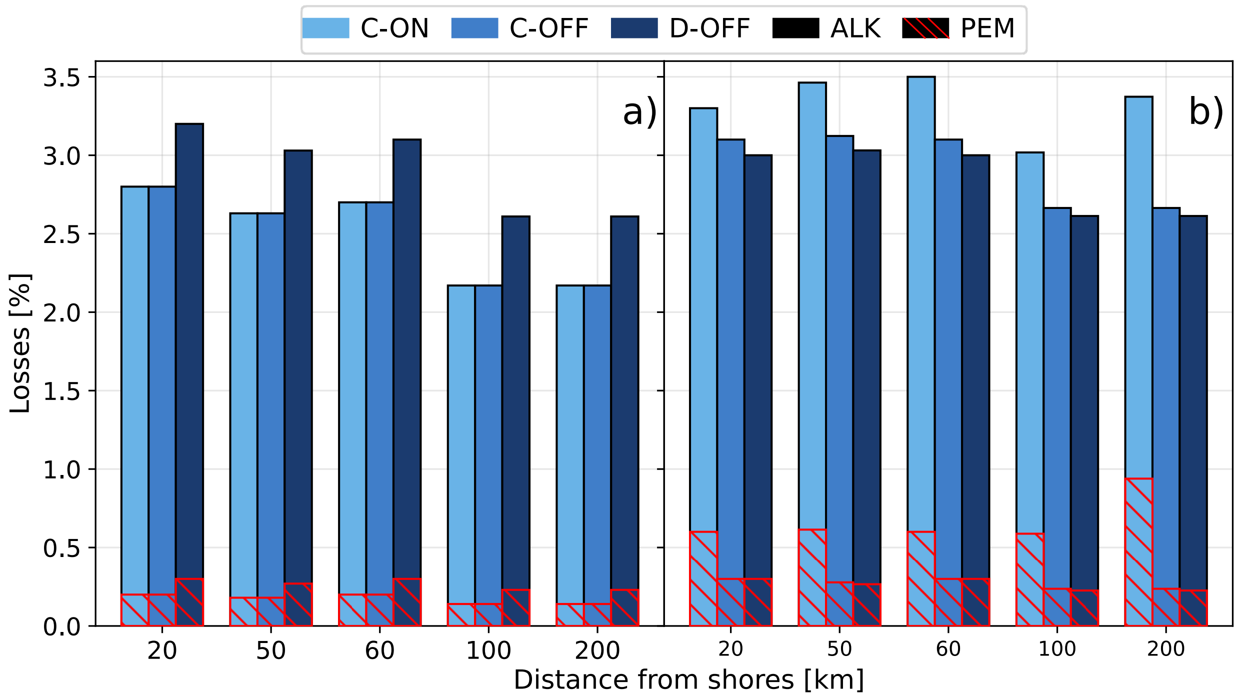

Figure 2.18: Overview of the operational behavior of the offshore configurations with PEM and ALK, with the inclusion of additional wind park sites HKZ (20 km) and IJV (60 km).

2.6 Discussion

After a short reflection on results in relation to the scientific literature (Section 2.6.1), the implications of this work for stakeholders are discussed (Section 2.6.2). Section 2.6.3 offers a reflection on the limitations of the study.

2.6.1 Comparison to literature

Compared to the literature, the LCoH estimates of the expert-validated benchmark scenarios align with studies that project 5–6€/kgH_2 in favorable scenarios [44,80]. For C-ON, the findings of this study are generally lower than the values reported by Hill et al. [50], which are similar to the higher-bound scenarios in this study. Many studies report LCoHs of 2–4€/kgH_2, aligning with lower bound cost and higher bound technology scenarios in this research, while the higher bound cost and lower bound technology scenarios herein adopted, particularly for D-OFF and C-ON, are up to 10.1€/kgH_2 for C-ON and 10.5€/kgH_2 for D-OFF. Frowijn et al. [81] recently estimated the LCoH of three system configurations, finding an LCoH range of 1.5–10.8€/kgH_2 across scenarios, with D-OFF as the most competitive. The study focuses on analyzing the assumed benefits of D-OFF. As a result, it uses a less detailed modelling approach, excludes economies of scale, and assumes a constant offshore energy input, which contributed to lower LCoHs in some scenarios.

As a reference, the average European competitive bids for green hydrogen production range from 5.8 to 13.5€/kgH_2, with an average of 9.8€/kgH_2 for the Netherlands [82]. In a recent study by TNO, the current LCoH for green hydrogen production was found to be 12–14€/kgH_2 for the Netherlands [83]. This highlights the critical role of selected input data and detailed, location-specific modelling, as the difference in configurations translates into different hydrogen production rates, energy flows, and transmission infrastructure needs, and ultimately LCoHs.

In this study, PEM electrolyzers are the most cost-effective option for all scenarios. However, other studies have reported different findings. Some do not address the debate and select only one of the two or do not specify which electrolyzer is included [40,44,54]. Hill et al. [50] found that PEM is outperformed by ALK, which is also the conclusion of Lei et al. [84] and Singlitico et al. [53]. These diverging outcomes are explained by the lower TRL of PEM, with correspondingly less beneficial parameters and higher CAPEX costs. However, Lei et al. [84] and Singlitico et al. [53] do not consider the difference in operational characteristics between electrolyzer technologies. PEM electrolyzers perform better with the variable wind energy input due to their wider operational range, resulting in a lower LCoH.

In most studies, centralized offshore electrolysis achieves the lowest LCoH [45,53,85], as in this study. However, Calado et al. [51] found onshore electrolysis to be more cost-effective due to the option to purchase low-cost grid electricity, which has been disabled for their C-OFF system configuration analysis. The choice between onshore and offshore electrolysis extends beyond the economic potential and operational dynamics, especially at larger scales. Besides cost implications, installing several offshore cables compared to a single pipeline may delay or alter development, with permitting—potentially taking multiple years per cable or pipeline—being a potential bottleneck. Potential delays in project development for onshore electrolysis may be more substantial than for offshore system configurations, especially when considering repurposed existing pipelines. Repurposing may entail a cost decrease of three to four times compared to new pipelines [75,86], but the benefits in terms of LCoH are negligible, with improvements from 0.1 to 4 %. Repurposing natural gas pipelines for hydrogen transmission faces potential challenges, such as embrittlement [87].

As hypothesized by Jang et al. [45], many technical and economic benefits may arise from implementing D-OFF. In contrast to their work, however, D-OFF does not represent the most cost-efficient configuration. The economies of scale impact the LCoH more than the increased hydrogen production, the reduced need for electrical transmission infrastructure, and the absence of additional infrastructure to host the electrolyzers in the D-OFF. Consequently, the centralized offshore configuration is the most cost-effective, as in Singlitico et al. [53].

2.6.2 Implications for stakeholders

For stakeholders—including energy producers, policymakers, and investors—understanding the implications of power input intermittency on the cost of renewable hydrogen is crucial. This study enables assessing cost and operational performance in different system configurations, moving forward the existing debates on onshore versus offshore and centralized versus decentralized hydrogen production.

While the outcomes presented in this study depict offshore electrolysis as an interesting and viable solution, they show that policymakers should focus on centralized configurations. Besides the economic results—which present this configuration as the most cost-effective— the C-OFF offers several advantages, such as higher technology readiness and reduced challenges for the system development over D-OFF.

To inform investment decisions for large-scale production, further in-depth analysis is required to identify cost-optimal conditions and ensure the technical feasibility of each configuration. This underscores the need for a cautious approach when making decisions about hydrogen projects, as varying assumptions and configurations can lead to widely different economic results. Moreover, the variability in the outcomes highlights the risks of oversimplifying the complexities of production technologies, as such simplifications may not fully capture the variability and nuances that influence the production cost for each system configuration.

Equally important is the need for targeted incentives—such as subsidies, tax benefits, or other (financial) mechanisms—to kick-start the upscaling of the green hydrogen supply chain and close the competitiveness gap. Introducing green hydrogen into an energy system depends on developing large-scale, integrated supply chains that align production with demand. Investments in these supply chains and offtake installations are capital-intensive and risky, which makes industrial parties hesitant to invest without government support.

2.6.3 Limitations

This study does not include the costs or operational considerations of hydrogen storage. Instead, the focus is on the production, assuming hydrogen is delivered directly to the future Dutch hydrogen backbone. The onshore hydrogen transmission infrastructure can accommodate variable production [88]. It can be acknowledged that hydrogen storage is an important system component, but it is out of scope for this analysis. This allows focusing on the performance of the hydrogen production system, without accounting for supply-demand dynamics.

The cost of hydrogen has been evaluated, rather than the value. This choice has been made to provide guidance on the costs associated with the hydrogen production configurations. While the value of hydrogen could have led to different results, that the relative differences between system configurations would not be affected. A value-oriented perspective would allow shedding light on hybrid solutions—combining electricity and hydrogen production offshore [85]. This offers possibilities for arbitrage between these two energy vectors and overplanting of wind farms.

The economic findings confirm the uncertainty surrounding offshore wind-based hydrogen production, driven by the wide range of input parameters and the need to include multiple assumptions. Expert-validated scenarios are incorporated into the analysis, aiming to enhance the robustness of the cost projections. While the conducted analysis considers over 400 scenarios, this represents only an initial step toward exploring the full uncertainty space. A more comprehensive treatment of uncertainty remains an important direction for future research.

Similarly, the most cost-efficient system configuration for large-scale green hydrogen production is wind source and location dependent. The Dutch North Sea wind conditions are characterized by a favorable Weibull distribution. Different wind energy input profiles from other sea basins may lead to different conclusions.

This study focuses on the techno-economic evaluation of offshore hydrogen production configurations, highlighting the impact of the choice of electrolyzer technology, distance to shore, the choice for hydrogen pipelines or HVDC infrastructure, etc. The environmental impact of these technology choices and configurations is out of scope due to the complexity of these assessments. For example, when considering the electrolyzer choice, PEM electrolyzers use rare materials like platinum-group metals [53]. However, due to other factors such as system lifetime, efficiency differences, and manufacturing impacts, no clear winner emerges between ALK and PEM technologies in terms of overall environmental impact [89]. Similarly, a comparison between the environmental impact of electrical cables and hydrogen pipelines may be challenging. Multiple factors, such as material requirements, installation procedures, and impact on local biodiversity, contribute to the overall environmental impact of the system. Optimizing the wind farm layout may reduce the inter-array distance and thus the footprint of the farm. The benefits related to this optimization may be limited if one considers, e.g., the influence on biodiversity. A comprehensive analysis of trade-offs between cost, efficiency, environmental impact, and other factors would require an explicit multi-objective optimization approach, which has been identified as a promising topic for future work.

2.7 Conclusions

The study aims to contribute to the ongoing discourse on selecting an approach to producing green hydrogen based on offshore wind on a GW-scale: Onshore centralized electrolysis (C-ON), Offshore centralized electrolysis (C-OFF), and Offshore decentralized electrolysis (D-OFF). An innovative high-resolution, time-dependent simulation framework was employed to accurately analyze the operation of the system configurations, with a particular focus on the decentralized one. Unlike centralized systems, D-OFF has unique dynamics driven by the direct connection of electrolyzers to individual wind turbines. The proposed modelling framework allows analyzing system costs and the impact of operational behaviors under intermittent energy inputs, providing a robust foundation for informed decision-making.

For all system configurations, the wide range of estimated LCoHs—spanning from 3.0 to 10.5€/kgH_2 —reflects a wide variety in future costs and potential technological development. Benchmark scenarios were developed using expert-validated economic input data. The resulting LCoHs exhibited a narrower range, between 4.1 and 5.5€/kgH_2. For all system configurations, the most significant cost driver was the wind farm cost, followed by the electrolyzer costs, and, in the case of C-ON, the electrical transmission infrastructure costs. The latter strongly depends on the distance to shore.

This analysis identifies offshore electrolysis—specifically C-OFF—as the most cost-competitive option, driven by the cost advantage of hydrogen transmission infrastructure over electrical export transmission infrastructure. This advantage grows with increasing distance from shore. Centralized configurations outperform decentralized ones, which are limited by the economies of scale. While D-OFF boosts hydrogen production rates, the gain is insufficient to achieve the lowest LCoH. Across all system configurations, PEM emerges as the most suitable choice. Both ALK and PEM face challenges due to intermittent supply. Under the assumptions made, enabled by the proposed framework based on time-dependent analyses and detailed wind data analysis, ALK is characterized by more strict technical constraints, resulting in worse performance and a higher LCoH than PEM. However, the long-term effects of intermittency on stack behavior, particularly for large-scale systems, remain uncertain.

The operational analysis realized due to the adoption of a time-dependent approach reveals how fluctuations in wind power, minimum load requirements of the electrolyzer, and stack degradation for each electrolyzer technology impact the energy losses for each system. The proposed model enables a detailed analysis of the differences between C-ON, C-OFF, and D-OFF. Results show that, while the decentralized configuration experiences relevant losses related to the operative constraints of the electrolyzers, it is characterized by the highest system-level efficiency, given the reduced energy conversion steps and transmission losses. This is emphasized by adopting PEM, which ensures continuous operation even with low power inputs. Stack degradation decreases the performance, decreasing hydrogen production, and increasing the LCoH. The outcomes of the analyses have been used for the studies later depicted in this thesis.

The study underscores the need for a detailed, time-dependent modelling framework combined with system designs tailored to specific offshore wind energy conditions. Researchers and policymakers should focus on developing adaptive operational strategies that maximize value as the starting point, going beyond cost. Integrating these insights into techno-economic models and energy system modelling frameworks will ensure that large-scale green hydrogen production aligns with the energy transition.

3 THE MEDITERRANEAN CHALLENGES: UNLOCKING POTENTIAL WITH FLOATING WIND

3.1 Challenges in floating offshore wind development: a review

The deployment of large-scale wind farms presents multiple challenges, including technical, economic, and environmental issues [90]. For instance, dense clusters of wind turbines may result in revenue reductions due to the wake interactions between aerogenerators. In fact, the more densely packed the turbines, the more relevant the impact of wakes [91]. The relevance of these losses can be assessed in large offshore wind farms, such as Horns Rev I & Nysted [92,93], where the reported AEP reductions span from 10 to 25%. Moreover, projections show that for very large-scale wind farms with conventional inter-turbine spacing [94] (e.g., 7 diameters in streamwise and 5 diameters in crosswind directions), AEP losses due to wakes could exceed 60% [95,96]. In addition, the evermore dense clustering of wind farms in the North Sea has caught the attention of project developers and researchers, which have highlighted potentially significant losses in production due to neighboring wind farm wake effects [97–99]. In addition, clustering offshore wind energy production in a single region can lead to curtailment and grid stability issues, as recently observed in many northern European countries [33,100–102]. Moreover, even in the absence of curtailment, clustering wind farms in a specific region could also lead to a "self-cannibalization" effect [100], where spot electricity prices are driven down by the high availability of wind energy in periods of high winds in a certain region [103].

Expanding offshore wind energy to other basins, which often have different characteristics from locations that have been exploited up to the current point, is seen in all reports as the only way to meet the ambitious targets in terms of offshore wind power generation [104]. In Europe, for example, focus is given to the Mediterranean Sea, as it borders countries with high energy needs that could strongly benefit from local wind energy generation. However, the Mediterranean Sea presents several unique challenges for offshore wind development [105], namely deep waters and a lower average wind resource. Therefore, tailored solutions are required to cost-effectively exploit these regions.

The key component to making offshore wind energy economically viable in deep waters are Floating Offshore Wind Turbines (FOWTs). In fact, despite the presence of installation sites that allow for the exploitation of shallow waters, such as the Adriatic Sea, they represent the vast minority of the available areas and usually experience unfavourable wind sources. However, FOWTs are still an emerging technology with high capital and operational costs [106]. Currently, only three floating offshore wind farms, namely Hywind Scotland (30 MW) [107], Kincardine (50 MW) [108], and WindFloat Atlantic (25 MW) [109], are operational and connected to the electrical grid, while several additional projects are in various stages of commissioning, construction, or planning [110]. Despite the rapid advancements in floating wind technology, the LCoE for floating wind remains substantially higher than that of fixed-bottom offshore wind [110]. Therefore, the large-scale installation of FOWTs in the Mediterranean Sea can not be adopted for the decarbonization of its energy systems, due to its cost, the regulatory aspects, the required harbor facilities, and the low technological maturity of some components like the integration of floaters. The International Renewable Energy Agency recently published a report that anticipates that global offshore wind capacity could reach nearly 1,000 GW by 2050. It emphasizes the potential of floating foundations to exploit deeper water resources, projecting that floating wind could account for 5% to 15% of total offshore capacity by mid-century [111], despite the current high-costs.

3.1.1 Floating farm design: the need for tailored solutions

To increase the competitiveness of floating wind it is necessary to drive LCoE down. From this point of view, according to many experts, FOWTs are a topic with significant margins in terms of technological learning potential [112–114] and significant cost reductions are foreseen within 2030, which could enhance the economic viability of floating wind and enable it to compete with the current costs of fixed-bottom offshore wind [115]. In fact, floating foundation designs have still not coalesced into one, or even a few archetypes. In addition, due to the low volumes of the floating market, turbines currently used in FOWT applications have been originally designed for bottom-fixed applications and readapted for floating foundations. Recently, the benefits of a more-tightly integrated design of the turbine and floater have been highlighted. Co-design, whereby the controller is designed together with the FOWT system [116], has shown promising results, with measurable reductions il LCoE of up to 4% that have been found in [117].

In addition to being able to benefit from a tighter integration with the floating substructures, recent literature has shown the benefits of tailoring the rotor characteristics to the installation site. In fact, Metha et al. [118] have found the optima power to rotor area ratio of offshore wind farms in the North Sea to be close to the industry standard for current offshore turbines, which feature relatively high ratio – i.e., specific power – of 300-350 W/m^2. Nevertheless, a measurable benefit in terms of LCoE can be found if scale of the optimum design and specific power are optimized on a site per site basis.

In this context, many researchers have found potential benefits in adapting the turbine diameter through optimization. Serafeim et al. [119] proposed a multidisciplinary optimization to reduce the LCoE of the DTU-10MW Reference Wind Turbine, aiming to estimate the optimum rotor diameter. Results show that the new rotor design, featuring a larger diameter (+3.7%) reduced the LCoE by 0.71% and increased AEP by 2.4%. Zalkind et al. [120] concentrated on system design for rotors with radii of 100 meters or greater, aiming to maximize the AEP while managing overall turbine loads to mitigate increases in operational (OPEX) and capital (CAPEX) expenditures. The framework for blade design examined several design variables, including blade length, cone angle, number of blades, rotor axial induction factor, and the distribution of rotor mass and stiffness to identify the most effective configuration. The authors concluded that an 11% enhancement in AEP for a 13MW wind turbine could be realized by extending the blade length by 25 m, corresponding to an increase of 25%, and reducing the induction factor, all while effectively controlling rotor loads. It must be noted that this approach relies on the optimization of a detailed aeroelastic design of the wind turbine. Therefore, the results in terms of LCoE might be affected by the selected testcase and by the achieved local optimum. In [121] Buck and Garvey emphasize economic optimization alongside AEP optimization, highlighting that capital expenditures represent the key factor contributing to the total turbine cost in the LCoE equation. They optimized various parameters, including blade chord, axial induction factors, and sectional lift coefficient across the blade span, aiming to minimize CAPEX while enhancing AEP. With reference to the NREL 5MW offshore turbine, the optimization process achieved a 1% reduction in CAPEX and a 1.4% increase in AEP, resulting in an overall improvement of 2.4% in the CAPEX/AEP ratio.

These analyses, while not all focused on offshore wind farms, suggest that LCoE can be improved by increasing rotor diameter and contextually decreasing specific power. As discussed later on in this study, this trend has indeed been ongoing over the last decade in the onshore market, where a slow but consistent reduction in specific power of new rotors can be observed [103]. In addition, while being able to provide valuable insights on the importance of integrated design on a component level, all these analyses neglect the mutual interactions between the wind turbines within a wind farm. However, changing the rotor diameter influences the wind turbine’s wake, in turn influencing inter-array wake losses.

To this end, some authors have included inter-array wake losses in their studies, although often in a simplified manner. Dykes et al. [122] performed a global sensitivity analysis to key wind turbine configuration parameters including rotor diameter, rated power, hub height, and maximum tip speed, by using the integrated wind plant system modeling tool WISDEM. They showed that the increase in turbine diameter might be beneficial to drive LCoE down. Wake losses are estimated as a percentage of the wind farm AEP. Mehta et al. [118] examine how the turbine’s rated power and rotor diameter influence various metrics at both the turbine and farm levels, aiming to identify the primary design drivers and understand how they affect different configurations. They developed an optimization framework able to minimize the LCoE and define the optimal turbine size. They found that reconfiguring the IEA 15 MW turbine for an installation site in the Dutch North Sea results in an optimal wind turbine with a rated power of 16MW (+6.7%) and a diameter of 236m (-1.5%), leading to a LCoE improvement of approximately 1%–2%. The increase in turbine-specific power with respect to reference is motivated by the high wind speeds of the studied sea basin. Wake losses are once more considered approximately, as the wind farm layout is not a design variable and is considered fixed in the study.

Both studies are based on complex multi-disciplinary design frameworks. Other authors have tackled the problem from a different perspective, using much simpler models based on empirical cost-scaling rules. Shields et al. [123] studied the impact of turbine upscaling and plant upsizing on various farm-level parameters. They found a reduction in LCoE by up to 20% when upscaling turbines from 6 to 20MW and upsizing the farm from 500MW to 2500MW capacity. However,

the study assumes a fixed cost per kW for the turbines and also limits the specific power of the turbines when upscaling. Ashuri et al. [124] optimized a 5MW reference turbine and scaled it up to 10 and 20 MW, respectively, to evaluate the effect of rotor and tower upscaling on LCoE. Their study claims an increasing LCoE trend when upscaling. However, the costs for balance of system (BoS) and O&M are assumed to scale with the rated power, with a fixed value for the exponent, following the relations presented in [125], thus strongly simplifying the complex relationships of the turbine with other elements of the farm. Sieros et al. [126] performed an upscaling study for turbines in the range of 5–20MW, with constant specific power, using classical similarity rules. The results showed an increase in the levelized production cost with turbine scale, for the same technology level. However, the focus of the study was on a simplified upscaling method, especially for the turbine, while the models for the rest of the wind farm were expressed simply as a percentage of turbine costs.
Finally, some researchers have shown that it is possible to focus on metrics other than LCoE as wind farm design drivers. The research conducted by Canet et al. [127], despite focusing on on-shore wind, shifts the focus from solely power generation and economic factors to long-term sustainability and lifetime CO2 emissions. This study established a relationship for CO_2 emissions that parallels the LCoE equation, defined as the environmental value minus the environmental cost divided by the total energy produced. Utilizing this new metric, the researchers optimized hub height and rotor diameter (D_R) to reduce environmental impact. Their findings indicated that the optimal configuration for environmental considerations does not align with the LCoE optimal configuration. More interestingly, they show for a test case in Germany that Low Specific Power (LSP) aerogenerators can be beneficial for both the cost of energy and the environmental impact due to the increased production at low wind speeds. Nevertheless, these results may not directly translate to offshore installations. In fact, inland installations do not require an upscaling of the offshore foundation or floating platform, which strongly affects the CAPEX of the system. Additionally, the wind farm layout is often constrained by terrain morphology, and thus it often does not represent a design variable for the system. If this is the case, the stronger wake effects due to the enhanced swept areas cannot always be offset by an increase in spacing between wind turbines, contrary to what may be possible offshore. These latter works put more emphasis on economic assessments, often prioritizing cost-related metrics over physical accuracy. While valuable for early-stage evaluations, such simplifications limit the ability to derive insights into the complex dynamic interactions that govern system behaviour. In addition, the cost-scaling rules employed in these studies often neglect the influence of swept area, and are based or nameplate power output, and are thus not suitable for studying the influence of rotor FOWT design on LCoE.

Another class of studies focuses on wind farm layout. In fact, considering wind farm layout in the design process allows for design techno-socio-economic tradeoffs between often conflicting interests such as the minimization of wake losses, the minimization of inter-array cable costs, the reduction of visual impact and the reduction of sea use, often contested with other activities such as tourism or fishing, to be evaluated. Furthermore, rotor diameter influences FOWT spacing significantly, as it impacts wake losses and thus energy production and structural loading. At the same time, FOWT spacing impacts the inter-array (IA) cable length, the cost of which per unit length is significant [128]. Moreover, considering the wind farm layout in the design process allows for additional design variables to be considered, such as the mooring lines, which can decrease inter-array wake losses significantly [129]. Many researchers have tackled this issue by developing and utilizing wind farm layout optimization tools. Yilmazlar et al. [130] presented a modular tool for preliminary estimation of the LCoE in wind farms, supporting early-stage design decisions through simplified models. While the tool effectively captures interactions between layout and cost components, such as the trade-off between reduced wake losses and increased cabling costs with larger turbine spacing, it does not perform any wind turbine design. Moreover, the case study is limited to a parametric analysis of inter-turbine spacing using FLORIS [131], varying only the distances between turbines without changing their orientation. Such parametric approaches may overlook more optimal solutions, as they fail to explore the full design space or account for the coupled effects of layout and turbine characteristics.The research conducted by Hietanen et al. [132] concentrated on optimizing the layout of offshore wind farms, aiming to decrease the LCoE for floating offshore wind installations by integrating floating-specific parameters with economic indicators. Their optimization routine identifies rotor placement across various offshore wind farms using an objective function that seeks to maximize AEP while adhering to constraints related to CAPEX and OPEX. While this optimization encompasses multiple parameters, its primary focus is not on the design of the wind turbines themselves but rather on the installation of rotors and the associated transmission requirements, which constitute significant costs for floating offshore wind farms. Cazzaro and Pisinger [133] addressed the scalability limitations of traditional methods by proposing a variable neighborhood search-based heuristic capable of efficiently optimizing layouts for large-scale offshore wind farms. Their method incorporates realistic constraints such as turbine spacing and foundation costs and demonstrates high performance even on problem instances involving thousands of potential turbine locations. Cao et al. [134] contributed a multi-objective optimization framework that considers not only power generation but also the distribution of streamwise turbulence intensity, a critical factor influencing turbine fatigue life. By integrating a turbulence-aware wake model and employing a genetic algorithm, their approach successfully reduces operational stress on turbines while maintaining energy production levels. Thomas et al. [135] presented a comprehensive comparative analysis of eight optimization methods applied to a standardized layout optimization case study, highlighting the importance of algorithmic transparency and reproducibility. Their results revealed that diverse methods can yield comparable performance when applied correctly, emphasizing the robustness of current optimization techniques. Lei et al. [136] proposed an adaptive genetic-particle swarm hybrid algorithm that dynamically modifies turbine positions to enhance conversion efficiency across varying wind scenarios and constraint sets. This approach achieved superior performance compared to a range of benchmark algorithms, underscoring the potential of hybrid metaheuristics. Finally, Yang et al. [137] advanced the field by shifting the optimization objective from power maximization to minimization of the LCoE, using an improved analytical wake model combined with a hybrid optimization strategy. Their method demonstrated notable gains in energy efficiency and cost-effectiveness, particularly in large-scale deployments. Collectively, these studies reflect the significant progress made in the development of increasingly sophisticated algorithms for optimizing wind farm layouts under realistic environmental and operational constraints. However, a common limitation across this body of work is the assumption of fixed turbine characteristics, regardless of the specific wind resource at a given site. By treating turbines as standardized components rather than as design variables that can be adapted to local wind conditions, these approaches may overlook substantial opportunities for improving overall wind farm performance.

In addition to the aforementioned classes of studies, some researchers have also focused on evaluating the impact of floating wind farms more broadly from an energy-system perspective. Martínez and Iglesias [138] evaluated LCoE across the Mediterranean using static wind resource data and basic power curve models, overlooking the dynamic effects of floating structures and atmospheric variability. Ghigo et al. [139] focused on minimizing platform weight to reduce costs, but their analysis did not capture the coupled dynamics of platform motion and turbine performance. Lerch et al. [140] performed a broad sensitivity analysis on LCoE for various floating wind farms concepts, yet their methodology was grounded in parameterized cost inputs and deterministic energy estimates. Similarly, Lanni et al. [141] explored floating wind farms for hydrogen production using a streamlined economic model that neglected the complex physical behaviour of floating systems in real sea conditions. While all these studies offer valuable insights into cost structures and deployment strategies, their reliance on simplified simulations limits their ability to represent the intricate physics of floating wind farms. Accurate assessment of energy production, structural loading, and long-term performance in floating systems requires integrated, high-fidelity models that couple aerodynamic, hydrodynamic, and control system interactions—elements that remain largely unaddressed in this research branch.

Overall, these analyses show that tailoring the wind turbine to the specific installation location by changing design parameters such as rated power, nominal rotor loading and blade length can benefit LCoE. At the same time, optimizing the wind farm layout, despite being an algorithmically complex problem due to the considerable number of design variables involved, can also benefit LCoE. While this literature review has also highlighted the existence of broader system-level studies focused on the impact of FOWTs in sea basins such as the Mediterranean, no study was found to date where the influence of design parameters on the wind farm layout has been studied. This gap highlights the need for an integrated optimization framework that considers both the spatial configuration of wind farms and the design of turbines, tailored to the unique wind profiles of each location.

3.1.2 Objectives and structure of the study

Based on the presented context, the objective of this study is to investigate the potential of LSP rotors in moderate wind speed offshore basins. To accomplish this objective a framework that is able to account for the influence of the wind farm layout and design parameters simultaneously in a physically consistent manner is developed. Furthermore, a detailed review of existing cost and mass scaling function for various turbine components is provided throughout the manuscript. A decrease in specific power is indeed a trend that has been ongoing for several years in onshore wind installations [103,142]: this trend has provided increased capacity factors for onshore wind projects despite them being developed in lower wind speed sites [143], and has led to the development of LSP rotor designs in academia [103]. In addition, despite the potential benefits of LSP rotors that have been discussed in the literature review in the previous section, this is a topic that is yet to be extensively explored for FOWTs. More specifically, both commercial and reference turbines developed by the academic community to date [144,145] are designed and optimized for those high wind speed conditions usually targeted by bottom-fixed applications [118]. As discussed, however, many offshore basins with significant development potential such as the Mediterranean Sea experience significantly lower average wind speeds (WSs) compared with northern European waters [146,147]. The overall energy conversion potential of commercial turbines in these sites is thus reduced. To this end, researchers are investigating (e.g., the EU project FLOATFARM [148]) the possibility of creating a new generation of FOWTs tailored to moderate wind speed deep-water sites and characterized by a lower specific power, i.e., the ratio between generator power and rotor swept area. From a technical perspective, lower specific power can be achieved by maintaining the same generator power and upscaling the rotor or by decreasing the generator power for a given rotor. In the context of

FOWTs, however, both strategies involve some drawbacks. The first approach leads to taller and heavier towers, which in turn result in a significantly increased overturning moment on the floating substructure, which needs to be increased in size, using more material and increasing cost. On the other hand, in the second strategy, it is apparent that the turbine and the substructure, designed to cope with higher aerodynamic loads, are underexploited and are therefore not cost-effective.

The present study aims to critically discuss the prospects of using LSP wind turbines in floating offshore installations in sites with moderate wind speeds. The workflow of the study is presented in **Figure 3.1**.

First, the literature review presented in the previous sections allowed for the definition of a broader framework of the problem. In particular, it is apparent that, contrary to the few studies presented to date (e.g., [149]), estimating FOWT prospects in new sea basins with simplified analyses that only estimate the aerodynamic AEP as a combination of statistic wind profiles (i.e., the wind distribution in the sites) and hypothetical power curves for this new rotors may result in unrealistic estimations. On the other hand, a comprehensive approach is needed, which must be able to evaluate the tradeoffs in terms of wake effects, cable costs, substructure, and turbine on CAPEX, OPEX, and energy production: a simple reanalysis of existing data cannot be sufficient for the scope.

Based on these outcomes, detailed reviews have been conducted on existing modeling tools and techniques for the main components of FOWT farms.

For each of these components, namely the rotor, the tower, and the floater, an extensive literature review, focused on how these component's mass and cost scale with FOWT size is first provided, followed by a discussion on how realistic scaling models for each of them can be derived and included a comprehensive simulation framework. This framework represented the key enabler to investigate how reduced-specific-power turbines can be effectively integrated into floating wind farms to enhance the economic viability of floating offshore wind projects in moderate wind speed conditions.

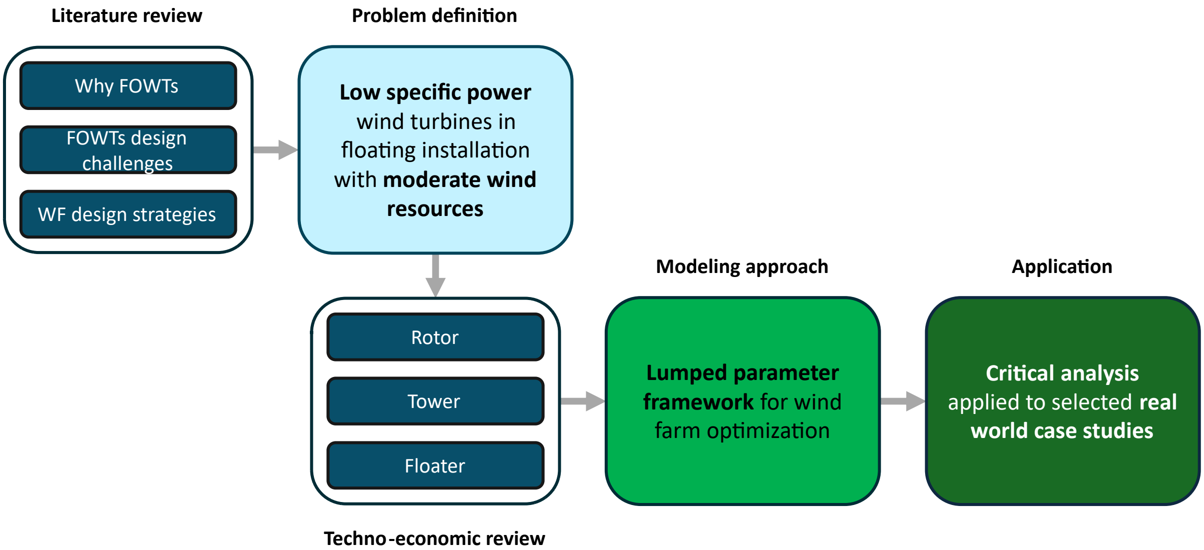

Figure 3.1: Workflow of the study. Review phases are highlighted with dashed boxes.

Although both the models and the conclusions are of general interest for all other installations with similar bathymetry, such as the Atlantic shores of the United States of America or waters around Japan, for the purposes of the present study, the Mediterranean Sea is taken as the case study to investigate critically the potential of LSP FOWTs due to its unique wind resource. By selecting the Mediterranean Sea as a case study, I had access to different sites that are representative of a quite broad spectrum of moderate wind conditions, thus allowing one to assess the complex interactions between turbine design variables and farm-level economics, offering insights into the prospects of the technology.

The study is structured as follows. The selected study cases are presented in Section 3.2. The review studies for each of the main system components and their implementation into a unique framework are reported in Section 3.3. Section 3.4 presents the optimization algorithm, while Section 3.5 discusses the results of the analyses on the Mediterranean case studies. These are followed by a critical discussion on the prospects of technology (Section 3.6). Final remarks, best practices, and possible further developments are finally outlined in Section 3.7.

3.2 Study cases

As discussed in Section 3.1, evaluating the techno-economic potential of LSP floating rotors requires going into the details of the selected study cases, as no high-level analysis based on aggregate data or average value has the potential to provide accurate insights.

3.2.1 Turbines

The present study considers four 15-MW wind turbines, purposefully designed for this analysis. Diameters range from 240 m, which corresponds to the current academia-designed reference 15MW wind turbine by IEA [144], to 330 m, in a 30 m step. Specific power ranges from 331.6 to 175.4 W/m^{2,} respectively. **Table 3.1** highlights the most significant parameters of the proposed WTs. Hub height is estimated by adding 30 m to the rotor radius in order to ensure sufficient sea clearance.

Table 3.1: Main design parameters for the IEA15MW RWT and the proposed FOWTs.

Wind Turbine	RWT [144]	MED15MW_240	MED15MW_270	MED15MW_300	MED15MW_330
Hub height [m]	150	150	165	180	195
Tower Height (H_T) [m]	130	130	145	160	175
D_R [m]	240	240	270	300	330
Specific power [W/m²]	331.6	331.6	262.0	212.2	175.4
Rated power [MW]	15	15	15	15	15
Cut in/out WS [m/s]	3/25	3/25	2.8/25	2.6/25	2.5/25
Rated WS [m/s]	10.7	11.3	10.5	9.9	9.5

Although the literature lacks clear guidelines on how to calculate minimum sea level clearance of the blades, I decided to operate in similitude with the most recently developed FOWTs, namely the IEA 15 and 22 MW RWT [144,145], where the same length has been set as the minimum tip clearance from the sea. The turbines are installed on semi-submersible platforms with a 20 m freeboard height. The naming scheme of the turbines, shown in **Table 3.1**, reflects the area of interest for the turbines (MED – Mediterranean Sea), the rated power of the machines, and their diameter.

3.2.2 Farm layout

The four turbine designs are used to estimate the overall performance of wind parks in various strategic locations in the Mediterranean Sea. Each farm is supposed to have a total installed capacity of 1.005 GW, i.e., obtained by the deployment of 67 FOWTs. Regarding the electrical infrastructure, one central substation has been included to accommodate the electricity infrastructure needed for the voltage increase needed to deliver electricity through the high voltage alternating current export cables (HVAC). The electricity is transmitted to the point of delivery (POD) onshore using the HVAC technology, considering the reduced costs, with respect to the direct current cables [150], related to an export distance that does not exceed 60 km. In order to simplify the infrastructure needs, any onshore electrical systems have been neglected, assuming the POD is located in close proximity to the shores. Notably, the design does not incorporate an energy storage system, emphasizing direct integration with the grid and focusing only on the production system. As better described in Section 3.4.4, for each installation site, the available area for the wind farm is assumed to be square, with a surface area of 450 km^2. The available sea lot has been assumed oriented with its upper side aligned parallel to the east-west direction for all the test cases.

3.2.3 Wind dataset

Wind speed data is sourced from the ERA5 reanalysis database [151]. A time span of thirty years has been selected, from 1993 to 2023. ERA5 provides the wind source data at a maximum height of 100 m above sea level (a.s.l.). To account for the height difference between the ERA5 data source (100 m) and the turbine hub heights, which range between 130 and 175 m, a power-law shear factor was employed to extrapolate wind speeds. The shear exponent of 0.1 has been selected relying on the findings of Yan et al. [152] for regional offshore conditions, ensuring consistency with expected atmospheric dynamics over the sea.

3.2.4 Installation sites

The installation sites selected for this work have been chosen to represent the several wind resource conditions across the Mediterranean Sea. As shown in **Figure 3.2**a, this water basin experiences a high variability of wind resource. Additionally, even in the most promising sites such as the Gulf of Lyon, there is a significant difference in the energy content with respect to the class I reference Weibull [153]. While the latter experiences an energy density of 340.5 kWh/m^2, the installation site in France is characterized by an energy content of 182.4 kWh/m^2, much closer to the 167.3 kWh/m^2 of the class III reference source. This is also consistent with the average wind speed experienced by the installation sites. These values range between 5.6 and 7.6 m/s, highlighting moderate wind regimes much closer to the 7.5 m/s of the Class III than to the 10 m/s of the Class I [153]. **Figure 3.2**a also shows a comparison between the Class I wind source and the Weibull in an installation site in the Dutch North Sea (Nederwiek) [154], which provides a wind resource similar to the one of the reference class, corroborating the hypothesis that existing offshore wind turbines have been tailored to this sea region.

Table 3.2: Installation sites comparison.

Wind Turbine	Lyon	Sicily	Sardinia	Cyprus
Average WS [m/s]	7.6	7.4	6.4	5.94
Weibull shape factor (k) [-]	1.79	1.89	1.72	1.89
Export distance [km]	20	60	35	25
Average sea depth [m]	85	390	300	350
Prevalent wind direction [-]	W-N-W	N-N-W	W-N-W	W
Source [-]	[156]	[157]	[158]	

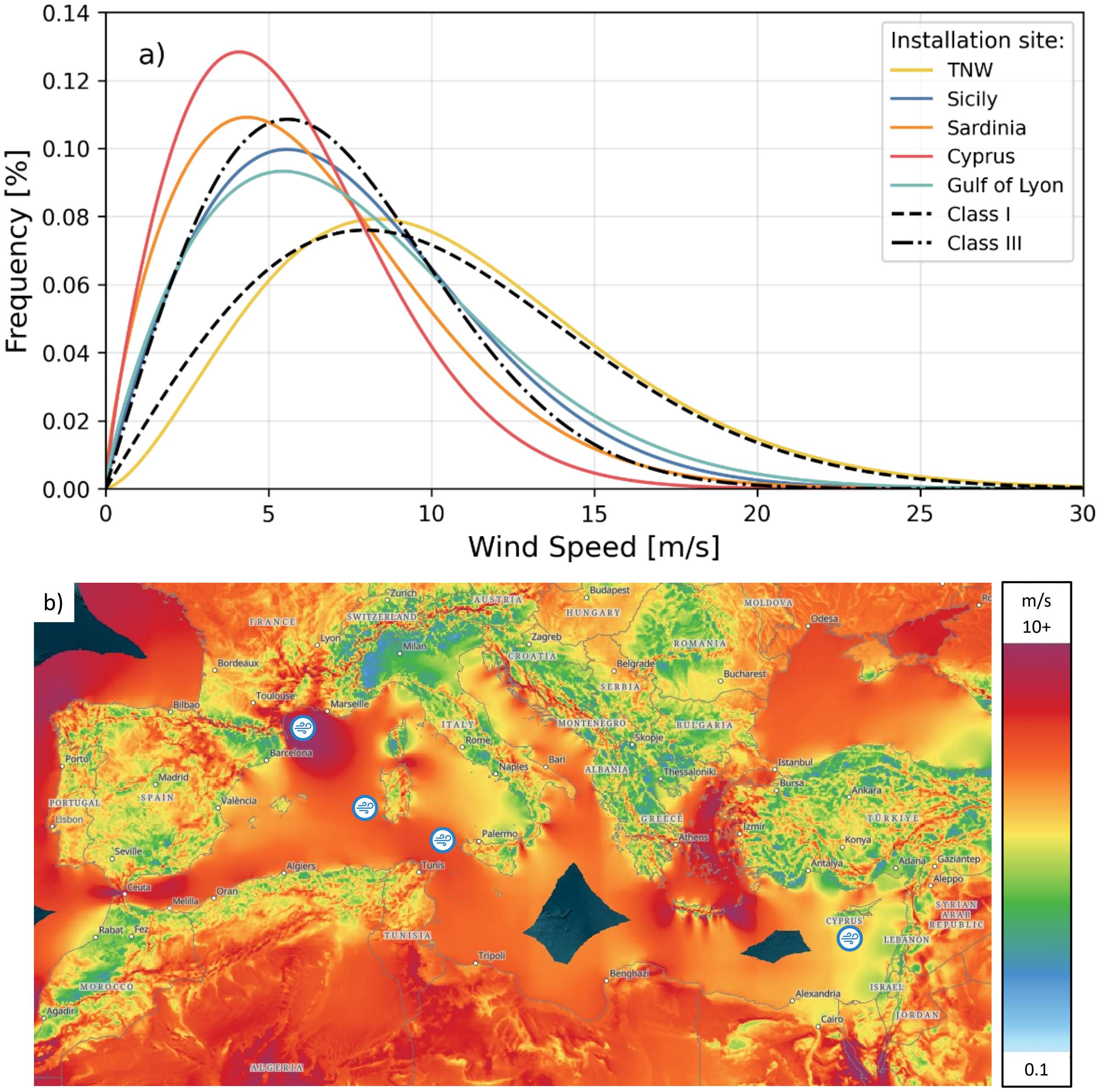

Figure 3.2: Comparison between the Weibull (a) of the considered installation sites (b) at 100 m asl. Wind speed map from Global Wind Atlas[1].

[1] map obtained from the Global Wind Atlas version 3.3, a free, web-based application developed, owned and operated by the Technical University of Denmark (DTU). The Global Wind Atlas version 3.3 is released in partnership with the World Bank Group, utilizing data provided by Vortex, using funding provided by the Energy Sector Management Assistance Program (ESMAP). For additional information: https://globalwindatlas.info

As shown by the contour map in **Figure 3.2**b [155], the chosen sites in the Mediterranean range from Cyprus, characterized by the lowest average wind energy, to Lyon, which experiences the most favorable wind conditions. Overall, a significant range of “moderate” wind scenarios is considered, allowing for a robust assessment of the LSP turbine technology.

Table 3.2 summarizes the main characteristics of selected installation sites.

3.3 FOWT cost and scaling models: review and critical assessment

Despite the presence of some cost and mass scaling laws in the open literature, WT upscaling in unconventional offshore environments represents a gap in existing research. While a few approaches have been proposed in previous studies, they consider the upscaling of both rotor swept area and installed power [159], and do not match the purpose of this analysis. Other validated cost and mass scaling models proposed in the literature [125,160] instead focus on onshore or fixed-bottom WTs. In alternative, as shown in section 3.1.1, many of the existing studies propose approaches in which the full aeroelastic design of a wind turbine is performed. In the next sections, a novel, simpler approach is proposed based on a synthesis of the most credited data available both in the relevant academic literature and in industry reports. This system-level method entails the adoption of scaling laws for the replacement of the complex algorithms and procedures needed for the structural and aerodynamic design of aerogenerators. Therefore, it allows for easy preliminary analyses on the feasibility of a WT with a fixed specific power in an installation site characterized by a known Weibull curve, while remaining physically consistent. As discussed, this complex assessment is key if one wants to get a sufficiently reliable overview of the problem, since all the studies presented to date fail in capturing the complex implications of upscaling FOWTs.

3.3.1 Rotor performance

In order to isolate the effect of specific power variation on LCoE and avoid the results being affected by a specific aerodynamic design, the IEA 15MW FOWT [144] is taken as a reference. The scaled rotors defined in this study are assumed to be aerodynamically similar and have the same performance maps in terms of power, thrust, and torque coefficients of the reference rotor [161]. While representing a simplification, this assumption is thought to be quite realistic, as the aerodynamic efficiency of the reference rotor is still at the edge of current standards. The power output of a wind turbine can be expressed as a function of the wind speed, power coefficient, and the rotor area as in Eq. 3.1:

$$P = \frac{1}{2} * \rho * A * Cp(\lambda, \beta) * WS^3 \qquad 3.1$$

where ρ represents the air density, A the WT swept area, and Cp the power coefficient as a function of the main turbine operating parameters, tip-speed ratio, and blade pitch angle. As Eq. 3.1 indicates, in the assumption that the same power coefficient can be maintained, the power output scales favorably as the swept area increases. If power in Eq. 3.1 is fixed to the design, or rated, power output, the rated wind speed (WS_{DES}) (Eq. 3.2) at which such power is produced decreases as the swept area increases:

$$WS_{DES} = \sqrt[3]{\frac{P_{DES} * 2}{A * Cp * \rho}} \quad 3.2$$

Therefore, an increase in specific power in the form of an increase in rotor diameter while maintaining generator power constant results in a shift to the left of the wind turbine power curve.

Similarly to power output, thrust (T), the total axial aerodynamic force of the rotor, can also be expressed as a function of swept area and wind speed as in Eq. 3.3:

$$T = \frac{1}{2} * \rho * A * Ct(\lambda, \beta) * WS^2 \quad 3.3$$

where Ct is the thrust coefficient of the rotor. Both these high-level parameters are important as power directly influences turbine output and plant revenue and thrust is directly correlated to aerodynamic loading on the structure and also influences wake strength and development. Both parameters, however, cannot be estimated directly but rather depend on the operational parameters λ (tip-speed ratio – TSR) and β (blade pitch angle), which in turn depend on the specific rotor aerodynamic design. Assuming similarity to the IEA 15MW FOWT, the operational strategy can be determined. If the rotor speed is between the minimum (ω_{min}) and maximum (ω_{max}) the rotor operates at the IEA 15MW design TSR of 9, where optimal performance is reached. The TSR is defined in Eq. 3.4:

$$\lambda = \frac{\omega R}{WS} \quad 3.4$$

The minimum and maximum rotor speeds can be derived in analogy to the IEA 15MW by imposing that the scaled rotors operate at the same TSR as the reference turbine at cut-in (Eq. 3.5):

$$\lambda = \frac{\omega_{IEA15}^{cut-in} R_{IEA15}}{WS_{IEA15}^{cut-in}} = \frac{\omega_i^{cut-in} R_i}{WS_i^{cut-in}} \quad 3.5$$

Which leads to:

$$\omega_i^{cut-in} = \frac{R_{IEA15}}{R_i} * \frac{WS_i^{cut-in}}{WS_{IEA15}^{cut-in}} * \omega_{IEA15}^{cut-in} \quad 3.6$$

Eq. 3.6 relates the cut-in rotor speed to the radius of the reference and scaled machines, to the cut-in rotational speed of the reference machine and to the cut-in wind speed of the reference and scaled turbine. The latter parameter, however, is unknown. This limitation can be overcome by imposing that the scaled turbines must produce the same power as the reference IEA 15MW machine at cut-in (Eq. 3.7):

$$P_{cut-in} = \frac{1}{2} \rho \pi R_{IEA15}^2 C_p {WS_{IEA15}^{cut-in}}^3 = \frac{1}{2} \rho \pi R_i^2 C_p {WS_i^{cut-in}}^3 \quad 3.7$$

Eq. 3.7 can be inverted and simplified to obtain Eq. 3.8:

$$\frac{WS_i^{cut-in}}{WS_{IEA15}^{cut-in}} = \left(\frac{R_{IEA15}}{R_i}\right)^{2/3} \tag{3.8}$$

Which allows the cut-in wind speed of the scaled rotors to be determined. Finally, if this expression is substituted into Eq. 3.6, the cut-in minimum rotor speed (Eq. 3.9) is determined:

$$\omega_i^{cut-in} = \left(\frac{R_{IEA15}}{R_i}\right)^{5/3} * \omega_{IEA15}^{cut-in} \tag{3.9}$$

The same procedure is then repeated at the rated wind speed, where all designs must output 15MW of power, to determine the nominal rotor speed and rated wind speed. If the rotational speed required to maintain the optimal TSR of $\omega = \lambda WS/R$ is lower than the minimum rotational speed as determined in Eq. 3.9, the rotor operates at the minimum rotational speed.

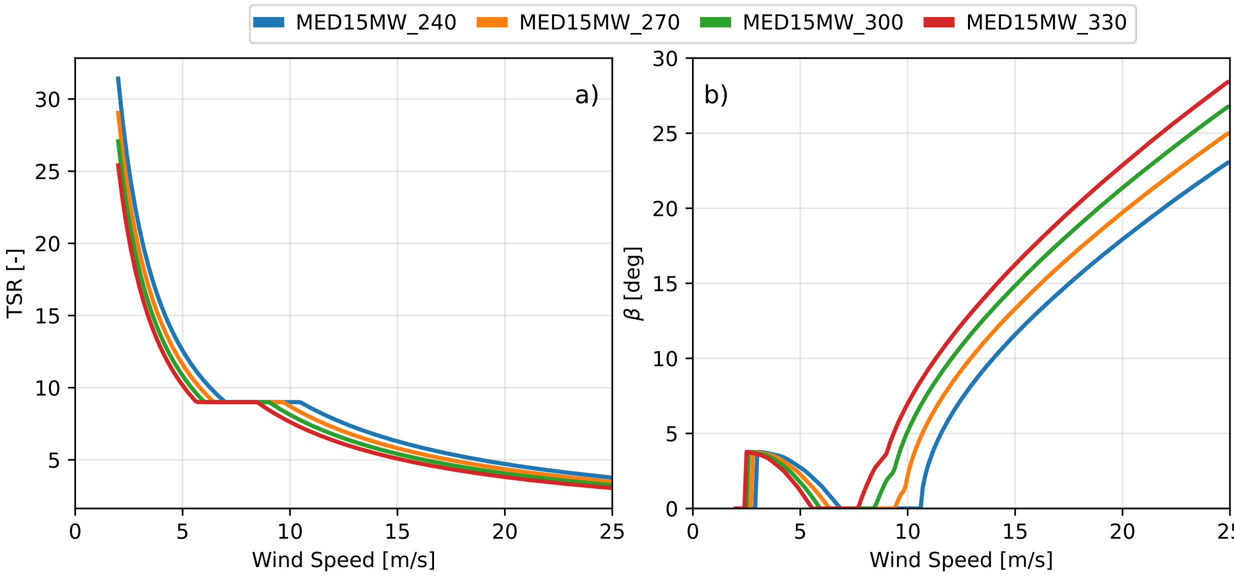

Figure 3.3: WT power curves in the laminar (a) and turbulent (b) free stream wind conditions.

A power-maximizing pitch angle is numerically selected for the resulting TSR from the *Cp* map, ultimately resulting in the non-zero pitch angle shown in **Figure 3.3**b when the TSR (shown in **Figure 3.3**a) exceeds the IEA 15MW-nominal value of 9. As shown in **Figure 3.3**, four different aerodynamically similar rotors have been evaluated in this study, with diameters, ranging from 240 to 330 m, in a 30 m step, corresponding to a specific power that ranges from 331.6 to 175.4 W/m^{2,} respectively. Once the operational point is set, rotor power and thrust can be determined from the *Cp* and *Ct* maps, respectively. The obtained values of thrust and power are shown in **Figure 3.4** and **Figure 3.5.**

In order to limit the aerodynamic loads on the upscaled rotors, peak shaving, whereby the blades of the turbine are feathered before rated power is reached in order to shave load, is also implemented. As better explained later in the study, the use of peak shaving is a common load-reduction technique and is especially significant in load-constrained LSP rotors. As shown in [145], this technique allows for significant peak load reduction with often minimal AEP losses. The effect of this strategy is highlighted in the rotor thrust curves in **Figure 3.4**. In addition, the increase in blade pitch required to limit rotor thrust can be seen in **Figure 3.3**b, where all curves except the one relative to the MED15MW_240 FOWT, which does not employ peak shaving, feature a more gradual "knee" before the rated wind speed. From a model perspective, if rotor thrust exceeds a user-specified threshold, the pitch angle that is able to satisfy the imposed constraint is determined numerically from the *Ct* response curve. Finally, the newly determined combination of TSR and pitch angle is then used to determine rotor power.

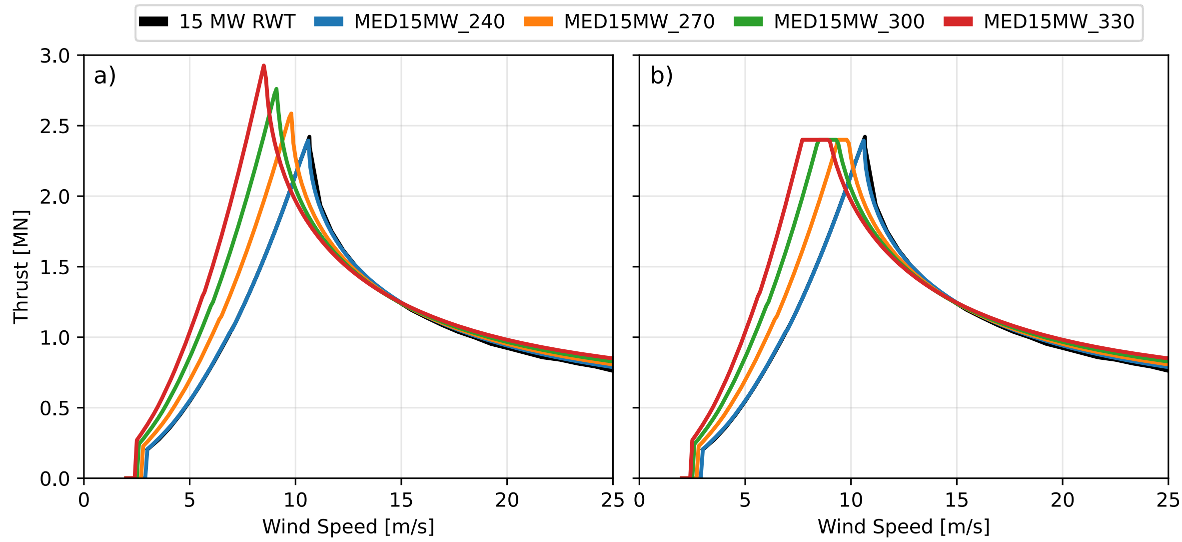

Figure 3.4: WT thrust curves without (a) and with (b) active pitch control.

In the final step, rotor power is corrected for the effect of turbulence intensity using the empirical model of Saint-Drenan et al. [162], using the average turbulence intensity from the FINO1 [163] offshore installation site as representative of the turbulence intensity in a generic offshore site. The effect of turbulence intensity (TI) on the rotor power curve is shown in **Figure 3.5**. This effect has been neglected in almost all the techno-economic feasibility studies presented to date on the topic, but it is thought to have a non-negligible effect on the final results, especially around rated wind speeds.

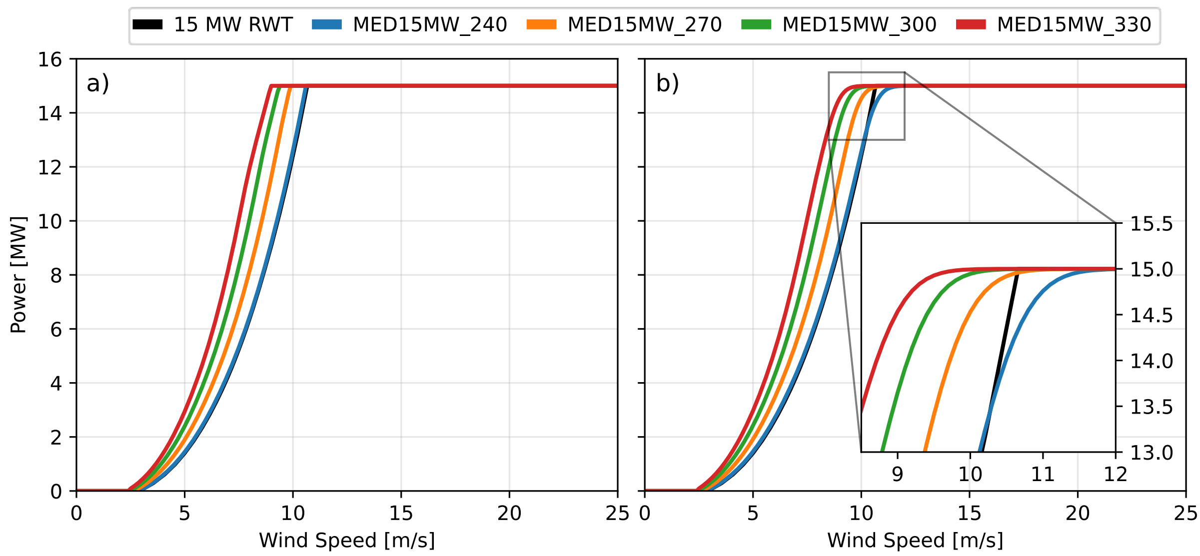

Figure 3.5: WT power curves in the laminar (a) and turbulent (b) free stream wind conditions.

3.3.2 Component mass and cost

Changing rotor-swept areas leads not only to a different performance of the turbine, but also to different loads. In turn, changing the loads means that the structural properties and cost of the turbine change. In order to account for the effect of such load changes, without performing a complete re-design of the machine, a simplified correlation-based approach has been prioritized.

3.3.2.1 Tower

The NREL cost and scaling model [125] is used as a basis to determine the mass and, consequently, the cost of the FOWT towers. In analogy to this model, the mass of the tower (M_T) as a function of its height (L_T) is determined according to a power law $M_T = \alpha L_T^{\beta}$. Floating towers are generally designed to be stiff-stiff, with natural frequencies placed above the 3P excitation range. As such, mass scaling correlations determined for onshore towers are inaccurate if applied to FOWTs. Therefore, in order to calibrate the law an extensive literature review has been performed. However, due to the deployment of only a few demonstrators, only the seven sources listed in **Table 3.3** have been included. Starting from the existing literature, a correlation has been developed relying on the relationship between M_T and L_T. The trendline resulting from the fitting reported in 3.10 has been adopted to obtain the M_T of the new WTs relying only on their L_T.

$$M_T = 1479.457 * L_T^{1.396} \tag{3.10}$$

Figure 3.6 and **Table 3.3** show the results of the fitting for the MED FOWTS (orange points). The outcomes obtained show a good agreement with the literature data, highlighted by the trendline coefficient of determination (R_2) equal to 0.8.

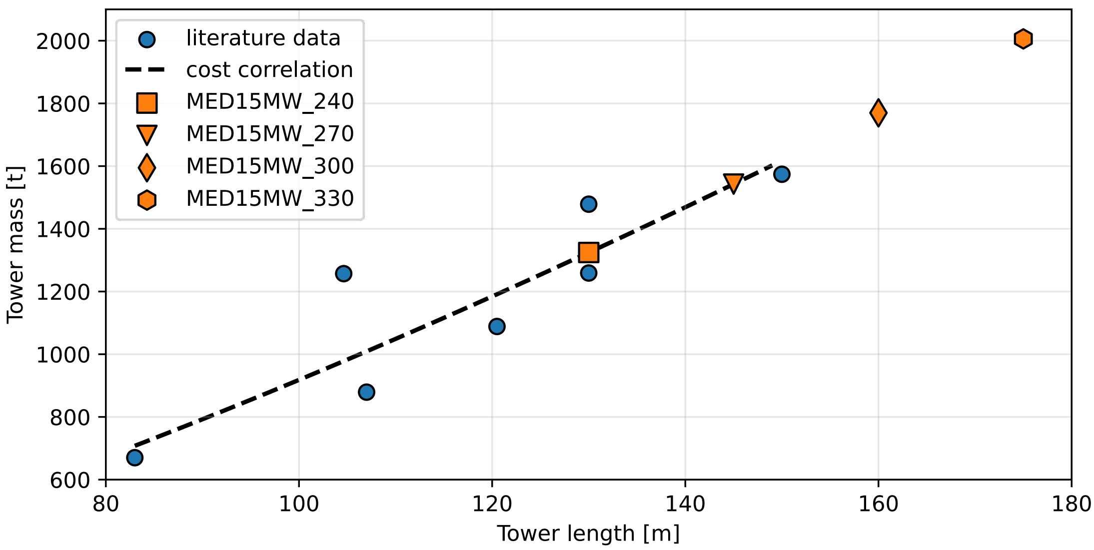

Figure 3.6: M_T literature and proposed data relying on the introduced correlation.

3.3.2.2 Rotor Nacelle Assembly

An approach similar to the one adopted for the tower has also been adopted for the RNA. For the RNA, the DTU mass scaling model has been selected due to its development specifically tailored for offshore wind farms [160]. However, as shown in **Table 3.4**, to estimate the effect of the increased D_R on blade masses, the correlation developed by NREL [125] has been utilized. This model, in fact, allows for the choice of the turbine class, which leads to a more accurate fit for the specific requirements of the test case analyzed.

Table 3.3: Existing and proposed FOWTs' M_T and H_T.

Wind Turbine	P [MW]	H_T [m]	M_T [t]	Source [-]
Hywind	6.0	83.0	670.0	[107]
10 NAUTILUS	10.0	107.0	879.0	[164]
10MW OO-STAR	10.0	104.6	1257.0	[164]
15MW Volturn US-S	15.0	130.0	1259.0	[159]
15MW Corewind	15.0	120.5	1088.5	[165]
IEA-15-240-RWT	15.0	130.0	1478.6	[166]
IEA-22-280-RWT	22.0	150.0	1574.0	[167]
MED15MW_240	15.0	130	1324.4	-
MED15MW_270	15.0	145	1542.6	-
MED15MW_300	15.0	160	1769.9	-
MED15MW_330	15.0	175	2005.8	-

Specifically, rotor mass (M_R) has been calculated with Eq. 3.11 in **Table 3.4**, where the exponent is related to class III turbines with carbon fiber spar caps. No additional FOWT-specific calibration was performed as blades are amongst the least affected components, loads-wise, when a turbine is installed on a floating foundation [168,169].

In order to univocally define the center of mass of the turbine (H_{COM}), the mass of the nacelle (M_{NAC}) needs to be accounted for. This parameter accounts for the weight of the nacelle housing *per se*, which is supposed to be independent of rotor size and the internal components. The dependency on D_R for the parts mentioned above is modelled with the DTU mass scaling model as shown in **Table 3.4**. Specifically, the masses of rotor, hub (M_{HUB}), pitch bearings (M_{PB}), pitch system (M_{PS}), and drivetrain bedplate (M_{BP}) are strongly affected by D_R, and an increased rotor swept area leads to increased masses and loads. Regarding the generator (M_{GEN}), equation 3.10 shows a dependency on rated torque (φ_{DES}), which is again directly related to the D_R.

Finally, mass correlations for minor components, such as the nacelle and drivetrain bedplate, can be found in the documentation of the model [160] and are not herein reported.

Table 3.4: Mass scaling equations for the main RNA components.

Component	Mass Equation	Equation number	Source
Rotor	$M_R = 3 * 0.5 * (0.5 * D_R)^{2.44}$	3.11	[125]
Hub	$M_{HUB} = 6 * 10^3 + 0.1 * D_R^{2.5}$	3.12	[160]
Pitch bearings	$M_{PB} = 5 * 10^2 + 0.07 * D_R^{2.5}$	3.13	[160]
Pitch system	$M_{PS} = 5 * 10^2 + 0.03 * D_R^{2.5}$	3.14	[160]
Drivetrain generator	$M_{GRN} = 35 * 10^3 * \varphi_{DES}^{0.7}$	3.15	[160]

To estimate the cost of each of the RNA's components, the cost scaling model developed by DTU has been utilized [160]. Costs are estimated as a function of the component masses. Specifically, Eq. 3.16 shows the linear relation between the cost of the specific component (C_i) and its mass, where β represents the cost scaling factor.

$$C_i = \beta * M_i \tag{3.16}$$

Eq. 3.11 is applied to all RNA components, as well as to the tower and blades. The specific value of β is reported in [160] for each component.

The resulting mass of the WTs is reported in **Table 3.5**, with a focus on the H_{COM}. This parameter has been calculated as in Eq. 3.17, by assuming the RNA H_{COM} at the hub height, and the tower H_{COM} at 40 % of the H_T. This assumption is consistent with the data reported in [166,167], where the average tower center of mass is located at about 40% of the tower height.

$$H_{COM} = \frac{0.4 * L_T * M_T + H_{HUB} * M_{RNA}}{M_{tot}} \tag{3.17}$$

From **Table 3.5** it is apparent how an increased D_R leads to a higher center of mass. In a floating context, this increase is particularly relevant as it affects the overturning moment of the turbine. In addition, **Table 3.5** shows a difference in M_{TOT} and H_{COM} between the 15 MW RWT and the MED15MW_240. In fact, while the IEA reference turbine is a result of a full aeroelastic design, for the proposed turbine the mass scaling relationships mentioned in this section have been utilized. This allowed a fair comparison between the new WT designs.

Table 3.5: Proposed FOWTs' M_R, M_{TOT} and H_{COM}.

Wind Turbine	D_R [m]	M_R [t]	M_{TOT} [t]	H_{COM} [m]	OM_{STD} [MNm]	OM_{PS} [MNm]
IEA-15-240-RWT [166]	240	1478.6	2425.8	92.97	594.4	594.4
MED15MW_240	240	1324.4	2244.2	91.46	569.7	569.7
MED15MW_270	270	1542.6	2521.5	98.72	682.1	650.4
MED15MW_300	300	1769.9	2818.2	106.22	803.9	737.9
MED15MW_330	330	2005.8	3134.2	113.97	936.9	833.2
IEA-22-280-RWT [167]	283	1574.0	2769.5	117.10	784.4	784.4

3.3.2.3 Floater

The floating foundation is designed to keep the installed turbine stable and resist the external actions of the wind and waves. In addition to being able to resist dynamic wind and wave-induced moments, the substructure must be able to resist static forces. Aerodynamic rotor loading is a large part of these overturning forces. As the platform inclines, however, the turbine acts as a reversed pendulum on the structure, and weight forces also tend to overturn the structure. In this respect, the higher the turbine mass and the higher the center of gravity of the turbine, the higher the gravity-induced overturning moment is. While the effect of the component weight cannot be overcome, a reduction of overturning moment can be achieved by reducing peak aerodynamic thrust through the use of peak-shaving. As shown in **Table 3.5**, peak shaving can reduce overturning moment significantly, with reductions that range between 5 and 11% on the current test cases.

The semisubmersible floating platform has been adopted due to its improved stabilization properties and easy installation with respect to the other floaters. The adopted semi-sub geometric configuration consists of three vertical steel columns, interconnected by horizontal pontoons. These columns are partially submerged to provide buoyancy, while the pontoons enhance structural integrity and provide heave damping. The central deck, supported by the columns, houses the WT.

The decrease of WTs' specific power results in the redesign of floating support structures able to deal with enhanced masses and overturning moments. To this end, while scaling laws, which allow for the determination of floater mass from variation in high-level parameters do not exist yet in the industrial field, some approaches have been proposed in the literature. The upscaling method proposed by Wu et al [170] for semi-submersibles focuses on scaling the pitch restoring stiffness proportionally to maintain the maximum static pitch angle. This stiffness is derived from considering the waterplane area moment, submerged volume, buoyancy, and position of the center of gravity. Two distinct scaling approaches are compared to increasing the moment of the waterplane area. The *Distance & Radius Scaling* method simultaneously scales both the column radius and the distance between columns using the same scale factor, while the *Distance Scaling* method adjusts only the distance between columns. Key observations include that increasing column radius increases platform mass and the heave natural period, while increasing column distance elevates the center of gravity and metacentric height but slightly reduces the heave natural period. Design adjustments in the 15 MW reference system mitigate these effects by increasing ballast mass to lower the center of gravity and increasing added mass to lengthen the heave natural period. Despite the accuracy of this method, it implies the geometrical design of the platform. Roach et al [171] developed an upscaling model based on generalized scaling relations. The methodology consists of a variation of the platform geometric parameters, constraining the platform pitch angle under rated wind turbine thrust, and identifies key scaling trends: platform dimensions scale by a factor of 0.75, while steel mass scales by a factor of 1.5, assuming constant wall thickness. Unlike prior studies focused on specific designs, this approach provides scalable relations applicable to other triangular semi-submersible platforms with three outer columns and a centrally mounted turbine. However, this iterative approach involves the adoption of a complete hydrodynamic model. In their work, Sergiienko et al. [172] resumed the standards [173,174] and best practices [175,176] for the design, construction, and maintenance of FOWTs, identifying the main technical parameters: floatability, maximum roll and pitch angle, freeboard height, minimum draught, and dynamic response to wind and waves.

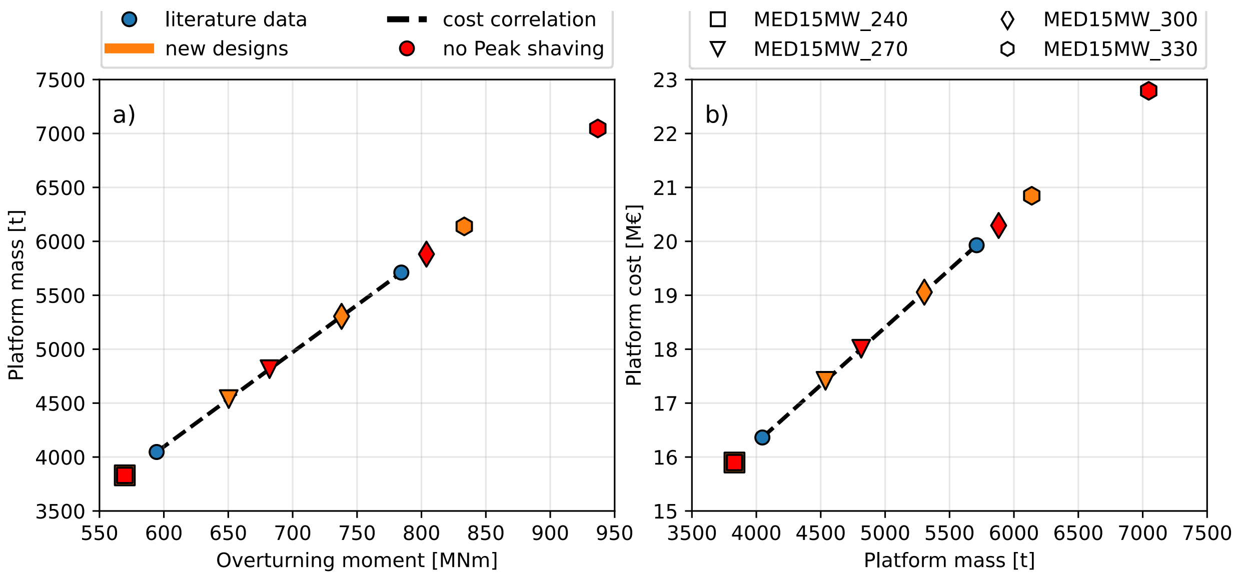

Figure 3.7: (a) platform mass - literature and proposed data relying on the introduced correlation. (b) platform cost - literature and proposed data relying on the introduced correlation. Red markers indicate platform mass and cost of proposed designs without the adoption of peak shaving.

One of the critical design criteria for ensuring the stability of a semi-submersible platform during wind turbine operation is the ability to generate sufficient restoring moments to counteract pitch and roll motions. To prevent the platform from exceeding the maximum allowable static angle of inclination under the largest rotor thrust, the hydrostatic stiffness in pitch and roll must meet the overturning moment, which is mainly caused by weight and aerodynamic thrust.

To this end, in this work, an approach similar to [172] has been adopted. For semi-sub platforms, the total restoring stiffness in pitch is predominantly governed by the contribution from the waterplane area. This contribution can thus be associated with the overturning moment of the upscaled turbine to quantify the resulting increases in mass and costs.

As floating wind turbines are a novel technology, mature cost models for the floating substructures have not yet been developed. From this point of view, the wide variety of existing foundation designs introduces additional challenges. Therefore, the IEA 15MW and IEA 22MW RWTs are used to develop cost and scaling functions, as both machines are installed on a steel four-column semi-submersible foundation. In addition, the geometry of the IEA 22MW foundation was determined through an optimization process using the IEA 15MW design as a baseline [177]. While the external geometry of the floaters has been carefully studied, less consideration has been put into the structural design of the foundations, as they have not been designed in detail. Both the IEA 15MW [178] and IEA 22MW FOWTs [179] feature steel columns of 50 mm in thickness and box-shaped pontoons with a wall thickness of 40 mm, which connect the main columns to the central one. The four columns are also connected via steel trusses above the waterline with a wall thickness of 20 mm. Once the wall thickness and the floaters' external shapes are known, it is possible to compute the steel mass for the columns, pontoons, and braces. The cost is obtained by multiplying the component weight by the manufacturing cost of the stiffened columns of 3120 $/t [180] and of 6250 $/t for pontoons and trusses. These values account for raw material costs and manufacturing, but do not include transportation costs [180]. According to the author's knowledge, the maximum OM is available only for the 15 [166] and 22 MW [167] RWTs proposed by the IEA. To this end, due to a lack of additional data, a linear relationship between OM and the platform mass (M_F) has been developed as in Eq. 3.18:

$$M_F = 0.009 * OM - 1157984.96 \tag{3.18}$$

Figure 3.7 shows the comparison between the new FOWTs and the RWTs in terms of mass. Despite the same rotor-swept area and thrust, it is apparent how the correlation results in a mass decrease from the IEA15-MW-RWT to the MED15MW_240. This is due to the reduced OM already discussed and shown in **Table 3.5**. Furthermore, the effect of peak shaving is clear in this image. The adoption of an active pitch control strategy to mitigate the thrust resulted in mass decreases in the range between 6% and 13%. The same approach has then been adopted to correlate overturning moment and platform cost. To this end, a linear relation between the semi-sub costs (C_F) and the platform's mass has been formulated as in Eq. 3.19:

$$C_F = 2.143 * M_F + 7689597.25 \tag{3.19}$$

The lack of abundant publicly available cost data for floating foundations is a limiting factor of this study. Nevertheless, the methods adopted to estimate the cost and mass of the IEA 22MW and IEA 15MW floaters are aligned with the current state-of-the-art. **Figure 3.8**a shows a comparison between the masses of the semi-sub floaters available in literature (blue dots) and the ones estimated in this study. Despite the relevant amount of data, the values of the overturning moment that the platform has to balance are not available, and correlating these two parameters is not possible. In addition, many datasets do not include cost, as the scarcity of data shown in **Figure 3.8**b demonstrates. Focusing once more on **Figure 3.8**a, an increase in WT swept area is inherently related to an increased overturning moment and thus to heavier floaters. However, this plot shows how technological progress resulted in lighter platforms. The right area of the chart includes recently developed demonstrators or concepts, such as the platforms for the IEA 15 and 22 MW in red, which experience lower estimated masses with respect to WT's nominal power and rotor diameter. Concerning floater costs, **Figure 3.8**b shows the differences between the proposed designs (orange), the literature data (blue dots) and the IEA references wind turbines (red). Information gathered during discussions with industry members, including project developers, consultants, and hull manufacturers is summarized in the shaded areas in **Figure 3.8**b. According to such industry insiders, the cost of European-manufactured steel hulls, represented by the green-colored ellipsis, is now more than double that of the Chinese-manufactured floaters, which are currently the most competitive on the market. However, these costs are based on projections of a limited number of units produced. The cost estimations performed in this work assume the development of technology combined with large-scale commercialization.

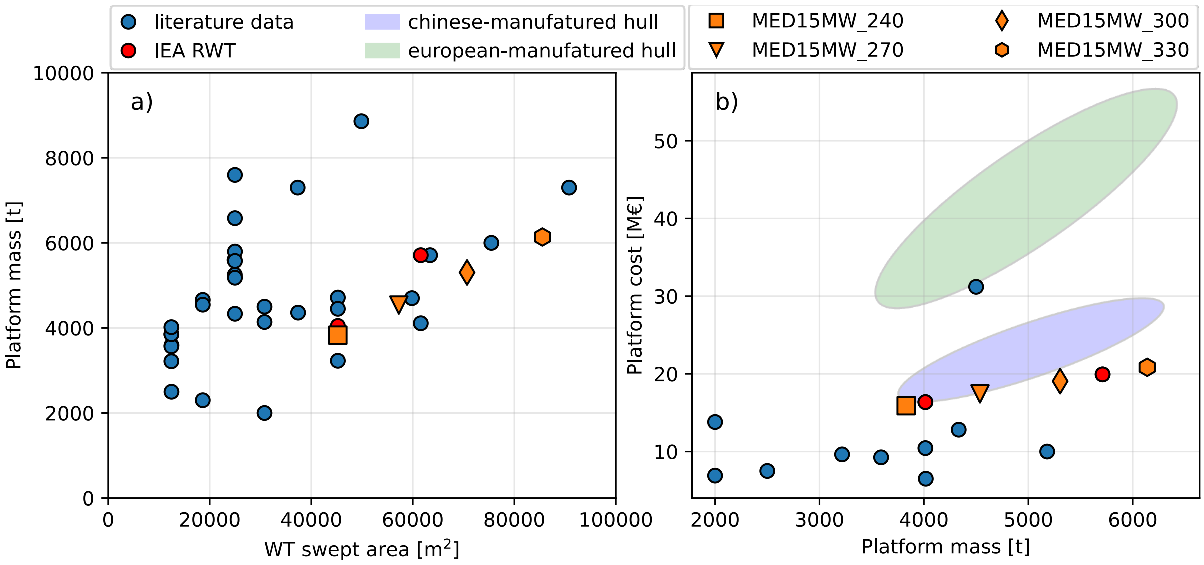

Figure 3.8: Comparison between the results and literature data for platform masses and costs.

Delving more in-depth, the marginal cost of the turbine components, as determined using the cost and scaling functions developed in this section, is summarized in **Figure 3.9:** WT CAPEX breakdown for the designed aerogenerators.. The platform represents about 55% of the whole turbine cost. This is consistent with a reduction of about 5% of the total cost due to the implementation of peak shaving.

Focusing on the economic impact that the swept area increase has on the cost of the single component, it is apparent how, while the weight of most of the WT components decreases with respect to the total cost, the impact of the rotor and tower increases. This is consistent with the assumptions adopted in the cost scaling method proposed, where the rotor price shows the highest sensitivity to the size. However, while the impact of peak shaving has been considered in terms of its effect on wind turbine performance, it has not been considered in terms of its potential to decrease the rotor weight. In fact, the reduction of maximum thrust on blades may lead to a reduction in structural material in the rotor, due to the lower loads, and thus to a CAPEX reduction. No cost and scaling function that accounts for the effect of peak shaving on rotor mass has been found at the current stage and this effect can currently be considered only by performing a full aero-elastic design.

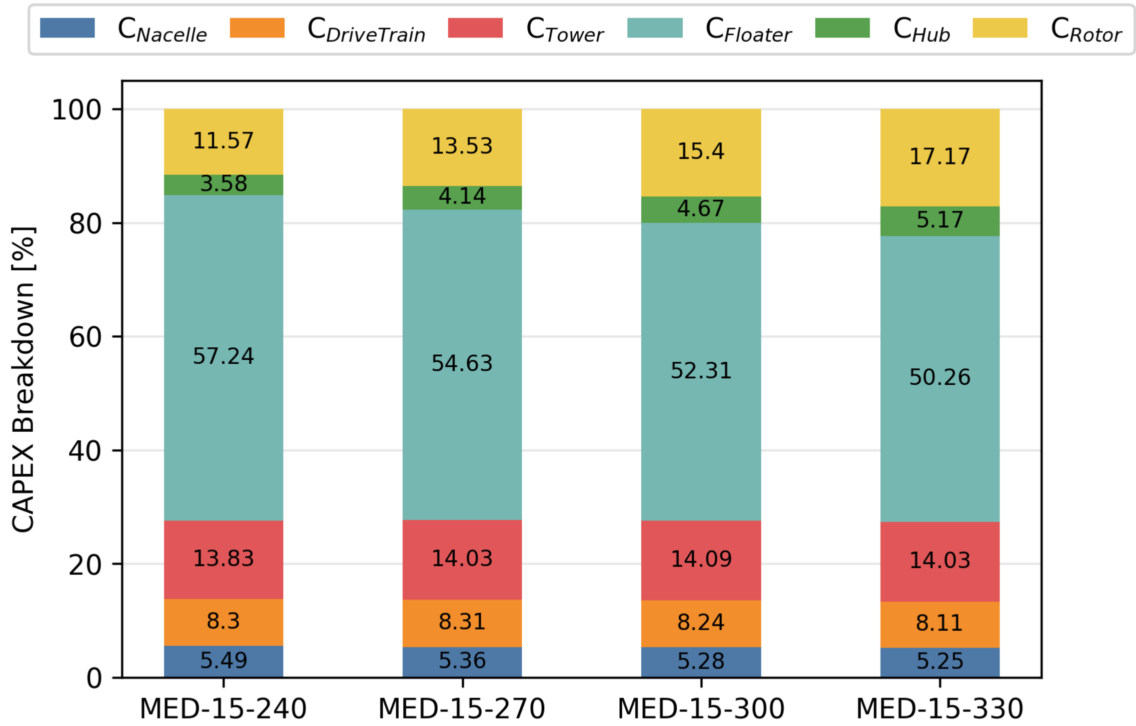

Figure 3.9: WT CAPEX breakdown for the designed aerogenerators.

The results presented in this study can therefore be assumed to conservatively favor the smaller rotor designs, which feature less peak shaving, from an economic point of view. Finally, looking at **Figure 3.9**, insights into how to reduce the WTs CAPEX can be provided. It is apparent that the floater has the highest weight on cost. While the other components have already experienced a large deployment, both in onshore and offshore environments, floating platforms represent the less developed and widespread technology, counting only a few demonstrators. To this end, due to its large share of total costs, lowering floater costs has the potential to drive down overall FOWT LCoE.

3.3.3 OPEX increase

Besides the increased capital requirements due to the larger swept areas, as rotor size increases, OPEX is also expected to rise [9,19,35]. The adoption of larger rotors with more flexible blades introduces relevant alterations in the aeroelastic behavior of the WT, resulting in larger mechanical stresses. These enhanced loads have the potential to activate novel failure mechanisms within the turbine, leading to variations in failure rates and necessitating the implementation of alternative and potentially more expensive maintenance strategies [181]. However, few research efforts have been made on analyzing the impact of the specific power decrease and rotor upscaling on operational costs [168]. In this study, the approach proposed by Mehta et al. [118] has been adopted. Specifically, operational costs encompass several factors such as insurance, logistics, and other associated expenses, while maintenance costs include both preventive and corrective maintenance for the turbine and the balance of plant. While the total OPEX depends on multiple variables unrelated to the WT swept area per se, such as number of turbines and rated power, vessel costs exhibit a linear scaling relationship with the rotor diameter [182] to mimic the costs faced during actual operation of floating offshore systems, which require different vessel types and times to perform repairs as rotor size increases. To this end, the DTU scaling model has been modified in order to assess these $OPEX$ variations by including a multiplication factor estimated through the ratio between the reference and the actual rotor diameter, as in Eq. 3.20:

$$OPEX_{NEW} = OPEX_{BASE} * \frac{D_{NEW}}{D_{BASE}} \tag{3.20}$$

where the subscripts new and base represent the turbine with the increased diameter and the reference one, respectively.

3.4 Optimization model

In this study, the TopFarm wind farm analysis and optimization framework [183], developed by the DTU, has been adopted to determine the optimal wind turbine and cabling layout that minimizes LCoE in a specific location. TopFarm enables comprehensive and efficient exploration of design variables while balancing conflicting objectives such as maximizing energy production and minimizing costs, by implementing optimization strategies. The optimization model, focusing on the intra-farm wake loss calculation strategy, IA cable layout optimization, and the definition of the objective function and constraints is presented in this section.

3.4.1 Power production assessment

PyWake [184] is a Python-based wind farm simulation tool designed to model the performance of wind farms under various conditions. It has been adopted to estimate the AEP of a WF layout in a specific site. Several key factors collectively influence the AEP of a WF layout, the wind resource, turbine characteristics, and the interactions between turbines within a wind farm. The wind farm model integrates the site information, wind turbine model, and wake model on the entire wind farm computing key metrics such as the annual energy production (AEP), wake losses, and turbulence intensity for the specified wind farm layout and wind resource conditions.

The installation site determines the long-term average wind speed, which is described using Weibull curves, and the wind rose, which specifies the directionality of the wind. As specified in Section 3.2.3, the long-term statistical representation of the site is obtained using one-hour average data from the ERA5 reanalysis database [185] at 100 m above sea level. Additional environmental factors, such as surface roughness and terrain effects have been neglected due to the offshore installation. The average wind speed is scaled from 100 m to the turbine hub-height using a power law with an exponent of 0.11, typically adopted in an offshore environment [186]. The adoption of a statistical approach ensures good accuracy for the calculation of the LCoE, and the upgrade to a time-dependent strategy would only have resulted in a computational cost increase.

The wind turbine is modelled through the turbine's power curve, which relates wind speed to power output and the thrust curve, which determines the extent of momentum extraction by the turbine and, consequently, the intensity of the wake for a given wind speed.

The wake model describes the time-averaged behavior of the wake generated by each turbine, including how it expands and impacts the downstream WTs, predicting the velocity deficit and turbulence intensity within the wake. In this work, the Bastankhah model has been adopted [187]. This advanced analytical wake model describes the wake as a Gaussian profile, capturing a more realistic distribution of velocity deficits and turbulence [188] with respect to simpler approaches [189]. The "LinearSum" model has been adopted [190] to estimate the effective wind speed at each WT location within the farm given by the superposition of different wakes. To account for partial overlapping between a downstream rotor and an upstream wake, the Gaussian overlapping model available within PyWake has been adopted, in accordance with existing guidelines [191]. Finally, the turbulence models in PyWake are utilized to estimate the added turbulence in the wake from one aerogenerator to downstream WTs within the wind farm. Pywake's "GCLTurbulence" has been adopted herein [192].

3.4.2 IA cables layout

Two different strategies can be used in TopFarm to determine the total inter-array cable length: the simplified approach proposed in [193] and the detailed tool Edwin [194]. The two approaches differ in several key details.

The basic optimization model adopted is a reimplementation of the *Travelling Salesman Problem* (TSP). It is representative of the behavior of a salesman who must visit multiple locations while minimizing travel distance. The adoption of this approach is reasonable, especially for onshore wind turbines, where IA cables often follow maintenance roads connecting the turbines. Once the grid optimization is performed, the cable costs are estimated by multiplying the specific costs by the total length of the IA network. In addition to the TSP assumption, the electrical cables used to connect the wind turbines within a wind farm are designed to carry specific voltage levels, which define the maximum number of turbines that can be connected per cable. However, such design constraints that introduce a higher level of complexity are not considered in [193], and the model assumes idealized cables capable of transmitting all the electricity produced by the connected turbines.

As an alternative, Edwin relies on the Esau-Williams heuristic algorithm developed by Souza de Alencar [195]. The algorithm minimizes the total cable length by identifying sub-optimal solutions that closely approximate exact solutions. The Esau–Williams heuristic is applied by constructing a minimal-cost spanning tree for a graph with designated roots, nodes, and capacity constraints. In this study, the offshore substations serve as the roots of the spanning tree, while the FOWTs act as the nodes as shown in **Figure 3.10**. The algorithm permits sub-branches along a given string while ensuring that the maximum number of nodes per string is not exceeded. Edwin includes actual cable constraints, such as the maximum voltage allowed by the electrical network and the section of the cables, defining the number of WTs that can be connected. Additionally, it enables the optimization of the location of the offshore substation within the wind farm.

Both approaches have been tested during the model build-up phase. According to the preliminary results, Edwin leads to relevant cost savings, with cable length decreases up to 50 km. In addition, despite the increase in computational burden, the resulting IA cable layout is more realistic. To this end, this tool has been included in the wind farm layout optimization framework for the analyses performed.

Concerning the IA cable specification, the same component adopted in [128] has been chosen. Specifically, cables characterized by a cross-section of 800 mm^2 and a nominal capacity of 90 MW have been selected as a valuable option, allowing for the connection of a maximum of 6 FOWTs per cable. This, combined with the spatial distribution of the aerogenerators, resulted in six cables connecting six WTs and five cables connecting five WTs for all the analyzed configurations.

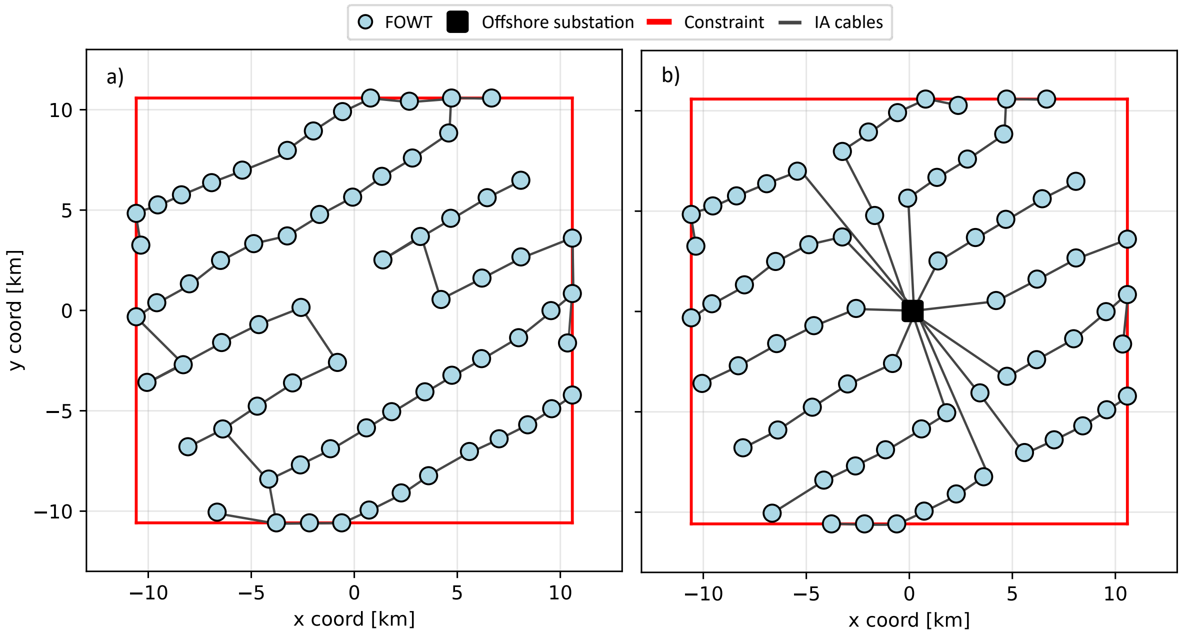

Figure 3.10: Optimal IA cable layout obtained with the TSP reimplementation (a) or Edwin (b).

3.4.3 Objective function

This study utilizes LCoE as the objective function for the optimization problem. LCoE provides a holistic approach by accounting for all elements impacting generation costs, such as CAPEX and OPEX. It is calculated as the ratio of the total discounted costs incurred over the facility's lifetime (n) to the total discounted energy output (E_{prod}) over the same period. As the electricity is derived from a renewable source, fuel costs are not included, as shown in Eq. 3.21, where r represents the interest rate:

$$LCoE = \frac{\sum_{y=0}^{n} \frac{CAPEX_y + OPEX_y}{(1+r)^y}}{\sum_{y=0}^{n} \frac{E_{prod,y}}{(1+r)^y}} \qquad 3.21$$

3.4.4 Wind farm optimization algorithm

The optimization process in this study is driven by the capabilities of the TopFarm framework, which leverages computational tools to solve the complex, multidisciplinary problem of wind farm design. At its core, TopFarm utilizes the OpenMDAO library [196], a powerful open-source framework developed for multidisciplinary optimization, to link the modules within the optimization tool. The core of the optimization process is shown in **Figure 3.10**. The optimization framework proposed operates as an iterative process, as shown in **Figure 3.11**, aimed at minimizing the LCoE. In each iteration, a new WF layout is evaluated. The process begins by estimating the Annual Energy Production (AEP) of the proposed layout using the PyWake library. Then the optimal layout of the inter-array cables is determined by solving the sub-optimization problem described in the previous section. This problem focuses on minimizing the total cable length while the location of the WTs is fixed. Once the cable layout is optimized, the framework estimates the CAPEX and OPEX for the current wind farm configuration using the cost models presented in detail in Section 3.3. This leads to the calculation of the LCoE as a final step. The newly calculated LCoE is then compared with the value obtained in the previous iteration. This comparison continues across iterations until the convergence criterion is met. Specifically, convergence is reached when the change in the objective function between iterations is below the predefined tolerance value, set at $1*10^{-8}$.

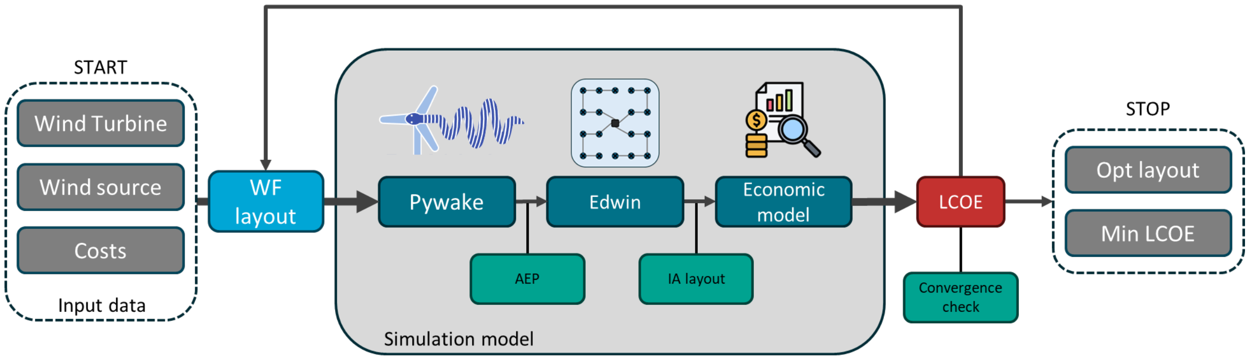

Figure 3.11: Schematic representation of the optimization model.

In this study, the “Constrained Optimization BY Linear Approximations” optimization algorithm (COBYLA) has been employed, a local-search method that does not rely on gradient computation. COBYLA is a gradient-free optimization algorithm that uses linear approximations to solve non-linear, constrained optimization problems. This makes it particularly well-suited for problems involving discontinuities or non-smooth objective functions, such as those arising from the interaction of turbine wakes or discrete design variables like turbine selection.

3.4.5 Constraints

The optimization model used in this study encompasses several essential constraints to ensure that the wind farm design is both feasible and aligned with technical, regulatory, and operational requirements. One of the key constraints is the minimum turbine distance, which ensures the required separation between turbines needed to preserve structural integrity. This distance is typically defined as a multiple of the turbine D_R, following industry standards to balance energy yield with turbine durability and operational reliability. Specifically, $4D_R$ has been set as the minimum WT spacing, according to the guidelines proposed in [197–199]. **Figure 3.12** shows a schematic representation of the minimum IA distance for floating offshore wind turbines. The report [200] published by the consortium composed of BVGA associates, Catapult, The Crown Estate, Crown Estate Scotland, and Floating Offshore Wind Centre of Excellence, presents a detailed description of the best practices for FOWTs. Specifically, it states that the WT displacement allowed by the mooring lines corresponds to around 35% of the sea depth of the installation sites. Therefore, taking the IEA-15-240-RWT and a sea depth of 160 m as a reference, the allowed motion is equivalent to 0.25 D_R for each WT, and the distance between the WT and the column where the mooring is connected ranges between 0.2 D_R and 0.3 D_R [201]. It is apparent that the minimum distance needed is about two D_R, which reaches the amount mentioned in [197–199] with an appropriate safety factor.

The wind farm design is also restricted to a predefined allowed sea lot for installation, reflecting the geographic and regulatory limitations of the site. Although not specifically evaluated in this study, and despite constraining a wind farm to a specific area may not lead to the global minimum LCoE, wind farms are often assigned specific sea lots. These constraints are generally defined in order to account for neighboring environmental exclusion zones, land-use policies, or proximity to infrastructure like shipping lanes or residential areas.

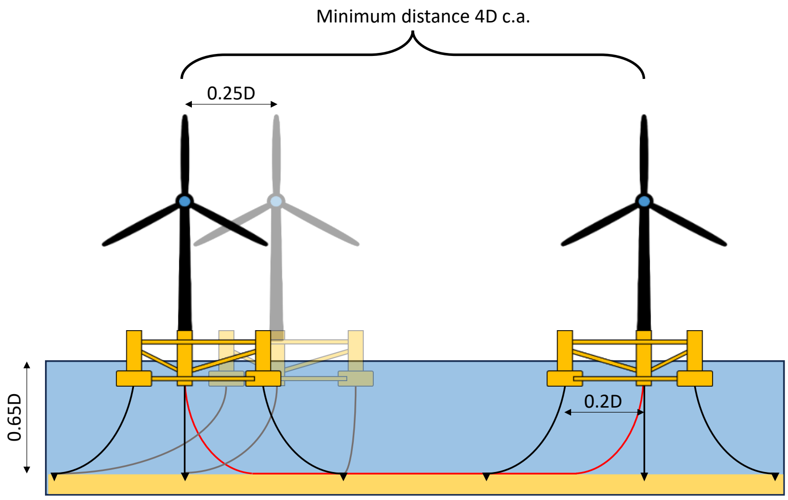

Figure 3.12: Scheme for minimum IA distance between WTs.

In this study, the wind farms are constrained to a 450 km^2 lot. While a rectangular sea lot may affect the WT location with respect to the prevalent wind direction, a squared one enables a comparison *ceteris paribus* between the different case studies proposed. Although true independence from wind directionality would have been achieved by using a circular installation area, this shape has never been adopted for offshore wind farms, which are generally polygon-shaped according to the author's knowledge.

3.5 Results

This section makes use of the optimization model synthesized in Section 3.4 to critically assess the potential of LSP rotors in the four installation areas in the Mediterranean Sea that were selected as representative of those average-wind speeds areas that are under study worldwide to expand FOWT technology. It is worth remarking that the outcomes presented in this section refer to the 1GW wind farm layout resulting from the proposed holistic optimization model and are therefore thought to represent the most realistic estimations at hand for possible industrial application of the technology.

3.5.1 Technical results of the optimization

Figure 3.13 shows the energy production potential in the four selected sites and apparently demonstrates how the strategy adopted for the reduction of the specific power increased the

AEP in all cases. However, the variation (Δ) of AEP with respect to the one obtained with the 240-meter diameter rotor is affected by the Weibull curve of the specific site. In fact, while Lyon shows the most promising wind speed distribution (**Figure 3.2**) and the highest AEP for all the tested rotor diameters, it experiences the lowest benefits from the increase of swept area (**Figure 3.13**b).

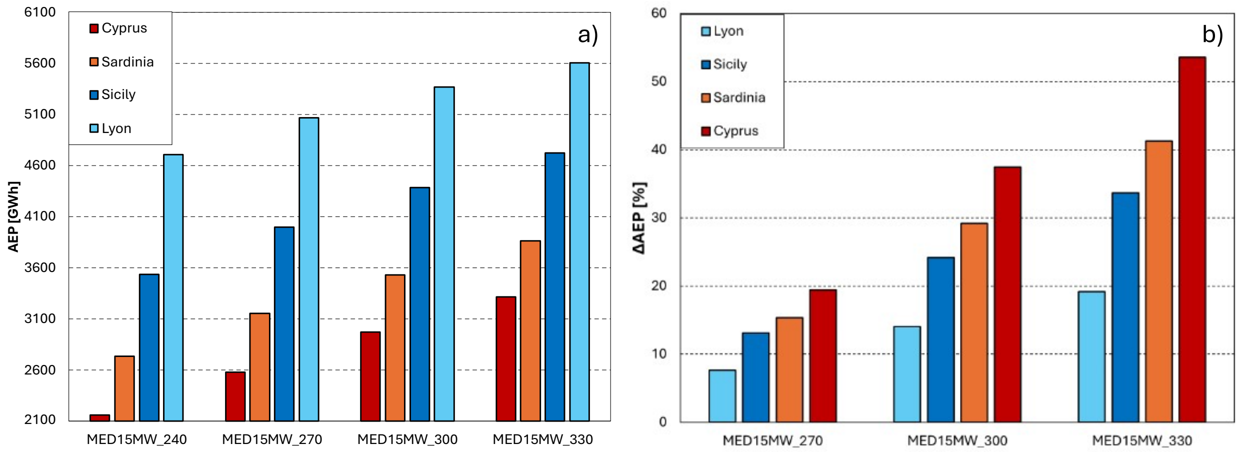

Figure 3.13: Comparison between the AEP and the AEP variation in the different installation sites for the new aerogenerator designs.

On the other hand, while Cyprus is characterized by the worst wind source (as testified by the low AEP in **Figure 3.13**a, it is the site experiencing the highest improvements. These trends are consistent with the assumption behind this work, which promotes the installation of larger blades to enhance wind energy exploitation at the lower wind speeds in the Weibull distribution. Additionally, the distribution of the AEP with respect to the wind speed improves the understanding of these results. **Figure 3.14** shows the energy production potential of the 1GW wind farm in the French and Cypriot sites for the MED15MW_240 and MED15MW_330, respectively. While the AEP of the French case is higher for both aerogenerators, the installation site in Cyprus benefits more from the specific power decrease, as the opportunity for AEP improvement are greater the more time the turbine spends below rated power.

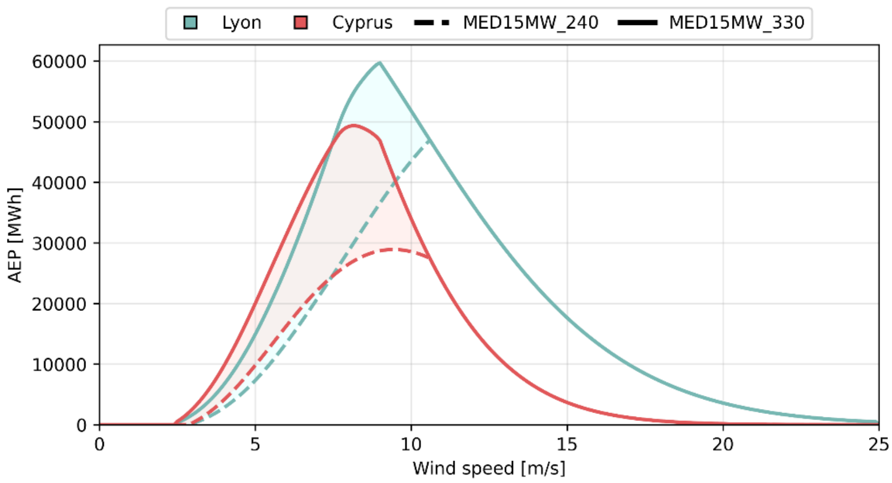

Figure 3.14: Comparison between the AEP distribution in the French and Greek installation sites for the MED15MW_240 and MED15MW_330.

Further considerations can be made by looking at the wind speed deficits induced by wakes. As shown in **Figure 3.4**, lower specific power leads to higher maximum thrust at reduced wind speeds, resulting in stronger wakes. Additionally, larger rotors extend the length of the wake, increasing its area of influence. These effects are depicted in **Figure 3.15**, where the difference in the downwind speed deficit between isolated MED15MW_240 and MED15MW_330 rotors is shown.

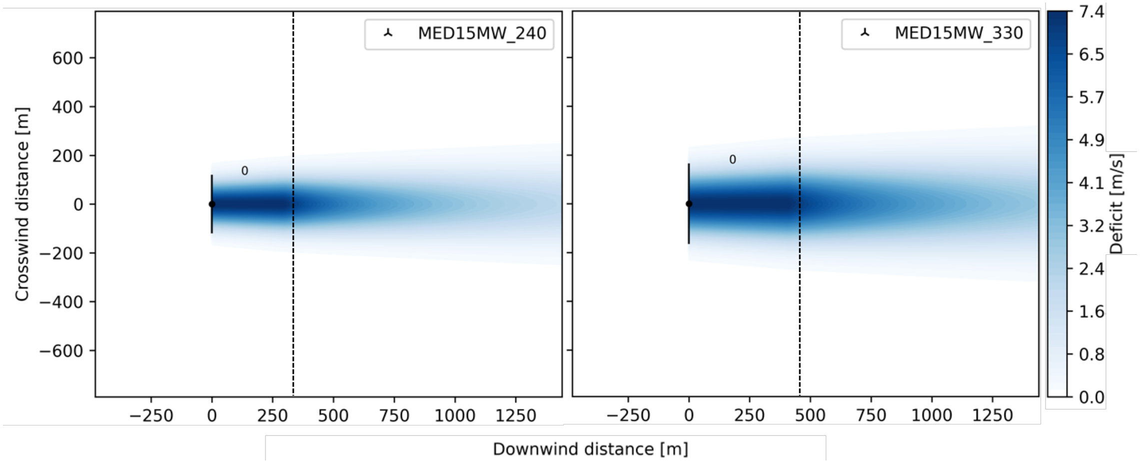

Figure 3.15: Comparison between the wake effects of the MED15MW_240 and the MED15MW_330 WTs.

The wind speed deficit contour, estimated by imposing the same thrust for both turbines, shows a more severe velocity decrease with the MED15MW_330, depicted by the larger dark blue area, which is extended further from the rotor position, as highlighted by the dashed vertical line. Such an effect has the direct consequence of affecting the optimal distance between the turbines. **Figure 3.16**a shows the comparison between the optimal wind farm layout obtained for the wind farm located in Sicily with the MED15MW_240 (light blue) and the MED15MW_330 (blue) WTs. It is apparent how the increased impact of wake losses, which increase from 3.5% to 3.7%, respectively, in the optimized configuration, induced by the larger swept areas results in an increased optimal spacing between turbines. It is worth noting that the optimal solution features increased turbine spacing despite the increasing cable costs, as the increase in AEP offsets the increase in CAPEX. Furthermore, starting from the initialization position (grey), in both cases, the orientation of WTs clusters resulting from the optimization process is N-NW. This can be justified by the wind source in the Sicilian installation site, where the prevalent wind direction corresponds to the orientation of the farms (see Appendix A). Particularly noteworthy is the comparison between the initial and final wind farm layouts. In fact, the choice of a starting configuration close to the optimal one, estimated by the author via sensitivity analyses in previous works [128], sensibly reduced the computational time required for the optimization.

The same trend can be observed for Cyprus in **Figure 3.16**b, where the prevalent wind direction is W-SW. In this installation site, the reduced global IA cable length of about 5% with respect to the Italian case suggests a lower average distance between turbines. This is again consistent with the wind speed distribution of Cyprus, whose average velocity is shifted towards lower values. Concerning wakes, the higher swept area leads to an increase in losses from 3.5% to 4%. The higher upper bound compared with the one in the Italian site can be justified by looking at the thrust curve of the turbines and at the wind speed distribution. The lower average wind speed experienced in Cyprus -equivalent to 5.6 m/s- is closer to the velocity that maximizes the thrust for the MED15M_330, leading to a stronger impact of wake losses.

This result, however, depends on the boundary conditions of the optimization. For instance, given the reliance on IA cables, whose impact on LCoE has been estimated at about 5%, variations in the cost of this component can significantly affect the overall economic feasibility. Therefore, a sensitivity analysis of the cable price, decreasing this value from 750 to 500 €/m, driven by market fluctuations or project-specific factors, has been performed in order to explore a wider design space and evaluate new techno-economic trade-offs.

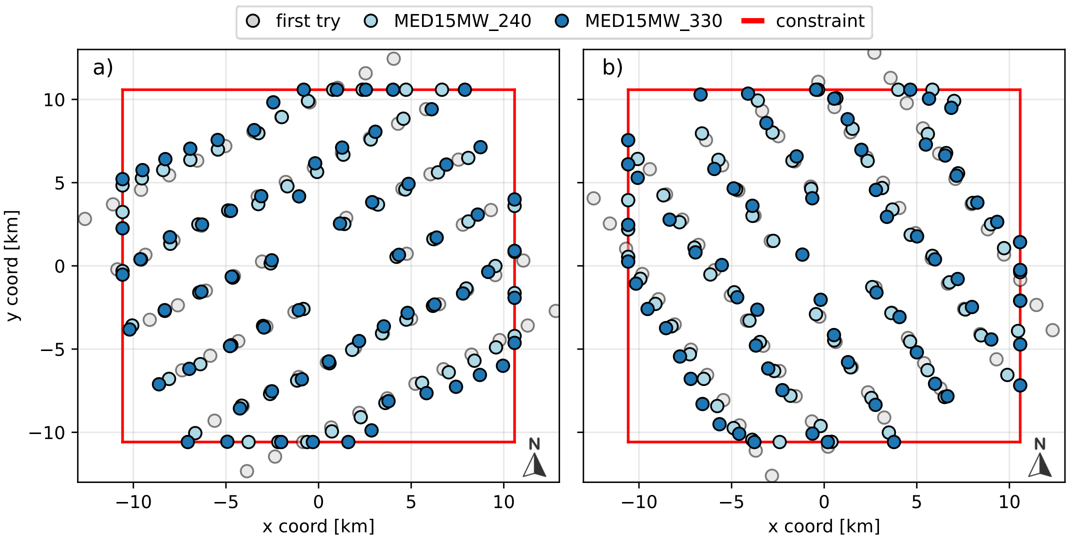

Figure 3.16: Comparison between the optimal layout obtained in Sicily (a) and Cyprus (b) for the wind farms with the MED15MW_240 and the MED15MW_330 WTs.

This economic range has been defined by subtracting 30% from the reference value, identified as 750 €/m. Decreased cable costs per km result in a lower CAPEX with the same WF layout. On the other hand, enhanced spacing between WTs leads to reduced wake losses. Specifically, a decrease in inter-array cable cost allows for an increased distance between the WTs, as shown in **Figure 3.17**, leading to the reduction of wake losses and thus higher AEP.

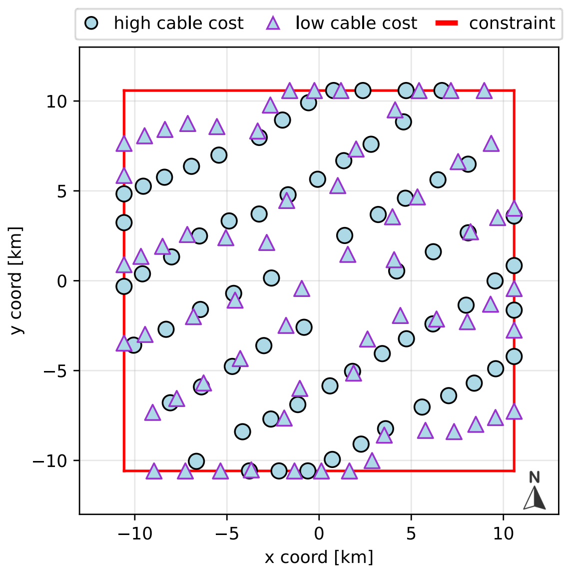

Figure 3.17: Comparison between the optimal layout obtained in Sicily with two different IA cable costs for the MED15MW_240.

Despite the global increase in the length of the cables, spanning from 14 to 30 km depending on the rotor diameter, the CAPEX for the electric infrastructure has experienced a decrease due to the new optimal layout. This, combined with the higher energy production potential, resulted in a lower LCoE.

3.5.2 Environmental analysis

The WTs' environmental impact is gaining momentum in the scientific community and the public interest and, according to experts in the field, this will be a criterion for upcoming tenders [202,203]. However, a complete life cycle analysis would require a detailed design of the system, including the installation and decommissioning procedures, which is completely site-dependent and can hardly be generalized in a global assessment as the one proposed here. To this end, a simplified approach for the evaluation of the environmental impact of floating wind farms has been proposed, relying only on the amount of steel required by WTs and floaters. According to **Table 3.6** and **Figure 3.6** and **Figure 3.7**, larger swept areas lead to increased masses and thus to enhanced steel consumption. This results in higher CO_2 emissions that are not necessarily balanced by the increased AEP during the WT lifetime. **Table 3.6** shows that the amount of steel needed for each turbine-floater assembly varies significantly with the specific power, leading to a CO_2 emission increase that ranges between 20 and 60% with respect to the 240-meter diameter rotor when a carbon footprint of 1.85 t of CO_2 per ton of produced steel is adopted [204]. On the other hand, the enhanced AEP resulting from the increased swept areas (**Figure 3.13**) leads to a wind farm's carbon footprint reduction. Focusing on the Italian electricity mix, the average carbon emissions per MWh of electricity produced in 2024 are about 270 kg/MWh, consistent with a share of 49% of renewables [205]. While the deployment of the MED15MW_330 results in an increased carbon payback period (CPBP) -from nine months of the MED15MW_240 to about one year in the installation site in Sicily- the environmental benefits on the whole lifetime of the wind farm are relevant. Assuming a constant carbon emission for the whole plant lifetime, the 30 years of operation of the wind farm in Sicily can help to avoid the emissions of more than 38 Mt of CO_2, with the WT with the highest swept area, corresponding to an improvement of more than 33% with respect to the base 15 MW WT.

Figure 3.18 shows the comparison between the CO_2 saved by the new WTs designs in the different installation sites.

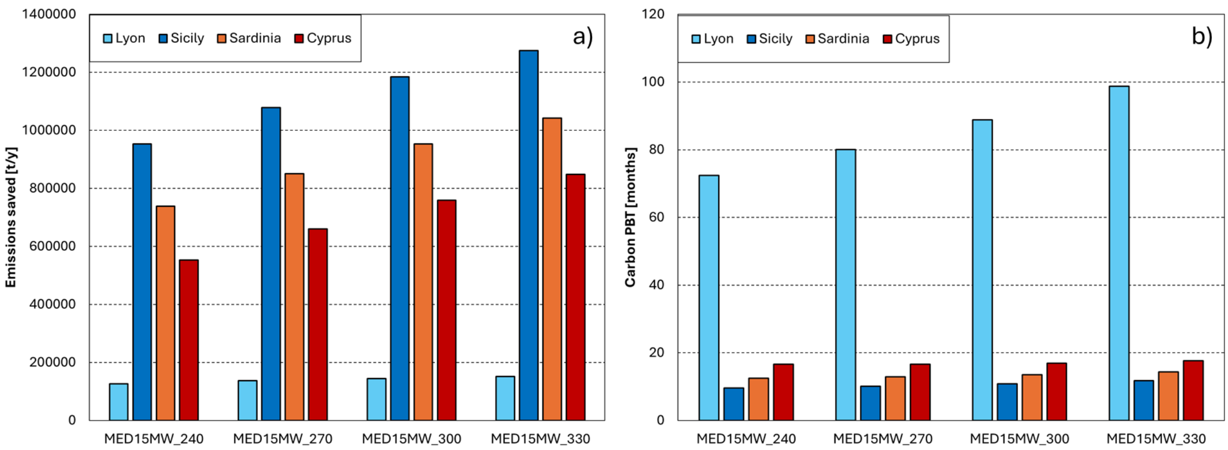

Figure 3.18: Comparison between the carbon emissions saved and the carbon PBT for the tested WTs in the different installation sites depending on the emission factor of each Country [207].

It is apparent that the most impactful factor is the carbon emission per unit of produced energy of the specific country. The site in the Gulf of Lyon, despite the highest AEP, experiences the lowest emission factor -27 kg/MWh [206] due to the high shear of nuclear energy, and thus the lowest saving potential. This results in the highest CPBP, with periods of up to eight years to reach neutrality. However, even in this extreme scenario, the adoption of WTs with lower specific power is beneficial in terms of emissions saved per year. Finally, **Figure 3.18** also allows for a comparison of the Italian sites. Despite the lower global emissions saved per year, the higher ΔAEP of Sardinia results in an enhanced environmental benefit in the adoption of the MED15MW_330, with a yearly carbon footprint reduction increase of up to 41% with respect to the base turbine.

Table 3.6: Steel consumption and CO_2 production increase for the single turbine-floater assembly due to higher swept areas.

Wind Turbine	MED15MW_240	MED15MW_270	MED15MW_300	MED15MW_330
Steel consumption [t]	6100.74	7265.11	8534.95	9917.91
CO2 emissions [t]	11286.36	13440.46	15789.66	18348.14

3.5.3 Economic results of the optimization

Although the increased swept area impacts positively the capacity factor of the wind farms, and thus their AEP, this study aims mainly to assess to what extent a tailored WT can minimize the LCoE in a specific site by pursuing a trade-off between increased expenditures and the higher AEP. The comparison between **Figure 3.13** and **Figure 3.19** shows how, while the AEP always rises, the LCoE trend strongly depends on the wind source. The relevant ΔAEP depicted for Cyprus leads to a minimum cost of energy obtained with the WT with the lower specific power. This is consistent with the Weibull of this site, which shows a high amount of energy at the lower wind speeds.

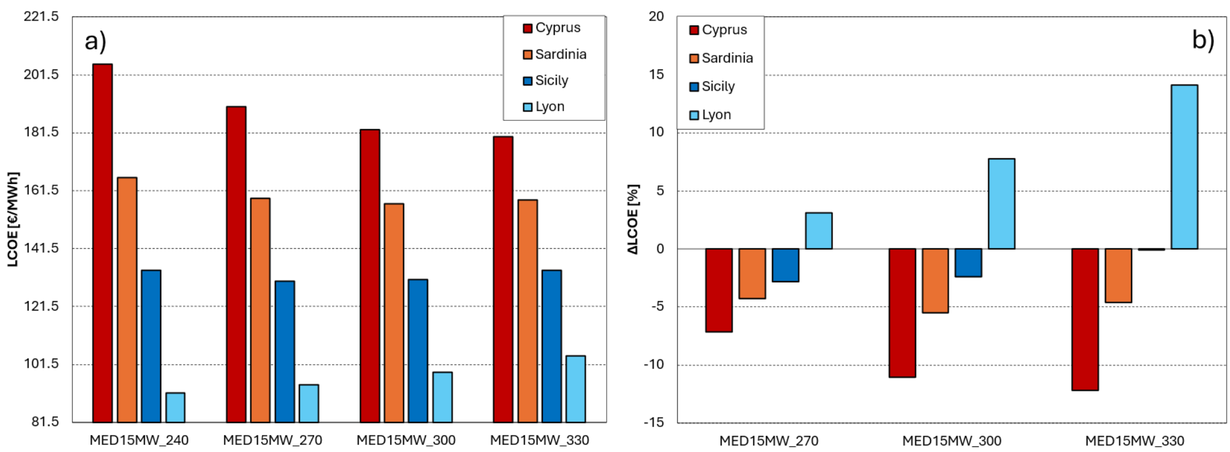

Figure 3.19: Comparison between the LCoE and the LCoE variation in the different installation sites for the new aerogenerator designs.

To this end, the more the operation curve is shifted towards lower wind speeds, the larger the benefits. Regarding the Italian sites, the wind energy distribution is translated towards higher wind speeds with respect to Cyprus. In these scenarios, the sensitivity analysis to the rotor diameter identifies MED15MW_270 and 300 as the optimal solutions for Sicily and Sardinia, respectively, as shown by the ΔLCoE in **Figure 3.19**b. This is again consistent with the wind resource of the two sites, which shows a higher average wind speed in Sicily than the one in Sardinia. Finally, while the site in the Gulf of Lyon experiences an increase in AEP, the higher CAPEX related to the larger swept area offsets the enhanced production potential, leading to a negative impact on costs. **Figure 3.19** shows how the optimal situation is represented by the turbine with the reference rotor diameter and further decreases in the specific power result in higher LCoE. This can be justified again by looking at the wind speed distribution in **Figure 3.2**. The Weibull in this site is the closest to Class I, which has been taken as a reference for the design of the IEA RWT with a rotor diameter of 240 m. IA cable costs affect only the LCoE, without modifying the optimal rotor swept area for the specific site. **Figure 3.20** shows the comparison between the LCoEs obtained with IA cable costs of 750 €/m (hatched bars) and 500 €/m (solid bars). The hatched bars, representative of the base case study, always exceed the LCoE depicted by the solid bars. When less expensive IA cables are used, the LCoE decreases as a consequence of the lower wake losses and reduced CAPEX. On the other hand, the unchanged optimal WTs emphasize a lack of direct dependency between the IA cable costs and the optimal swept area. From these preliminary results, it has been noticed that the optimal rotor diameter per se is influenced only by the wind speed distribution in a specific site.

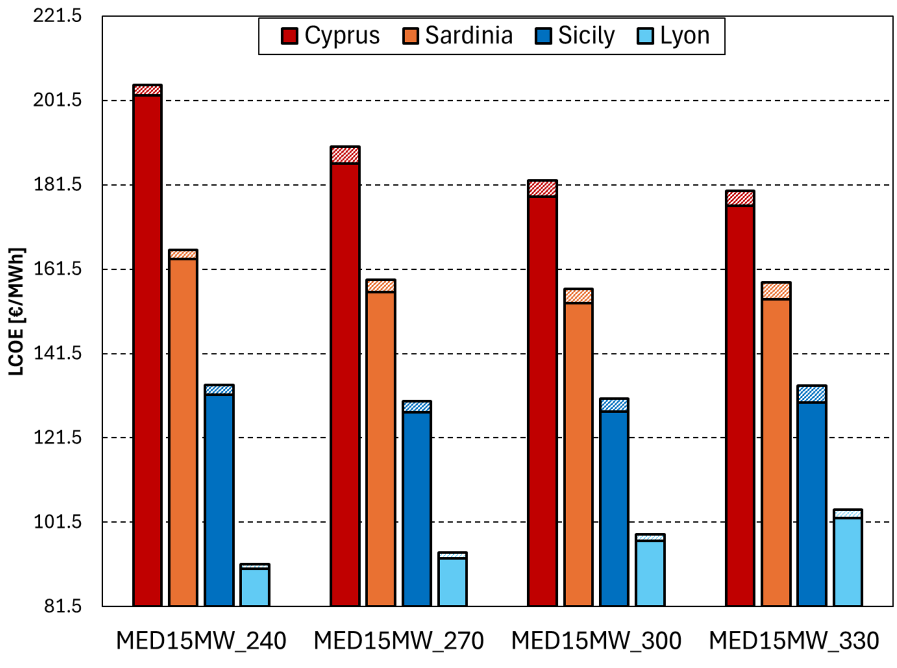

Figure 3.20: Comparison between the LCoE in the different installation sites for the new WT designs with different IA cable costs.

3.6 Discussion

The findings of this study underscore the potential of LSP wind turbines as a key technological advancement for regions with moderate average wind speeds, such as those prevalent in many

Mediterranean countries. In alignment with the stated objectives, this discussion synthesizes the key findings and provides a broader perspective on their implications.

First, the literature review highlighted a significant gap in current methodologies, particularly the oversimplification in estimating the AEP based solely on wind profiles and hypothetical power curves. As shown in many studies, such approaches risk overlooking complex but critical interactions between turbine design, farm layout, and economic performance. By contrast, the comprehensive approach adopted in this review underscores the necessity of integrating detailed cost and performance drivers, such as wake losses, substructure design, and cabling costs, into early-stage feasibility analyses. In particular, this study clarified that the promise of LSP turbines in moderate wind areas affects not only their aerodynamic efficiency but also their energy system implications. The detailed component-level review revealed how changes in rotor size and specific power influence the mass and cost scaling of rotors, towers, and floaters. These impacts are not independent; for example, larger rotors associated with LSP configurations tend to require taller towers and more robust floating structures, which may offset some of the expected energy gains. However, in the context of moderate wind sites where capacity factors are inherently lower, LSP turbines offer a valuable trade-off by improving AEP without significantly increasing operational expenditures. Despite lower specific power rotors being hampered by higher CAPEX, in fact, several key advantages have been highlighted. By optimizing the WT swept area, despite the increased costs, both the LCoE and the environmental impact of aerogenerators can be reduced. Additionally, this approach leads to higher capacity factors, which may also be beneficial for expanding renewable energy capacity in sea basins with moderate wind speeds and deep waters that have not yet been exploited with conventional offshore wind technology. In addition, lowering specific power increases the availability factor, which is often valuable in energy grids with high penetration of intermittent renewable energy. From this perspective, the results are of interest for future analyses by both policymakers and relevant stakeholders, including energy producers, private investors, and utility companies that could push forward the development of a new generation of rotors tailored for specific markets. Increased investment in this technology could, in fact, not only contribute to renewable energy targets but also help enhance grid resilience and promote sustainable development of regions such as the Mediterranean one. By selecting the Mediterranean Sea as a case study, this study was able to contextualize theoretical findings within real-world site conditions, including variations in wind resource, water depth, and infrastructure availability. This region-specific analysis demonstrated that while LSP FOWTs may not be universally optimal, their strategic deployment in select moderate-wind locations could bridge the gap between current technology limitations and future offshore wind expansion goals.

A comparison between the results obtained in this study and those presented in previous works highlights both the evolution of cost trends and the limitations inherent in certain modeling approaches. For instance, the wind farm specific CAPEX estimated in this work ranges between 3480 and 5100 €/kW, whereas [105] reported a lower range of 3200 to 4550 €/kW. While the lower bound is in line with the literature, the upper-bound CAPEX found herein is influenced by the use of low specific power wind turbines, which increases CAPEX. Therefore, due to this metric not considering the AEP improvement of the larger rotors, energy production benefits cannot be quantified against their higher capital costs, making a direct comparison with this study [105] challenging.

Further comparison can be made with the work of Serri et al. [149], who reviewed LCoE estimates for wind projects in the Mediterranean Sea. Their reported LCoE range of 63 to 156 €/MWh aligns well with the present results, particularly for high-wind-resource areas such as Sicily and the Gulf of Lion. Conversely, sites characterized by lower average wind speeds, such as Cyprus and Sardinia, show consistency with the upper bound reported by Martínez and Iglesias [138], where the LCoE can reach up to 250 €/MWh. These parallels support the validity of the developed modeling framework and highlight the critical role of site-specific wind conditions in determining economic viability.

While the presented model is comprehensive and physically consistent, technical and economic limitations should be acknowledged to contextualize the results accurately. The impact of peak shaving on blade weight has not been considered. A reduction in loads due to peak shaving could result in lighter blades due to the lower aerodynamic loads. However, accurately assessing this effect requires a detailed structural design, which is beyond the scope of this study. Consequently, the results presented here represent a conservative scenario (i.e., additional reductions in LCoE are at hand), that still offers meaningful insights into the proposed solution. Additionally, the impact of turbulence on WT thrust has been neglected, leading to a conservative estimation of wake effects. This simplification may result in an overestimation of wake losses, which would likely lead to slightly improved outcomes if turbulence effects were included. This assumption is adequate for the comparative scopes of the study. Finally, no sensitivity analysis has been performed on the occupied area due to a lack of literature data on costs per unit surface for sea lots. As a result, any potential improvement in surface efficiency in terms of energy output per square kilometer of sea surface, would favor larger, more productive rotors, under the constraint of a set permitted sea lot and set number of permitted turbines of set specific power.

Concerning economic assumptions, no sensitivity analysis on the costs of platforms and other ancillary components, such as export cables and offshore substations, has been conducted. For all these components, the cost scaling models described in the methods section have been consistently applied. These models are based on established industry standards, empirical data, and literature values, ensuring a realistic and standardized approach to cost estimation across the project. Any fixed cost increases or decreases would uniformly affect all turbines and installation sites analyzed, thus preserving the comparative nature of the study’s conclusions. Therefore, variations in these costs could introduce uncertainty into the LCoE estimations, but they would not change the optimal turbine configuration for the installation sites. On the other hand, modifying the platform cost correlation by increasing or decreasing the dependency of the expenditure by the swept area may affect the optimal WT for a specific site. However, according to the limited amount of data available in the literature, arbitrary adjustments to the relation presented in Section 3.3 would be arbitrary, and was thus considered irrealistic.

Finally, while more complex economic metrics, such as the Cost of Value of Energy (CoVE) [209,210], are increasingly explored in academic literature and energy tender evaluations, I opted to use the LCoE due to its widespread adoption and suitability for comparative analyses. In this study, LCoE was particularly appropriate as different turbine configurations have been compared to evaluating the benefits of larger rotors. Metrics like CoVE require time-dependent simulations of wind power output and detailed local market data, which were not available for this preliminary analysis.

3.7 Conclusions

In the study, current trends in offshore wind technology have been first critically reviewed, demonstrating that a new generation of floating wind turbines featuring LSP values, in order to better convert moderate wind speeds, can potentially disclose new sea basins and provide an increase in wind power generation needed to meet renewable energy targets. The same review showed, however, that the analyses presented to date failed in reliably estimating the potential of this technology because they made use of simplified models, which either focus on turbine components disregarding the influence of wake losses and inter-array cable layouts, or consider these effects but model the cost of turbine components using simplified cost scaling laws, which often do not include all the relevant physics. This, in turn, has led to significantly biased estimates, since changing the specific power of a FOWT has a number of implications that must be modeled.

On these bases, a new methodology for preliminarily designing LSP floating wind turbines has been developed and presented. The methodology's underlying assumptions are based on a synthesis of the best data available from academia and industry, which were reviewed and examined in the study. Once developed, the methodology, which also includes a wind farm optimization tool, has been used to assess the impact of LSP FOWTs in four case studies in the Mediterranean Sea, which – thanks to their variable characteristics in terms of wind distributions – are thought to be representative of a large number of potential moderate-wind installations worldwide.

The main takeaways of the study can be summarized as follows:

- LSP wind turbines are clearly shown to offer a promising solution in unconventional sea basins with moderate average wind speeds, both from an environmental and economic perspective. However, the optimal specific power is highly dependent on the wind resource characteristics of each site. Therefore, a comprehensive approach like the one presented here, which can go beyond the simple rotor, is mandatory to get reliable estimations.
- The lower the average wind speed, the greater the benefit due to the LSP. Among the selected study cases, a decrease in specific power has shown to lower LCoE for Sicily, Sardinia, and Cyprus. For these cases, the optimal specific power ranges from 261 W/m^2 for Sicily (similar to a Class II site) to 175 W/m^2 for Cyprus, where the Weibull distribution approaches Class 4 conditions.
- Wind turbines with higher swept areas might be suboptimal in installation sites with higher average wind speeds. Although the reduced specific power results in enhanced energy production, the improvement does not compensate for the CAPEX increase, leading to higher LCoE, such as in the French site analyzed, where the reference 240 m rotor represents the most cost-effective solution.
- Wind turbines with larger swept areas also offer a reduced environmental impact compared to conventional designs. The benefits related to the increased energy output exceed the higher steel consumption, potentially lowering the overall ecological footprint. This holds true also in the cases of high wind speeds (such as the one in France discussed before), where no LCoE improvements are obtained.
- While uncertainties in component costs, such as those related to inter-array pipelines, can influence the LCoE and optimal layout, they do not necessairily affect the identification of the optimal turbine for a specific site.
- Comprehensive simulation models, such as the one developed for this study, are mandatory for critical analysis of FOWT technology, and are thought to provide in the future support to policymakers, stakeholders, and researchers for fostering the development of offshore wind in new sea basins.

4 MITIGATING GRID CONGESTION IN OFFSHORE WIND: COMPARATIVE MODELING OF LI-ION BATTERIES AND HYDROGEN

4.1 Introduction

The reduced visual and acoustic impact, coupled with increased restrictions imposed on available onshore sites for the installation of renewable energy facilities, promotes a progressive rise in the deployment of offshore technologies within the European energy landscape in the coming years [211]. In regions like the European Union, high population densities, limited land availability, and strong political commitment to decarbonization make offshore wind particularly attractive despite capital costs that are currently significantly higher than onshore wind [6]. These countries often have well-developed maritime infrastructure and proximity between offshore sites and demand centers, which helps to reduce transmission losses and integration costs [212].

In contrast, resource-rich nations such as the United States, Australia, or parts of the Middle East may have vast land areas with high onshore wind or solar potential, reducing the immediate need for offshore solutions [212]. Additionally, their lower population densities and dispersed demand centers can make offshore wind less economically favorable unless targeted for specific coastal regions. Despite the crucial role of power production from renewable energy sources (RES) in the energy transition, the integration of a substantial number of large-scale facilities in national electrical grids poses significant challenges. In particular, for Mediterranean countries, and specifically for Italy that is taken here as a case study, large-concentrated installations of renewable energies can:

- affect the stability and reliability of the power grid, due to significant fluctuations associated with the non-dispatchable RES.
- generate grid congestion during peak hours of production.
- lead to the planned reduction of renewable plants' power output, namely curtailments.

As described in the scenarios presented in [213], a massive increase in installed RES capacity by 2030 or 2050 may result in significant energy waste related to curtailments. In addition to these challenges, the large power flows introduced by offshore wind farms, particularly FOWT technology, may exceed the capacity of the existing Mediterranean grid infrastructure [128].

Although the co-location of wind and solar [214,215] and hybrid storage systems [216,217] may be beneficial in flattening production profiles and increasing the flexibility of control strategies; managing electric energy curtailments will become a critical aspect of offshore wind integration in the near future.

To this end, the development of advanced energy storage systems (ESS) and grid management solutions, and the adoption of electrolysis plants, becomes imperative. Various strategies are being explored to address this issue.

The challenges related to the planned reduction of the power output to prevent grid overloads and congestions may be mitigated by producing green hydrogen from energy surplus. Compared to batteries, green hydrogen is a versatile energy carrier that can be used for long-term storage, both in liquid and gaseous phases, and can act both as a fuel for various applications, including fuel cells or combustors and as a key element in industrial processes in the so-called hard-to-abate sectors [218]. However, few research efforts have been spent on the exploitation of curtailments from FOWT farms in the Mediterranean Sea, and in general on the production of Hydrogen to reduce the associated energy waste. Specifically, Wang et al. [219] evaluated the feasibility of producing hydrogen from curtailments of renewable energy sources (RES) in order to feed fuel cells electric vehicles. The analyses show that the use of electrolysis can provide relevant benefits to mitigate the effects of intermittency of RES. In their study, Park et al. [220] demonstrated how comprehensive system modeling can be used to assess the economic viability of producing green hydrogen from curtailed solar and onshore wind renewable energy using actual meteorological data. Results show an LCoH of around 5.9$/kg, consistent with the findings of this study. In [221], McDonagh et al. showed that the coupling of Offshore wind farms and electrolysis has a good potential to increase the revenues of a plant thanks to the exploitation of curtailed power. The findings depict an LCoH of 3.77€/kg for a wind farm located in the Irish Sea. Biggins et al. [222] proposed a stochastic optimization to maximize the revenues of a system composed by wind farms, batteries and electrolyzers. Results show that hydrogen production increases the average revenue and curtailed wind utilization significantly more than the Li-ion battery. However, although many research efforts were spent to evaluate hydrogen production costs from wind power, in most of these studies a simplified model to convert electricity into hydrogen is used. The adoption of a conversion factor, such as the one adopted by Yan et al. in [223], may result in relevant overestimation of the producibility. Finally, Gambou et al [224] highlighted that relying solely on efficiency-based models is insufficient and that more comprehensive approaches incorporating the stack degradation processes are needed to properly simulate long period time spans. While the simple models can be useful for initial design and analysis, they cannot accurately capture the thermal behavior of the electrolyzer [225].

Parallel to research efforts that have been spent on hydrogen as a way to reduce curtailment impact due to the evolving nature of electrolysis technologies, one promising approach, especially in the short term, involves the use of large-scale lithium-ion batteries (BESSs) to store excess energy and mitigate grid congestion [226]. In [227,228], batteries are selected as potential ESS to be employed for mitigating short-term fluctuations in renewable production and to increase power quality. Moreover, the results presented in [229] show that, despite the higher grid losses, locating the battery onshore, near the point of delivery, contributes to increasing the earnings from the system. Finally, according to [230], batteries are located directly in turbines to minimize the temporal misalignment between production and demand. Despite the reduction of land occupation and grid losses, the results of the above-mentioned study show a high rate of degradation due to the relevant number of charging and discharging cycles. However, large BESS capacities result in relevant expenditures, due to the high costs associated with this component [231], which requires multiple replacements during the plant's lifetime. Additionally, the use of brand-new BESS (NBESSs) generates environmental pollutants, including hazardous waste and greenhouse gases, in manufacturing and recycling [231]. As such, the environmental impact of this storage technology may undermine the tender system, which is expected to include these aspects for new farms [202,203]. At the same time, the global market for electric vehicles is growing rapidly and is expected to reach 16 % of the total vehicle market share by 2030 [232]. These vehicles, to guarantee adequate performance in terms of autonomy and reliability, typically use BESS with a lifespan of around 10 years in the vehicle, corresponding to 80 % of the component's state of health (SOH) [233–235]. Despite this replacement, taking place before the effective end of life of the battery is reached, the remaining capacity of the storage system meets the less strict reliability criteria required by power plants set around 70 % [236]. To this end, second-life batteries (SBESSs) can mitigate the environmental burden of this energy storage strategy by increasing the lifetime of the battery by a further 5-7 years, thus reducing the need for new batteries and contributing to targets set by the EU regulatory framework for batteries [237–239]. A growing body of research has explored the potential of SBESSs primarily in the context of energy storage for stationary applications. For instance, in [240] the authors investigated the feasibility of using second-use EV batteries as shared storage among prosumers, analyzing financial and environmental break-even points under different carbon pricing scenarios, and highlighting their role in enhancing self-consumption rates without incentives. Another line of research addressed the technical barriers to SLB deployment, proposing advanced cell regrouping techniques using Particle Swarm Optimization and Genetic Algorithms to enhance performance, reduce degradation, and minimize environmental impact through lifecycle optimization [241]. Additionally, studies have focused on the systemic and policy-level challenges to SLB adoption, employing multi-criteria frameworks to prioritize barriers such as cost and technology, while aligning the discussion with broader sustainability goals and circular economy principles [242]. Nevertheless, although these contributions offer valuable insights into SLB feasibility, performance, and policy integration, the utilization of SBESS specifically to mitigate the efficiency and economic impact of curtailments remains underexplored to date.

4.1.1 Main scientific contributions and novelty

Regarding BESS, existing literature predominantly focuses on power quality and load shifting for relatively small-scale plants, often overlooking detailed analyses on how to consider and reduce the impact of curtailments on the economy of large-scale wind farms. Moving from this background, this present study aims to fill this gap, addressing the pressing issue of energy curtailment resulting from the rapid integration of intermittent offshore wind power into the grid in Mediterranean countries, where infrastructure upgrades may lag behind new renewable installations. Specifically, it investigates how the inability of the grid to immediately absorb the full output of offshore wind farms can lead to wasted energy and lost revenue. Additionally, the purpose of the performed analyses is to estimate the LCoH obtained by exploiting the energy from curtailments.

While results are specific to the selected case study, the present analyses are potentially of use in all other locations facing similar issues. The key novelties of this work can be summarized as follows:

- analysis of the behavior of a complex electrolyzer model that includes the effects of temperature variation and aging of the stack, thanks to the adoption of a time-dependent approach.
- in-depth investigation of BESS as a cost-effective and sustainable solution for managing this curtailed energy and improving the economic performance of offshore wind farms.
- extensive comparison between the adoption of brand-new and second-life BESSs from electric vehicles, quantifying both the economic and environmental trade-offs of these technologies.

In this study, Section 4.2 reviews the economic and regulatory aspects related to the extension of the life of batteries beyond their first application. After a description of the methods adopted to estimate the power production of a floating offshore wind farm in the western marine area of Sicily with a minute resolution, Section 4.4.3 showcases the assumptions made to analyze energy reductions and the revenues introduced by the adoption of BESSs and ALK electrolyzers. Furthermore, a new cost metric has been introduced. Starting from the standard formulation for LCoE, a market-dependent levelized cost of energy (mLCoE) has been considered to account for the decreased power production due to the energy market. Both cost metrics, along with the net present value (NPV) and LCoH, are used in Section 4.5 for the techno-economic comparison between the adoption of hydrogen or SBESSs and NBESSs for the mitigation of curtailment impact. Finally, some considerations on the environmental impact of batteries and the benefits related to their lifetime extension are proposed.

4.2 Second-life batteries

The increasing adoption of renewable energy sources has led to a growing interest in SBESSs as a sustainable solution for energy storage. However, several challenges hinder their widespread implementation, including technical uncertainties, performance degradation, and safety concerns. Additionally, the regulatory framework remains fragmented, with existing guidelines and standards still lacking comprehensive directives for SBESS applications. In this section, an extensive yet critical review of these aspects is presented, aimed at highlighting the feasibility of the coupling of this technology with FOWTs.

4.2.1 Existing SBESS projects

Beyond technical and regulatory aspects, economic feasibility plays a crucial role in determining the viability of SBESSs, influencing their potential deployment in various applications such as grid support, peak shaving, and renewable energy integration. Although SBESS technology has not yet reached a maturity level that guarantees profitability and reliability, large-scale installations of this technology are drawing attention in stationary applications. Concerning the adoption as an auxiliary power unit, a well-known example is that of the Mobility House, a German company specializing in electric mobility, which helped design a second-life application for the Johan Cruyff Arena [243]. This application enables emergency power supply for at least one hour in the case of power outages. It is a three-megawatt system, composed of batteries recovered from Nissan vehicles, that temporarily stores solar energy from the stadium roof during periods of low demand, and releases it when needed [244]. Another example of a second-life application as a reserve power source can be found in Yellowstone National Park. Thanks to a collaboration between Toyota and Yellowstone, more than 200 battery packs that once powered Toyota Camry Hybrids have now been reused as an energy storage system, powering the five buildings on the Lamar Buffalo Ranch [245]. Finally, the Second Life plant in Elverlingsen is an example of how electric vehicle batteries can be reused to support the transition to more sustainable energy. Located in an area that once housed coal-fired power generation, the facility makes use of second-life batteries from Mercedes vehicles. With 1920 modules, this system offers a capacity of 9.8 MWh and an installed power of 8.96 MW, contributing not only to the stability of the power grid but also to environmental sustainability [246,247]. However, the installation of SBESSs to mitigate the impact of curtailments on floating offshore wind farms represents a gap both in literature and in industrial applications. Therefore, this study can serve as a guideline for exploring this pioneering application.

4.2.2 Battery passport

The large-scale deployment of SBESSs is highlighting some challenges related to this kind of technology. Issues such as cell inhomogeneity and compatibility may reduce economic revenues and lead to relevant safety concerns. In [248], a thorough examination of the key challenges associated with SBESSs is presented: safety concerns, such as thermal runaway, are explored along with possible solutions. Additionally, the issue of cell inhomogeneity is addressed by reviewing both passive and active balancing techniques. Another focal point of their study is the compatibility of second-life batteries, assessing whether their electrical properties can fulfill the performance demands for energy storage. Previous research suggests that while the limited availability of suitable batteries may hinder profitability in the short term, integrating SBESSs with wind farms remains an attractive and feasible option.

In this context, the Battery Passport proposed by the European Commission emerges as a key tool, an initiative designed to ensure transparency and sustainability in battery management [239]. Through the accurate tracking of batteries, the passport makes it possible to keep track of the origin of materials, production practices, and disposal methods. This approach not only promotes producer accountability but also provides consumers with valuable information, enabling them to make more informed and sustainable choices.

According to the European guidelines, starting on 1 January 2027, batteries are required to be labelled with information that identifies the battery and specifies its key characteristics, including details about lifetime, charging capacity, the presence of hazardous material, and potential safety hazards. This information should be available to battery owners to support battery reuse, repurposing, or remanufacturing efforts [249,250].

However, according to current guidelines, the passport does not include detailed information about the BESSs' first life. Integrating this into the global passport offers several advantages. First, it provides a complete picture of the health of the battery at the time of decommissioning from primary use, which is critical in determining whether the battery can be reused, whether upgrading is required, or whether it needs to be recycled. Knowing the residual capacity and operational history of the battery enables second-life market participants to make informed decisions about possible reuse. This integration reinforces the role of the Global Passport as a central tool in battery lifecycle management, ensuring that every battery can be used to its full potential [250].

4.2.3 Techno-economic impact

Techno-economic assessments conducted for SBESS applications in two wind farms on the Spanish island of Tenerife indicate an increase in revenue, with internal rates of return improving from 10 % to 14 % [231]. A cost sensitivity analysis reveals that, although subsidies are not crucial in these cases, a 15 % capital expenditure incentive could enhance profitability resilience in the event of declining electricity prices. Moreover, the study highlights the environmental advantages of this approach, which could prevent approximately 0.7–1.2 kilotons of BESS-related waste and result in savings of around 5–7 million € in battery recycling expenses. Another important aspect is the comparison between NBESSs and SBESSs. In [251], the authors analyze the financial benefits of second-life versus new batteries in wind farms, employing a dynamic degradation model to assess capacity. Case studies conducted in the USA and Denmark suggest that, under current wind energy and lithium-ion battery pricing, reusing batteries is not financially beneficial for the examined wind farms. However, if wind energy prices decline significantly faster than battery prices, second-life batteries could become a more viable option in the future.

Concerning costs, several elements should be included for SBESSs: the cost of recovering and purchasing the battery, the cost of future disposal, and the economic return from recovering valuable materials through recycling. However, both brand-new and second-life BESSs share these last two values. To this end, due to the comparative analyses performed in this study, future disposal costs and the return from material recovery have been neglected. Exactly as with the evaluation procedure, there are no regulated and standardized strategies for the estimation of the CAPEX of SBESSs yet. Among the various proposals analyzed, the approach adopted in [234] and summarized in Eq. 4.1 has been selected as the most detailed. The purchase cost of the SBESS (C_{USED}) is estimated considering the price of the new battery with the same capacity (C_{NEW}), ranging from 110 and 190 €/kWh [252,253], and coefficients to account for the SOH (F_{SOH}), the repurposing costs (F_{REUSE}), and the incentives (F_{DISC}):

$$C_{USED} = C_{NEW} * F_{SOH} * (1 - F_{REUSE} - F_{DISC}) \tag{4.1}$$

According to the literature review performed in [234], the C_{USED} ranges from 44 to 100 €/kWh. These cost estimations have been confirmed by other studies where the average price for SBESSs has been set at 85 €/kWh, as in [254].

4.3 Study cases

This section depicts the study cases selected for this work. After the description of the wind turbines adopted, the installation sites in Sicily and Sardinia are shown.

4.3.1 Wind turbines

In this current study, the 15 MW reference wind turbine (WT) proposed by the IEA for offshore installations is adopted [166]. Despite the early commercial stage experienced by FOWTs of similar scale, this choice is consistent with a time scale starting in 2030, when it is foreseen that these turbine sizes will have attained complete maturity and undergone extensive commercialization. **Table 4.1** reports the reference data for the adopted WTs.

Table 4.1: IEA 15 MW reference data.

Hub height	Rotor diameter	Rated power	Cut in/out wind speed	Rated wind speed
150 m	242 m	15 MW	3 - 25 m/s	10.6 m/s

Recent findings [255] established a lifetime of 30 years for those WTs. Planned extraordinary maintenance could, in fact, extend the operation for an additional five years, instead of the 25 commonly considered, without significantly affecting the performance. This assumption, considering a lifetime of 30 years also for the whole power plant, leads to avoiding replacement costs for the generators. Regarding floating platforms, mooring systems, and energy delivery to shore, the assumptions extensively described in [256], are herein adopted. Specifically, due to the depth of the seabed and the metocean conditions characteristic of the site, the semi-submersible platform with catenary moorings is selected. Finally, intra-array electric cables with a capacity of 90 MVA and HVAC export cables are adopted as the most cost-effective solution in this specific case.

4.3.2 Sicily: Wind farm layout and installation site

This study is focused on a sea lot located approximately 60 km from the western shores of Sicily, where previous feasibility projects were presented to the Italian authorities [257]. This study aims to estimate the LCoE for a wind farm with the potential integration of Li-ion batteries in a time horizon starting in 2030. In order to minimize the costs associated with energy production, a layout optimization is needed.

Table 4.2: Wind farm layout spacing description.

Layout L-l	13d-5d	13d-6.25d	13d-7.5d	13d-10d
Intra-array distance [km]	3.25-1.25	3.25-1.56	3.25-1.87	3.25-2.5
Sea lot extension [km^2]	292.5	365.04	437.58	585

Wind farms are composed of sixty-seven 15 MW WTs, for an overall rated power of 1.005 GW. The optimal layout of offshore wind farms poses significant challenges, including submersible cables and moorings. Furthermore, wake effects significantly affect power production, as most of the rotors work at suboptimal efficiency due to slower and more turbulent wind, thus reducing the revenues from wind farms. For these reasons, an extensive sensitivity analysis on WT distance is performed to find the optimal tradeoff between the increasing capital costs in ancillary devices and the decreasing wake effects associated with more distanced configurations. The LCoE minimization is achieved by adopting a rectangular-shaped layout and varying the intra-array distance, as shown in **Table 4.2**, where the configurations are described using the spacing in the wind (L) and crosswind (l) direction expressed in WT diameters (d).

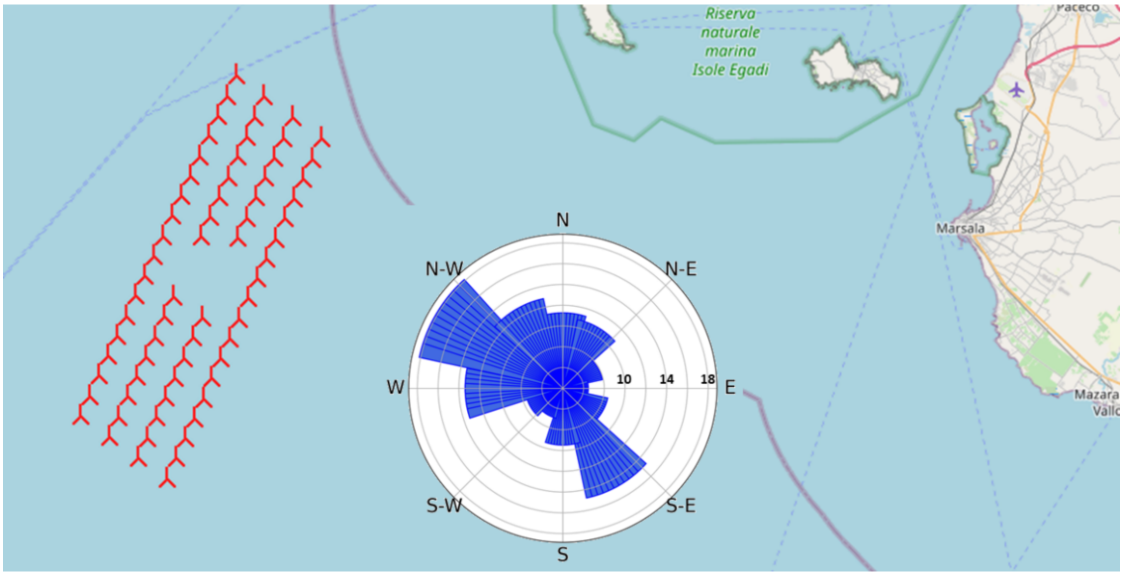

Figure 4.1: Example of wind farm layout with wind rose of the specific site in terms of frequency [%].

Moreover, to maximize the energy capture while minimizing wake effects on downstream wind generators, the orientation of the cluster of rotors was set considering the prevalent wind direction from the west-northwest, as depicted in **Figure 4.1**. Finally, the environmental footprint of each configuration, described in **Table 4.2** by means of occupied surface, ranges from approximately 290 to 504 km^2.

4.4 Methodology

This section presents the methodology adopted in this work. After the description of the assumption made to estimate the wind power and to refine resource data, the curtailment strategy and battery modeling are explained. Finally, the determination CAPEX and OPEX adopted for the LCoE and NPV estimations is shown.

4.4.1 Wind data

The adoption of detailed battery models in smart energy system analyses requires power inputs with an appropriate time resolution to account for a realistic behavior of the storage device. In particular, a one-minute resolution has been considered a good trade-off between accuracy and computational cost to properly assess the effects of charge and discharge cycles on the state of health (SOH) and efficiency of the component [258]. However, the use of wind data with this time resolution could lead to significant errors in wind power production assessment. Wind power curves provided by WT manufacturers are typically averaged over ten-minute intervals [259], and using wind data on a minute basis would prevent an accurate evaluation of the real performance of the generator, which fluctuates significantly on such small time scales due to turbulence in the incident flow. Therefore, while a ten-minute scale is adopted in order to correctly estimate the wind power generation from the available wind speed, a subsequent refinement strategy is used to obtain the time-varying power output on a one-minute basis. Nevertheless, obtaining wind data with a ten-minute resolution at the typical hub height of modern rotors is challenging, considering the lack of offshore direct measures, the reduced elevation of measurement stations, and the hourly resolution of reanalysis databases.

Considering the lack of detailed guidelines on how to refine the coarse wind dataset to match the desired time resolution, the author adopted a strategy based on the variability of the measured data at mast elevation with respect to the hourly average. As described in **Figure 4.2**, both the ERA5 database [151] and measured data from an existing offshore mast near the site [257] are used.

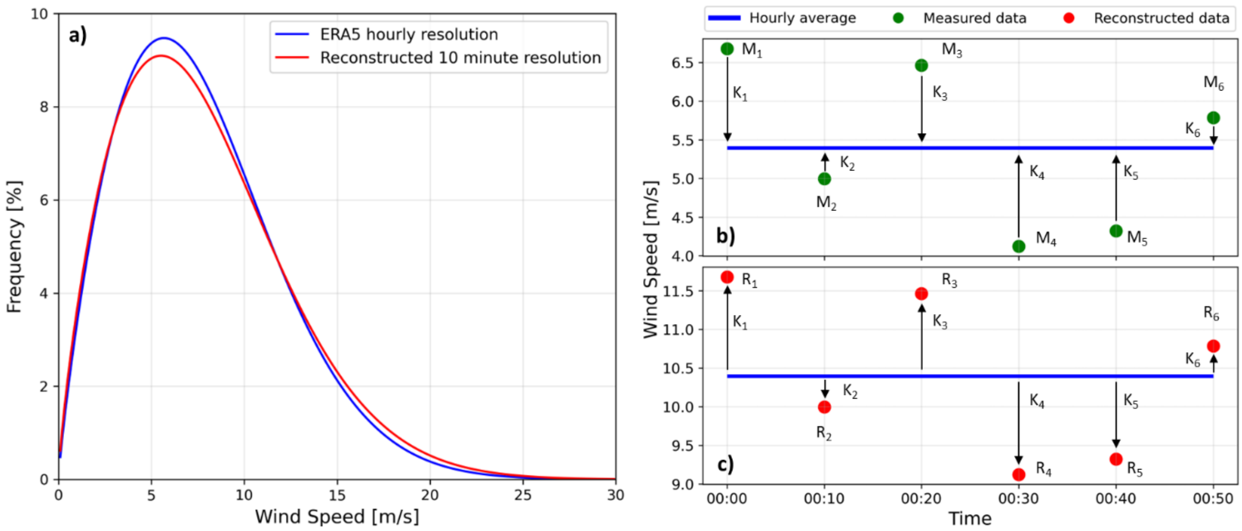

Figure 4.2: a) Comparison between Weibull curves of ERA5 and the reconstructed data at 100 m a.s.l: b) procedure to evaluate the wind variation of the measured data; c) evaluation of the ten-minute series at 100 m a.s.l.

The first one provides the hourly average wind speed at the selected site. The second one, which includes the mean, minimum, and maximum wind speed on a ten-minute basis, provides the wind variation with respect to the mean. The refinement process for those three wind velocities can be outlined in two steps:

- **Figure 4.2**a: Extrapolation of the wind variation (k_i) from the measured data as the ratio between each value (M_i) and their hourly mean (blue line)
- **Figure 4.2**b: Application of the extrapolated variation to the reanalysis data, by multiplying hourly data of ERA5 at 100 m above sea level (a.s.l.) (blue line) by k_i.

Despite the conservation of the average wind speed, this approach results in increased variability of the source, as depicted by the red line in **Figure 4.2**a, and in a slight decrease in the median velocity. However, given the cubic dependence between wind speed and WT power production, the refinement to the ten-minute resolution leads to a difference of 4.3 % in the annual energy production (AEP). Considering that the loss of such information is intrinsic to the refinement process, and according to the author's experience, the introduced error is deemed acceptable for conducting detailed analyses based on coarse databases. Furthermore, to accurately define the wind source, the following assumptions are made:

- Wind direction is considered constant with elevation, and the measured data from the buoy is used.
- The hourly atmospheric temperature of ERA5 is kept constant, considering the reduced variation rate of this quantity.

4.4.2 Power production calculations

In this study, the commercial software windPRO [260] was adopted due to its wide utilization in the design, development, and evaluation processes of wind projects. Time-dependent analyses are conducted to evaluate the ten-minute power production starting from the data described in the previous section. For this work, the author adopted the procedure extensively described in [256], adopting the N.O.J. wake model [189] and neglecting factors such as the surface roughness and orography due to the offshore site. Finally, given the need to conduct analyses over time horizons longer than the two years provided by measurements, with periods of interest spanning ten years, the estimated power dataset at ten-minute intervals is extended to achieve the desired length. Specifically, considering the peculiar behavior of wind in certain months of the year, it was chosen to reconstruct the missing months by randomly shuffling the days from those same months computed in previous years. With respect to a simple repetition of the available years to reach the required ten-year time span, this randomization allows for increased variability in the repeated periods, while statistically respecting the seasonal variability of the wind resource. However, although the wind power reconstructed dataset has a duration of a decade, a plant lifetime of thirty years is assumed. For simulating the entire operational period of the plant, therefore, it was decided to rely on the available dataset to extrapolate the final results. This choice is due to the reduction of computational efforts and is consistent with the lifespan of the battery, which is considered the most critical component.

In order to accurately estimate the cyclic wear of the battery, once the ten-minute mean (P_{AVG}), minimum (P_{MIN}), and maximum (P_{MAX}) power productions are estimated relying on the resource above, an additional refinement process is adopted to obtain a power resolution of one minute. To this end, the iterative procedure adopted [261] is based on the random generation in a range limited by P_{MIN} and P_{MAX} of eight power values, whose average is P_{AVG}. This approach, considering that the average power generation is preserved, prevents the errors that would have been included in the production estimation based on a minute resolution of the wind source.

Figure 4.3 summarizes in a scheme the overall process used to obtain 1-min wind power data starting from 1-hour wind speed data.

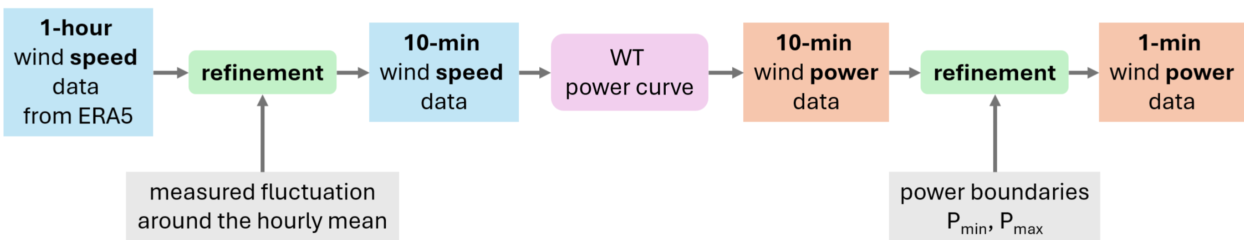

Figure 4.3: Scheme of the overall process used to obtain 1-min wind power data starting from 1-hour wind speed data.

4.4.3 Curtailments

Curtailments represent the planned reduction of power output from wind farms during periods of electrical grid congestion, predominantly impacting non-programmable renewable energy sources. The “Global Ambition Italia” scenario depicted by TERNA for 2040 [213] anticipates a substantial adoption of these sources, leading to an estimated 11 TWh/year of curtailed energy, constituting around 5 % of the projected renewable energy production. However, this percentage is indicative, given the significant variability in grid capacity across different regions. Hence, this study examines three scenarios, varying the annual curtailed energy from 5 % to 10 % or 15 % of the plant AEP. Additionally, the planned power output reduction is estimated as a percentage of the farm's nominal power, as described in **Table 4.3**, in order to match the target annual curtailed energy. Those reductions are scheduled throughout daylight hours, with a distribution centered on 1:00 p.m., and modelled with two distinct time-dependent approaches:

- *Homogeneous distribution (S1)*: the curtailed energy is equally distributed throughout the year. Over the 24 hours, the curtailed energy is concentrated during the six central hours of the day, typically when the grid congestion is higher. This reduction is applied to every day of the year without distinctions.
- *Seasonal distribution (S2)*: the planned reduction of power output is concentrated during the summer, with peaks of eight hours per day, six hours in spring and autumn, and valleys in winter (four hours). In this case, both the potential issues induced by the seasonal fluctuation of renewables and the daily trend of grid conditions are accounted for. Additionally, in order to consider weather variability, a randomization process that preserves the mean hours per day has been applied for winter months.

Table 4.3: Curtailment description in terms of power reduction.

Scenario		5 %	10 %	15 %
S1	Power reduction [%]	12	27	47
S2	Power reduction [%]	12	29	51

Furthermore, in this work, the curtailed energy is assumed to be remunerated (E_{cost}) as a percentage of the LCoE. This assumption is consistent with the present regulation and, even if it will probably be changed in the future, it is considered in this study as an incentive to promote the installation of large capacities of renewable power plants. According to the author's experience, three different scenarios are considered, assuming an E_{cost} is equal to 0 %, 25 %, and 50 % of the LCoE, as in previous works [128] in collaboration with a publicly funded Italian research company.

4.4.4 Battery modelling

Among the existing electrochemical ESS technologies, this study considers Li-ion batteries due to their high round-trip efficiency and ability to withstand charge and discharge cycles [215]. Specifically, the Nickel-Manganese-Cobalt (NMC) Python-based model described in [258] was employed. To this end, the battery is charged when the wind farm's power generation is limited by curtailments and discharged when the production is lower than the 1 GW nominal output. In order to obtain accurate results, a degradation model is also considered, accounting for the reduction in available capacity due to cyclic wear. Finally, given the continuous use of the battery and the reduced idle periods, a calendar ageing model is not included, as it refers to situations where the state of charge (SOC) of the component remains high, without undergoing discharging cycles for extended periods. Moreover, in order to obtain a more conservative assessment of the battery degradation, the fit for the estimation of the end-of-life cycles (EOL) presented in [215] for the MC PHEV-1 / Samsung SDI 94 Ah battery [262] has been adopted. Specifically, the resulting coefficients A and B reported in equation 4.2 are equal to 1512.45 and -0.9684.

$$EOL_{cycles} = A * (\Delta SOC)^B \quad 4.2$$

A decrease in SOH leads to lower performance of the battery, consistent with energy and economic losses. Moreover, the SOH reflects the residual life of the component. While the same initial SOC has been assumed, equal to 95 %, the most relevant difference between brand-new and second-life BESSs is in the initial SOH, set at 80 % for the latter [233–235]. This initial SOH has been assumed to account for prior degradation from SBESSs first use, including calendar and cycling ageing. As mentioned in the introduction and highlighted by the dashed blue line in **Figure 4.4**, this SOH value represents the EOL limit for the BESSs installed in electric vehicles. On the other hand, the replacement of the component occurs for both technologies when 70 % of SOH is reached (red dashed line in **Figure 4.4**) or after a maximum operation time of ten years [236]. Finally, due to the current limitations of battery passports, detailed first-life data for second-life batteries are often unavailable, introducing potential variability in module performance. To maintain consistency, this study evaluates SBESS performance under idealized conditions.

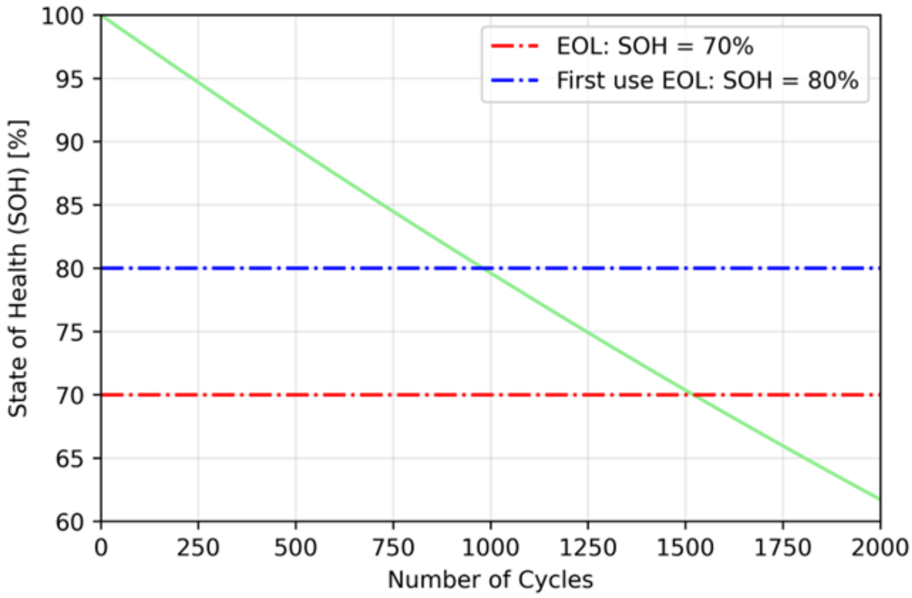

Figure 4.4: SOH decrease due to cyclic operation of the BESS for the two degradation fittings tested.

4.4.5 Electrolyzer modelling

To assess the impact of the electrolyzer system size, a sensitivity analysis has been conducted by varying the size between 10 and 990 MW. This range was selected based on some preliminary analyses, which showed that these dimensions are optimal for a 1 GW power plant within the described scenarios. Although the maximum power available for the electrolysis facility, about 300 MW, is higher than the 90 MW considered, the limited amount of time when that power occurs leads to smaller optimal capacities. Given the lack of spatial constraints and the constant power input resulting from the centralized onshore configuration, ALK technology has been considered herein. The computational model of the electrolyzer previously described in Section

2.3.1.2 has been adopted, setting the time step size to 1 min to ensure consistency in the comparison with the BESS case. Within this timeframe, one can estimate the efficiency variations relying on the estimation of the overpotentials due to losses. Values of current density equal to 10 kA/m2 and voltage of 1.89 V were considered as design parameters of the cell. To carry out the economic analysis and calculate the LCoH, a 30-year timespan was assumed for the electrolyzer, with a stack replacement after 10 years (based on the results presented in Chapter 2), costing 40% of the CAPEX. Moreover, this study assumes that curtailed renewable energy, which would otherwise be wasted, is used to produce green hydrogen. This assumption allows for focusing solely on the expenditures associated with the electrolysis plant, neglecting hydrogen storage and pipelines due assumption of direct use near the production area. Therefore, electricity expenses were accounted for considering that energy is valued as the feed-in tariff assumed (0% or 50% of the LCoE).

4.4.6 Metrics for cost estimation

The estimation of costs related to the generation of electricity is key for this work. Specifically, the LCoE is employed as the primary metric for the evaluation of the layout optimization of the wind farm. LCoE represents the cost associated with the production of a single unit of energy with a specific technology and the price at which energy must be sold to recover capital ($CAPEX$) and operational ($OPEX$) expenditures during the plant's lifetime. Notably, this metric is obtained with the ratio between the actualized sum of costs projected throughout the lifespan of the plant and the actualized sum of energy that the plant will generate within the same timeframe. Furthermore, the same metric can be used to accurately consider the impact of curtailments on the revenues of the wind farm. The inclusion of the grid constraints in the estimation of the producibility leads to a decrease in the amount of energy produced to account for the non-production due to curtailments. In this case, considering the unchanged $CAPEX$ and $OPEX$, the costs for energy production would experience a significant increase. To this end, in this study, the market-dependent LCoE depicted by equation 4.3 is used to estimate the real minimum price at which energy should be sold, assuming no remuneration for curtailments.

$$mLCOE = \frac{\sum_{t=1}^{n} \frac{(CAPEX_t + OPEX_t)}{(1+i)^t}}{\sum_{t=1}^{n} \frac{E_{grid,t}}{(1+i)^t}} \tag{4.3}$$

Where t represents the present year, n is the plant lifetime, i is the discount rate, and E_{grid} is the energy delivered to the grid.

The other metric used to estimate the impact of the adoption of an energy storage system is the NPV. This parameter allows for the evaluation of the profitability of a planned investment by assessing its present value through the difference between the future discounted cash flows (cf) and the initial CAPEX, as specified in equation 4.4. Specifically, cfs are estimated as the sum of the revenue obtained from energy input to the grid and the remuneration expected for the energy not injected during curtailment. The difference between the plant with and without a BESS is considered in the increase in the initial capital cost and the replacement expenditures for the battery over the system's lifespan.

$$NPV = \sum_{t=1}^{n} \frac{cf_t}{(1+i)^t} - CAPEX \tag{4.4}$$

For the NPV calculation, some assumptions about the electricity pricing are required. In this study, according to the guidelines proposed by the FER2 regulation, a feed-in tariff has been assumed, valuing the energy injected into the grid at 185 €/MWh [263].

Finally, the LCoH has been selected as a cost metric for the definition of hydrogen cost. Again, the same approach presented in Section 2.3.2 has been adopted for the calculation.

4.4.7 Component costs

The accurate estimation of CAPEX and OPEX is crucial for computing the LCoE and NPV of a wind-powered energy system. However, due to the limited number of existing plants, estimating the actual and projected costs of floating offshore wind turbines (FOWTs), floating platforms, and all related components is complex. In this work, the same assumptions and methodology described in [256] have been adopted, with the specific capital expenditures described in **Table 4.4**. Considering the sensitivity analysis performed on the distance between WTs, the costs for intra-array cables are expressed as the range resulting from the least and most spaced configurations. To deal with the uncertainty related to the costs of Li-ion batteries for analyses conducted over a timeframe starting from 2030, it has been decided to perform sensitivity analyses by varying the battery cost, with values per unit of capacity ranging from 110 to 190 €/kWh for both $BESS_{OPT}$ and $BESS_{RE}$. This assumption is consistent with the future projections presented by [252,253].

Table 4.4: Specific Expenditures for the case study.

Component	Capex
Wind turbines [M€/MW/unit]	1.034
Platform [M€/MW/unit]	0.696
Intra-array cables [M€/kW/km]	0.008
Export cables [M€/MW/km]	0.011
Moorings [M€/MW/unit]	0.035
Installation [M€/MW]	0.169
NBESS [€/kWh]	110-190
SBESS [€/kWh]	50-130

Concerning SBESSs, due to the assumptions presented in Section 4.2, a CAPEX that ranges between 50 and 130 €/kWh has been considered. This assumption includes both the lower CAPEX of the technology and the economic incentives due to the reduced environmental impact. Finally, a storage system replacement cost of 70 % of the initial CAPEX is adopted [264], assuming the substitution of NBESSs and SBESSs with the same technology at the end of the storage lifetime. While the SBESSs experience lower replacement costs, the higher number of substitutions during the plant lifetime and the possible enhanced energy losses due to degradation may affect the revenues.

Concerning electrolyzers, to account for projections to 2030, a literature analysis has been conducted. Regardless of the size of the plant, the CAPEX of electrolyzers was set 1000€/kW, to simulate the worst-case scenario [265]. This value has been selected based on the extensive amount of data available in the literature, which has been summarized in a box and whisker plot (**Figure 4.5**). In this plot, a box spans from the first to the third quartile, with a vertical solid line representing the median value and a vertical dashed line indicating the average value. The chosen value represents the upper bound of the range, resulting in a conservative assumption for projections up to 2030. Additionally, according to the literature [224], a stack lifetime of ten years has been assumed, leading to two substitutions of the component during the wind farm lifetime. This assumption is consistent with the evaluation of a degradation lower than 20% of the nominal performance after 10 years of operation. Considering that the stack contains the most expensive components, the replacement costs were set at 40% of the capital expenditure for the electrolyzer. Finally, in order to take into account economies of scale, the approach shown in Section 2 has been adopted.

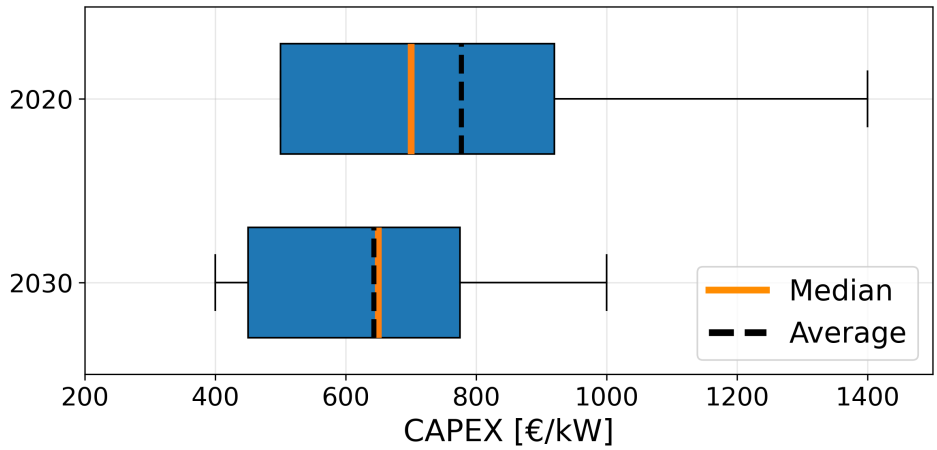

Figure 4.5: ALK electrolyzers CAPEX in 2020 and in 2030.

4.5 Results

This section presents an overview of the wind farm performance in different configurations and scenarios. The outcomes for the analyzed layouts are described in terms of AEP and LCoE to highlight the effects of wake losses and component costs in the optimization. Furthermore, mLCoE is adopted to estimate the real costs per unit of energy in each curtailment scenario for the specific installation case. Finally, concerning the utilization of batteries, the results of the time-dependent analyses are presented to estimate the size that maximizes the wind farm NPV. In this study, a sensitivity analysis on the interest rate (i) is performed to account for the uncertainties in the component and energy market for a time horizon starting from 2030. To this end, values of 5 %, 7 %, and 9 % are adopted.

4.5.1 Wind farm layout optimization

Before the analysis of the effectiveness of installing a BESS, this section shows results of the wind farm itself in terms of energy production and cost of energy, considering aerodynamic losses and cable costs. Optimizing the wind layout to minimize the LCoE means finding the best trade-off between higher energy production and higher installation costs. As expected, upon examination of **Table 4.5**, an increase in wind turbine intra-array spacing enhances the energy production, due to the decrease in wake effects. However, although the 13d-10d layout is not the most spaced in the along-wind direction, the increased distance in the crosswind direction promotes a reduction of wake losses, which results in the highest AEP.

Table 4.5: Wind farm AEP and LCoE for the analyzed layouts with different interest rates i.

Layout L-l	r	13d-5d	13d-6.25d	13d-7.5d	13d-10d	14d-7.5d	15d-7.5d
AEP [GWh/y]	-	3268.5	3308.3	3334.7	3368.9	3341.0	3347.3
LCoE [€/MWh]	5 %	107.20	106.61	106.18	106.77	106.04	106.17
LCoE [€/MWh]	7 %	121.67	121.00	120.52	121.19	120.36	120.51
LCoE [€/MWh]	9 %	137.28	136.52	135.98	136.73	135.79	135.97

The adoption of L (distance in wind direction) equal to thirteen WT diameters leads to an almost full wake recovery, resulting in small improvements with a further increase of this parameter. As depicted by **Table 4.5**, an increase in AEP is not necessarily related to a decrease in energy costs. Despite the minimum wake losses and higher capacity factors, higher WT spacing leads to enhanced CAPEX and OPEX. For this specific installation site, the optimal wind farm layout is represented by the 14d-7.5d configuration.

4.5.2 mLCoE

Based on the outcomes of the previous section, the optimal layout has been chosen to investigate the effects of curtailments on energy costs. To this end, the time-dependent analysis enables the estimation of the yearly impact of curtailments on energy production. Without a BESS, non-production affects the revenues of the wind farm. The accurate estimation of curtailments is crucial. **Figure 4.6**a shows the net yearly energy production and the curtailed AEP for both S1 and S2 in the different scenarios. The plot represents both the seasonal and homogeneous scenarios because, as mentioned in the previous sections, despite the different distribution of daily curtailments in S1 and S2, the total amount of non-produced energy is equivalent.

Figure 4.6b shows the LCoE and the mLCoE for the curtailment scenarios considered with different discount rates. The red bar in the chart represents the result obtained neglecting curtailments, corresponding thus to the standard LCoE generally adopted in literature.

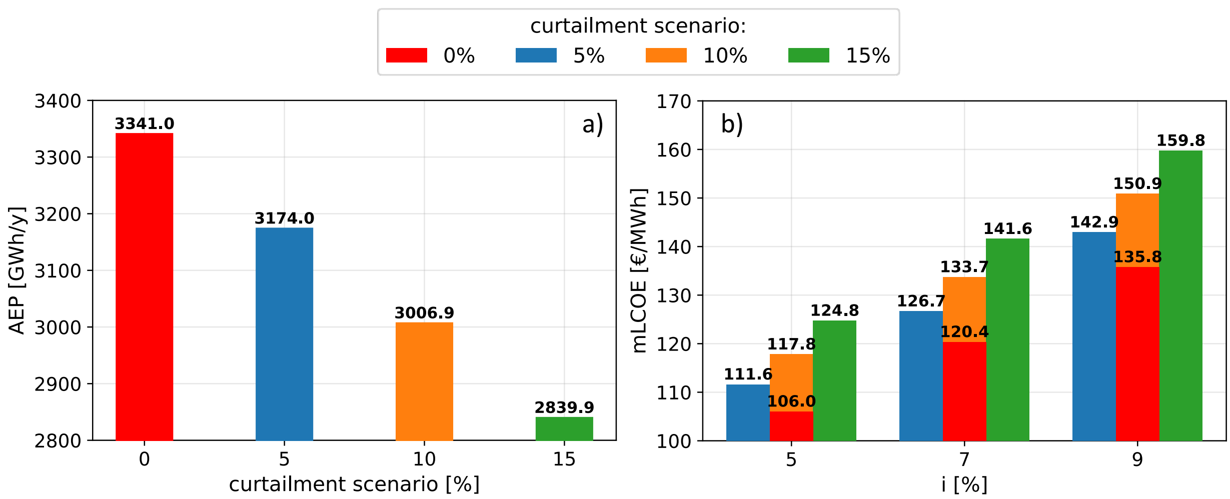

Figure 4.6: AEP (a) and mLCoE (b) in different curtailment scenarios for the discount rates analyzed.

As expected, the decrease in energy production results in a significant increase in generation costs. Curtailment scenarios of 5 %, 10 %, and 15 % lead to a rise in energy costs of 5 %, 11 %, and 18 %, for all the interest rates considered. Low values for E_{cost} lead to relevant economic losses in the revenues of the wind farm, especially if the price of the energy sold to the grid is close to the LCoE. To this end, the inclusion of the mLCoE results in more accurate cost projections to deal with the tender system of the energy market.

4.5.3 LCoH

Based on the results of Section 4.5.1, the 14d-7.5d layout has been chosen for the 15 MW WTs farms, to investigate the cost of possible green hydrogen production. It is worth noticing that the present study does not consider any cost related to hydrogen storage and transport. The following results must then be considered as only related to the production step of the hydrogen value chain. In order to justify the adoption of a detailed electrolyzer model, a comparison between a statistical and a time-dependent approach is proposed herein. Therefore, curtailments have been accounted as a fixed percentage of the AEP for every hour of the year (statistical approach) and with a distribution to consider grid congestion throughout the day (as described in Section 4.4.3). The comparison between those two approaches allows one to estimate the limitations of the common practice for preliminary analyses. To this end, **Figure 4.7** shows the comparison between the two described curtailment distributions during 24 h of simulation.

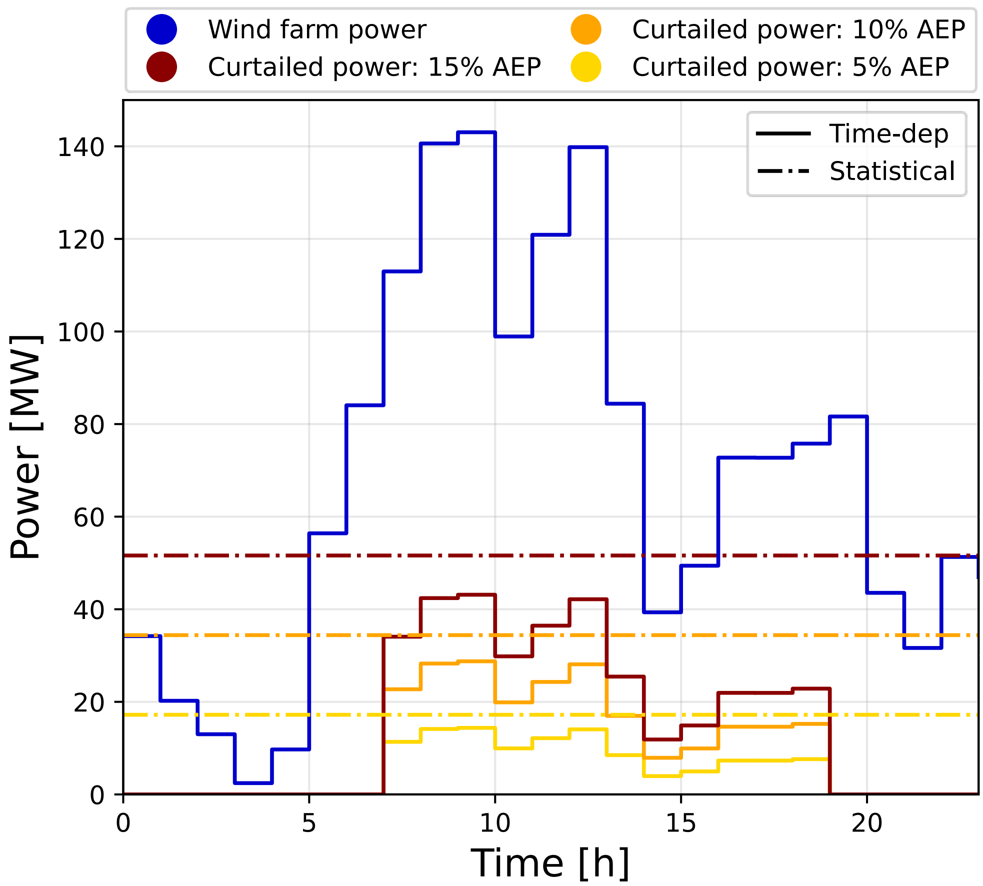

Figure 4.7: Power production and curtailed power for the time-dependent and statistical approach, in all curtailment scenarios.

A statistical approach translates, in the time domain, into a constant power input available for the electrolyzer. Therefore, even during a day on non-constant production form the wind farm, as the one shown in the image, a constant power input to the electrolysis facility is considered, leading to an overestimation of the CF of the component. On the other hand, the time-dependent approach results in a more realistic power input estimation, also due to the clustering of curtailments during the central hours of the day, when the probability of going through grid congestion is higher. Even if the total curtailed energy is equivalent in both situations, the time distribution of the available energy affects the estimation of hydrogen production.

Indeed, during a day of low production, as the one shown in **Figure 4.7**, the statistical approach shows a higher curtailed power throughout the whole day for all curtailment scenarios.

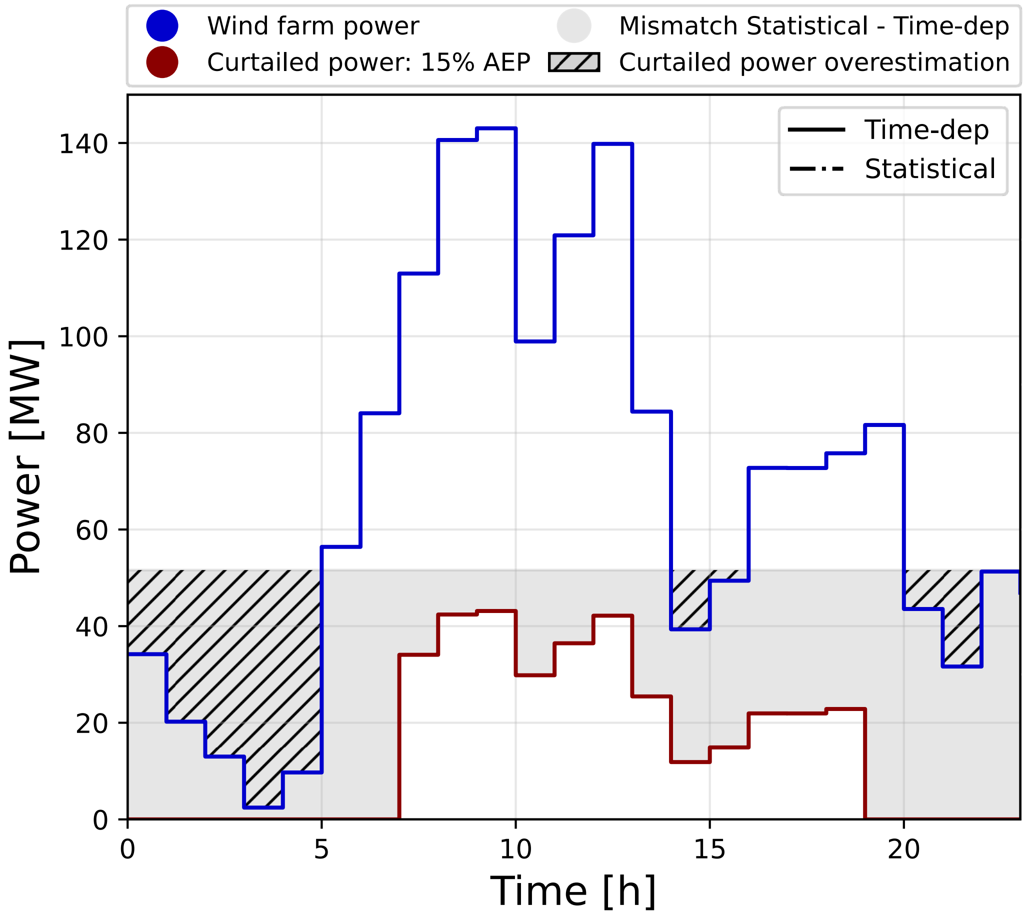

Figure 4.8: Power production and curtailed power for the time-dependent and statistical approach, the 15% AEP curtailment scenario.

Figure 4.8 highlights, time-step per time-step, the differences between the approaches in the scenario characterized by the higher curtailed energy in the same 24 h of **Figure 4.7**. In detail, the grey area represents the difference in energy available for the electrolyzer. A constant distribution of curtailed energy during the year leads to a relevant overestimation of the curtailed energy in the off-peak hours, while in the time-dependent scenario, all the wind farm power is fed into the grid. As highlighted by the hatched light grey area in the plot, this trend may result in energy availability even larger than the wind farm production. Those two aspects, combined with the constant power input to the electrolysis facility, result in an underestimation of the LCoH between 1 and 2 €/kg. The statistical approach has been discarded, justifying the adoption of the electrolyzer model.

Figure 4.9 shows the dependence of the LCoH and the CF in S1 and S2 on the size of the electrolyzers while varying the energy value in the 10% curtailment scenario. It is apparent that, despite the low LCoH estimated, the CF of the electrolysis facility remains low. Despite the small capacities installed with respect to the available energy during curtailment hours, this is consistent with large periods of inactivity of the component, when the wind farm output is fed directly into the grid. On the other hand, the low costs associated with hydrogen production result in a relatively low LCoH. A comparison can also be done between the curtailment scenarios and the energy values considered. It is apparent how the seasonal distribution of the curtailment leads to higher LCoH.

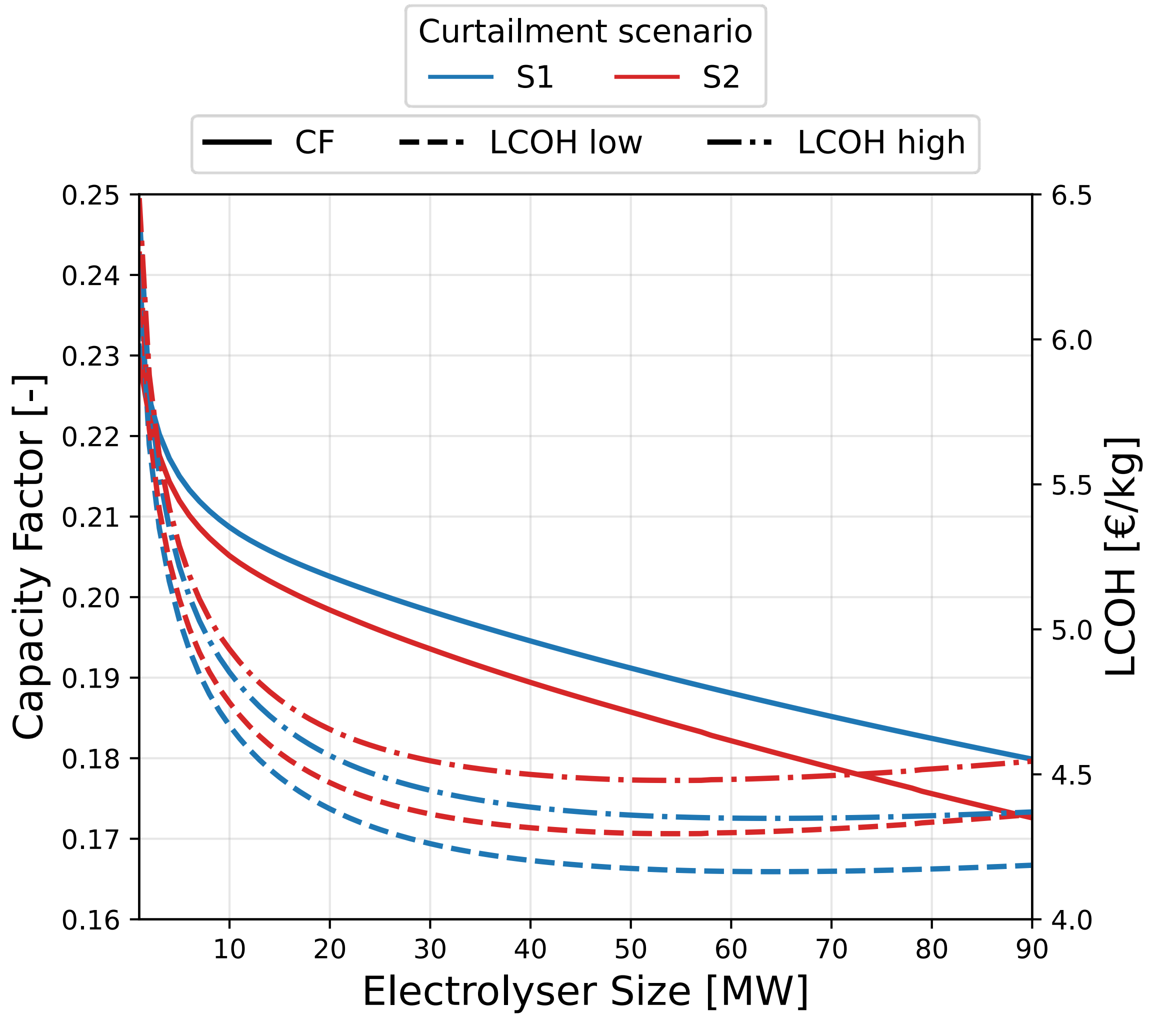

Figure 4.9: LCoH and capacity factors in S1 and S2 in the 10 % curtailment scenario.

The less homogeneous distribution of the available energy, in fact, results in higher energy underexploitation, as testified by the lower CFs at the same electrolyzer capacity. This results in lower optimal electrolyzer capacities and, therefore, lower hydrogen production per year. Finally, as expected, the higher energy costs associated with the *LCoH high* scenario lead to higher production costs. **Table 4.6** shows the optimal electrolyzer sizes resulting from the analyses that have been then used for the estimation of the NPV.

Table 4.6: Optimal electrolyzer sizes and LCoH in the different curtailment scenarios.

Parameter	Energy cost scenario	S1	S2
Electrolyzer capacity [MW]		64	55
LCoH [€/kg]	LCoH low	4.164	4.29
	LCoH high	4.348	4.47

4.5.4 NPV

This section describes the assumptions made and the results of the previously mentioned scenarios for the estimation of the Li-ion ESS contribution. In order to compare the storage plant with the base one, an accurate description of the energy remuneration scheme is needed. For the curtailed energy, the same E_{cost} is assumed for both plant configurations. This approach allows us to consider the potential revenues from curtailments as positive cash flow. The base plant does not generate energy during hours of curtailment. On the other hand, the BESS can store the energy produced in such moments and further inject it into the grid when the system is allowed to. This additional source of income may contribute to enhancing the NPV when higher than the additional installation and substitution costs of the BESS. Finally, in this section, only the results for i equal to 7 % are shown, while an LCoE of 120.36 €/MWh is considered.

Figure 4.10 shows the influence of NBESS costs on the NPV of the wind farm after 30 years of operation in different curtailment scenarios. Specifically, an E_{cost} of 0 % (a), 25 % (b), and 50 % (c) of the plant LCoE is reported for the S1, S2, and no BESS scenarios.

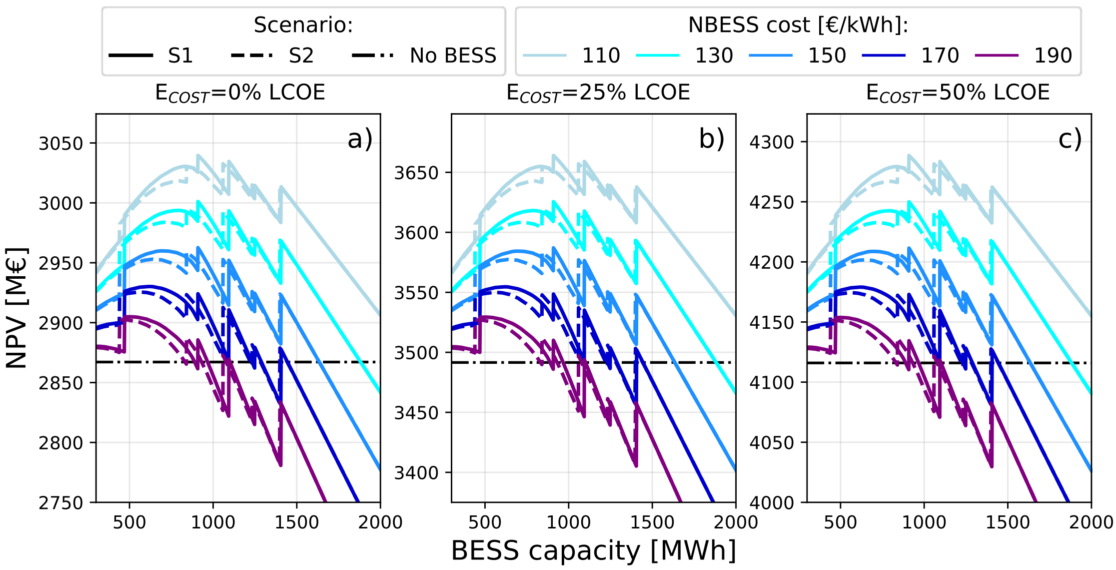

Figure 4.10: NPV of the wind farm in the 5 % curtailment scenario and a curtailed energy remuneration of 0 % (a), 25 % (b), and 50 % (c) of the LCoE with the adoption of the NBESS.

It is apparent how the base plant (dash-dot black line at the bottom) experiences lower revenues over the plant lifetime in all the configurations analyzed. A seasonal scenario (dashed line) results in a lower contribution of the storage system, if compared to the S1 condition (solid line), where a homogeneous power flow to the battery improves the performance of the component, increasing the amount of exploited energy. Furthermore, an increase in storage costs (different colors) leads to a relevant decrease in the wind farm's NPV and the battery's optimal size. Specifically, a rise of 20 % in BESS cost results in a reduction of the revenues of 1 %. This is due to enhanced capital expenditure for the system with the same energy available for storage. Regarding E_{cost} variation, while an increase in the remuneration of curtailed energy enhances the absolute value of the NPV, it does not affect the relative revenues with respect to the base plant. Specifically, an optimal range of BESS capacity between 700 and 900 MWh is estimated, which leads to maximum NPVs ranging from 3000 to 3100 M€, from 3600 to 3730 M€, and from 4240 to 4350 M€ for E_{cost} values of 0 %, 25 %, and 50 % of the LCoE, respectively.

Figure 4.11 illustrates how variations in NBESS (a-c) and SBESS (d-f) costs impact the wind farm's NPV over a 30-year operational period under different curtailment scenarios. Specifically, Ecost values of 0 % (a, d), 25 % (b, e), and 50 % (c, f) of the plant LCoE are analyzed for the homogeneous (S1) and seasonal (S2) curtailment distribution during the year, with respect to the base scenario. The base plant (dash-dot black line) generates lower revenues with respect to the one with NBESS throughout its operational lifetime, if the storage is properly sized. However, when SBESSs are implemented, the storage system results in a cost-effective solution only when the BESS cost is below 70 €/kWh. In fact, while for the NBESS the replacements along the plant's lifetime range from 4 to 6, in the second life scenario, the number of substitutions spans between 15 and 6, leading to relevant cost increases.

Higher storage costs (represented by different colors) lead to a significant decline in both the wind farm's NPV and the battery's optimal capacity. Specifically, a 20 % increase in BESS costs results in approximately a 1-2 % reduction in revenues. This is attributed to higher capital expenditures on the system, despite the available energy for storage remaining unchanged. Regarding variations in E_{cost}, while an increase in the remuneration of curtailed energy raises the absolute NPV, it does not influence the relative revenue difference compared to the base plant.

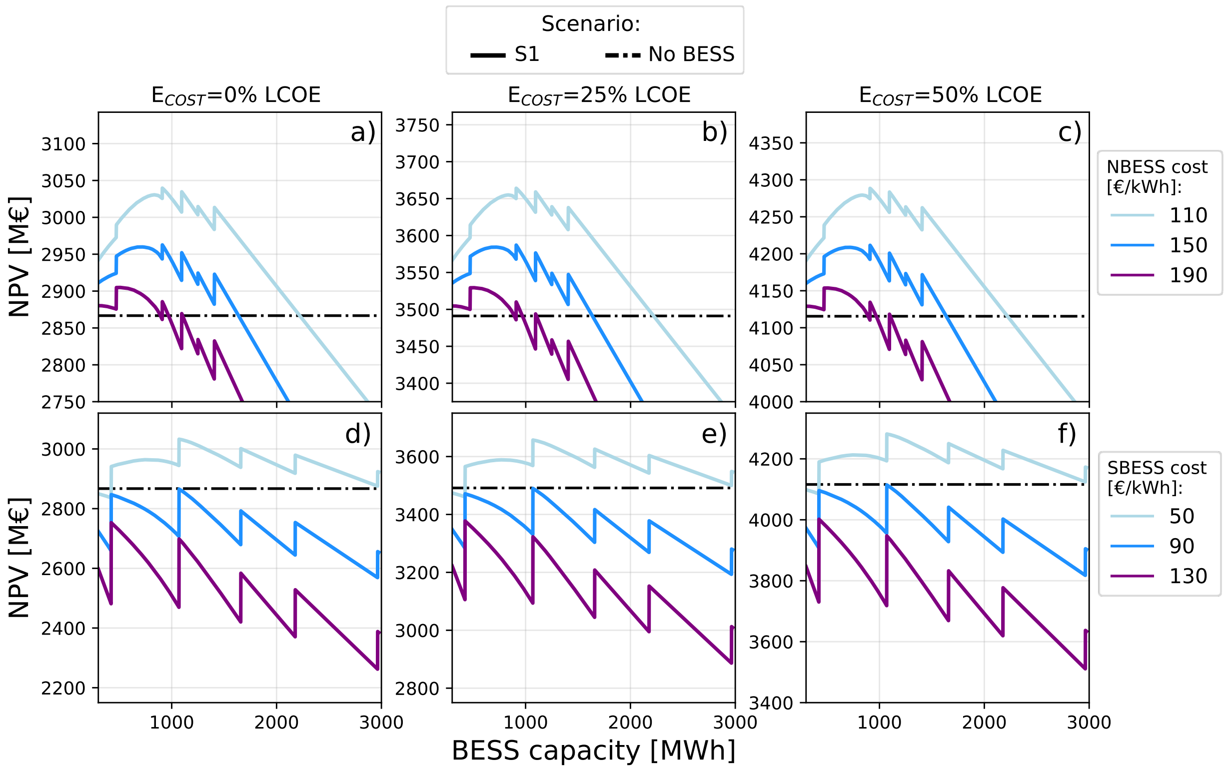

Figure 4.11: NPV of the wind farm in the 5 % curtailment scenario and a curtailed energy remuneration of 0 % (a, d), 25 % (b, e), and 50 % (c, d) of the LCoE for the NBESS (above) and SBESS (below).

A few words should be spent on the trend of NPV for both technologies. The discontinuities observed with increasing BESS sizes are due to the reduction of storage replacements during the plant's lifetime. Larger sizes reduce the number of operating cycles, with lower depth of discharge under the same energy dispatch conditions.

As a result, the overall degradation of the battery system is mitigated, extending the functional lifespan of the component. Consequently, storage systems with larger capacities undergo fewer full equivalent cycles over time, which directly translates into a reduced need for BESS module substitutions. This dynamic offsets part of the increased CAPEX associated with scaling up the storage system. Therefore, while larger capacities result in enhanced CAPEX, proper sizing leads to economic benefits even with oversized storage. This balance explains why the NPV trend displays peaks at specific storage sizes, those that are large enough to significantly reduce degradation without incurring unnecessary oversizing costs. These optimal points reflect configurations where the trade-off between CAPEX and replacement cost is most favorable.

In **Figure 4.12**, the effects of a curtailment scenario of 5 % (blue), 10 % (orange), or 15 % (green) of the AEP are shown. In detail, the results show that adopting a brand-new storage system is always convenient regardless of the curtailment distribution throughout the year.

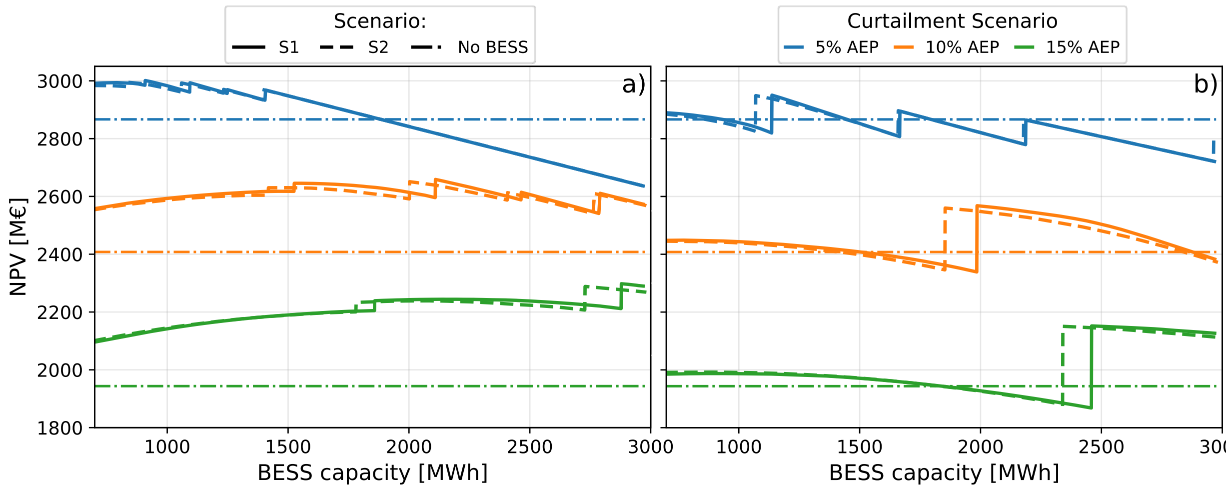

Figure 4.12: NPV of the wind farm with an Ecost of 0 % of the LCoE and a BESS cost of 130 €/kWh for the NBESS (a) and 70 €/kWh for the SBESS (b).

Moreover, an increased reduction of the wind farm output leads to a decreased amount of energy valued at the market energy price, assumed to be equivalent to 185 €/MWh. This is consistent with the decrease of the NPV shown in the plot for the base plant (dash-dot line) with all the E_{cost} assumed. In addition, the revenues in S2 (dashed line) are 0.4 % lower than those in S1 (solid line).

Delving deeper into details, a few words should also be spent on the comparison between NBESS and SBESS. **Figure 4.12**b illustrates how, with both technologies, the S2 (dashed line) results in a lower contribution from the storage system compared to the S1 condition (solid line), where a more uniform power flow to the battery enhances its performance by increasing the amount of utilized energy.

As the wind farm's output reduction increases, the amount of energy valued at the market price decreases accordingly. This aligns with the decline in NPV observed for the base plant without storage (dash-dot line) across all considered scenarios. Furthermore, a higher level of curtailed energy results in lower storage efficiency and a diminishing gap between the new and second-life BESS, improving the cost efficiency of the latter. Therefore, an increase in curtailed energy leads to lower storage effectiveness and a reduction of the gap between the two scenarios from 2 % to 1 % for a power reduction of 5 % and 15 % on the AEP, respectively. As expected, the optimal size of the storage, depicted in the outcomes above, is about 9 %, 16 %, and 38 % smaller than the one that leads to the minimum energy waste.

Figure 4.13 shows how the increased remuneration for the curtailed energy affects the increase in the NPV (ΔNPV) due to the battery, varying the BESS cost. The results demonstrate that, while the remuneration of 50 % of the LCoE leads to an overall higher income, the ΔNPV is not affected by increases in the price of curtailed energy, due to the proportional increase in revenues from the base plant. Therefore, just one bar is shown in this plot to represent the maximum earnings from a configuration, regardless of curtailment remuneration. On the other hand, a higher amount of curtailed energy results in enhanced ΔNPV due to the increased weight of energy exploitation. As expected, while the most cost-effective case is characterized by a low percentage of energy allocated to curtailments, valued with the highest remuneration and low battery costs, the higher impact on the revenues is obtained in a curtailment scenario where the energy reduction is equivalent to 15 % of the AEP. A few differences can be observed when comparing the NBESS and SBESS. While the adoption of NBESSs is always beneficial for the wind farm, SBESSs can result in economic losses. However, in all the analyzed configurations, the non-homogeneous curtailment distribution in S2 always leads to worse exploitation of the storage system, leading to economic losses.

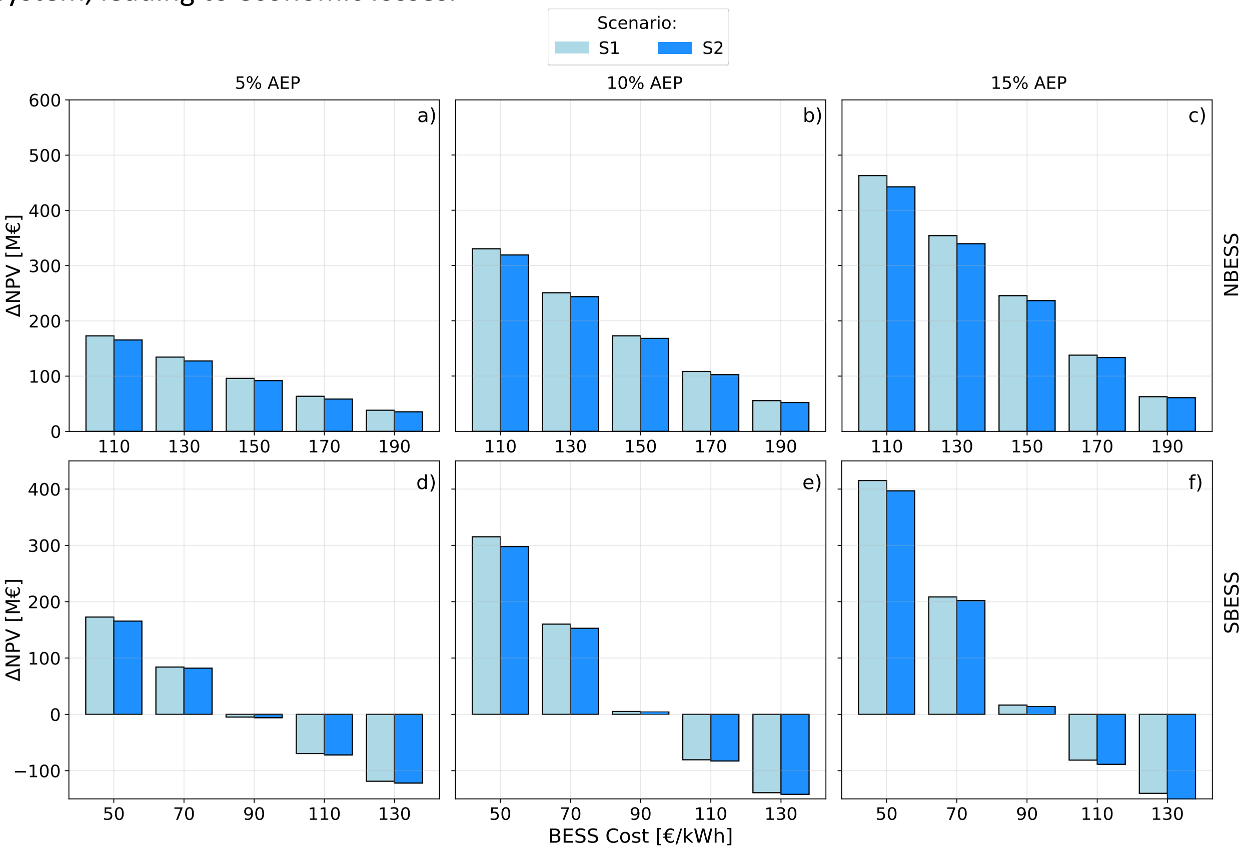

Figure 4.13: NPV Variation in the configuration with the optimal BESS size varying battery cost for different curtailed energy remuneration and wind farm output reduction of 5 % (a), 10 % (b), and 15 % (c) of the AEP with the NBESS (above) and SBESS (below).

These results can be compared with those obtained using hydrogen to mitigate curtailments. **Figure 4.14** shows the NPV of the plant equipped with the electrolysis facility varying the hydrogen remuneration in the LCoH low scenario. Consistent with the results in terms of LCoE, it is apparent that even with a low price per kg of hydrogen, the investment results to be cost-effective. Depending on the curtailment distribution, hydrogen prices of 4.64 and 4.29 €/kg result in the same NPV of the base plant (dash-dot line). On the other hand, a few words should be spent on the comparison with BESS. The dotted line highlights the revenues associated with both NBESS and SBESS, with specific CAPEX of 130 and 70 €/kW, respectively. Despite the high hydrogen remuneration needed to obtain the same NPV (between 8.50 and 9.50 €/kg), these values are obtained for the upper bound of the ALK specific capex in projections to 2030. Therefore, considering this conservative scenario, hydrogen can be a competitor of batteries in curtailment mitigation.

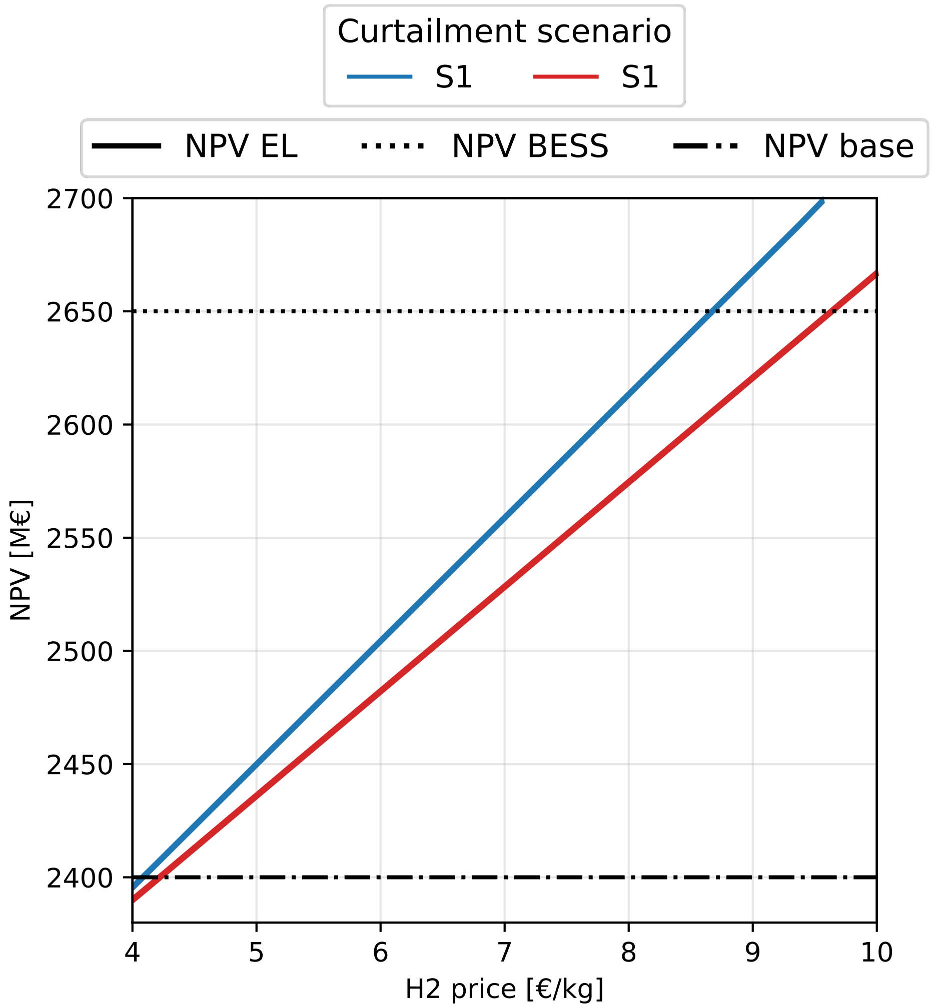

Figure 4.14: Comparison between the NPV of the electrolysis, the BESS and the base solution in S1 and S2 in the 10 %, LCoH low curtailment scenario.

4.5.5 Preliminary environmental analysis

While a comprehensive Life Cycle Assessment (LCA) could provide a more complete picture of the environmental impacts associated with these battery systems, such an analysis falls beyond the scope of this study. In fact, conducting a full LCA is a stand-alone effort that requires detailed inventory data, which is currently unavailable. Nevertheless, a preliminary environmental evaluation is important in a study like the present one and can still be conducted based on available data—particularly the reported carbon footprint of the batteries. This allows for an initial estimation of their potential climate impact, complementing the economic results presented earlier.

A realistic degradation scenario is crucial to estimate the number of replacements of the BESS during the wind farm's lifetime. Starting from a minimum number of three substitutions, a maximum of 6 and 18 replacements can be observed with the NBESS and SBESS, respectively. However, although this affects the wind farm's revenues worse when a second-life technology is adopted, the environmental benefits related to the adoption of SBESSs are relevant. In fact, while the adoption of a brand-new storage system dedicated to the wind farm is associated with a carbon footprint of 263 kg CO_2-eq/MWh [266], the environmental impact of SBESS can be neglected. Specifically, the adoption of this technology can save up to 2400 t CO_2-eq, depending on the number of replacements for the component, as shown in **Figure 4.15**.

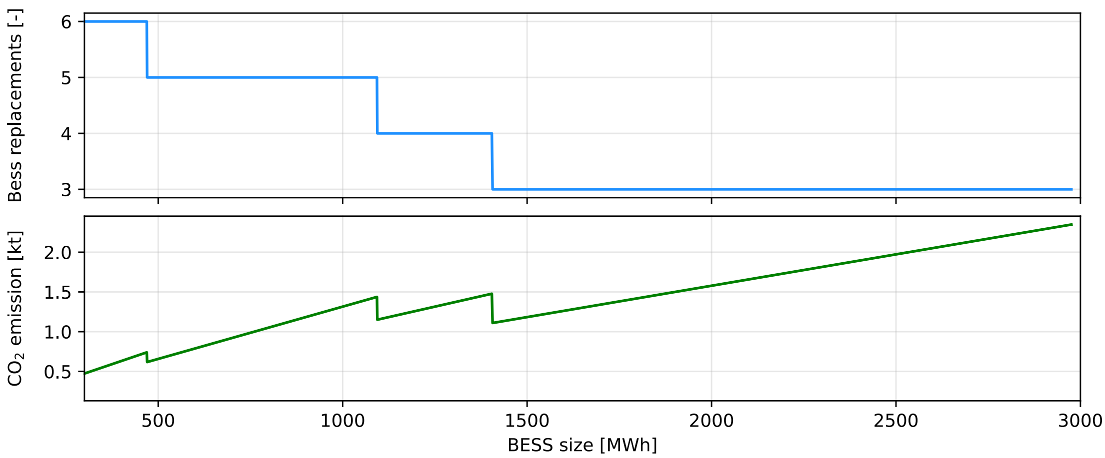

Figure 4.15: Battery replacements and environmental impact of the storage after thirty years of operation of the plant.

On the other hand, the lifetime extension, estimated to range from two to five years despite the limited useful SOH range (from 80 % to 70 %), allows for better exploitation of the BESS, which would otherwise have been decommissioned. This may be beneficial for the revenues of the system equipped with the SBESS. The competitiveness of this solution can be enhanced with further incentives to reduce the CAPEX of this technology, or with future CO_2 taxes proposed by policymakers to discourage the adoption of NBESSs when it is not required.

Finally, it is important to note that a full life cycle comparison, including the production and decommissioning phases, would not impact on the relevance of the results in this context. For the purposes of this preliminary assessment, it has been assumed that a similar environmental impact occurs during these two phases for both new and second-life BESS, given the lack of detailed component-level data. The environmental interest of the comparison lies primarily in the reuse of second-life batteries that would otherwise have been decommissioned despite the remaining SOH. This approach allows for a meaningful evaluation of the benefits derived from extending the functional life of battery systems, rather than focusing on impacts that are assumed to be equivalent across both options.

4.6 Discussion

This study examines the comparison between the integration of large-scale BESS and electrolysis facilities with offshore wind farms strategies to mitigate curtailments and improve grid stability, while also comparing the potential of new versus second-life batteries. Although the concept offers significant prospects for enhancing the flexibility and resilience of renewable energy systems, FOWTs, large-scale storage technologies, and electrolyzers remain in the preliminary stages of large-scale deployment, facing a complex set of technical, economic, and regulatory challenges.

Offshore wind’s potential is widely recognized, yet its growth is hampered by high capital costs, complex grid integration, and logistical challenges. Most current offshore wind farms located close to shore use high voltage alternating current (HVAC) transmission, which is technically simpler and less expensive over shorter distances. In contrast, high-voltage direct current (HVDC) becomes more efficient and cost-effective for transmitting power over longer distances, especially in far-offshore projects [267,268]. However, for the near-shore farms studied in this work, HVAC remains the preferred solution due to its lower upfront infrastructure requirements and maturity.

Despite projections of future cost reductions for 2050, offshore wind's current LCoE remains high, underscoring the urgency of making early-stage projects more viable against fossil fuel-based electricity. Improving early project viability will require targeted policy support, such as feed-in tariffs, investment tax credits, contracts for difference, and long-term power purchase agreements, along with financial tools like public-private partnerships and loan guarantees. Technological advancements, including larger turbines, floating foundations, and digital monitoring, as well as streamlined permitting and local supply chain development, are also key to reducing costs.

Crucially, this work highlights the emerging role of hydrogen and battery storage, both new and second life, as a tool for optimizing offshore wind integration. While second-life batteries offer a potentially lower-cost and more sustainable alternative, they present additional uncertainties around performance and lifecycle that need to be addressed through further research and pilot projects. Conversations with industry stakeholders have revealed that most of upcoming offshore wind farms, especially in the Mediterranean Sea, are expected to be coupled with battery systems to improve grid alignment and reduce volatility. This coupling is seen as a way to mitigate operational risk for grid operators, increase revenue stability for plant owners, and enhance investor confidence in offshore wind infrastructure. On the other hand, technical advancements for electrolyzers may improve the impact of economies of scale, putting the focus on this technology as a competitor of large-scale BESS. The results, in fact, show how the break-even price of hydrogen to reach the same NPV of the BESS plant is between 8.5 and 9.5 €/kg. Additionally, the adoption of electrolyzers not only contributes to greater system flexibility but also supports Europe’s broader strategic objective of enhancing energy autonomy. While large-scale batteries’ supply chains are currently dominated by China and other non-European countries, electrolyzers rely on components and industrial know-how that can be more readily developed and manufactured within Europe. This reduces the risk of dependency on external suppliers and strengthens the resilience of the European energy transition.

A limitation of this study is the evaluation of the behavior of the system with the ALK technology in the worst-case expenditure scenario, while the evaluation of other electrolysis technologies and more CAPEX scenarios may result in a complete overview of hydrogen potential in curtailment impact mitigation.

4.7 Conclusions

The study investigates the effects of curtailments on the revenues of offshore wind farms potentially installed in a site in the Mediterranean Sea, comparing the adoption of ALK electrolyzers, brand-new and second-life BESS to avoid energy waste during different curtailment scenarios.

For large-scale farms, such as the 1 GW plant considered in this study, curtailments represent a significant issue, especially in installation contexts where grid requirements are particularly strict. However, while curtailments significantly impact costs, the adoption of BESS, as well as ALK electrolyzers, can mitigate revenue losses.

The key findings of this work are listed below:

- Curtailments increase production costs, with mLCoE rising by 5 % to 18 % depending on the curtailment level.
- BESS integration improves financial performance, increasing the NPV by 30 % when a brand-new storage is adopted.
- Although second-life BESSs require lower CAPEX to be viable, they can help to increase the NPV up to 30 % with respect to the base plant.
- ALK integration improves financial performance when hydrogen prices higher than 4.2 €/kg are considered.
- Hydrogen and BESS solutions may reach the same NPV when a hydrogen remuneration of 8.5-9.5 €/kg is adopted.
- Despite the storage systems, production costs remain below the feed-in tariff, ensuring economic feasibility despite market uncertainties.
- The lifetime extension of BESS can be beneficial for the environmental impact, leading to a carbon footprint reduction of up to 2400 t CO_2-eq.

Finally, while the NBESSs are always beneficial for the revenues of the system, SBESSs lead to positive incomes only when their CAPEX is below 70 €/kWh, corresponding to an expenditure 30 % lower than the current average in the literature. This result is consistent with literature findings, highlighting how SBESSs need relevant incentives to match the brand-new related revenues.

5 FROM WIND TO HYDROGEN: COMPARATIVE EVALUATION OF ELECTROLYZER TECHNOLOGIES AND COST REDUCTION PATHWAYS

5.1 Introduction

The transition to a low-carbon energy system is crucial for mitigating climate change, with the European Union targeting net-zero emissions by 2050 [238]. Green hydrogen is a key pillar of this transition, offering a scalable solution for decarbonizing hard-to-abate sectors. However, achieving competitive hydrogen production costs depends not only on the availability of renewable energy but also on the effective integration of electrolysis technologies with variable power sources. Offshore wind presents a promising energy source for green hydrogen production due to its higher capacity factors compared to onshore wind [271] or other renewables like photovoltaics [272], while maintaining a moderate LCoE. The deployment of green hydrogen production facilities is particularly relevant in the Mediterranean area [273], in which historically several hard-to-abate industries are located close to ports, like steel production [274], shipyards [275] and others. These businesses are aiming to undertake the transition towards more sustainable industrial processes; however, such a scenario is yet to take off.

The electrolyzer technology strongly influences hydrogen production efficiency. Although ALK represents the most widespread technology due to its cost-effectiveness and maturity [276], it faces significant operational limitations, including high minimum power thresholds and long cold start-up times [277]. These constraints can lead to substantial energy curtailment when integrated with fluctuating wind power. Conversely, PEM and anion exchange membrane (AEM) electrolyzers offer wider operational ranges, faster response times after shutdowns, and improved flexibility, making them more suitable for coupling with offshore wind farms [277,278].

Within this context, many studies have explored different electrolyzer technologies, including ALK, PEM, and AEM, offering comparisons in terms of performance, cost, scalability, and integration with intermittent power sources. Looking at the most recently developed technology, some studies delved deeply into the AEM, reflecting its potential as a bridge between the mature ALK and PEM systems. In their review, Bernat et al. [279] highlighted the role of AEM electrolysis in meeting global energy transition targets and emphasized the necessity for continuous research and commercialization efforts to advance this technology. Gul et al. [280] expanded the analysis of AEM electrolysis by modeling an integrated renewable energy system that combines solar, wind, and biogas inputs to produce hydrogen using excess or curtailed power. Their model demonstrates how AEM electrolyzers can be effectively incorporated into community-scale energy solutions, achieving substantial CO_2 reductions and delivering hydrogen at competitive costs, even under uncertainty in demand and supply conditions. On the other hand, the simplified modelling approach adopted for the simulation of renewable energy production can lead to the underestimation of the complex physics related to the coupling with electrolyzers. Additionally, these studies are focused on a single technology and do not provide a comparison between the existing electrolysis solutions. In this regard, Yang et al. [281] undertook a cost comparison of ALK, PEM, and AEM technologies using a bottom-up modeling approach that incorporates material properties, operating parameters, and manufacturing assumptions. Their projections suggest that, while ALK currently offers the lowest hydrogen production cost, AEM and PEM could surpass ALK in cost-effectiveness in the medium to long term, provided there are significant technological breakthroughs. Further comparative insights are offered by Wang et al. [282], who conducted a rigorous experimental comparison of ALK and PEM electrolyzers operating at identical hydrogen production rates. Their analysis includes dynamic ramping behavior, energy consumption, and integration with solar power systems. The study finds that PEM exhibits higher energy efficiency and responsiveness, especially under fluctuating conditions, characteristics that are critical for future hybrid electrolysis strategies. Similarly, Rashid et al. [283] provide a broad review of water electrolysis technologies, analyzing key thermodynamic and kinetic parameters, electrode materials, and system efficiencies. They stress the long-standing technological barriers, including high energy consumption, low durability, and capital intensity, which continue to limit widespread deployment.

Looking at the interactions between electrolyzer and energy systems, Tofighi-Milani et al. [284] modeled the dynamic interaction between PEM and ALK electrolyzers and the grid. This study demonstrated that PEM electrolyzers offer faster frequency response capabilities. Schmidt et al. [285] used expert-validated data to estimate future trends in capital cost, efficiency, and lifetime for ALK and PEM technologies. Their findings suggest that despite cost reductions through technical development and scaling, technological dominance of PEM is far from ensured. Moving towards larger scales, Reksten et al. [286] conducted a techno-economic assessment of PEM and ALK plants, projecting that the current capital expenditure (CAPEX) gap between the two technologies could narrow significantly by 2030, with learning rates of 25–30%. However, no direct coupling with renewable electricity sources, such as wind or photovoltaic, has been considered, resulting in the overlooking of the impact of minimum loads, variable efficiency, and cold startups on hydrogen production. Benghanem et al. [287] explored the use of both PEM and ALK electrolyzers powered by photovoltaic systems, focusing on how variations in electrolytes (e.g., KOH and seawater) and electrode materials affect hydrogen output and overall system efficiency. Their results underscore the higher performance and lower voltage requirements of

PEM systems compared to ALK, especially when seawater is used as an electrolyte. The study also highlights the critical influence of solar irradiation and material choice on system productivity. However, these studies do not perform a techno-economic comparison of the different technologies when coupled with renewable energy sources such as wind power.

This review identifies several key limitations within this body of work. Unlike most previous studies, this present work emphasizes critical factors such as wake effects, different power inputs, electrolyzer minimum load constraints, detailed component-level modelling, and integrated simulation of system interactions, all essential for evaluating the cost-efficiency and operational performance of various configurations. To adequately capture these factors, high-resolution temporal modelling is required. However, many previous works [47,48,288–290] only partially include these aspects, as their primary focus often lies outside of analyzing operational-level interactions and their impact on system performance and cost.

A majority of existing studies apply hourly time resolution and rely on empirical wind data [48,277,288,291–293] or model-derived datasets [289,290,294]. Despite using real-world wind inputs, only a few incorporate wake losses or calculate turbine-specific energy output [46,293], which is crucial for the estimation of variable electrolyzer efficiency and technical constraints. Some researchers have provided more detailed representations of electrolyzer operations [277,290], while others focus on minimum load thresholds [291,293] or thermal performance [288,292]. However, all these contributions are not often included in the same study, as well as the degradation due to the operation of the component. Experimental studies by Kojima et al. [55], Kuhnert et al. [56], and Nguyen et al. [57] have shown that both ALK and PEM electrolyzers are vulnerable to accelerated degradation under variable input conditions. Singlitico et al. [277] estimate costs for three North Sea-based configurations, including dynamic modelling of wind farms and electrolyzers. Their results underline the importance of scale, particularly for smaller electrolyzers, which incur higher specific costs. They evaluate two operational modes: one where the electrolyzer runs at a constant power level ('hydrogen-driven') and another that utilizes only surplus electricity ('electricity-driven').

Jang et al. [290] investigate centralized and decentralized offshore hydrogen production systems and calculate the LCoH and net present value using fixed capacity factors and cost assumptions. While this method enables straightforward cost comparisons, it lacks temporal variability and detailed dynamic simulation. Rogeau et al. [294] also analyze all the hydrogen production configurations in the North Sea for multiple future time horizons (2020, 2040, and 2050), offering a detailed cost breakdown across infrastructure components. However, their approach simplifies hydrogen production by assuming static conversion efficiencies and fixed loss factors, without simulating dynamic system behavior. In contrast, the model used in this study explicitly accounts for electrolyzer variability and fluctuating wind inputs. All three studies utilize a single data set and perform sensitivity analyses to evaluate cost impacts, but they do not explore a broader parameter space that captures future technological uncertainties. The approach proposed herein draws from both academic and industrial sources to create a more robust and representative dataset, though challenges remain in fully capturing system uncertainties. Finally, previous research by Mehta et al. [293] has investigated the benefits of optimizing wind turbines specifically for hydrogen production, highlighting that such designs, typically featuring higher specific power, can slightly reduce the LCoH compared to turbines optimized for the LCoE. Additionally, this study suggests that electrolyzer oversizing can be an effective strategy for the electrolyzer analyzed. However, the analysis is limited to systems using PEM electrolyzers and relies on detailed aero-servo-elastic turbine redesigns for the North Sea region. It does not explore alternative, system-level optimization methods or focus on areas with lower average wind speeds. Additionally, it neglects to examine whether minimizing LCoE necessarily leads to the lowest LCoH, key aspects that remain insufficiently addressed.

5.1.1 Contribution and novelty

Table 5.1 offers a summary of the existing literature on offshore wind-based hydrogen production. While the studies presented in **Table 5.1** collectively offer some interesting insights into the development, optimization, and application of individual electrolysis technologies, a clear gap remains. Indeed, none of existing studies addresses a holistic comparison that simultaneously considers multiple electrolyzer technologies and multiple offshore wind power input sources, varying the specific power of aerogenerators, evaluated across both technical and economic dimensions. Most comparative analyses focus either on technological performance under isolated conditions or on economic projections with limited integration of dynamic operational variables. Moreover, the interaction between power source characteristics and electrolyzer behavior is often underexplored, despite its relevance for real-world implementation.

Table 5.1: Summary of the existing literature on techno-economic simulation models of offshore wind-based electrolysis.

Source	Temporal resolution	Electrolyzer technology	Sensitivity to power input source	Electrolyzer operation	Stack degradation
Rogeau et al. [40]	Annual	PEM	x	x	x
Egeland and Sartori [49]	Hourly	PEM-SOEL	x	✓	x
Komorowska et al. [44]	Annual	PEM	x	x	x
Vu Dinh et al. [46]	Hourly	PEM	x	x	x
Singlitico et al. [53]	Hourly	ALK-PEM-SOEL	x	✓	✓
Hill et al. [50]	hourly	ALK-PEM	x	✓	x
Calado et al. [51]	Hourly	ALK-PEM-SOEL	x	✓	x
Jang et al. [45]	Annual	ALK-PEM	x	✓	✓
Song et al. [47]	Hourly	ALK-PEM-SOEL	x	x	x
Zhuang et al. [48]	Hourly	-	x	x	x
Mehta et al. [52]	Hourly	PEM	x	✓	x
Rezaei et al. [54]	Hourly	PEM	x	✓	✓
Kojima et al. [55]	Annual	ALK-PEM	x	x	✓
Kuhnert et al. [56]	Annual	PEM	x	x	✓
Nguyen et al. [57]	Annual	ALK-PEM	x	x	✓
Travaglini et al [67]	10 min	ALK-PEM	x	✓	✓
This work	**10 min**	**ALK-PEM-AEM**	✓	✓	✓

In order to fully exploit the advantages offered by large operational range electrolyzers, it is essential to evaluate how different electrolysis technologies perform under varying wind conditions and to optimize system-wide design choices that enhance their operational efficiency. The strong targets set by Mediterranean countries for the decarbonization of their energy systems [238] present an interesting case study for offshore wind-to-hydrogen integration. However, the Mediterranean Sea poses significant challenges for the deployment of wind energy due to its deep waters and lower average wind speeds compared to the North Sea [146,147]. The unique bathymetry of this region necessitates the deployment of floating offshore wind turbines

(FOWTs) rather than fixed-bottom designs. However, existing FOWTs are predominantly optimized for high-wind environments, which may not be suitable for Mediterranean conditions. By adopting low-specific-power FOWTs with larger rotor-swept areas, energy capture can be improved, leading to a higher yearly energy input combined with a more stable power supply for electrolyzers, which may mitigate the LCoH. In fact, beyond turbine design, wind farm layout optimization also plays a crucial role in reducing the LCoH, considering the relevant impact of LCoE on hydrogen production costs [296]. Wake interactions between turbines impact energy production, especially in low-wind-speed regions, while high inter-array cable costs further affect overall system economics. Achieving an optimal balance between wake loss reduction and cable cost minimization is thus essential for providing a stable, cost-effective energy supply to electrolyzers. To capture the full impact of wind variability on hydrogen production, this study employs a time-dependent modeling approach. Using ten-minute resolution simulations, the model assesses power fluctuations, curtailments due to minimum load thresholds, and the thermal effects influencing electrolyzer efficiency in a centralized offshore configuration. Additionally, the present study differs from existing literature since it focuses exclusively on dedicated wind-powered hydrogen systems. In addition, a more complex electrolyzer model is provided, as well as a more sophisticated wind farm simulation to explore component interactions in greater detail.

Building on this background, this work aims to address the critical gaps mentioned above by conducting a systematic comparison of various hydrogen production technologies, ALK, PEM, and AEM, under different power input scenarios. The latter are included by varying the FOWT and installation site in the Mediterranean. Specifically, existing reference FOWTs developed by the IEA [144] are optimized for the high average wind speeds typical of the North Sea [118], making them less suitable for regions like the Mediterranean Sea, where average wind speeds are significantly lower [146,147]. To improve wind energy capture under such conditions, previous studies [297] have suggested that lowering the specific power, by means of increasing the rotor diameter while maintaining the same generator power, can shift the power curve of the turbine towards lower wind speeds. This approach has been shown to yield a reduction in the LCoE in certain geographical contexts. The present study investigates whether the same benefit translates to hydrogen production. Specifically, it has been explored whether wind turbines with lower specific power configurations are also advantageous when used to power electrolyzers for green hydrogen production in dedicated centralized onshore configurations. This issue has been addressed across different electrolysis technologies, ALK, PEM, and AEM, utilizing the resulting LCoH as a cost metric. The novelty of this work lies in its integrated assessment of rotor sizing and electrolysis technology, focusing on:

- The techno-economic impact of increasing rotor size on hydrogen production in low-wind-speed regions.
- Whether the turbine configuration that minimizes LCoE also minimizes LCoH.
- Whether this optimal configuration varies across electrolysis technologies.

To this end, both technical performance metrics, such as efficiency, minimum load thresholds, and lifetime, and economic parameters have been considered. Through this comprehensive analysis, the study provides a robust framework for evaluating green hydrogen production pathways in realistic contexts, thereby informing future policy, investment, and research priorities in the hydrogen economy.

The study introduces a novel methodology to understand how the rotor swept area of the FOWT affects the operational parameters and cost effectiveness of the solution. The procedure is conducted through a three-step approach:

1. Wind farm layout optimization, relying on the trade-offs between wake losses, AEP, and cable costs, in order to achieve the lowest possible LCoE for each FOWT technology analyzed.
2. Time-dependent wind farm simulations, starting from the optimal layout to estimate the available power for the electrolysis facility, time step per time step.
3. Time-dependent electrolyzer simulation to compare the different electrolysis operational constraints under realistic power input conditions.

By leveraging electrolyzer flexibility and system-wide optimization, this study provides insights into how hydrogen production can be effectively integrated into Mediterranean energy systems. The following sections discuss LCoE minimization strategies, analyze the relations between rotor diameter (D_R) and electrolyzer techno-economic performance, outline the methodology used, present the key results, and offer recommendations for future research and deployment strategies.

After the description of the contribution of this work to literature and the main novelties, Section 5.2 depicts the methods adopted, pointing out the techno-economic assumptions made, and the related impact on the results. Study cases and results are shown in Sections 5.3 and 5.4, with emphasis being put on the discussion of the main outcomes obtained. Final remarks, best practices, and possible further developments are finally suggested in Section 5.6.

5.2 Methods

In this section, the methodology adopted for the evaluation of the LCoH for each electrolysis technology is described. After the definition of the framework adopted for optimizing the floating wind farm layout, the setup adopted in Pywake for the time-dependent simulation of the farm is presented. Finally, the electrolyzer model is described, pointing out the differences between the technologies utilized.

The framework developed is based on a three-step procedure, as shown in **Figure 5.1**, aimed at comparing the electrolysis technologies proposed and evaluating the impact of lowering the FOWT specific power on the LCoH. The proposed method is not iterative. After the optimization of the wind farm layout, time-dependent wind power and hydrogen output are simulated, adopting the models described below. This strategy can be described as follows:

1. **LCoE minimization**: Minimizing the LCoE is essential, as the resulting electricity is used as the energy input for green hydrogen production via electrolysis. Since electricity costs are among the major drivers of the LCoH [296], reducing the LCoE directly contributes to a lower hydrogen production cost. To this end, the open-sourced TopFarm optimization tool has been employed. Based on key inputs such as the wind turbine type, the wind resource data, and cost parameters, this tool generates an optimized wind farm layout that minimizes the LCoE by balancing the minimization of wake losses and layout-dependent capital expenses. This optimized layout is then used as input for the subsequent simulation module to estimate the time-dependent power generation, which serves as the energy input profile for the hydrogen production system. This kind of optimization has been performed considering only the LCoE as objective function. The

statistical approach based on the Weibull distribution provided by TopFarm, in fact, does not allow for the analysis of the relationships between available power and electrolyzer constraints. Therefore, the wind farm layout can be optimized only for LCoE minimization.

2. **Time-dependent power production**: To evaluate the impact of renewable energy variability on hydrogen production, a time-dependent simulation approach has been adopted. The wind farm power output has been estimated using PyWake, an open-source modeling tool capable of simulating detailed wind flow interactions between turbines. Starting from the optimal layout, the simulation has been conducted with a 10-minute time resolution, allowing for an accurate representation of the short-term fluctuations in wind power availability. This time-dependent power profile has then been used as input to the hydrogen production module, enabling the assessment of the electrolyzer's performance under variable operating conditions.
3. **Time-dependent hydrogen production**: A Python-based electrolyzer model has been employed to simulate hydrogen production under variable operating conditions. The model takes into account key dynamic factors such as efficiency variation with load, calendar degradation, operating temperature effects, as well as shutdown and cold start-up delays. This enables a realistic representation of the electrolyzer's behavior when subjected to fluctuating power input from the wind farm. By integrating the time-dependent power data obtained from PyWake, the model allows for an accurate estimation of the actual hydrogen production over time. This approach highlights how renewable energy variability not only affects hydrogen output but also impacts long-term system performance, efficiency, and overall utilization of the component.

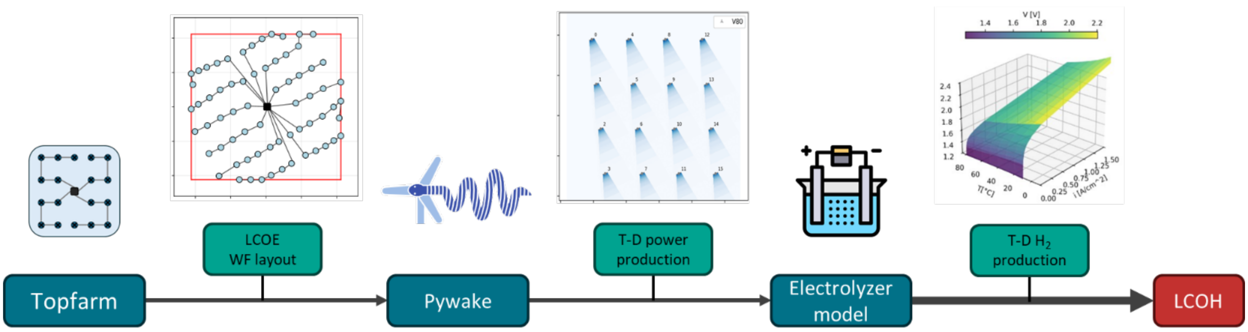

Figure 5.1: Overview of the LCoH calculation procedure.

Finally, for each installation site, this whole optimization-simulation approach has been repeated varying the wind turbine type.

5.2.1 Wind farm optimization model

For the wind farm layout optimization, the framework presented in Section 3.4 [297] has been adopted. This model utilizes the TopFarm framework, developed by DTU [183] and based on the OpenMDAO [196] multidisciplinary design and optimization framework, to minimize the LCoE, customized to take into account floating farm costs as in [297]. TopFarm facilitates a structured exploration of design variables and implements advanced optimization algorithms to resolve trade-offs between energy yield and capital costs. The core objective is to minimize the LCoE by jointly optimizing WT location and inter-array (IA) cable routing within a defined maritime area.

The optimization workflow, illustrated in **Figure 5.2**, operates iteratively. In each iteration, the tested wind farm layout is evaluated by first estimating the Annual Energy Production (AEP) using the PyWake library [184] with a statistical approach based on the Weibull distribution of the specific site. Subsequently, IA cable routing is optimized with Edwin [194] as a sub-problem with fixed WT locations, aiming to minimize total cable length. Cost estimations for CAPEX and operational (OPEX) expenditures are then computed using the models described in Travaglini et al. [297], leading to the calculation of the LCoE. This value is compared with previous iterations, and the process continues until convergence, defined as a change in the objective function smaller than 1×10^{-8}. Considering the mismatch between the height of source data and aerogenerators, wind speed values are extrapolated to the turbine hub height using a power-law profile with an exponent of 0.11 [186], commonly applied in marine environments.

Table 5.2 summarizes the main settings of the wind farm layout optimization.

Table 5.2: Settings of the wind farm layout optimization.

Parameter	Value
Objective	LCoE minimization
tolerance	$1\cdot10^{-8}$
driver	COBYLA
Minimum turbine spacing	4 diameters [197–199]
Available sea lot	450 km^2
Wake effects model	Bastankhah Gaussian [187]
Effective wind speed	LinearSum superposition model [190]
Rotor-wake overlapping	PyWake's Gaussian method [191]
Added turbulence	LCoE minimization

Optimization is performed using the COBYLA (Constrained Optimization BY Linear Approximations) algorithm, a gradient-free local search method suitable for non-smooth, constrained problems. Its robustness in handling discontinuities, such as those from wake interactions and discrete variables, makes it particularly appropriate for this application.

The optimization model incorporates several constraints to ensure technical and regulatory feasibility. A key constraint is the minimum spacing between turbines, set at 4 D_R, in line with industry best practices [197–199]. This accounts for structural integrity, operational reliability, and mooring-induced WT displacement, which is approximately 0.25 rotor diameters per turbine based on a 160 m sea depth reference and IEA-15-240-RWT characteristics [201].

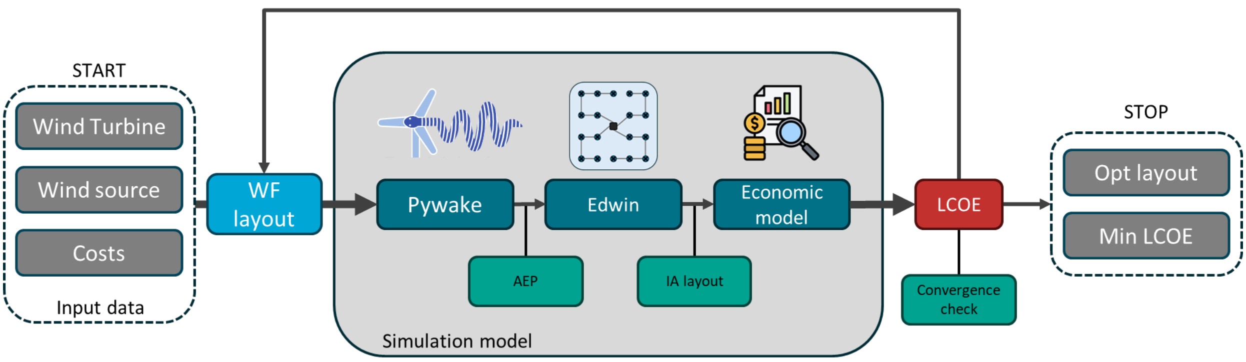

Figure 5.2: Schematic representation of the optimization model.

Additionally, the turbine layout is constrained within a predefined 450 km² squared installation area, reflecting real-world site allocation practices. Although site-specific constraints may not yield the global LCoE minimum, they reflect realistic design limitations due to environmental exclusion zones, infrastructure, and policy boundaries. The use of a square installation area allows for consistent comparison across scenarios, even though irregular polygonal shapes are more typical of offshore wind farm boundaries.

Turbine performance is modeled using manufacturer-provided power and thrust coefficient curves, capturing both energy conversion efficiency and wake generation. Wake effects are modeled using the Bastankhah Gaussian wake model [187], which offers improved accuracy over simpler formulations [188,189] by representing the wake velocity deficit with a two-dimensional Gaussian distribution. The effective wind speed at each turbine is calculated using the "LinearSum" superposition model [190], and the partial rotor-wake overlap is treated using PyWake's Gaussian overlap method following established guidelines [191]. Finally, the added turbulence from wake interactions is computed using the "GCLTurbulence" model [192], providing estimates of increased turbulence intensity downstream of each rotor.

5.2.2 Wind farm simulation model

To evaluate the time-dependent performance of the wind farm layouts resulting from the first step of the optimization, this study employs the PyWake library [184], a Python-based simulation tool designed for wind farm modeling and analysis. PyWake is used to compute the AEP, wake losses, and turbulence intensity based on site-specific wind conditions, turbine characteristics, and turbine-to-turbine interactions.

Concerning the wind resource, a time-step length of ten minutes has been selected. The use of wind data with higher resolution could, in fact, lead to significant errors in wind power production assessment. Wind power curves provided by manufacturers are usually averaged over ten-minute intervals [259]. While using wind data on a one-hour basis would not allow for the estimation of power output variability on hydrogen production, datasets with a higher resolution would lead to significant errors in the evaluation of the performance of the generator, which experiences significant fluctuations on small time scales. For offshore conditions, surface roughness and terrain effects are neglected. Concerning the setup for the wake model, the wake overlapping, the turbulence, and wind source extrapolation to wind turbine hub height, the same setup described In Section 5.2.1 has been adopted.

5.2.3 Electrolyzer model

In this study, three electrolyzer technologies have been compared, accounting for their technical constraints, performance, and expenditures. To limit computational costs, the lumped parameter model presented in Section 2.3.1.2 has been adopted. An electrolyzer is a device that enables water splitting for hydrogen production via an electrochemical process driven by an external power input. Its behaviour is commonly characterized by a polarization curve, which relates cell voltage to current density and serves as a basis for performance modelling. While the behavior of the ALK can be reproduced by focusing exclusively on the linear portion of the polarization curve, due to the minimum load threshold of 20% of the nominal power, PEM and AEM experience a wider operational range. **Figure 5.3** shows the differences between the efficiency surfaces of the three electrolyzer technologies. To mimic the behavior of the system also in part-load, a non-linear modeling of the polarization curves is required. Besides the more restricted operational range, the ALK experiences a lower sensitivity to temperature fluctuations, as shown by the slope of the surface in **Figure 5.3**, and better manages heat losses.

In all considered technologies, the polarization curve experiences parallel upward shifts due to thermal and temporal degradation. Specifically, lower operating temperatures require higher voltages to sustain the same current density (**Figure 5.3**), as well as prolonged operation increases voltage requirements over time due to calendar aging. Both these mechanisms induce a higher power consumption to produce the same amount of hydrogen, leading to lower efficiency. These effects can be summarized in Eq. 5.1, where the operating voltage (V) is assessed by adding the overvoltages to the design voltage of the new stack at reference temperature ($V_{T0,h0}$).

$$V = V_{T_0,\,h_0} + V_{degr} \cdot h_{EL} + V_T \cdot (T_{rated} - T_{EL}) \tag{5.1}$$

As shown by Equation 5.1, while the effect of calendar aging depends linearly on the number of working hours (h_{EL}) of the electrolyzer and can be reversed only by replacing the stack, the thermal effects are defined only by the difference between rated (T_{rated}) and operational (T_{el}) temperature of the specific time step. Both the thermal and the degradation overvoltages are accounted for with a linear relationship thanks to the adoption of wear (V_{degr}) and temperature (V_T) coefficients, in μV/h and μV/°C, respectively.

To effectively account for the temperature effect, 3D surfaces describing the voltage variation according to the current density and the operating temperature have been obtained. Due to the limited maturity of technology and the scarcity of data available in the current literature, the AEM polarization curve presented herein has been extrapolated from preliminary results provided by two industrial partners collaborating with the research group. To preserve industrial secrets, the y-axis labels and the color bar have been intentionally omitted.

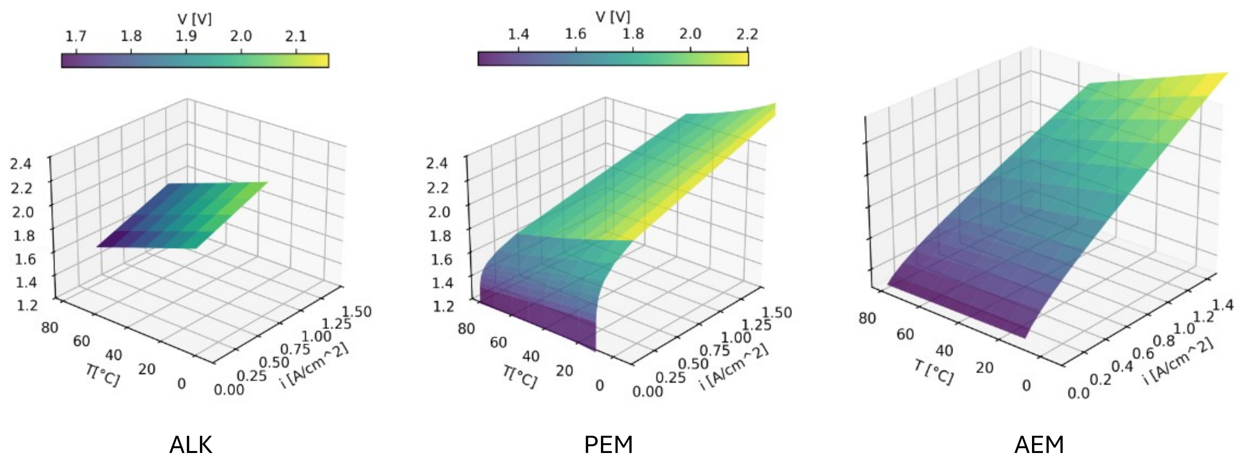

Figure 5.3: Polarization surfaces of the electrolysis technologies compared.

Once the operating voltage is known, the conversion factor (φ) can be estimated as in Eq. 5.2. The φ describes the transfer function between input energy and the hydrogen flow rate. This coefficient can be estimated by the ratio between the maximum hydrogen production ($H_{2,flow}$) and the ideal current (I_{id}), the V, and the number of cells (n_{cells}).

$$\varphi = \frac{H_{2,flow}}{I_{id} \cdot V \cdot n_{cells}} \tag{5.2}$$

The hydrogen production rate is assumed to be directly proportional to the current density. As the current increases, hydrogen is produced up to the rated flow rate.

Concerning the control strategy of the power input, the power fed to the stack is partitioned equally between all the modules that can be activated, considering the minimum power thresholds of each technology. Despite the higher energy loss potential, this approach is focused on the minimization of the shutdowns of the modules. The high impact of component shutdowns on stack degradation, in fact, could sensitively reduce the useful lifetime of the component [298,299]. Additionally, a review of the dynamic operation of electrolyzers highlights that flexible operation with frequent shutdowns and startups significantly increases degradation compared to steady or balanced partial load operation, which supports the benefit of equal power partitioning to reduce shutdown frequency [300,301]. Therefore, enhanced energy losses have been preferred to minimize the number of replacements. Additionally, this strengthens the assumptions of linear stack degradation with operating hours, disregarding the power input previously described. On the other hand, aforementioned energy losses due to minimum load thresholds must be considered as power not converted into hydrogen and not as waste. Due to the centralized nature of the selected hydrogen production configuration, the unconverted energy is fed into the grid. Even if it is not directly translated into a benefit for the LCoH calculation, it enhances the feasibility of the entire system. To this end, the total hydrogen production can be estimated relying on the φ and the energy input (E_{in}) as in Eq. 5.3.

$$H_2 = \varphi \cdot E_{in} \tag{5.3}$$

The thermal model captures the stack temperature evolution, which affects voltage variations in subsequent timesteps. Temperature variation (ΔT) of the electrolyte solution is computed as in Eq. 5.4:

$$\Delta T = \frac{Q_{gen} - Q_{loss}}{m \cdot c_p} \tag{5.4}$$

where Q_{gen} is the generated heat, Q_{loss} is the thermal loss, m is the mass, and c_p is the specific heat capacity of the solution, for the ALK modeling, or the stack, for PEM and AEM. The geometry of the electrolyzer system, in fact, plays a key role in heat distribution and dissipation. While for the ALK thermal modeling the approach proposed by Superchi et al. [258] has been adopted considering the gas-liquid separator as the primary heat loss component, the stack has been considered for heat generation and losses for all the other technologies analyzed, as in Tiktak et al. [302]. While thermal power is generated during electrolysis, as the cell voltage exceeds the thermoneutral voltage, thermal losses occur via multiple resistances: internal tank convection, wall conduction, air gap convection, container conduction, and external air convection. For the refrigeration of the stack, the model takes into account a cooling loop that avoids the stack temperature exceeding the maximum operating one.

The operating temperature also serves to evaluate when the component shuts down. In this work, a minimum working temperature of 35°C has been assumed for all technologies, which is consistent with the assumption made in [67]. To consider the impact of cold start-up time on curtailments and hydrogen production, the power consumption of the electrolyzer after the shutdown is utilized only to bring the stack temperature to the nominal operating value, without hydrogen production. Therefore, a start-up time for each electrolyzer technology is needed before restoring its production potential. According to Singlitico et al. [277], while for the ALK, a start-up time of 20 min has been considered, just one time step, corresponding to 10 min, has been set for PEM and AEM.

5.2.4 Techno-economic metrics and financial assumptions

To understand the degree of exploitation of the technologies involved in this study, the Capacity Factor (CF) of the wind farm and electrolyzer has been computed (Eq. 5.5). For the wind farm, the CF is estimated as the ratio between the energy that the farm produces in a year and the energy that the same farm would produce if it could maintain the nominal power production over the same period. Regarding the electrolyzer, the CF is the ratio between the energy that the device processes over a year and the energy that it would process when fed by a constant power input sufficient for the nominal hydrogen production over the same period.

$$CF = \frac{E_{actual}}{E_{nominal}} \tag{5.5}$$

Another technical metric used to study the degree of exploitation of the electrolyzers is the utilization factor (UF): the ratio between the exploited and the available energy to the electrolysis facility (see Eq. 5.6). While the numerator is the same as considered for the CF, the denominator is now equal to the energy produced by the wind farm feeding the electrolyzer. This metric allows for the direct estimation of the impact of cold startups and minimum power requirements from the modules on the operation of stacks.

$$UF = \frac{E_{actual}}{E_{available}} \tag{5.6}$$

Table 5.3: Settings of the wind farm layout optimization.

Component	assumption	Reference
Intra-array cables	750 €/m	[297]
Export cable	2.7 M€/km	[128]
Electrical substation	324 €/kW	[160]
Installation costs	~300 €/kW	[160]
Project costs	700 €/kW	[160]
Discount rate	7%	-
Project lifetime	30 years	[255,303]
Sea lot dimension	21x21 km	[297]
Distance from shore	60 km (Sicily) 40 km (Cyprus)	[157], [304]
Water depth	390 m (Sicily) 350 m (Cyprus)	[157], [304]
FWF cost	DTU cost model	[160]

The TopFarm framework used to optimize the layout of the wind farm aims at minimizing the LCoE, here calculated as in Eq. 3.21 . The main financial assumption behind the LCoE calculation, as the lifetime of the plant and the discount rate, are summarized in **Table 5.3**. The following analyses aim at estimating the LCoH of the hydrogen produced by the various combinations tested, computed as in Eq. 2.4. The LCoH differs from the LCoE because it considers the hydrogen mass produced in a year ($M_{H2,produced}$) instead of the AEP. The installation cost of the electrolyzer is the object of a sensitivity analysis presented in Section 5.3.2.

5.3 Case study

In this section, the case study selected for the analyses is described. After the definition of the considered wind farm, the electrolysis facility is depicted, focusing on the electrolyzer configuration and design parameters. Finally, the installation sites are described, highlighting the key features such as wind source, bathymetry, and distance from the shores.

5.3.1 Wind farm

In this study, the power input to the electrolysis facility is provided by a dedicated offshore wind farm with a total installed capacity of 1.005 GW. All the generated power is exclusively allocated for hydrogen production, with no export to the electricity grid. The wind farm is composed of sixty-seven 15-MW FOWTs optimized for high-efficiency electricity generation in offshore sites characterized by moderate wind speed. To evaluate the impact of turbine swept areas on the overall hydrogen production system, four different wind farm configurations have been assessed in both installation sites (**Table 5.4**).

In this study, the four wind turbines proposed in Travaglini et al. [297,305] have been selected con conduct the analyses. While keeping the same generator power, these turbines differ in the D_R, which varies from 240 to 330 m. This results in decreased specific power, leading to a better harnessing of the wind source at lower wind speed, as shown in **Figure 5.4**.

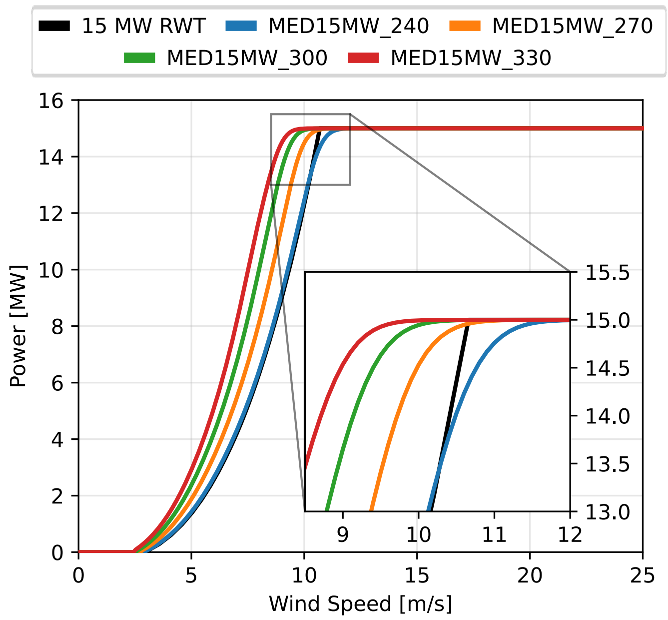

Figure 5.4: Power curves of the wind turbines adopted in this study [297,305].

Larger swept areas result in a reduction in cut-in and rated wind speeds, extending the wind turbine's operational range and enhancing its ability to harness wind energy under suboptimal conditions, thereby increasing the overall energy yield. As a result of this improved low-wind performance, capacity factors are typically enhanced. The turbine operates closer to its rated capacity over a broader spectrum of wind conditions, leading to larger annual energy production without necessitating an increase in generator size or rated power. Additionally, the attainment of rated power at lower wind speeds contributes to a reduction in power output variability. This smoothing effect, which becomes more pronounced with increasing D_R, improves the stability of the power supply to the electrolyzer. However, larger swept areas enhance the costs of both turbines and floaters, leading thus to the need to conduct a trade-off analysis between expenditures and AEP increases. While the number of turbines remains consistent across all scenarios to maintain the same total power capacity, each case explores different turbine technologies, varying the rotor swept area, allowing for an assessment of performance under varying operational dynamics and wind response behaviors.

By evaluating these distinct configurations within the same site and system boundaries, the study isolates the influence of turbine selection on power availability for electrolysis and, in turn, hydrogen yield and system utilization.

Table 5.4: Design parameters for the different wind turbines considered.

FOWT type	Diameter [m]	Power [MW]	Specific power [W/m^2]	Cut-in-rated wind speed [m/s]
MED15_240	240	15	332	3-11.8
MED15_270	270	15	262	2.8-11
MED15_300	300	15	212	2.6-10.4
MED15_330	330	15	175	2.5-10

5.3.2 Electrolysis facility

This test case examines a centralized onshore electrolysis configuration, as in **Figure 5.5**, in which the electricity from a dedicated offshore wind farm is used exclusively for hydrogen production. The generated electricity is transmitted to shore via high-voltage subsea export cables, where it feeds directly into a 1 GW electrolysis facility located near the point of delivery. This establishes a closed-loop energy system in which all generated electricity is consumed by the electrolyzer when its technical constraints allow for it. In this case, despite being delivered to the shores, surplus power exported is considered a curtailment since it does not contribute to the hydrogen production. Concerning electric cables, due to the export distance being lower than 70 km in both installation sites analyzed, the high voltage alternating current technology has been chosen for the energy transportation as per standard practice in the literature [306,307].

The electrolyzer operates under variable input conditions due to the intermittent nature of wind energy and is assumed to be entirely isolated from the electrical grid. Therefore, its operation is modeled to reflect real-world performance characteristics. These include variations in efficiency at partial load, degradation over time due to calendar aging, and a minimum operational threshold, as described in Section 5.2.3. The energy consumption and cost contributions of the reverse osmosis unit used for water desalination are considered negligible, and therefore excluded from the LCoH calculations, as supported by prior studies [67]. Finally, it is assumed that the produced hydrogen is supplied directly to the end user, without the need for intermediate storage. As such, hydrogen storage infrastructure and its associated costs are not included in the estimation of the LCoH. This assumption is justified by the comparative nature of the study, which aims to assess the benefits related to the adoption of larger swept area wind turbines for hydrogen production.

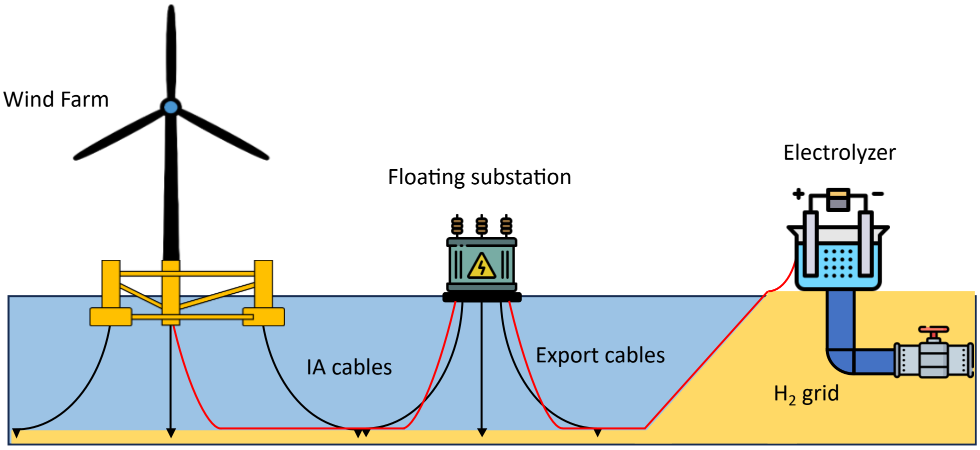

Figure 5.5: Centralized onshore configuration scheme.

The electrolyzer system is modeled based on key performance and operational parameters that represent current commercial and near-commercial technologies. This study considers three electrolyzer technologies: ALK, PEM, and AEM. Each technology offers distinct advantages in terms of efficiency, flexibility, system integration, and capital expenditure, making them suitable for various use cases in green hydrogen production. **Table 5.5** summarizes the most relevant design variables, such as nominal efficiency, minimum load ratio, start-up time, and operational temperature. Regarding technical parameters, three scenarios have been selected: the optimistic (OPT), the pessimistic (PES), and the average (AVG). For the ALK and PEM electrolyzers, the parameter values are sourced from an exhaustive literature review conducted in Travaglini et al. [67], while specific references for the less mature AEM technology are provided in the table. Some of the data related to AEM technology, however, cannot still be found in reports or scientific papers and have been extrapolated based on industrial collaborations of the research group with two companies in the field. Such data can therefore be considered to be absolutely realistic, even though the exact values used in the study do not pertain to a specific device to preserve industrial secrets. This structured approach facilitates a comparative assessment of how each electrolyzer type interacts with the fluctuating power supply from the wind farm and how their technical characteristics influence overall hydrogen yield, system responsiveness, and energy utilization efficiency.

Table 5.5: Design parameters for the different wind turbines considered.

Parameter	ALK [67]			PEM [67]			AEM [69, 71]		
Scenario [-]	OPT	AVG	PES	OPT	AVG	PES	OPT	AVG	PES
Cell power [kW]		9.45			2.735			5	
Minimum load [%]		20			5			5	
T_{rated} [°C]		70			80			70	
Cold startup time [min]		20			10			10	
ϕ [kg/MWh]	21.2	19.3	18.0	20.3	19.0	17.2	21.0	20.7	19.8 [310]
Electrical η [%]	70.8	64.3	59.9	67.7	63.4	57.4	70.0	69.0	66.1
V_{degr} [μV/h]	4	5.04	6.85	4.29	6.6	4.85	5.26	10.1	15.0

Concerning expenditures, **Table 5.6** depicts the four scenarios assumed, grouped in lower (LB) and higher bound (HB), average, and reference case. Also in this case, values for ALK and PEM are derived from [67], while for AEM, references are reported in the table. Finally, the combination of all the depicted input data leads to an overall amount of 216 scenarios.

Table 5.6: Design parameters for the different wind turbines considered.

Parameter	ALK [67]				PEM [67]				AEM			
Scenario [-]	HB	AVG	REF	LB	HB	AVG	REF	LB	HB	AVG	REF	LB
CAPEX [€/kW]	1000	663.9	727.8	350	1400	1309	812	500	1200 [311]	931[312]	662 [313]	451 [309]
OPEX [%CAPEX]	4	3	3	2	4	2.6	2.6	1.5	7 [313]	2.6 [312]	5 [313]	1.5 [309]
C_{repl} [%CAPEX]	55	47.5	47.5	40	55	47.5	47.5	40	55 [311]	47.5 [312]	47.5 [313]	40 [309]

5.3.3 Installation sites

In order to investigate the impact of wind turbine specific power on hydrogen production in low-to-moderate wind speed environments, two offshore locations in the Mediterranean Sea have been selected. Both sites are characterized by moderate average wind speeds, which make them representative for assessing system performance under unconventional wind conditions. While the methodology adopted in this study is general and applicable to a broad range of locations, the specific sites were selected due to their particular relevance. As discussed, in the Mediterranean Sea the presence of energy-intensive industries such as steel factories and shipyards, which are actively exploring green hydrogen as a decarbonization strategy, makes these areas of particular interest. Additionally, the selected sites have been chosen primarily for their proximity to the coast, considering the direct use of hydrogen as one of the requirements for the installation of a wind-to-hydrogen farm. This is essential to ensure the feasibility of a centralized onshore configuration for hydrogen production and distribution. While the selected locations do not necessarily exhibit optimal wind conditions, as heavy industrial consumers are not always situated in high-wind areas, the study aims to demonstrate the producibility of wind energy even in moderate or low-resource contexts. Finally, the selection has been influenced by the limited availability of offshore wind data with a ten-minute temporal resolution, which is essential for capturing wind variability and conducting high-fidelity energy simulations. Specifically, the key features of the selected sites are summarized below and in **Table 5.7**:

- **Sicily**: this installation site is located 60 km away from the northwestern coast of Sicily, resulting in a point of delivery installed close to Marsala. Several projects have been presented to the Italian authorities for the deployment of floating wind farms in this area [157] due to the relatively good wind source, placed between IEC wind classes III and II [186], as testified by the statistical distribution of the wind velocity in **Figure 5.6**.
- **Cyprus**: this installation site is located about 40 km off the southern coast of Cyprus, with the point of delivery located near the city of Larnaca. Despite the low average wind speed (sub IEC class III [186]) compared to the average of the Mediterranean Sea, it remains among the most favorable locations for offshore wind development around Cyprus due to its suitable bathymetric conditions.

Concerning the statistical distribution of wind speed, data at 100 m above the sea level are sourced from the ERA5 reanalysis database [151], selecting a period from 1993 to 2023 for both installation sites. The Weibull distributions adopted for the layout optimizations are shown and compared in **Figure 5.6**.

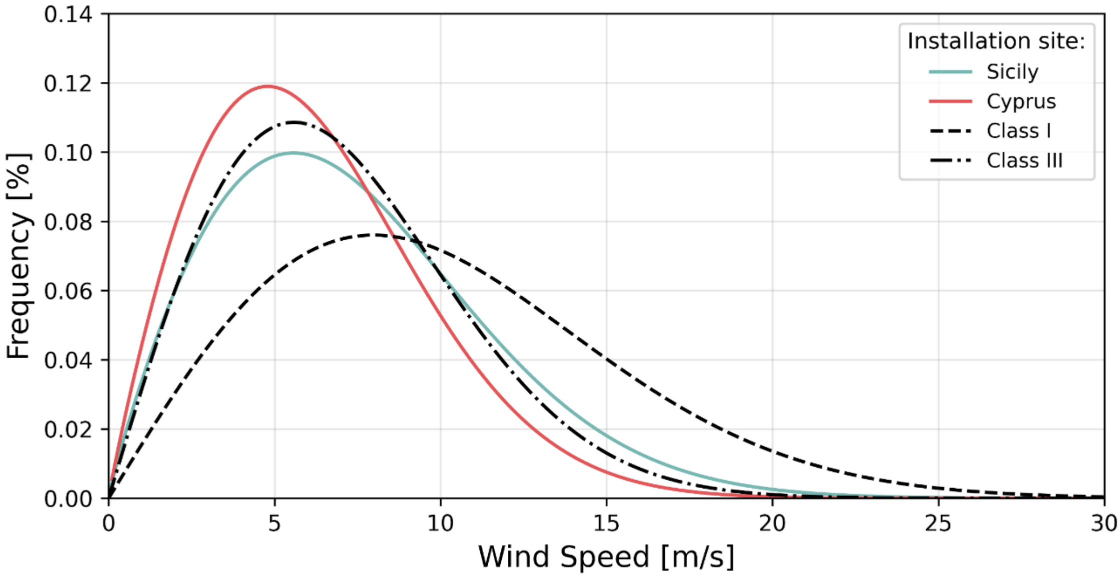

Figure 5.6: Weibull curve of the wind source at 100 m asl for the installation site in Sicily and in Cyprus.

Additionally, to define the wind source fully, the two wind roses are presented in **Figure 5.7**, showing north-northwest in Sicily (a), and west in Cyprus (b) as the prevalent wind directions. On the other hand, for the time-dependent analyses, data have been obtained from two different sources.

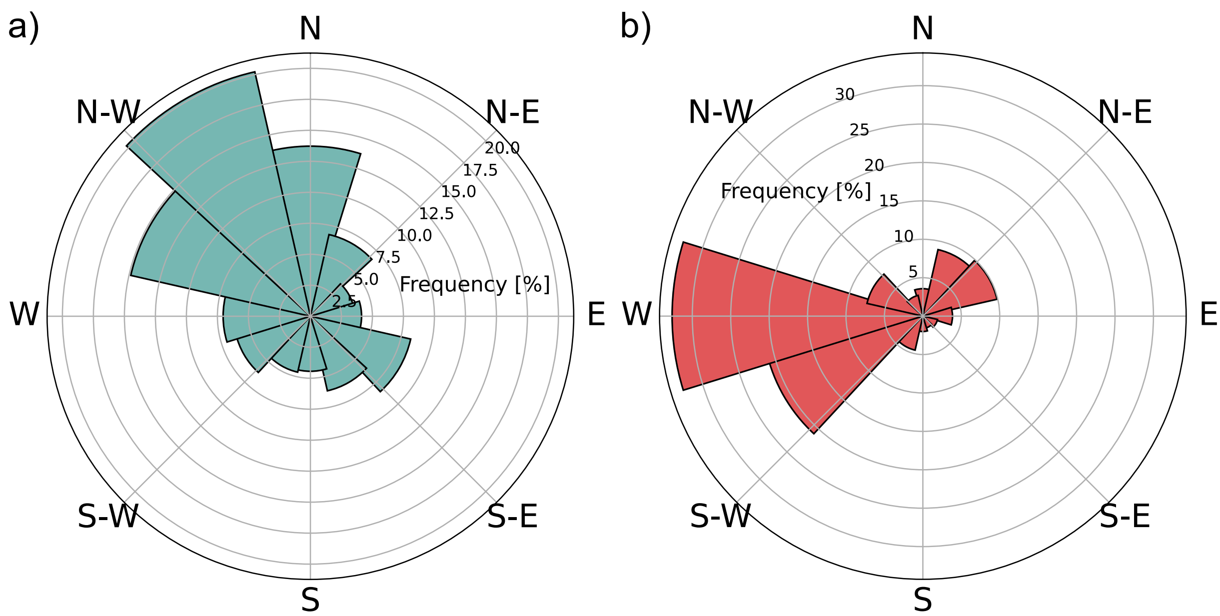

Figure 5.7: Wind rose distribution of the wind source at 100 m asl for the installation site in Sicily (a) and in Cyprus (b).

In the Italian installation site, the same dataset with a resolution of 10 minutes at 100 m above the sea level presented in [314], and described in detail Section 4.4.2, has been adopted. Due to the lack of high-resolution offshore wind data at turbine hub height, a two-step procedure has been developed to refine hourly reanalysis data fund in ERA5 to a ten-minute resolution using variability patterns observed in local mast measurements. First, a set of scaling factors has been derived by comparing ten-minute measured values with their hourly average. Then, these factors have been applied to scale the hourly ERA5 wind speeds at 100 m a.s.l., thereby generating synthetic ten-minute wind time series. This method preserves the hourly mean but increases variability and slightly reduces the median speed. Nevertheless, regarding the installation site in Cyprus, ten years of data have been provided by Vortex [315]. This company runs non-linear flow models that scale large atmospheric patterns down to fine spatial resolutions, generating modelled wind resource data suitable for long-term techno-economic analyses and siting procedures.

Table 5.7: Design parameters for the different wind turbines considered.

Site	Longitude [°]	Latitude [°]	k [-]	Median WS [m/s]	Sea depth [m]	Export distance [km]
Sicily [157]	11.6	37.8	1.89	7.4	390	60
Cyprus [304]	34.4	33.7	1.83	5.6	350	40

5.4 Results

This section presents the technical and economic results of the conducted analyses, focusing on the influence of rotor diameter increase on electrolyzer operation. After a first description of the main outcomes obtained in terms of energy yield and LCoE due to the specific power decrease, the evaluation of the effects of increasing rotor diameter and varying electrolyzer technologies on the LCoH and overall energy utilization is presented. Drawing on the optimization model outlined in Section 5.3.1, this analysis explores the feasibility of using low-specific-power rotors across the two selected Mediterranean sites. These outcomes have been used for the estimation of the LCoH and the comparison of ALK, PEM, and AEM electrolyzer behavior under fluctuating power input conditions.

5.4.1 Wind farm optimization

Figure 5.8 illustrates the energy production potential across the two selected locations, clearly indicating that the strategy of reducing specific power leads to an increase in AEP. Nevertheless, the AEP variation (Δ) relative to the baseline case with a 240-meter rotor diameter depends on the specific wind speed distribution at each location. For instance, although Sicily experiences the most favorable wind speed profile (as highlighted in **Figure 5.6**) and consistently delivers the higher AEP for all rotor sizes, increasing the rotor swept area results in an improvement lower than the one in Cyprus (**Figure 5.8**b). Therefore, the site in Cyprus shows a more pronounced benefit from the larger rotors. These observations align with the underlying premises of this study, which encourages larger rotor blades to maximize wind energy capture, particularly in the lower wind speed ranges of the Weibull distribution.

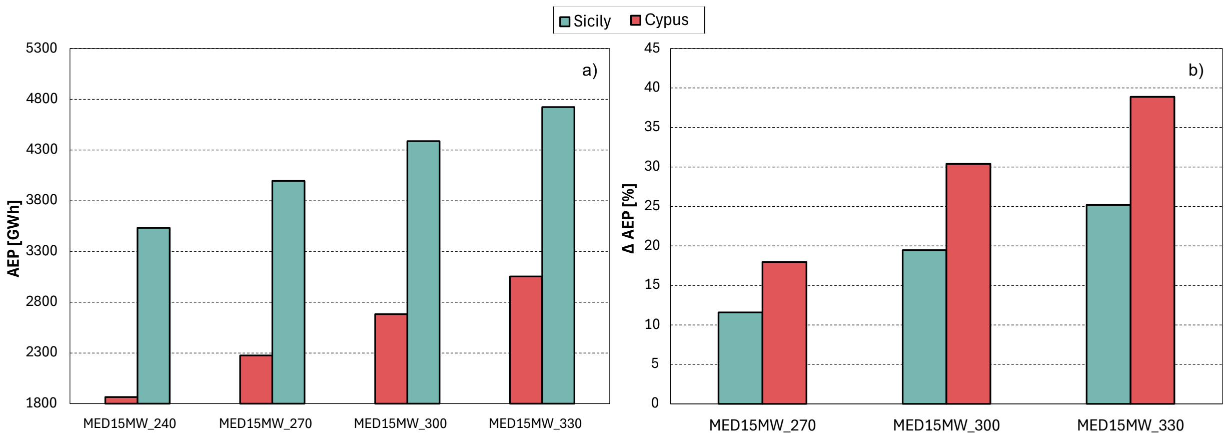

Figure 5.8: Comparison between the AEP and the ΔAEP in the two installation sites for the new aerogenerator designs.

While increasing the rotor swept area enhances the AEP, and consequently the capacity factor, of wind farms, one of the primary objectives of this study is to evaluate how site-specific wind turbine design can reduce the cost of the input energy to the electrolyzers by balancing increased capital investment against gains in AEP. A comparison between **Figure 5.8** and **Figure 5.9** reveals that, although AEP consistently improves with larger rotor diameters, the LCoE response is highly dependent on the wind resource characteristics of each location. For example, the substantial ΔAEP increase observed in Cyprus results in the lowest LCoE when employing the turbine with the lowest specific power (MED15_330). This is consistent with the site's Weibull distribution, which indicates a significant portion of energy availability at lower wind speeds. Accordingly, the higher the shift of the turbine's operational curve towards lower wind speeds, the more substantial the cost benefit. On the other hand, the Italian site exhibits more favorable wind profiles compared to Cyprus. Here, sensitivity analysis on rotor diameter highlights MED15MW_270 as the most cost-effective solution, as shown by the ΔLCoE in **Figure 5.9**b.

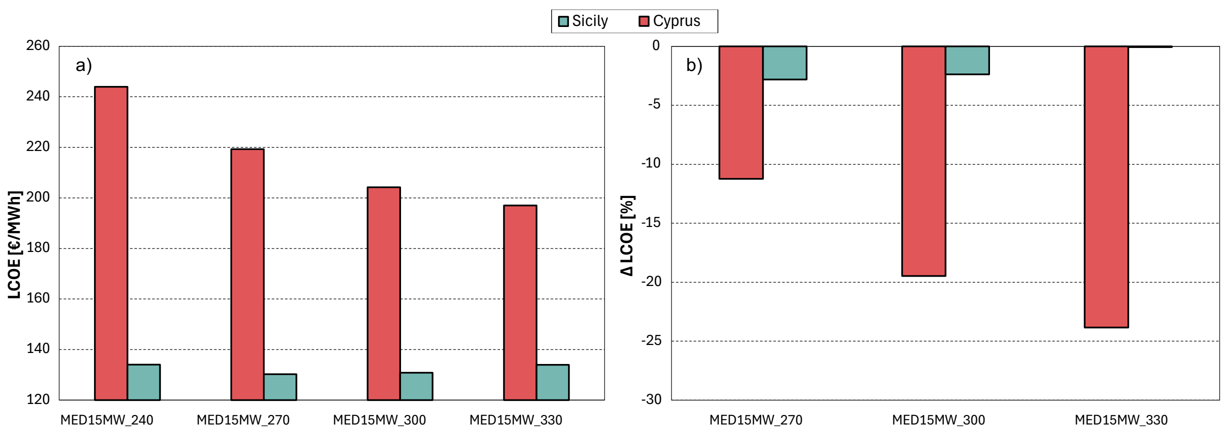

Figure 5.9: LCoE and ΔLCoE in the two installation sites for the new aerogenerator designs.

Figure 5.10a compares the optimal wind farm layouts in Sicily using the MED15MW_240 (light blue) and MED15MW_330 (blue) wind turbines. The results clearly show that the increased rotor size rises wake losses from 3.5% to 3.7% in the optimized layout. This increase drives a corresponding rise in optimal turbine spacing to mitigate wake interactions. Notably, this larger spacing remains convenient despite the resulting higher cable infrastructure costs, as the additional energy production compensates for the CAPEX increase. From the initial turbine arrangement, both configurations converge towards an orientation aligned along the N-NW axis, a result of the prevailing wind direction at the Sicilian site (see **Figure 5.7**).

A similar pattern is apparent in **Figure 5.10**b for the wind farm in Cyprus, where the prevalent wind direction is W-SW. In this case, the total IA cable length is approximately 5% shorter than in Sicily, indicating a generally closer turbine spacing. This is consistent with Cyprus's lower average wind speed, which promotes more packed layouts. Concerning wake effects, increasing the rotor diameter also increases wake losses from 3.5% to 4%. This higher upper limit, compared to the Sicilian site, is explained by examining the turbine thrust curve and Cyprus's wind speed profile. The average wind speed of 5.6 m/s at this location is near the peak thrust value for the MED15MW_330, intensifying wake interactions among turbines.

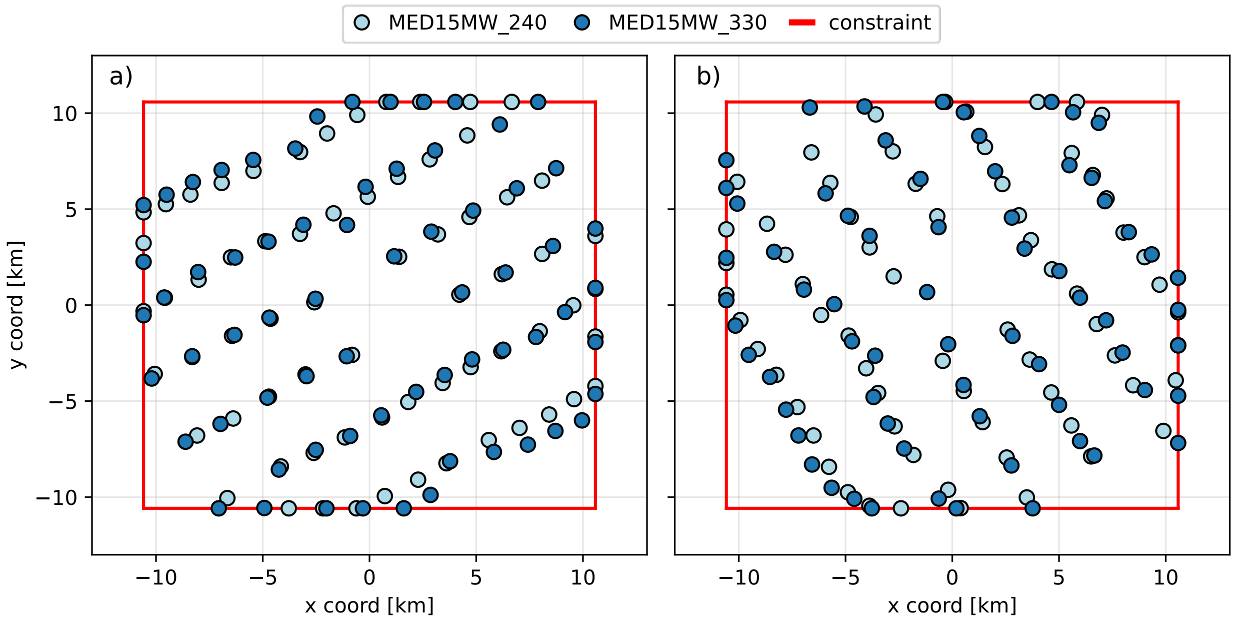

Figure 5.10: Wind farm optimal layout comparison for the MED15MW_240 and MED15MW_330 for the installation site in Sicily (a) and in Cyprus (b).

5.4.2 Hydrogen production

Figure 5.11 shows the statistical distribution of the wind farm power production from the two configurations characterized by the lowest LCoE in the two installation sites considered. The graphs show the number of occurrences per year, corresponding to 10-minute timesteps considered for the analysis, in which the power production of the farm is comprised in a certain range. The power production span, starting from zero and up to the nominal power production of 1 GW, has been divided into twenty bins of 50 MW.

The wind farm is coupled with electrolyzers with the same nominal capacity, and, because of the technical limitations of these devices, a minimum power output from the wind farm must feed the stacks to start hydrogen production. Every time the power produced by the wind farm is lower than that value, depending on the electrolysis technology considered, these devices cannot be activated. From the statistical point of view, this means that the first bins of power production cannot be converted to hydrogen.

For PEM and AEM technologies, the minimum power input is 5% of the nominal one, corresponding to 50 MW for this case. With these technologies, only the first bin of the available power remains unexploited (white bar in **Figure 5.11**). On the other hand, ALK electrolyzers require at least 200 MW, corresponding to 20% of their nominal power, to start the reaction. As such, the first four bins of power production cannot be converted into hydrogen (white and light blue bars in **Figure 5.11**) and are fed into the grid. While this amount of energy may lead to an economic benefit in a real-world plant for electricity and hydrogen cogeneration, in this case it is just neglected for the estimation of LCoH.

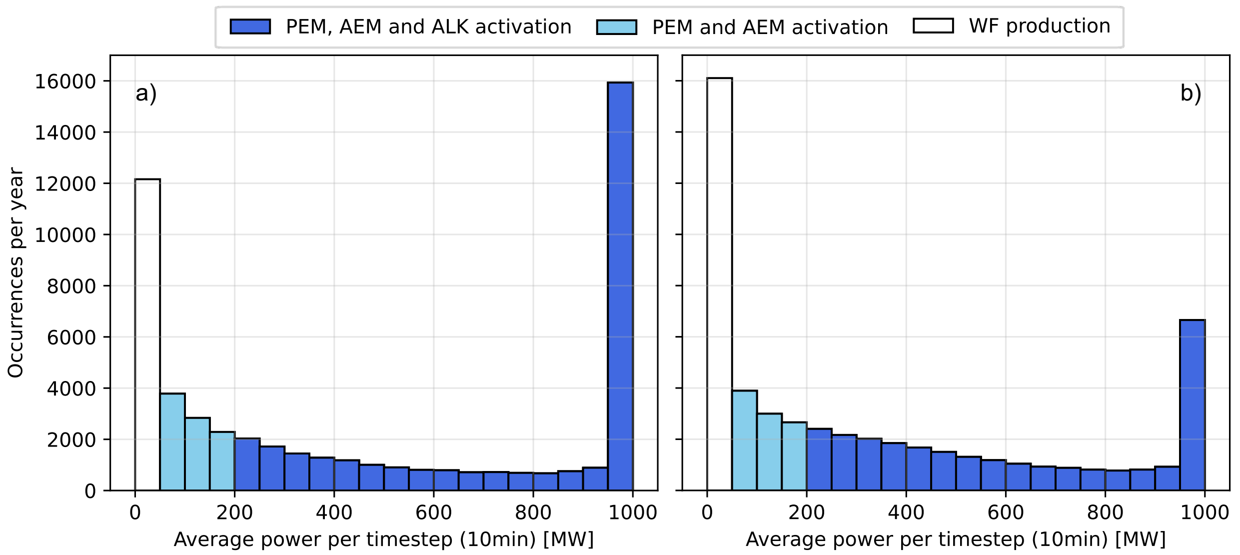

Figure 5.11: Wind farm power production distribution for the installation site in Sicily (a) and in Cyprus (b) with the MED15_270 and MED15_330, respectively.

The power production from the wind farm in Sicily, composed of wind turbines with a rotor diameter of 270 meters, is represented in **Figure 5.11**a. The bin with the highest probability of occurring is the one comprising the nominal power production. Indeed, every time the wind speed is higher than the rated one, the farm produces a power output equal to the maximum one. When the farm is not producing at the nominal level, there is a higher probability of producing at low percentages. The three bins of power production between 50 a 200 MW, wasted by the ALK electrolyzer, are characterized by a high probability of occurring. PEM and AEM electrolyzers are instead able to convert power to hydrogen during these instances, significantly increasing the number of working hours of these combinations.

Figure 5.11b shows instead the probability distribution of the power production from the MED15 330 wind farm in Cyprus. Due to the lower wind speeds, the number of occurrences at nominal power production is considerably lower than in the case of Sicily. The probability of producing power at a low percentage (50-200 MW) is slightly higher in this case, decreasing the chance of activating ALK technologies. This behavior represents an advantage from the gross H2 production, but may accelerate the stack degradation, a phenomenon further investigated in **Figure 5.17**.

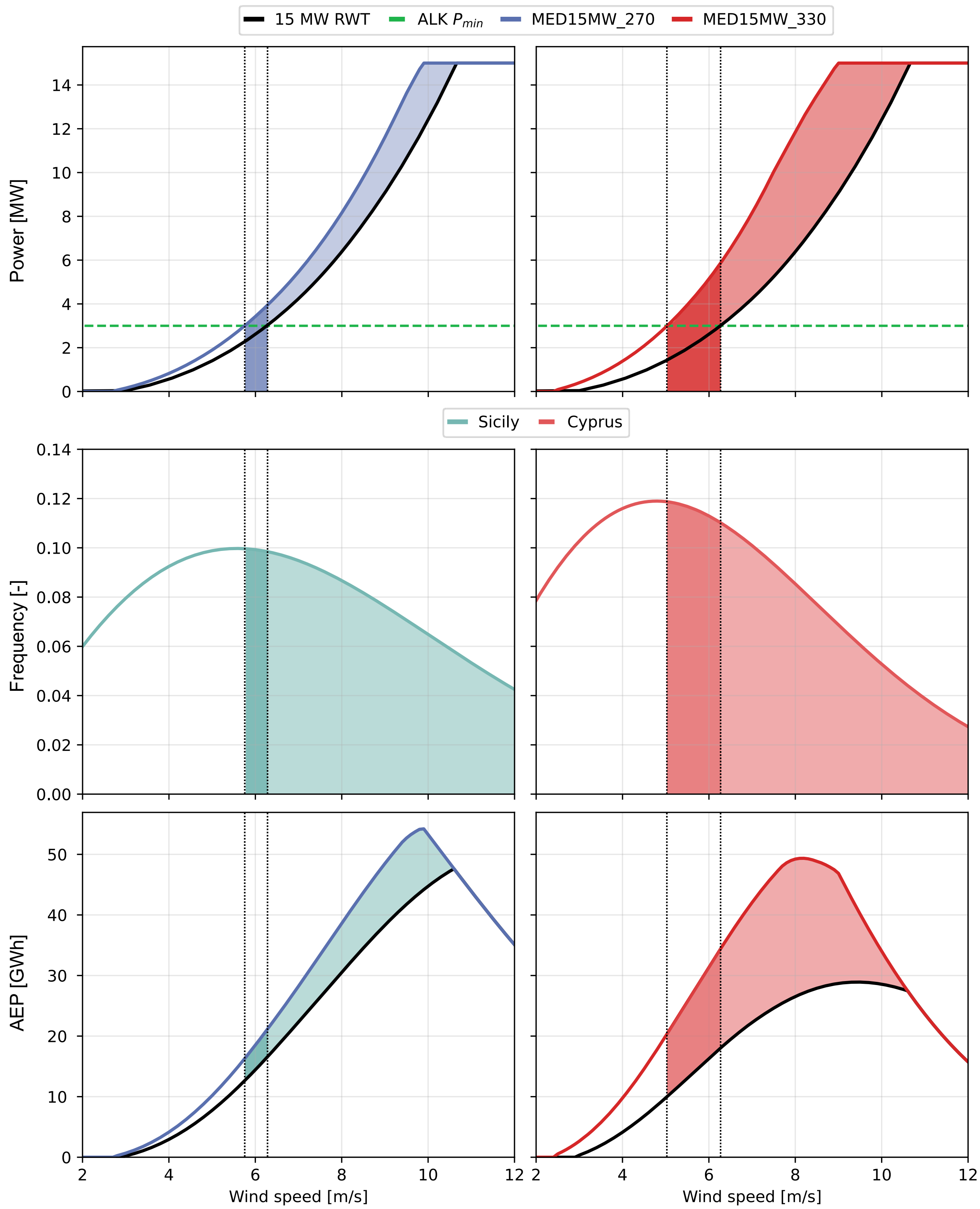

Figure 5.12: Gain in available energy for ALK electrolyzer between 240m and larger rotor diameter wind farms in Sicily (left) and Cyprus (right) considering the: a) shift of power curves and minimum power required by ALK electrolyzers, b) impact on available wind speeds from the point of view of wind resource characterizing the sites, c) gross AEP increment and gain in available energy for H2 production by ALK electrolyzers.

Hydrogen produced by alkaline electrolyzers is often characterized by a competitive cost due to the lower cost of alkaline electrolyzers compared to the other technologies, but the much higher power level required to start the gas production when compared to PEM and AEM types makes this technology less suitable for sites with low average wind speeds. The introduction of wind turbines with larger rotor diameters has the potential to consistently increase the energy share available for H2 production, even with high power requirements at low speeds. **Figure 5.12** shows the gain in available energy for hydrogen production with the ALK electrolyzer technology, comparing the adoption of the 240 m and larger rotor diameter wind farms in the two installation sites. The comparison considers the rotor dimensions that minimized the LCoE presented in the section above: 270m for Sicily (left) and 330m for Cyprus (right).

Figure 5.12a compares the 240m rotor diameter turbine and the larger rotor diameter turbine power curve with the minimum power required from ALK electrolyzers. The shift moves the minimum wind speed required to start hydrogen production towards lower values. In Cyprus (right), the selection of the 330m rotor diameter turbines moves the minimum wind speed from 6.15 to 5.1 m/s, a much higher shift than in Sicily (left), where the 270m rotor diameter turbines decrease it to 5.8 m/s.

The reduction of the minimum wind speed for hydrogen production has a direct effect on the wind resource available on the two sites, as shown in **Figure 5.12**b. The wind speed distribution in Cyprus (right) is shifted towards lower wind speeds than in Sicily (left). Therefore, the introduction of larger rotors in Cyprus has a higher potential of increasing the energy available for hydrogen production from ALK electrolyzers than in Sicily, driving the selection of 330m rotor diameter turbines instead of smaller ones.

Figure 5.12c shows the gross AEP increment brought by a larger rotor diameter and underlines the resulting gain in available energy for H2 production by ALK electrolyzers. A larger rotor diameter not only increases the AEP but also moves the energy production to available power levels at lower wind speeds. Therefore, the electrolyzers have additional energy for hydrogen production at all wind speeds, and a new portion of the AEP distribution becomes available for ALK electrolyzers.

In Sicily (left), the MED15_270 manages to increase the energy available for hydrogen production by 33%, and makes the energy produced between 5.8 and 6.15 m/s now available for ALK electrolyzers (+4%). The 330m rotor diameter turbine in Cyprus provides a much larger increment in AEP, better exploiting the lower wind speeds, and increases the available energy for ALK to a much wider extent (+55%). The shift of minimum wind speeds to start ALK production alone generates an increase of 8% in available energy for hydrogen.

Figure 5.13 presents the CF, as defined in section 5.2.4, of both the wind farm and the electrolyzer, varying rotor diameter and the installation site. As previously discussed in **Figure 5.8**, decreased FOWT specific power increases the energy production of the farm, and thus the CF of the plant. In Sicily, the CF of the wind farm increases from 43% to 53.8% if the rotor diameter increases from 240 to 330m. In Cyprus, the same variation makes the CF increase from 29.5% to 41.7%.

A similar increasing trend characterizes the CF of electrolyzers. However, the better exploitation of electrolyzers comes not only from the increase of AEP, but also from the shift of the minimum wind speed able to generate the minimum power required to start the electrolysis process, as shown in **Figure 5.12**. Additionally, the trend is strongly related to the installation site. Despite the higher values shown in Sicily for both wind and electrolyzers (**Figure 5.13**a), Cyprus experiences higher benefits due to the larger diameter, leading to a more relevant capacity factor increase. Finally, some differences can be noticed between the electrolysis technologies. While

PEM and AEM exhibit CFs close to that of the wind farm, ALK energy exploitation is lower. This is due to the stronger technical constraints on the minimum power threshold and cold start-up time that characterize this technology. On the other hand, the CF of this technology exhibits higher benefits related to the larger swept areas. Specifically, while PEM and AEM CFs experience an improvement of 25% and 42% for Sicily and Cyprus, respectively, ALK's energy exploitation rises by 28% and 47% in the corresponding sites.

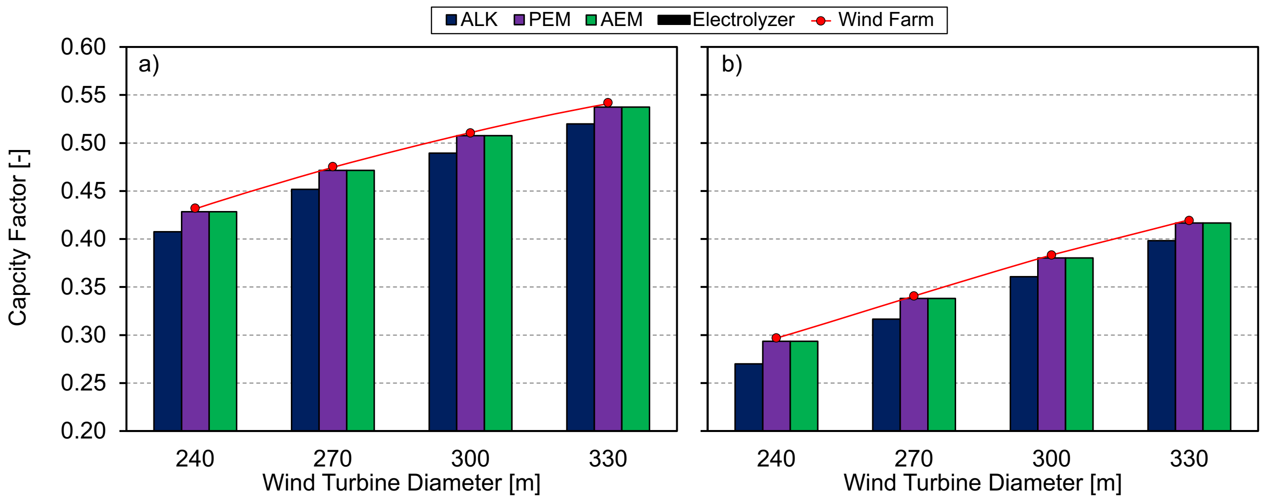

Figure 5.13: Wind Farm and Electrolyzer CF comparison in Sicily (a) and Cyprus (b).

Accordingly, **Figure 5.14** shows the results in terms of unexploited energy resulting from the technical operating constraints of three electrolyzer technologies in the two installation sites. The overall energy waste, represented by the bars in the plots, is composed of the combination of technical constraints such as minimum load thresholds (solid-colored segments) and the operational lag due to the cold start-up time of the component (hatched segments).

Across both sites, a clear differentiation emerges in the behavior of the three technologies. ALK experiences the highest unexploited energy due to its high minimum load requirement of 20% of nominal installed capacity. This threshold is frequently not met during low-wind periods, especially with smaller turbine diameters, leading to extended idle periods and significant underutilization of available wind energy. In this case, the benefit related to lower specific wind turbines is apparent. The larger amount of energy available to the system related to the larger diameters leads to an increase in energy consumption of 17%. On the other hand, PEM and AEM electrolyzers, which share a more flexible minimum load threshold of 5%, display markedly lower wastes. Their higher operational responsiveness allows them to operate under a broader range of wind power inputs, resulting in more effective energy capture and less effective impact of low specific power wind turbines. The performance trends of PEM and AEM are nearly overlapping, consistent with their similar technical constraints.

Additionally, while thermal startup losses (hatched areas) are similar across all technologies, they represent a higher percentage of the total unexploited energy for PEM and AEM, due to their overall lower energy waste. This underscores the importance of minimizing shutdown occurrences even for highly flexible electrolyzers, as startup thermal losses become a more dominant share of the overall inefficiencies. Comparing the two geographical contexts yields further insights. Cyprus exhibits higher unexploited energy related to the minimum load threshold, especially for ALK systems (**Figure 5.14**b). This is attributed to more frequent occurrences of low wind power, during which the farm cannot meet the operating threshold of the electrolyzers. On the other hand, despite the higher average wind resource, Sicily experiences larger durations of wind scarcity. This results in more cold startups and shutdown events (**Figure 5.14**a). Consequently, thermal losses due to frequent shutdowns are reduced in Cyprus, even for less responsive technologies.

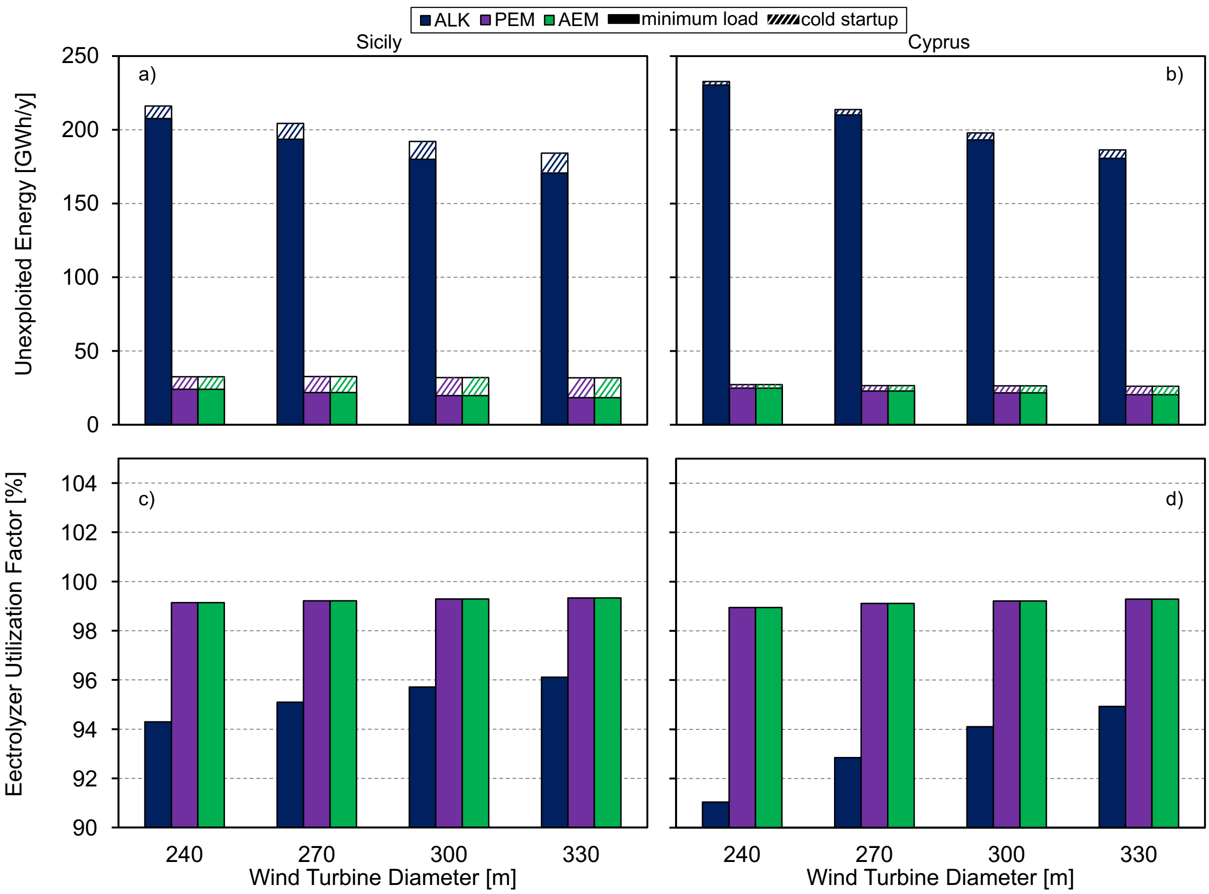

Figure 5.14: Unexploited energy and Electrolyzer Utilization Factor comparison due to electrolyzer technical constraints in Sicily (a, c) and Cyprus (b, d).

Figure 5.14 also shows the trend of the electrolyzer utilization factor (UF). This parameter, defined in Section 5.2.4, allows for a better understanding of energy usage. Consistent with the plots above, while the site in Cyprus (d) experiences lower UF, the electrolyzers benefit most from the specific power decrease (see the ALK trend in blue). However, thanks to the faster response to shut down and wider operational range, the difference between AEM and PEM in the installation sites is reduced and close to the nominal value. Also in this case, ALK is the technology that benefits most from the specific power decrease. While PEM and AEM exhibit UF improvements lower than 0.5%, ALK exceeds 4% at the installation site in Cyprus.

In further detail, **Figure 5.15** illustrates the time-dependent behavior of the wind-powered electrolysis system, offering insight into the dynamic interaction between available wind energy, wasted energy, and hydrogen production. **Figure 5.15**a compares the available input energy obtained with the MED15_240 farm (red area) to the wastes for ALK (blue area) and AEM (green area). From the plot, it is apparent that the blue area frequently exceeds the green. This reflects ALK's higher minimum load threshold, which prevents it from operating during partial-load conditions, leading to more frequent idle periods and greater energy waste. The green area, which overlays the blue, is shown only when the power input falls below 5% of nominal electrolyzer capacity and is not enough to trigger hydrogen production. This dual-color structure emphasizes the greater flexibility of the AEM electrolyzer, which can continue to operate in low-input conditions that forces the ALK system to shut down. Concerning PEM, it exhibits a similar behavior, and its trend has been left out of the plot to avoid repetitions.

On the other hand, **Figure 5.15**b presents the corresponding hydrogen production profiles, resulting from the input energy shown above. Here, the blue area corresponds to the periods when both ALK and AEM are producing hydrogen, while the green area represents the additional hydrogen output generated exclusively by AEM during time-steps when ALK is idling due to insufficient input power. It is again apparent how, thanks to the less strict technical constraints, AEM maintains partial production for a wider range of power inputs, contributing to a more continuous and resilient hydrogen supply.

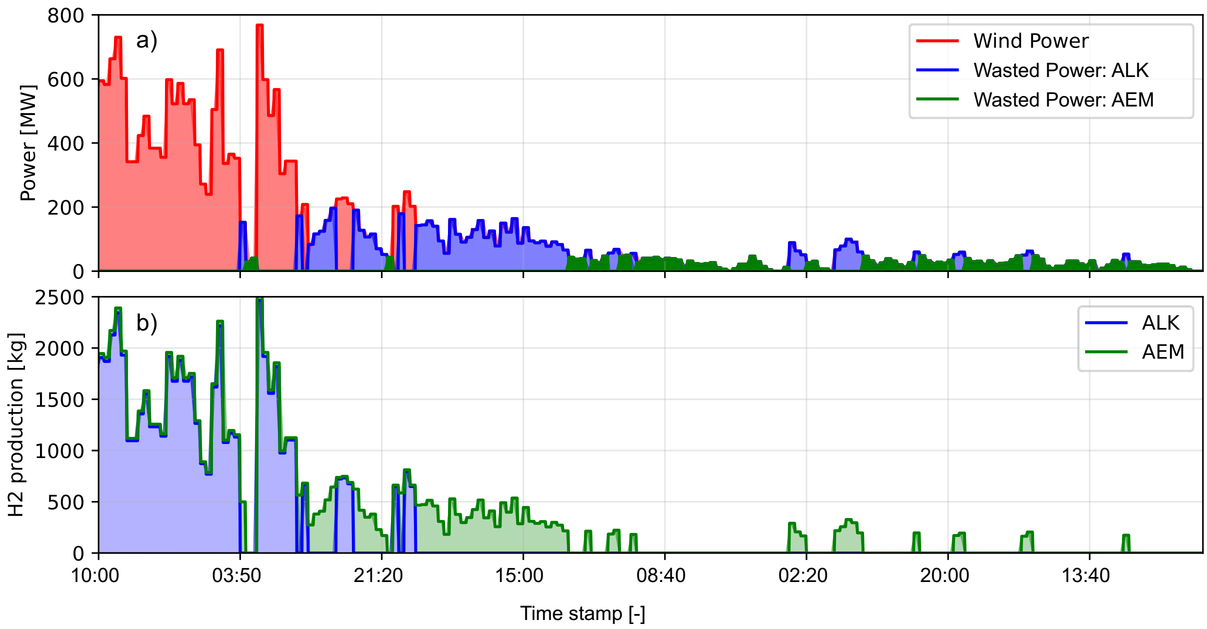

Figure 5.15: Time-dependent behavior of the system in terms of produced and exploited power a), and hydrogen production b) during seven days of operation with the MED15_240 FOWT. PEM trends have been omitted due to similar behavior to AEM technology.

Figure 5.16 presents the annual hydrogen production achieved for each electrolyzer technology and wind turbine rotor, in the two considered installation sites. The red error bars in the plot represent the variability in output associated with different electrolyzer efficiencies. This plot allows for investigating the impact of the three different conversion and three degradation factors considered for each electrolyzer in order to account for a pessimistic, optimistic, or average development of the technology, respectively, in a time horizon starting from 2030 (**Table 5.5** in Section 5.3.2). Several key trends can be highlighted. Sicily (**Figure 5.16**a) consistently outperforms Cyprus (**Figure 5.16**b) in terms of total hydrogen production, regardless of technology or turbine size. This is primarily driven by a higher annual wind energy yield, enabling longer and more consistent operation of the electrolyzers and thus enhancing hydrogen output.

Among the electrolyzer technologies, PEM experiences the highest hydrogen production across most of the configurations. This is due to its lower minimum load threshold and high responsiveness, which allow it to exploit a broader range of wind energy conditions. The error bars offer additional insight into the sensitivity of each technology to efficiency assumptions.

While PEM and ALK show greater uncertainty in production estimates due to the wider set of data found in the literature, AEM's narrower range margins reflect the lack of data in the literature and therefore the limited development of technology.

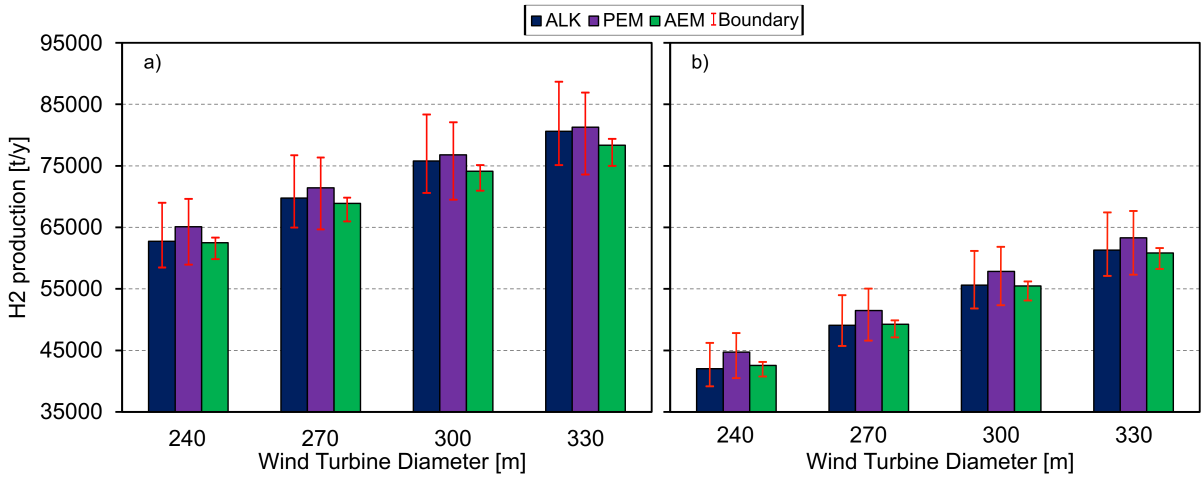

Figure 5.16: Hydrogen production comparison in Sicily (a) and Cyprus (b) varying the turbine diameter.

In line with **Figure 5.13**, ALK demonstrates a steeper improvement in hydrogen production with an increasing rotor diameter compared to PEM and AEM. Finally, despite the worst performance in terms of energy exploitation and the comparable nominal conversion efficiency experienced by the ALK, hydrogen production is similar to that of the other technologies. This is primarily attributed to lower degradation rates and higher average conversion efficiency over time. **Figure 5.17**a, in fact, shows how the ALK experiences an average ϕ higher than the other technologies, equivalent to 19.64 kg/MWh with respect to the 18.59 kg/MWh for PEM and 17.04 kg/MWh for AEM, which balances the reduced energy exploited. Despite the trend shown reproducing the behavior of the systems in the Sicilian case, adopting the MED15_240 in the average technical scenario and optimal degradation, the results can be extended to all the simulated configurations, as testified by **Table 5.8**. The yearly average ϕ trend depicted in the image for the OPT degradation scenario highlights the impact of degradation on stack performance. It is apparent how the operation of the component leads to the wear of the electrolyzer, which results in a decreased conversion efficiency of the stack. Additionally, ALK's stricter technical constraints on minimum power input lead to fewer operating hours with respect to the technologies with wider operational ranges. As a result, due to the linear degradation model based on the voltage increase per operating hour, PEM and AEM exhibit faster wear, even if the operation occurs far from the nominal power input of the electrolysis facility. This is consistent with the trends shown in **Figure 5.17**a. ALK, in fact, experiences better performance over a longer operational period compared to the other electrolyzers, resulting in higher overall system efficiency.

Although the AEM exhibits a higher degradation rate, as indicated by the higher slope with respect to the other trends, it allows for a greater degradation before requiring component replacement. Therefore, despite the lower ϕ for about half of the plant lifetime, the AEM with the degradation scenario selected experiences fewer replacements than PEM, which undergoes two replacements during the period analyzed.

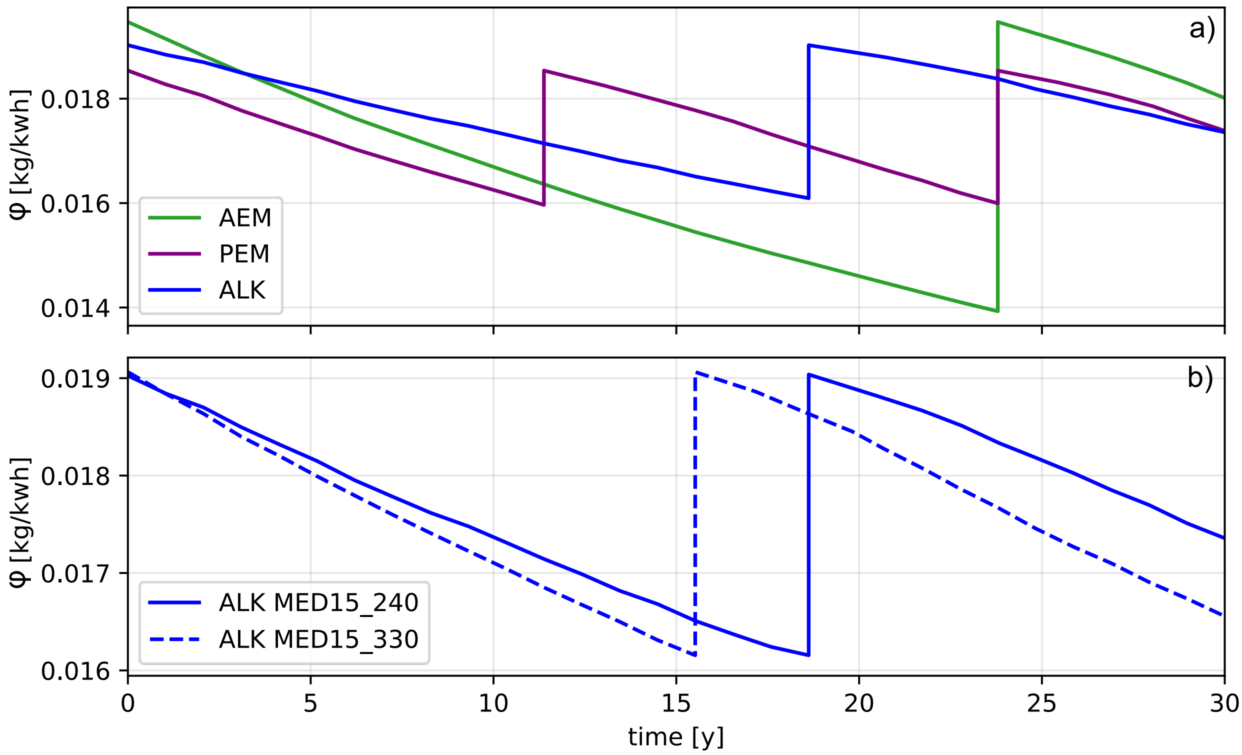

Figure 5.17: Time-dependent variation of the yearly average ϕ in Sicily comparing the three technologies with the MED15_240 (a), and the behavior of ALK with the MED15_240 and MED15_330 (b) in the optimal degradation scenario.

Finally, **Figure 5.17**b compares the performance of the alkaline electrolyzer when coupled with two different wind turbine types. The adoption of the turbine with a larger rotor diameter enables energy harvesting at lower wind speeds, effectively increasing operational hours. However, this also leads to increased stack degradation, resulting in a higher number of component replacements over time. In this case, despite the lower average ϕ over the plant lifetime, corresponding to 19.48 kg/MWh with respect to the 19.64 kg/MWh of the system coupled with the MED15_240, the increased available energy and power exploitation allowed by the MED15_330 leads to enhanced hydrogen production, as highlighted by **Figure 5.16**. **Table 5.8** provides a comprehensive overview of the results obtained in this study in terms of LCoE, LCoH, component replacement, and yearly average ϕ depending on FOWTs' specific power. The trend that can be observed is that lower specific power turbines result in more electrolyzer replacements as well as lower average conversion factors. The same trend can also be observed in adopting wide operational range electrolyzers. Finally, it is apparent that the rotor size that minimizes the LCoE also minimizes the LCoH.

Figure 5.18 presents the distribution of LCoH across all analyzed scenarios, encompassing the three electrolyzer technologies, the four wind turbine models, the two installation sites, and the different economic and technical conditions, for an overall combination of 216 simulations. In detail, this number of simulations results from the combination of three values of the conversion factor and three values of the degradation factor with the four economic scenarios.

Table 5.8: Summary of the results obtained for the technical average scenario.

		FOWT diameter [m]	240	270	300	330
Sicily		LCoE [€/MWh]	134.04	130.27	130.86	133.55
	ALK	Average ϕ [kg/MWh]	19.64 – 19.37	19.58 – 19.42	19.52 – 19.36	19.52 – 19.43
		Substitutions [-]	1 – 2	1 – 2	1 – 3	1 – 3
		LCoH [€/kg]	5.32 – 6.50	5.25 – 6.33	5.33 – 6.53	5.49 – 6.60
	PEM	Average ϕ [kg/MWh]	18.59 – 18.51	18.59 – 18.47	18.58 – 18.46	18.56 – 18.46
		Substitutions [-]	2 – 3	2 – 3	2 – 4	2 – 4
		LCoH [€/kg]	5.35 – 7.19	5.29 – 6.98	5.37 – 7.31	5.55 – 7.36
	AEM	Average ϕ [kg/MWh]	17.05 – 16.79	17.08 – 16.82	17.13 – 16.74	17.11 – 16.70
		Substitutions [-]	1 – 3	1 – 3	1 – 3	1 – 3
		LCoH [€/kg]	5.39 – 7.75	5.34 – 7.49	5.41 – 7.467	5.59 – 7.57
Cyprus		LCoE [€/MWh]	243.94	219.30	204.19	196.98
	ALK	Average ϕ [kg/MWh]	19.59 – 19.45	19.61 – 19.45	19.58 – 19.36	19.56 – 19.33
		Substitutions [-]	1 – 2	1 – 2	1 – 2	1 – 2
		LCoH [€/kg]	8.03 – 9.82	7.47 – 8.99	7.19 – 8.53	7.13 – 8.39
	PEM	Average ϕ [kg/MWh]	18.61 – 18.57	18.59 – 18.54	18.59 – 18.53	18.59 – 18.51
		Substitutions [-]	2 – 3	2 – 3	2 – 3	2 – 3
		LCoH [€/kg]	7.79 – 10.47	7.38 – 9.70	7.17 – 9.24	7.14 – 9.05
	AEM	Average ϕ [kg/MWh]	16.89 – 16.74	16.96 – 16.81	17.01 – 16.81	17.05 – 16.80
		Substitutions [-]	1 – 3	1 – 3	1 – 3	1 – 3
		LCoH [€/kg]	7.95 – 11.36	7.49 – 10.45	7.27 – 9.93	7.25 – 9.69

As shown in **Figure 5.18**, the defined design space allows for the estimation of a range of LCoH instead of a single fixed value. This may give an idea of potential future scenarios. While the central part of each vertical distribution appears to be the densest of scatters, corresponding to the average technical and economic scenarios, the upper and lower boundaries should be considered as the maximum and minimum LCoH that can be estimated with the assumptions made, and not just as outliers. Finally, to simplify the readability of the figure, the plots in **Figure 5.18** are clustered for installation site (Sicily above and Cyprus below), while the columns represent the wind turbines considered.

Across all scenarios, the ALK consistently yields the lowest LCoH values, underscoring its cost-effectiveness despite the comparable hydrogen production potential. Additionally, the wind turbine that minimizes the LCoH aligns with that for minimizing the LCoE, reflecting the dominant influence of electricity cost on hydrogen production economics.

The impact of wind turbine rotor diameter on LCoH is notably more pronounced in Cyprus, where the adoption of the MED15_330 turbine significantly reduces hydrogen production costs, bringing the minimum LCoH in Cyprus closer to the higher levels estimated for Sicily. This trend mirrors the behavior seen in LCoE, where larger rotor diameters improve energy capture and cost efficiency more substantially in Cyprus due to site-specific wind conditions. However, a significant cost difference exists between the average values in the two installation sites, with Cyprus exhibiting approximately 3 €/MWh higher LCoH compared to that in Sicily.

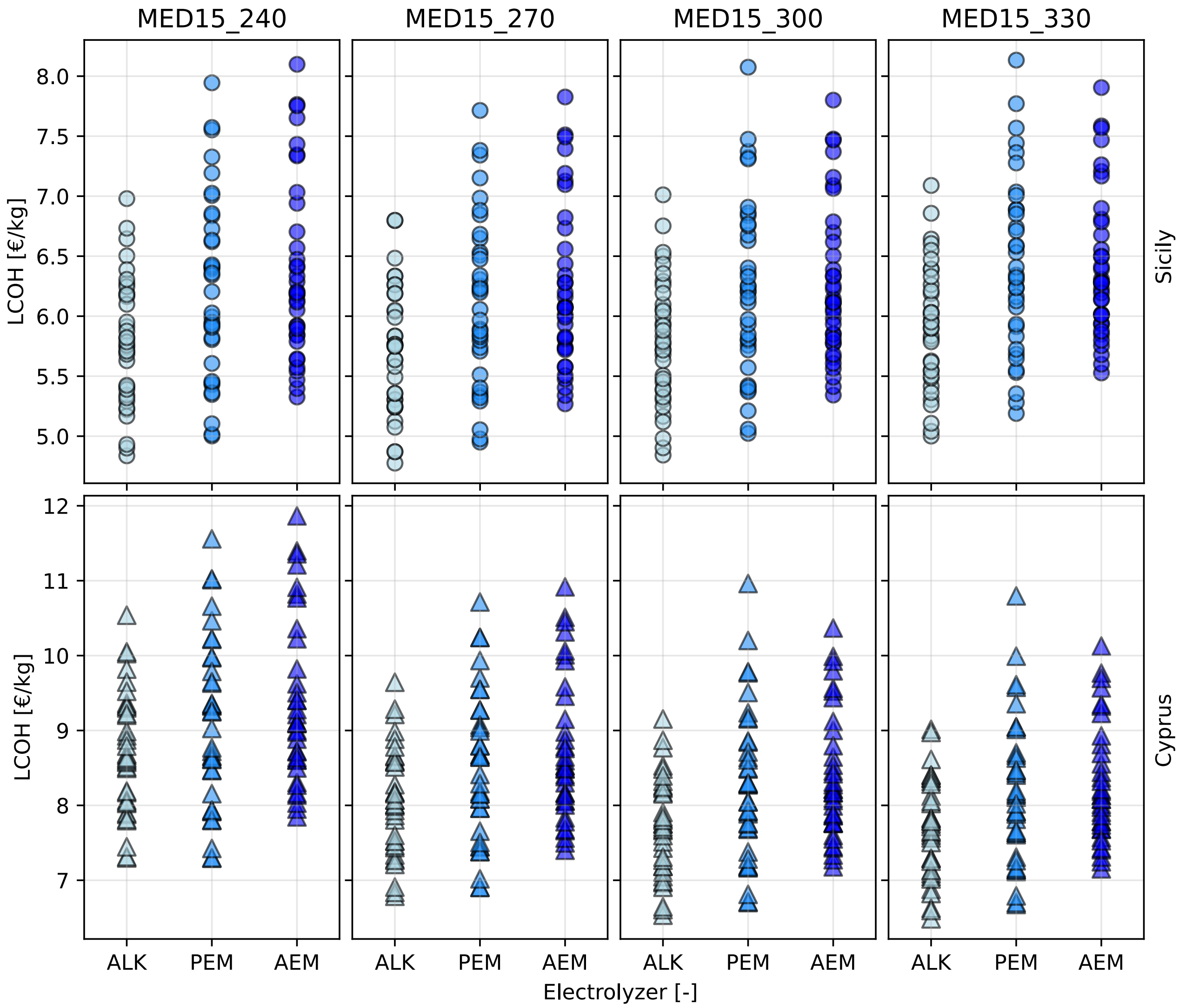

Figure 5.18: LCoH distribution across all the scenarios analyzed, considering uncertainty in efficiencies, degradation factors, and costs.

5.5 Discussion

This study presents a comprehensive assessment of how electrolyzer technology and local wind characteristics jointly affect the efficiency, reliability, and economic viability of renewable hydrogen production. Using two study cases like those of Sicily and Cyprus, characterized by low-to-moderate wind speeds, allows to magnify the differences between the behavior of the different electrolyzers. The analysis of these two sites demonstrates in particular that system performance does not rely only on average wind speeds but is strongly affected by wind intermittency and its interaction with the operational flexibility of electrolyzers. In this context, the ability of technologies such as PEM and AEM to operate at lower power thresholds and respond dynamically to fluctuating input conditions, combined with the benefits resulting from the adoption of low-specific-power wind turbines, provides a significant advantage in terms of energy exploitation.

Sicily's higher wind resource consistently enables higher hydrogen output across all configurations. While PEM electrolyzers result in enhanced total hydrogen production, ALK electrolyzers lead to the lowest LCoH due to higher conversion factors and lower degradation over time. Additionally, ALK is the technology that benefits most from scaling up wind turbine diameter, particularly when the wind resource distribution is shifted towards lower velocities. This points to a trade-off between flexibility and robustness. While PEM and AEM technologies are better suited to environments with high variability and frequent low-wind events, ALK electrolyzers, given the high ϕ and durability, are competitive in more stable, high-energy settings where downtime is minimal. Therefore, the importance of turbine rotor size also emerges as a critical variable. Larger rotors capture more of the low-wind spectrum, smoothing out fluctuations and reducing the frequency of electrolyzer shutdowns. This effect can be particularly beneficial to technologies with higher startup thresholds, such as ALK, mitigating one of their primary drawbacks. Considering large-scale electrolysis facilities, tailored solutions for green offshore hydrogen production can include the use of high-efficiency alkaline electrolyzers as a stable baseload, complemented by PEM or AEM technologies that enable increased overall output by effectively operating during periods of low wind availability. However, this issue may be overcome by the adoption of a smart control strategy for the electrolyzer. Advanced power input partitions to the different electrolyzer modules may represent a solution, but further analyses should be performed on the impact of different wear among the stacks of the same electrolyzer facility. On the other hand, this would require a more detailed electrolyzer model which falls out of the scope of this study. The interplay between rotor sizing and electrolyzer design suggests that tailored optimization strategies, matching technological characteristics to local resource patterns, are essential for achieving cost-effective hydrogen production.

Regarding the economic aspects, the LCoH is highly sensitive to both the choice of electrolyzer and the specific site configuration. While PEM systems yield the highest production and lowest shutdown frequency, the ALK systems achieve the lowest LCoH in both installation sites. This is due not only to their lower capital cost per unit capacity, but also to their robustness under high-load conditions. These findings are broadly consistent with previous studies in the field. While previous studies have highlighted the potential benefits of hydrogen production costs introduced by higher specific power wind turbines [293], the results presented herein reveal a contrasting trend. In the context of the Mediterranean Sea, and particularly in regions like Cyprus, where wind resources are notably weaker compared to areas such as the North Sea, turbines with lower specific power proved to be more effective. This divergence arises from the local wind profile, which is skewed towards lower wind speeds, making larger rotors (and thus lower specific power) more efficient for harnessing energy. As a result, the LCoH experiences relevant reductions, with savings up to 1.50 €/kg H_2, corresponding to a 17% decrease in Cyprus. These findings suggest that turbine optimization for hydrogen is completely region-specific, with local wind conditions playing a pivotal role in determining the most cost-effective design approach. Another interesting comparison can be made by looking at the LCoH found in the literature. While studies focused on the North Sea have proposed average hydrogen costs of 3-4 €/kg [67,277], average prices of 5-6 €/kg have been estimated for the Mediterranean Sea [128], which are consistent with the outcomes of this study.

Additionally, a comparison with the outcomes obtained for the Dutch North Sea should be addressed. In the North Sea (**Figure 2.8**), dedicated offshore fixed bottom wind farms coupled with centralized or decentralized electrolysis show relatively favorable LCoH, with minimum values reaching ~3 €/kg in the most optimistic cases. This cost level is a key benchmark for the economic competitiveness of green hydrogen. Interestingly, the cost distribution remains in a relatively narrow range across distances from shore, with only a moderate increase at larger distances. Both ALK and PEM electrolyzers perform similarly, although PEM tends to exhibit slightly higher variability in LCoH. In this case, the combination of high CF and the possibility of adopting bottom-fixed foundations keeps LCoH relatively low in the North Sea.

On the other hand, the Mediterranean scenarios (**Figure 5.18**) show systematically higher LCoH values, with minimum costs approximately 3 €/kg above those obtained in the Dutch case. This offset is consistent across all configurations and represents a significant barrier to achieving parity with Northern European benchmarks. Two main drivers explain this difference:

- Floating offshore wind adoption: unlike the North Sea, the Mediterranean cases rely on floating offshore wind technology. The higher CAPEX and OPEX associated with floating foundations directly translate into increased hydrogen production costs.
- Lower CFs: Mediterranean wind resources are generally less favorable than those in the North Sea. The adoption of low-specific-power wind turbines improves the CF and brings costs down compared to conventional designs, but even in optimized scenarios, production levels remain below the benchmark represented by the North Sea.

The comparison also shows that in the Mediterranean, the choice of electrolyzer technology plays a larger role. AEM electrolysis is included in the Mediterranean assessment, and its cost performance is less favorable, with systematically higher LCoH compared to ALK and PEM. This further increases the gap in achievable costs between the two regions.

Another noteworthy observation is the cost distribution spread. In the North Sea cases, costs remain clustered, and the variation between the lowest and highest values is relatively modest. In the Mediterranean, however, the spread is wider, reflecting higher sensitivity to local wind resource conditions (see the difference between Sicily and Cyprus) and technology configurations. This suggests that site-specific optimization will play a more critical role in Southern Europe compared to Northern Europe, where high CFs can be more consistently guaranteed.

Overall, the results underline that while advances such as low specific power turbines can help narrow the gap between Mediterranean and North Sea hydrogen production, structural differences in wind resources and offshore technology requirements maintain a persistent cost disadvantage. Overcoming this gap would likely require either significant cost reductions in floating wind, relevant incentives from the governments, or hybrid approaches (e.g., combining offshore and onshore renewable resources, integrating solar PV) to improve capacity factors and reduce LCoH volatility.

From a technical perspective, future reductions in minimum power thresholds and startup times will be crucial for enhancing electrolyzer integration into renewable energy systems. Attention should be paid to electrolyzer control strategies. In configurations where electrolyzer stacks are connected in series rather than parallel, better utilization of partial power input is possible, even if this introduces a higher frequency of shutdowns of the modules. Smarter control algorithms that minimize downtime while preserving system longevity could offer significant gains in performance and economic return.

Nonetheless, several limitations must be acknowledged. The degradation model employed does not currently capture the impact of fluctuating power input or frequent shutdowns, which could significantly influence the lifespan and stack efficiency, particularly under highly variable wind conditions. Moreover, although other electrolysis technologies, such as Solid Oxide Electrolyzers, are gaining momentum, they have not been included in this study due to their limited commercial deployment and the scarcity of performance data in the literature. This exclusion narrows the generalizability of the findings to currently more mature electrolyzer technologies. Only centralized, onshore hydrogen production systems have been considered.

While this choice reflects the relatively short distances from shore for both installation sites and the immaturity of decentralized offshore hydrogen infrastructure, it limits extrapolation to offshore or distributed production paradigms, which may lead to different economic and technical outcomes. Finally, the wind farm optimization has been performed only by selecting the LCoE as the objective function. Although the LCoH may lead to a different optimized layout, the statistical approach allowed by TopFarm can result in significant errors due to the impossibility of accounting for the electrolyzer technical constraints. Future works on this topic may be aimed at comparing the optimal wind farm layout obtained by looking at energy or hydrogen costs.

5.6 Conclusions

In conclusion, this study advances the body of knowledge by showing some of the cross-interactions taking place when the design of an offshore renewable hydrogen production system is at hand. Electrolyzer flexibility, wind resource variability, and turbine configuration all interact in defining the system operation and LCoH. The key points can be summarized as:

- **Electrolyzer flexibility vs. cost trade-off:** The ability of PEM and AEM to better operate under variable and low-power conditions enhances hydrogen production efficiency in intermittent power input scenarios. However, ALK electrolyzers, despite the lower flexibility, at the time of writing, remain the most cost-effective solution due to lower degradation rates and capital costs.
- **Local wind patterns**: The performance of offshore wind-to-hydrogen systems is highly site-specific. With reference to the study cases analyzed herein, Sicily's stronger and more consistent wind distribution yields greater hydrogen output, while in Cyprus low-specific-power turbines with larger rotors are needed in order to improve energy capture under lower average wind speed conditions.
- **Turbine-electrolyzer synergy**: Turbines with lower specific power values smooth wind power fluctuations and allow for the exploitation of low wind speeds, which is particularly beneficial for electrolyzers with higher minimum operating thresholds like ALK. Tailoring turbine design to local wind profiles significantly enhances system efficiency and reduces hydrogen costs.
- **Economic sensitivity to design choices**: LCoH exhibits strong variations by site and configuration, with reductions up to €1.50/kg (or 17%) in Cyprus when using optimized turbine-electrolyzer pairings. This underscores the need for region-specific optimization strategies rather than one-size-fits-all solutions.

Technology selection should therefore be deeply contextualized, leveraging site-specific resource profiles to align electrolyzer characteristics and wind energy capture for optimal performance and economic efficiency. As electrolyzer technology continues to evolve and control systems become more sophisticated, future work should integrate more detailed degradation models and expand the scope to include emerging configurations and offshore scenarios.

6 CONCLUSIONS

This thesis has investigated the techno-economic feasibility, design choices, and system-level interactions that shape the future deployment of offshore wind-to-hydrogen systems. By combining high-resolution modeling of offshore hydrogen production configurations, an in-depth analysis of low specific power FOWTs, a comparative assessment of battery and hydrogen storage options for curtailment mitigation, and a region-specific evaluation of electrolyzer–turbine synergies, this work has contributed to a more integrated understanding of how renewable hydrogen can be produced and delivered at scale in diverse Mediterranean and European contexts.

The main findings and their implications are summarized and synthesized below.

Offshore hydrogen production configurations. The comparative analysis of C-ON, C-OFF, and D-OFF configurations has shown that offshore electrolysis is not only technically feasible but also increasingly competitive when integrated with large-scale offshore wind farms. Among the three options, C-OFF consistently emerges as the most cost-competitive configuration, driven by the relative cost advantage of hydrogen transmission pipelines over HVDC cables at increasing distances from shore.

The wide LCoH range across scenarios in the North Sea (3.0–10.5 €/kg) reflects both technological uncertainty and the heterogeneity of input assumptions. When benchmarked against expert-validated parameters, however, costs narrow to a more plausible band of 4.1–6.5 €/kg H_2, in line with recent literature estimates for early large-scale projects. These findings reinforce the view that offshore electrolysis will remain more expensive than fossil-based hydrogen in the near term, but that it is already approaching levels considered viable under supportive policy frameworks and carbon pricing.

Decentralized offshore electrolysis resulted to be the less cost-effective solution despite its higher system-level efficiency. Nevertheless, D-OFF may retain strategic value in specific contexts, such as where modular deployment, shorter permitting timelines, or redundancy in infrastructure are considered.

A clear conclusion emerging from this work is that the choice of electrolyzer matters, but the ranking of technologies depends strongly on operational conditions. While PEM electrolyzers are best suited to handle the variability of wind power input, the lower cost and durability of ALK maintain their competitiveness under stable, high-energy conditions. This underlines the importance of aligning technology selection with site-specific wind profiles and operational strategies.

Low specific power floating wind turbines. The assessment of LSP FOWTs demonstrated their potential in moderate-wind regions such as the Mediterranean Sea. By lowering specific power and enlarging rotor diameter, LSP turbines increase capacity factors and enhance the economic viability of sites traditionally considered marginal for offshore wind. This strategy reduces the LCoE, helping to expand offshore wind deployment to new sea basins.

However, the study also revealed that the LSPs are not beneficial a priori. In high-wind environments, such as those in the North Sea or parts of the French Mediterranean coast, larger rotors do not compensate for the associated cost increase, leading to higher LCoE. Optimal turbine design is therefore highly site-specific, requiring integrated design methodologies that account simultaneously for aerodynamic performance, structural scaling, floating substructure costs, wake effects, and cable layouts.

From an environmental standpoint, LSP turbines may reduce the overall ecological footprint of offshore wind deployment. By generating more energy per unit of material, they help balance the increased resource intensity of larger machines. This aligns with the broader objectives of sustainable and resource-efficient energy transitions.

Storage integration and curtailment mitigation. The analysis of curtailment management strategies confirmed that both BESS and electrolyzers can play a significant role in improving the financial viability of offshore wind farms. For a 1 GW plant in the Mediterranean Sea, curtailments were shown to energy raise production costs by up to 18 %, but the integration of storage, whether through hydrogen production or large-scale batteries, can mitigate substantial revenue losses.

Brand-new BESSs improve NPV by up to 30 %, while SLBs, although more uncertain in terms of lifespan and performance, provide a promising low-cost alternative if their CAPEX falls below ~70 €/kWh. On the hydrogen side, ALK electrolyzers become attractive once hydrogen prices exceed ~4.2 €/kg, with break-even conditions relative to BESS achieved between 8.5 and 9.5 €/kg.

These results suggest that hybridization strategies, in which batteries are used for short-term balancing and electrolyzers for long-term conversion into hydrogen, may represent the most robust pathway forward. From a policy perspective, however, targeted incentives will be needed to de-risk both battery and hydrogen investments, given their capital intensity and evolving supply chains.

Site-specific turbine–electrolyzer synergies. The regional case studies of Sicily and Cyprus highlighted the critical role of local wind resource distributions in determining both hydrogen output and LCoH. While Sicily's stronger winds support higher production across all electrolyzer types, Cyprus demonstrated how low-specific-power turbines with larger rotors can enhance hydrogen production by capturing low-wind events and smoothing variability.

The interplay between turbine sizing and electrolyzer flexibility revealed that no single electrolyzer technology dominates across contexts:

- PEM and AEM excel under variable, low-wind conditions thanks to their lower minimum load requirements.
- ALK remains the most cost-effective under stable, high-load conditions, especially when coupled with large rotors that reduce shutdowns.

This underlines the necessity of tailored optimization, where turbine–electrolyzer pairings are designed in accordance with site-specific wind profiles. It also suggests that future offshore hydrogen systems may benefit from hybrid electrolyzer facilities, combining alkaline stacks for baseload production with PEM/AEM stacks to capture residual low-wind energy.

Mediterranean vs. North Sea. A recurring theme across the analyses is the persistent cost gap between Mediterranean and North Sea offshore hydrogen production. In the Dutch North Sea, LCoH can fall to ~3 €/kg in optimistic scenarios, while Mediterranean sites remain ~3 €/kg higher across comparable configurations. This gap is driven primarily by:

- Floating wind reliance, which raises CAPEX and OPEX relative to bottom-fixed foundations.
- Lower capacity factors, even when optimized with LSP turbines.

The Mediterranean also exhibits wider LCoH variability, reflecting greater sensitivity to local conditions and technology configurations. This means that site-specific optimization is more critical in Southern Europe, while Northern Europe benefits from more uniformly favorable wind resources.

Bridging this cost gap will require a combination of technological innovation (e.g., cheaper floating platforms, advanced electrolyzer control strategies), hybrid renewable integration (wind + solar), and strong policy support to ensure investment certainty and accelerate learning curves.

Implications and future directions. The findings of this thesis provide actionable insights for different stakeholder groups:

- For policymakers: Centralized offshore electrolysis deserves priority in policy roadmaps with bottom-fixed applications, as it consistently outperforms alternatives under current conditions. However, incentives for floating wind, electrolyzers, and hybrid storage systems are necessary to ensure Mediterranean regions can participate in the hydrogen economy on competitive terms.
- For industry: The design of LSP turbines and turbine–electrolyzer pairings should be guided by site-specific conditions rather than generic benchmarks. Early movers may gain an advantage by developing flexible hybrid systems that combine multiple electrolyzer technologies or integrate hydrogen with battery storage.
- For researchers: The results highlight the importance of time-dependent, high-resolution modeling of system interactions. Future work should incorporate electrolyzer degradation under variable load, hybrid value-based metrics (beyond LCoH and LCoE), and multi-objective optimization that includes environmental and social dimensions alongside cost.

This thesis has shown that the pathway to large-scale offshore hydrogen production is neither linear nor uniform. Technological choices, site-specific wind regimes, infrastructure considerations, and market frameworks all interact in shaping outcomes. While Northern European basins currently enjoy a cost advantage, Mediterranean regions can still emerge as viable players through strategic deployment of LSP floating wind turbines, tailored turbine–electrolyzer configurations, and hybrid storage solutions. The competitiveness of offshore hydrogen will not be determined solely by minimizing costs but by maximizing value through system integration, grid resilience, and alignment with broader decarbonization strategies. By developing a deeper understanding of these complex interactions, this thesis contributes to building the knowledge base required for informed decisions in one of the most critical areas of the energy transition.

7 ACKNOWLEDGMENTS

I would like to express my sincere gratitude to Ansaldo Green Tech for hosting me during my PhD traineeship and for providing a valuable opportunity to gain experience and insights that greatly contributed to this research.

I am also thankful to the Faculty of Technology, Policy and Management at TU Delft for welcoming me during my research period abroad. This work was supported by the Italian National Recovery and Resilience Plan (PNRR), funded by the European Union – Next Generation EU programme.

8 LIST OF PUBLICATIONS

- Travaglini, R.; Superchi, F.; Papi, F.; Bianchini, A., (2026). " Towards offshore hydrogen production via floating wind turbines: a comparative study on main electrolyzer technologies in two Mediterranean case studies", Journal of Cleaner Production, Vol. 544, DOI: https://doi.org/10.1016/j.jclepro.2026.147653;
- Superchi, F.; Travaglini, R.; Bianchini, A., (2026). “Critical issues for the deployment of floating offshore hybrid energy systems comprising wind and solar: a case study analysis for the Mediterranean Sea”, Renewable Energy, Vol. 260, DOI: https://doi.org/10.1016/j.renene.2026.125194;
- Travaglini, R.; Frowijn, L.S.F.; Bianchini, A.; Lukszo, Z.; Bruninx, K., (2025). "Offshore or onshore hydrogen production? A critical analysis on costs and operational considerations for the Dutch North Sea", Applied Energy, Vol. 397, DOI: 10.1016/j.apenergy.2025.126290;
- Travaglini, R.; Papi, F.; Bianchini, A., (2025). "Floating wind farms in sea basins with moderate wind speeds: a critical assessment of the potential of low-specific-power turbines in reducing the LCoE", Renewable and Sustainable Energy Reviews, Vol. 222, DOI: 10.1016/j.rser.2025.115990;
- Travaglini, R.; Superchi, F.; Bianchini, A., (2025). "Mitigating curtailments in offshore wind energy: a comparative analysis of new and second-life battery storage solutions", Journal of Cleaner Production, Vol. 519, DOI: 10.1016/j.jclepro.2025.146055;
- Lanni, F.; Serri, L.; Manzini, G.; Travaglini, R.; Superchi, F.; Bianchini, A., (2025). "Techno-Economic Analysis of Sustainable Hydrogen Production from Offshore Wind Farms: Two Italian Study Cases", Processes, Vol 13(4), DOI: 10.3390/pr13041219;
- Travaglini, R.; Superchi, F.; Lanni, F.; Manzini, G.; Serri, L.; Bianchini, A., (2024). "Towards the development of offshore wind farms in the Mediterranean Sea: A techno-economic analysis including green hydrogen production during curtailments", IET Renewable Power Generation, VOl 18(15), DOI: 10.1049/rpg2.13135;
- Frowijn, L.S.F.; Bruninx, K.; Lukszo, Z.; Travaglini, R., (2024). "Comparative analysis of centralized and decentralized electrolysis in the Dutch North Sea", in Proceedings of ISGTEUROPE, DOI: 10.1109/ISGTEUROPE62998.2024.10863729;
- Travaglini, R.; Superchi, F.; Bianchini, A., (2024). "Design of a Reverse Osmosis Desalination Plant Powered by Renewables for a Small Mediterranean Island", Journal of Physics: Conference Series, DOI: 10.1088/1742-6596/2893/1/012028;
- Travaglini, R.; Melani, P.F.; Balduzzi, F.; Orlando, S.; Viti, V.; Bianchini, A., (2024), "A critical insight into the most effective CFD settings to model atmospheric stability in wind energy applications", Journal of Physics: Conference Series, DOI: 10.1088/1742-6596/2767/9/092031;

- Travaglini, R.; Superchi, F.; Lanni, F.; Manzini, G.; Serri, L.; Bianchini, A.,(2023). "Towards the development of offshore wind farms in the Mediterranean Sea: a techno-economic analysis on an Italian case study", in Proceedings of IET Conference, DOI: 10.1049/icp.2023.1552;

REFERENCES

[1] Petrini, F., Manenti, S., Gkoumas, K., and Bontempi, F., 2010, “Structural Design and Analysis of Offshore Wind Turbines from a System Point of View,” Wind Engineering, **34**(1), pp. 85–107. https://doi.org/10.1260/0309-524X.34.1.85.

[2] Esteban, M. D., Diez, J. J., López, J. S., and Negro, V., 2011, “Why Offshore Wind Energy?,” Renewable Energy, **36**(2), pp. 444–450. https://doi.org/10.1016/j.renene.2010.07.009.

[3] 2024, “Harnessing Offshore Wind While Preserving the Seas.” [Online]. Available: https://www.eea.europa.eu/en/analysis/publications/harnessing-offshore-wind-while-preserving-the-seas. [Accessed: 23-Aug-2025].

[4] WindEurope, 2020, *Offshore Wind in Europe Key Trends and Statistics 2019*. [Online]. Available: https://windeurope.org/wp-content/uploads/files/about-wind/statistics/WindEurope-Annual-Offshore-Statistics-2019.pdf. [Accessed: 28-Nov-2022].

[5] “Offshore Renewable Energy.” [Online]. Available: https://energy.ec.europa.eu/topics/renewable-energy/offshore-renewable-energy_en. [Accessed: 23-Aug-2025].

[6] WindEurope, 2023, “Wind Energy in Europe: 2023 Statistics and the Outlook for 2024-2030,” WindEurope. [Online]. Available: https://windeurope.org/intelligence-platform/product/wind-energy-in-europe-2023-statistics-and-the-outlook-for-2024-2030/. [Accessed: 10-Feb-2025].

[7] 2023, “World Energy Transitions Outlook 2023: 1.5°C Pathway.” [Online]. Available: https://www.irena.org/Publications/2023/Jun/World-Energy-Transitions-Outlook-2023. [Accessed: 11-Apr-2024].

[8] Lemasson, A. J., Somerfield, P. J., Schratzberger, M., McNeill, C. L., Nunes, J., Pascoe, C., Watson, S. C. L., Thompson, M. S. A., Couce, E., and Knights, A. M., 2022, “Evidence for the Effects of Decommissioning Man-Made Structures on Marine Ecosystems Globally: A Systematic Map,” Environmental Evidence, **11**(1), p. 35. https://doi.org/10.1186/s13750-022-00285-9.

[9] Topham, E., Gonzalez, E., McMillan, D., and João, E., 2019, “Challenges of Decommissioning Offshore Wind Farms: Overview of the European Experience,” J. Phys.: Conf. Ser., **1222**(1), p. 012035. https://doi.org/10.1088/1742-6596/1222/1/012035.

[10] Van Maele, T., Desplenter, N., Van Aken, I., and Degraer, S., 2023, *Vision Paper: Decommissioning Offshore Windparks in the Belgian Part of the North Sea | Tethys*. [Online]. Available: https://tethys.pnnl.gov/publications/vision-paper-decommissioning-offshore-windparks-belgian-part-north-sea. [Accessed: 23-Aug-2025].

[11] Bergström, L., Kautsky, L., Malm, T., Rosenberg, R., Wahlberg, M., Åstrand Capetillo, N., and Wilhelmsson, D., 2014, “Effects of Offshore Wind Farms on Marine Wildlife—a Generalized Impact Assessment,” Environ. Res. Lett., **9**(3), p. 034012. https://doi.org/10.1088/1748-9326/9/3/034012.

[12] Gimpel, A., Werner, K. M., Bockelmann, F.-D., Haslob, H., Kloppmann, M., Schaber, M., and Stelzenmüller, V., 2023, “Ecological Effects of Offshore Wind Farms on Atlantic Cod (*Gadus Morhua*) in the Southern North Sea,” Science of The Total Environment, **878**, p. 162902. https://doi.org/10.1016/j.scitotenv.2023.162902.

[13] ACTeon, BEF, European Climate, Infrastructure and Environment Executive Agency (European Commission), Fresh Thoughts, GRID-Arendal, Milieu, WUR, Ruskule, A., Oulès, L., Zamparutti, T., Dworak, T., Lieberknecht, L., Strosser, P., Gea, G., Veidemane, K., and Piet, G., 2021, *Guidelines for Implementing an Ecosystem-Based Approach in Maritime Spatial Planning: Including a Method for the Evaluation, Monitoring and Review of EBA in MSP*, Publications Office of the European Union. [Online]. Available: https://data.europa.eu/doi/10.2926/84261. [Accessed: 23-Aug-2025].

[14] ICES, 2024, *ICES Roadmap for Offshore Renewable Energy (ORE)*, ICES Convention, policies, and strategy. https://doi.org/10.17895/ices.pub.24990198.v2.

[15] "Scotland's Largest Offshore Wind Farm Now Fully Operational." [Online]. Available: https://www.sse.com/news-and-views/2023/10/scotland-s-largest-offshore-wind-farm-now-fully-operational/. [Accessed: 23-Aug-2025].

[16] 2019, *Offshore Wind Outlook 2019*. [Online]. Available: https://www.iea.org/reports/offshore-wind-outlook-2019. [Accessed: 22-Nov-2022].

[17] 2019, *COMMUNICATION FROM THE COMMISSION TO THE EUROPEAN PARLIAMENT, THE EUROPEAN COUNCIL, THE COUNCIL, THE EUROPEAN ECONOMIC AND SOCIAL COMMITTEE AND THE COMMITTEE OF THE REGIONS The European Green Deal*. [Online]. Available: https://eur-lex.europa.eu/legal-content/EN/TXT/?uri=celex:52019DC0640. [Accessed: 23-Aug-2025].

[18] "Wind Energy in Europe: 2024 Statistics and the Outlook for 2025-2030," WindEurope. [Online]. Available: https://windeurope.org/intelligence-platform/product/wind-energy-in-europe-2024-statistics-and-the-outlook-for-2025-2030/. [Accessed: 23-Aug-2025].

[19] 2021, *COMMUNICATION FROM THE COMMISSION TO THE EUROPEAN PARLIAMENT, THE COUNCIL, THE EUROPEAN ECONOMIC AND SOCIAL COMMITTEE AND THE COMMITTEE OF THE REGIONS on a New Approach for a Sustainable Blue Economy in the EU Transforming the EU's Blue Economy for a Sustainable Future*. [Online]. Available: https://eur-lex.europa.eu/legal-content/EN/TXT/?uri=celex:52021DC0240. [Accessed: 23-Aug-2025].

[20] "Technology Deployment," IEA. [Online]. Available: https://www.iea.org/energy-system/renewables/wind. [Accessed: 23-Aug-2025].

[21] Musial, W., Spitsen, P., Duffy, P., Beiter, P., Schields, M., and Mulas, D., *Offshore Wind Market Report: 2023 Edition*. [Online]. Available: https://api.everviz.com/share/U82RgDGdP. [Accessed: 23-Aug-2025].

[22] 2024, *Energy Transition Outlook 2024*, DNV. [Online]. Available: https://www.dnv.com/publications/energy-transition-outlook-2024/. [Accessed: 23-Aug-2025].

[23] Alves Ribeiro, J., Alves Ribeiro, B., Pimenta, F., M.O. Tavares, S., Zhang, J., and Ahmed, F., 2025, "Offshore Wind Turbine Tower Design and Optimization: A Review and AI-Driven Future Directions," Applied Energy, **397**, p. 126294. https://doi.org/10.1016/j.apenergy.2025.126294.

[24] 2024, "Windfloat Atlantic | Offshore Wind Energy," Windfloat Atlantic. [Online]. Available: https://www.windfloat-atlantic.com/. [Accessed: 08-Sep-2025].

[25] Wind Energy Technologies Office, 2024, *Floating Offshore Wind Shot: Progress and Priorities*, U.S. Department of Energy. [Online]. Available: https://www.energy.gov/eere/wind/floating-offshore-wind-shot-progress-and-priorities. [Accessed: 08-Sep-2025].

[26] emincer2, 2024, "1H 2024 Offshore Wind Market Outlook: Course Correct," BloombergNEF. [Online]. Available: https://about.bnef.com/insights/clean-energy/1h-2024-offshore-wind-market-outlook-course-correct/. [Accessed: 08-Sep-2025].

[27] "380 GW of New Offshore Wind Built by 2032," 4c Offshore. [Online]. Available: https://www.4coffshore.com/news/380-gw-of-new-offshore-wind-built-by-2032-nid27990.html. [Accessed: 08-Sep-2025].

[28] Dykes, K., Veers, P., Lantz, E., Holttinen, H., Carlson, O., Tuohy, A., Sempreviva, A. M., Clifton, A., Rodrigo, J. S., Berry, D., Laird, D., Carron, S., Moriarty, P., Marquis, M., Meneveau, C., Peinke, J., Johnson, N., Pao, L., Fleming, P., Bottasso, C. L., Lehtomäki, V., Robertson, A., Muskulus, M., Manwell, J., Tande, J. O. G., Sethuraman, L., Roberts, O., and Fields, J., 2019, "Results of IEA Wind TCP Workshop on a Grand Vision for Wind Energy Technology," 138. [Online]. Available: https://ntnuopen.ntnu.no/ntnu-xmlui/handle/11250/2596867. [Accessed: 08-Sep-2025].

[29] elia group, 2024, *Going Like The Wind by Elia Group - Issuu*. [Online]. Available: https://issuu.com/eliagroup/docs/5387_241015_elia_book_uk_bd_double_page. [Accessed: 17-Feb-2025].

[30] AZ, 2022, "Nederland maakt ambitie wind op zee bekend: 70 gigawatt in 2050 - Nieuwsbericht - Rijksoverheid.nl." [Online]. Available: https://www.rijksoverheid.nl/actueel/nieuws/2022/09/16/nederland-maakt-ambitie-wind-op-zee-bekend-70-gigawatt-in-2050. [Accessed: 19-Jun-2024].

[31] Neumann, F., Zeyen, E., Victoria, M., and Brown, T., 2023, "The Potential Role of a Hydrogen Network in Europe," Joule, **7**(8), pp. 1793–1817. https://doi.org/10.1016/j.joule.2023.06.016.

[32] Gea-Bermúdez, J., Bramstoft, R., Koivisto, M., Kitzing, L., and Ramos, A., 2023, "Going Offshore or Not: Where to Generate Hydrogen in Future Integrated Energy Systems?," Energy Policy, **174**, p. 113382. https://doi.org/10.1016/j.enpol.2022.113382.

[33] Glaum, P., Neumann, F., and Brown, T., 2024, "Offshore Power and Hydrogen Networks for Europe's North Sea," Applied Energy, **369**, p. 123530. https://doi.org/10.1016/j.apenergy.2024.123530.

[34] Capurso, T., Stefanizzi, M., Torresi, M., and Camporeale, S. M., 2022, "Perspective of the Role of Hydrogen in the 21st Century Energy Transition," Energy Conversion and Management, **251**, p. 114898. https://doi.org/10.1016/j.enconman.2021.114898.

[35] Panchenko, V. A., Daus, Yu. V., Kovalev, A. A., Yudaev, I. V., and Litti, Yu. V., 2023, "Prospects for the Production of Green Hydrogen: Review of Countries with High Potential," International Journal of Hydrogen Energy, **48**(12), pp. 4551–4571. https://doi.org/10.1016/j.ijhydene.2022.10.084.

[36] Zhou, Y., Li, R., Lv, Z., Liu, J., Zhou, H., and Xu, C., 2022, "Green Hydrogen: A Promising Way to the Carbon-Free Society," Chinese Journal of Chemical Engineering, **43**, pp. 2–13. https://doi.org/10.1016/j.cjche.2022.02.001.

[37] Schöffer, S. I., Frowijn, L. S. F., and van der Goot, W., 2022, *System Integration GW-Electrolyser: The Road to a 1-GW Electrolyser– Challenges and Opportunities*, Smart Delta Resources. [Online]. Available: https://www.smartdeltaresources.com/sites/default/files/inline-files/System%20integration%20GW%20electroFinal%20presentation.pdf.

[38] Timmers, V., Egea-Àlvarez, A., Gkountaras, A., Li, R., and Xu, L., 2023, "All-DC Offshore Wind Farms: When Are They More Cost-Effective than AC Designs?," IET Renewable Power Generation, **17**(10), pp. 2458–2470. https://doi.org/10.1049/rpg2.12550.

[39] Ibrahim, O. S., Singlitico, A., Proskovics, R., McDonagh, S., Desmond, C., and Murphy, J. D., 2022, "Dedicated Large-Scale Floating Offshore Wind to Hydrogen: Assessing Design

Variables in Proposed Typologies," Renewable and Sustainable Energy Reviews, **160**, p. 112310. https://doi.org/10.1016/J.RSER.2022.112310.

[40] Rogeau, A., Vieubled, J., de Coatpont, M., Affonso Nobrega, P., Erbs, G., and Girard, R., 2023, "Techno-Economic Evaluation and Resource Assessment of Hydrogen Production through Offshore Wind Farms: A European Perspective," Renewable and Sustainable Energy Reviews, **187**, p. 113699. https://doi.org/10.1016/j.rser.2023.113699.

[41] Pedersen, M. M., Forsting, A. M., Laan, P. van der, Riva, R., Romàn, L. A. A., Risco, J. C., Friis-Møller, M., Quick, J., Christiansen, J. P. S., Rodrigues, R. V., Olsen, B. T., and Réthoré, P.-E., 2023, "PyWake 2.5.0: An Open-Source Wind Farm Simulation Tool," DTU. [Online]. Available: https://gitlab.windenergy.dtu.dk/TOPFARM/PyWake.

[42] Superchi, F., Papi, F., Mannelli, A., Balduzzi, F., Ferro, F. M., and Bianchini, A., 2023, "Development of a Reliable Simulation Framework for Techno-Economic Analyses on Green Hydrogen Production from Wind Farms Using Alkaline Electrolyzers," Renewable Energy, **207**, pp. 731–742. https://doi.org/10.1016/j.renene.2023.03.077.

[43] NWP, "Gasunie legt Waterstofnetwerk Nederland aan," Nationaal Waterstof Programma. [Online]. Available: https://www.nationaalwaterstofprogramma.nl/inspiratie/2444173.aspx. [Accessed: 25-Nov-2024].

[44] Komorowska, A., Benalcazar, P., and Kamiński, J., 2023, "Evaluating the Competitiveness and Uncertainty of Offshore Wind-to-Hydrogen Production: A Case Study of Poland," International Journal of Hydrogen Energy, **48**(39), pp. 14577–14590. https://doi.org/10.1016/j.ijhydene.2023.01.015.

[45] Jang, D., Kim, K., Kim, K.-H., and Kang, S., 2022, "Techno-Economic Analysis and Monte Carlo Simulation for Green Hydrogen Production Using Offshore Wind Power Plant," Energy Conversion and Management, **263**, p. 115695. https://doi.org/10.1016/j.enconman.2022.115695.

[46] Dinh, Q. V., Dinh, V. N., Mosadeghi, H., Todesco Pereira, P. H., and Leahy, P. G., 2023, "A Geospatial Method for Estimating the Levelised Cost of Hydrogen Production from Offshore Wind," International Journal of Hydrogen Energy, **48**(40), pp. 15000–15013. https://doi.org/10.1016/j.ijhydene.2023.01.016.

[47] Song, S., Lin, H., Sherman, P., Yang, X., Nielsen, C. P., Chen, X., and McElroy, M. B., 2021, "Production of Hydrogen from Offshore Wind in China and Cost-Competitive Supply to Japan," Nat Commun, **12**(1), p. 6953. https://doi.org/10.1038/s41467-021-27214-7.

[48] Zhuang, W., Pan, G., Gu, W., Zhou, S., Hu, Q., Gu, Z., Wu, Z., Lu, S., and Qiu, H., 2023, "Hydrogen Economy Driven by Offshore Wind in Regional Comprehensive Economic Partnership Members," Energy Environ. Sci., **16**(5), pp. 2014–2029. https://doi.org/10.1039/D2EE02332F.

[49] Egeland-Eriksen, T., and Sartori, S., 2024, "Techno-Economic Analysis of the Effect of a Novel Price-Based Control System on the Hydrogen Production for an Offshore 1.5 GW Wind-Hydrogen System," Energy Reports, **11**, pp. 2633–2655. https://doi.org/10.1016/j.egyr.2024.02.016.

[50] Hill, S. J. P., Bamisile, O., Hatton, L., Staffell, I., and Jansen, M., 2024, "The Cost of Clean Hydrogen from Offshore Wind and Electrolysis," Journal of Cleaner Production, **445**, p. 141162. https://doi.org/10.1016/j.jclepro.2024.141162.

[51] Calado, G., Castro, R., Pires, A. J., and Marques, M. J., 2024, "Assessment of Hydrogen-Based Solutions Associated to Offshore Wind Farms: The Case of the Iberian Peninsula," Renewable and Sustainable Energy Reviews, **192**, p. 114268. https://doi.org/10.1016/j.rser.2023.114268.

[52] Mehta, M., Zaaijer, M., and Terzi, D. V., 2022, “Optimum Turbine Design for Hydrogen Production from Offshore Wind,” Journal of Physics: Conference Series, **2265**(4), p. 042061. https://doi.org/10.1088/1742-6596/2265/4/042061.

[53] Singlitico, A., Østergaard, J., and Chatzivasileiadis, S., 2021, “Onshore, Offshore or in-Turbine Electrolysis? Techno-Economic Overview of Alternative Integration Designs for Green Hydrogen Production into Offshore Wind Power Hubs,” Renewable and Sustainable Energy Transition, **1**, p. 100005. https://doi.org/10.1016/J.RSET.2021.100005.

[54] Rezaei, M., Akimov, A., and Gray, E. M. A., 2024, “Techno-Economics of Offshore Wind-Based Dynamic Hydrogen Production,” Applied Energy, **374**, p. 124030. https://doi.org/10.1016/j.apenergy.2024.124030.

[55] Kojima, H., Nagasawa, K., Todoroki, N., Ito, Y., Matsui, T., and Nakajima, R., 2023, “Influence of Renewable Energy Power Fluctuations on Water Electrolysis for Green Hydrogen Production,” International Journal of Hydrogen Energy, **48**(12), pp. 4572–4593. https://doi.org/10.1016/j.ijhydene.2022.11.018.

[56] Kuhnert, E., Mayer, K., Heidinger, M., Rienessel, C., Hacker, V., and Bodner, M., 2024, “Impact of Intermittent Operation on Photovoltaic-PEM Electrolyzer Systems: A Degradation Study Based on Accelerated Stress Testing,” International Journal of Hydrogen Energy, **55**, pp. 683–695. https://doi.org/10.1016/j.ijhydene.2023.11.249.

[57] Nguyen, E., Olivier, P., Pera, M.-C., Pahon, E., and Roche, R., 2024, “Impacts of Intermittency on Low-Temperature Electrolysis Technologies: A Comprehensive Review,” International Journal of Hydrogen Energy, **70**, pp. 474–492. https://doi.org/10.1016/j.ijhydene.2024.05.217.

[58] Travaglini, R., and Frowijn, L., 2025, “Hydrogen Production Simulation Model.” [Online]. Available: https://github.com/RTrava/H2_prod_sim.

[59] Sohoni, V., Gupta, S. C., and Nema, R. K., 2016, “A Critical Review on Wind Turbine Power Curve Modelling Techniques and Their Applications in Wind Based Energy Systems,” Journal of Energy, **2016**, p. e8519785. https://doi.org/10.1155/2016/8519785.

[60] Travaglini, R., Superchi, F., Lanni, F., Manzini, G., Serri, L., and Bianchini, A., 2024, “Towards the Development of Offshore Wind Farms in the Mediterranean Sea: A Techno-Economic Analysis Including Green Hydrogen Production during Curtailments,” IET Renewable Power Generation, **n/a**(n/a). https://doi.org/10.1049/rpg2.13135.

[61] Katic, I., Højstrup, J., and Jensen, N. O., 1987, “A Simple Model for Cluster Efficiency: European Wind Energy Association Conference and Exhibition,” EWEC’86. Proceedings. Vol. 1, pp. 407–410.

[62] Morten Lybech, T., 2021, “Introduction to Wind Turbine Wake Modelling and Wake Generated Turbulence.” [Online]. Available: https://help.emd.dk/knowledgebase/content/ReferenceManual/Wake_Model.pdf. [Accessed: 19-Apr-2023].

[63] Amores, E., Rodríguez, J., Oviedo, J., and Lucas-Consuegra, A., 2017, “Development of an Operation Strategy for Hydrogen Production Using Solar PV Energy Based on Fluid Dynamic Aspects,” Open Engineering. https://doi.org/10.1515/eng-2017-0020.

[64] Tiktak, J., 2019, “Heat Management of PEM Electrolysis: A Study on the Potential of Excess Heat from Medium- to Large-Scale PEM Electrolysis and the Performance Analysis of a Dedicated Cooling System.” [Online]. Available: https://repository.tudelft.nl/islandora/object/uuid%3Ac046820a-72bc-4f05-b72d-e60a3ecb8c89. [Accessed: 20-Jun-2024].

[65] Tomić, A. Z., Pivac, I., and Barbir, F., 2023, “A Review of Testing Procedures for Proton Exchange Membrane Electrolyzer Degradation,” Journal of Power Sources, **557**, p. 232569. https://doi.org/10.1016/j.jpowsour.2022.232569.

[66] van der Roest, E., Bol, R., Fens, T., and van Wijk, A., 2023, “Utilisation of Waste Heat from PEM Electrolysers – Unlocking Local Optimisation,” International Journal of Hydrogen Energy, **48**(72), pp. 27872–27891. https://doi.org/10.1016/j.ijhydene.2023.03.374.

[67] Travaglini, R., Frowijn, L. S. F., Bianchini, A., Lukszo, Z., and Bruninx, K., 2025, “Offshore or Onshore Hydrogen Production? A Critical Analysis on Costs and Operational Considerations for the Dutch North Sea,” Applied Energy, **397**, p. 126290. https://doi.org/10.1016/j.apenergy.2025.126290.

[68] Cooper, N., Horend, C., Röben, F., Bardow, A., and Shah, N., 2022, “A Framework for the Design & Operation of a Large-Scale Wind-Powered Hydrogen Electrolyzer Hub,” International Journal of Hydrogen Energy, **47**(14), pp. 8671–8686. https://doi.org/10.1016/j.ijhydene.2021.12.225.

[69] Lehmann, J., Wabbes, A., Miguelañez Gonzalez, E., and Scheerlinck, S., 2022, “Levelized Cost of Hydrogen Calculation from Off-Grid Photovoltaic Plants Using Different Methods,” Solar RRL, **6**(5), p. 2100482. https://doi.org/10.1002/solr.202100482.

[70] 2022, “General Information Nederwiek,” Offshorewind RVO. [Online]. Available: https://offshorewind.rvo.nl/cms/view/91063764-5eb7-428e-9c6e-e38fcf3adf22/general-information-nederwiek. [Accessed: 19-Jun-2024].

[71] 2021, “General Information TNW,” Offshorewind RVO. [Online]. Available: https://offshorewind.rvo.nl/cms/view/796048cf-12cb-4e90-8124-ae4eb73c1c49/general-information-tnw. [Accessed: 19-Jun-2024].

[72] Travaglini, R., Superchi, F., and Bianchini, A., 2024, “FEASIBILITY STUDY ON THE USE OF LARGE-SCALE LITHIUM-ION BATTERIES TO PREVENT ENERGY WASTES DUE TO CURTAILMENTS IN OFFSHORE WIND FARMS,” Rhodes, Grece. https://doi.org/10.52202/077185.

[73] “Global Wind Atlas 3.1 Released - DTU Wind and Energy Systems,” https://windenergy.dtu.dk. [Online]. Available: https://windenergy.dtu.dk/english/news/nyhed?id=31117952-71fb-4d24-bbe4-e100487c1709. [Accessed: 19-Apr-2023].

[74] NSWPHP, 2024, “Offshore Energy Hubs: Blueprints with Offshore Electrolysis | North Sea Wind Power Hub.” [Online]. Available: https://northseawindpowerhub.eu/files/media/document/NSWPH_Grid-integrated%20offshore%20Power-to-Gas_Discussion%20paper%20%231.pdf. [Accessed: 17-Feb-2025].

[75] EHB, 2022, *A European Hydrogen Infrastructure Cision Covering 28 Countries*. [Online]. Available: https://www.ehb.eu/files/downloads/ehb-report-220428-17h00-interactive-1.pdf.

[76] Dii, 2024, *Bulk Transport Options for Green Molecules*. [Online]. Available: https://www.solarpaces.org/wp-content/uploads/2024/02/MENA-2024-Dii-Bulk-Transport-Options-for-Green-Molecules.pdf.

[77] DNV, 2023, *Specification of a European Offshore Hydrogen Backbone*. [Online]. Available: https://aquaductus-offshore.de/wp-content/uploads/2023/03/DNV-Study_Specification_of_a_European_Offshore_Hydrogen_Backbone.pdf.

[78] van Uden, J., Ebersbach, N., Reijntjes, J., Ayivor, P., and Campagne, A., 2023, “Pathway 2.0 Techno-Economic Data.” https://doi.org/10.5281/zenodo.10101328.

[79] Gao, Q., Bechlenberg, A., Jayawardhana, B., Ertugrul, N., Vakis, A. I., and Ding, B., 2024, "Techno-Economic Assessment of Offshore Wind and Hybrid Wind–Wave Farms with Energy Storage Systems," Renewable and Sustainable Energy Reviews, **192**, p. 114263. https://doi.org/10.1016/j.rser.2023.114263.
[80] NSWPHP, 2023, *Hydrogen Turbine Electrolysis*. [Online]. Available: https://northseawindpowerhub.eu/files/media/document/424532-N-RP-0001%20-%20Concept%20Screening%20Report%20%28Hydrogen%20Turbine%20Study%29%20Rev%20B.pdf.
[81] Frowijn, L., Bruninx, K., Lukszo, Z., and Travaglini, R., 2024, "Comparative Analysis of Centralized and Decentralized Electrolysis in the Dutch North Sea," *2024 IEEE PES Innovative Smart Grid Technologies Europe (ISGT EUROPE)*, pp. 1–5. https://doi.org/10.1109/ISGTEUROPE62998.2024.10863729.
[82] EC, 2023, "Competitive Bidding - European Commission." [Online]. Available: https://climate.ec.europa.eu/eu-action/eu-funding-climate-action/innovation-fund/competitive-bidding_en. [Accessed: 29-Aug-2024].
[83] TNO, 2024, "Evaluation of the levelised cost of hydrogen based on proposed electrolyser projects in the Netherlands." [Online]. Available: https://publications.tno.nl/publication/34642511/mzKCln/TNO-2024-R10766.pdf. [Accessed: 18-Jul-2024].
[84] Lei, J., Zhang, H., Pan, J., Zhuo, Y., Chen, A., Chen, W., Yang, Z., Feng, K., Li, L., Wang, B., Jiao, L., and Jiao, K., 2024, "Techno-Economic Assessment of a Full-Chain Hydrogen Production by Offshore Wind Power," Energies, **17**(11), p. 2447. https://doi.org/10.3390/en17112447.
[85] NSWPHP, 2022, *Grid-Integrated Offshore Power-to-Gas*. [Online]. Available: https://northseawindpowerhub.eu/files/media/document/NSWPH_Grid-integrated%20offshore%20Power-to-Gas_Discussion%20paper%20%231.pdf.
[86] HyWay 27, 2021, *HyWay 27: Hydrogen Transmission Using the Existing Natural Gas Grid?*, Ministry of Economic Affairs and Climate Policy. [Online]. Available: https://www.hyway27.nl/en/latest-news/hyway-27-realisation-of-a-national-hydrogen-network.
[87] Martin, P., Ocko, I. B., Esquivel-Elizondo, S., Kupers, R., Cebon, D., Baxter, T., and Hamburg, S. P., 2024, "A Review of Challenges with Using the Natural Gas System for Hydrogen," Energy Science & Engineering, **12**(10), pp. 3995–4009. https://doi.org/10.1002/ese3.1861.
[88] NWP, 2021, *Werkplan Nationaal Waterstof Programma 2022-2025*. [Online]. Available: https://www.tweedekamer.nl/downloads/document?id=2021D41104. [Accessed: 28-Apr-2025].
[89] Krishnan, S., Corona, B., Kramer, G. J., Junginger, M., and Koning, V., 2024, "Prospective LCA of Alkaline and PEM Electrolyser Systems," International Journal of Hydrogen Energy, **55**, pp. 26–41. https://doi.org/10.1016/j.ijhydene.2023.10.192.
[90] Correia Martins, F. A., Van Zuijlen, A., and Ferreira, C. S., 2025, "Proof of Concept for Multirotor Systems with Vortex-Generating Modes for Regenerative Wind Energy: A Study Based on Numerical Simulations and Experimental Data," Wind Energ. Sci., **10**, pp. 41–58. https://doi.org/10.5194/wes-10-41-2025.
[91] Stevens, R. J. A. M., Gayme, D. F., and Meneveau, C., 2016, "Effects of Turbine Spacing on the Power Output of Extended Wind-Farms," Wind Energy, **19**(2), pp. 359–370. https://doi.org/10.1002/we.1835.

[92] Barthelmie, R. J., Hansen, K., Frandsen, S. T., Rathmann, O., Schepers, J. G., Schlez, W., Phillips, J., Rados, K., Zervos, A., Politis, E. S., and Chaviaropoulos, P. K., 2009, "Modelling and Measuring Flow and Wind Turbine Wakes in Large Wind Farms Offshore," Wind Energy, **12**(5), pp. 431–444. https://doi.org/10.1002/we.348.
[93] Barthelmie, R. J., Pryor, S. C., Frandsen, S. T., Hansen, K., Schepers, J. G., Rados, K., Schlez, W., Neubert, A., Jensen, L. E., and Necklemann, S., 2010, "Quantifying the Impact of Wind Turbine Wakes on Power Output at Offshore Wind Farms," Journal of Atmospheric and Oceanic Technology, **27**(8), pp. 1302–1317. https://doi.org/10.1175/2010JTECHA1398.1.
[94] Li, Y., Yu, W., Sciacchitano, A., and Ferreira, C., 2024, "Numerical Investigation of Regenerative Wind Farms Featuring Enhanced Vertical Energy Entrainment," Wind Energy Science Discussions, pp. 1–38. https://doi.org/10.5194/wes-2024-124.
[95] Dupont, E., Koppelaar, R., and Jeanmart, H., 2018, "Global Available Wind Energy with Physical and Energy Return on Investment Constraints," Applied Energy, **209**, pp. 322–338. https://doi.org/10.1016/j.apenergy.2017.09.085.
[96] Calaf, M., Meneveau, C., and Meyers, J., 2010, "Large Eddy Simulation Study of Fully Developed Wind-Turbine Array Boundary Layers," Physics of Fluids, **22**(1), p. 015110. https://doi.org/10.1063/1.3291077.
[97] Baas, P., and Verzijlbergh, R., 2022, *The Impact of Wakes from Neighboring Wind Farms on the Production of the IJmuiden Ver Wind Farm Zone - Whiffle*. [Online]. Available: https://whiffle.nl/document/the-impact-of-wakes-from-neighboring-wind-farms-on-the-production-of-the-ijmuiden-ver-wind-farm-zone/. [Accessed: 19-May-2025].
[98] Christiansen, N., 2022, "Regional Impacts of Offshore Wind Farms on the North Sea Hydrodynamics," doctoralThesis, Staats- und Universitätsbibliothek Hamburg Carl von Ossietzky. [Online]. Available: https://ediss.sub.uni-hamburg.de/handle/ediss/10273. [Accessed: 19-May-2025].
[99] Pettas, V., Kretschmer, M., Clifton, A., and Cheng, P. W., 2021, "On the Effects of Inter-Farm Interactions at the Offshore Wind Farm Alpha Ventus," Wind Energy Science, **6**(6), pp. 1455–1472. https://doi.org/10.5194/wes-6-1455-2021.
[100] 2024, "Lack of Grid Capacity Lets Output of Germany's North Sea Offshore Wind Turbines Drop in 2023," Clean Energy Wire. [Online]. Available: https://www.cleanenergywire.org/news/lack-grid-capacity-lets-output-germanys-north-sea-offshore-wind-turbines-drop-2023. [Accessed: 19-May-2025].
[101] Gea-Bermúdez, J., Das, K., Pade, L.-L., Koivisto, M., and Kanellas, P., 2019, *NSON-DK Day-Ahead Market Operation Analysis in the North Sea Region towards 2050*, 978-87-93549-61–6, Technical University of Denmark.
[102] Koivisto, M., Gea-Bermúdez, J., Kanellas, P., Das, K., and Sørensen, P., 2020, "North Sea Region Energy System towards 2050: Integrated Offshore Grid and Sector Coupling Drive Offshore Wind Power Installations," Wind Energy Science, **5**(4), pp. 1705–1712. https://doi.org/10.5194/wes-5-1705-2020.
[103] Swisher, P., Murcia Leon, J. P., Gea-Bermúdez, J., Koivisto, M., Madsen, H. A., and Münster, M., 2022, "Competitiveness of a Low Specific Power, Low Cut-out Wind Speed Wind Turbine in North and Central Europe towards 2050," Applied Energy, **306**, p. 118043. https://doi.org/10.1016/j.apenergy.2021.118043.
[104] Widuto, A., *EU Strategy for Offshore Renewable Energy Sources | Legislative Train Schedule*, European Parliament. [Online]. Available: https://www.europarl.europa.eu/legislative-train/theme-a-european-green-deal/file-offshore-wind. [Accessed: 03-Mar-2025].

[105] Zountouridou, E. I., Kiokes, G. C., Chakalis, S., Georgilakis, P. S., and Hatziargyriou, N. D., 2015, “Offshore Floating Wind Parks in the Deep Waters of Mediterranean Sea,” Renewable and Sustainable Energy Reviews, **51**, pp. 433–448. https://doi.org/10.1016/j.rser.2015.06.027.

[106] Stehly, T., and Duffy, P., 2021, “2020 Cost of Wind Energy Review.” https://doi.org/10.2172/1838135.

[107] Equinor, 2022, *HYWINDSCOTLAND The World’s First Commercial Floating Wind Farm*. [Online]. Available: https://www.equinor.com/energy/hywind-scotland. [Accessed: 26-Sep-2024].

[108] “Projects: Kincardine Offshore Wind Farm - Principle Power, Inc.” [Online]. Available: https://www.principlepower.com/projects/kincardine-offshore-wind-farm. [Accessed: 27-Sep-2024].

[109] Lucas, T. R., Ferreira, A. F., Santos Pereira, R. B., and Alves, M., 2022, “Hydrogen Production from the WindFloat Atlantic Offshore Wind Farm: A Techno-Economic Analysis,” Applied Energy, **310**, p. 118481. https://doi.org/10.1016/j.apenergy.2021.118481.

[110] Otter, A., Murphy, J., Pakrashi, V., Robertson, A., and Desmond, C., 2022, “A Review of Modelling Techniques for Floating Offshore Wind Turbines,” Wind Energy, **25**(5), pp. 831–857. https://doi.org/10.1002/we.2701.

[111] IRENA, 2019, *FUTURE OF WIND. Deployment, Investment, Technology, Grid Integration and Socio-Economic Aspects*. [Online]. Available: https://www.irena.org/-/media/files/irena/agency/publication/2019/oct/irena_future_of_wind_2019.pdf. [Accessed: 05-Feb-2025].

[112] Santhakumar, S., Heuberger-Austin, C., Meerman, H., and Faaij, A., 2023, “Technological Learning Potential of Offshore Wind Technology and Underlying Cost Drivers,” Sustainable Energy Technologies and Assessments, **60**, p. 103545. https://doi.org/10.1016/j.seta.2023.103545.

[113] Bento, N., and Fontes, M., 2019, “Emergence of Floating Offshore Wind Energy: Technology and Industry,” Renewable and Sustainable Energy Reviews, **99**, pp. 66–82. https://doi.org/10.1016/j.rser.2018.09.035.

[114] Shields, M., Beiter, P., and Nunemaker, J., 2022, *A Systematic Framework for Projecting the Future Cost of Offshore Wind Energy*, NREL/TP-5000-81819, National Renewable Energy Laboratory (NREL), Golden, CO (United States). https://doi.org/10.2172/1902302.

[115] DNV, 2024, *Floating Offshore Wind: The next Five Years*. [Online]. Available: https://www.dnv.com/focus-areas/floating-offshore-wind/commercialize-floating-wind-report/. [Accessed: 05-Feb-2025].

[116] Pao, L. Y., Pusch, M., and Zalkind, D. S., 2024, “Control Co-Design of Wind Turbines,” Annual Review of Control, Robotics, and Autonomous Systems, **7**(Volume 7, 2024), pp. 201–226. https://doi.org/10.1146/annurev-control-061423-101708.

[117] Abbas, N. J., Jasa, J., Zalkind, D. S., Wright, A., and Pao, L., 2024, “Control Co-Design of a Floating Offshore Wind Turbine,” Applied Energy, **353**, p. 122036. https://doi.org/10.1016/j.apenergy.2023.122036.

[118] Mehta, M., Zaaijer, M., and von Terzi, D., 2024, “Drivers for Optimum Sizing of Wind Turbines for Offshore Wind Farms,” Wind Energy Science, **9**(1), pp. 141–163. https://doi.org/10.5194/wes-9-141-2024.

[119] Serafeim, G., Manolas, D., Riziotis, V., and Chaviaropoulos, P., 2022, “Multidisciplinary Aeroelastic Optimization of a 10MW-Scale Wind Turbine Rotor Targeting to Reduced LCoE,” J. Phys.: Conf. Ser., **2265**(4), p. 042051. https://doi.org/10.1088/1742-6596/2265/4/042051.

[120] Zalkind, D. S., Ananda, G. K., Chetan, M., Martin, D. P., Bay, C. J., Johnson, K. E., Loth, E., Griffith, D. T., Selig, M. S., and Pao, L. Y., 2019, "System-Level Design Studies for Large Rotors," Wind Energy Science, **4**(4), pp. 595–618. https://doi.org/10.5194/wes-4-595-2019.

[121] Buck, J. A., and Garvey, S. D., 2015, "Redefining the Design Objectives of Large Offshore Wind Turbine Rotors," Wind Energy, **18**(5), pp. 835–850. https://doi.org/10.1002/we.1733.

[122] Dykes, K., Ning, A., King, R., Graf, P., Scott, G., and Veers, P., 2014, *Sensitivity Analysis of Wind Plant Performance to Key Turbine Design Parameters: A Systems Engineering Approach; Preprint*, NREL/CP-5000-60920, National Renewable Energy Lab. (NREL), Golden, CO (United States). https://doi.org/10.2514/6.2014-1087.

[123] Shields, M., Beiter, P., Nunemaker, J., Cooperman, A., and Duffy, P., 2021, "Impacts of Turbine and Plant Upsizing on the Levelized Cost of Energy for Offshore Wind," Applied Energy, **298**, p. 117189. https://doi.org/10.1016/j.apenergy.2021.117189.

[124] Ashuri, T., Zaaijer, M. B., Martins, J. R. R. A., and Zhang, J., 2016, "Multidisciplinary Design Optimization of Large Wind Turbines—Technical, Economic, and Design Challenges," Energy Conversion and Management, **123**, pp. 56–70. https://doi.org/10.1016/j.enconman.2016.06.004.

[125] Fingersh, L., Hand, M., and Laxson, A., 2006, *Wind Turbine Design Cost and Scaling Model*, NREL/TP-500-40566, National Renewable Energy Lab. (NREL), Golden, CO (United States). https://doi.org/10.2172/897434.

[126] Sieros, G., Chaviaropoulos, P., Sørensen, J. D., Bulder, B. H., and Jamieson, P., 2012, "Upscaling Wind Turbines: Theoretical and Practical Aspects and Their Impact on the Cost of Energy," Wind Energy, **15**(1), pp. 3–17. https://doi.org/10.1002/we.527.

[127] Canet, H., Guilloré, A., and Bottasso, C. L., 2023, "The Eco-Conscious Wind Turbine: Design beyond Purely Economic Metrics," Wind Energy Science, **8**(6), pp. 1029–1047. https://doi.org/10.5194/wes-8-1029-2023.

[128] Travaglini, R., Superchi, F., Lanni, F., Manzini, G., Serri, L., and Bianchini, A., 2024, "Towards the Development of Offshore Wind Farms in the Mediterranean Sea: A Techno-Economic Analysis Including Green Hydrogen Production during Curtailments," IET Renewable Power Generation, **n/a**(n/a). https://doi.org/10.1049/rpg2.13135.

[129] Mahfouz, M. Y., Lozon, E., Hall, M., and Cheng, P. W., 2024, "Integrated Floating Wind Farm Layout Design and Mooring System Optimization to Increase Annual Energy Production," J. Phys.: Conf. Ser., **2767**(6), p. 062020. https://doi.org/10.1088/1742-6596/2767/6/062020.

[130] Yilmazlar, K., Cacciola, S., Xiolesmy Alfonso Rodriguez, M., and Croce, A., 2022, "Development of Engineering Cost Models for Integrated Design Optimization of Onshore and Offshore Wind Farms," J. Phys.: Conf. Ser., **2265**(4), p. 042042. https://doi.org/10.1088/1742-6596/2265/4/042042.

[131] 2025, "NREL/Floris." [Online]. Available: https://github.com/NREL/floris. [Accessed: 19-May-2025].

[132] Hietanen, A. I., Snedker, T. H., Dykes, K., and Bayati, I., 2024, "A Novel Techno-Economical Layout Optimization Tool for Floating Wind Farm Design," Wind Energy Science, **9**(2), pp. 417–438. https://doi.org/10.5194/wes-9-417-2024.

[133] Cazzaro, D., and Pisinger, D., 2022, "Variable Neighborhood Search for Large Offshore Wind Farm Layout Optimization," Computers & Operations Research, **138**, p. 105588. https://doi.org/10.1016/j.cor.2021.105588.

[134] Cao, L., Ge, M., Gao, X., Du, B., Li, B., Huang, Z., and Liu, Y., 2022, "Wind Farm Layout Optimization to Minimize the Wake Induced Turbulence Effect on Wind Turbines," Applied Energy, **323**, p. 119599. https://doi.org/10.1016/j.apenergy.2022.119599.

[135] Thomas, J. J., Baker, N. F., Malisani, P., Quaeghebeur, E., Sanchez Perez-Moreno, S., Jasa, J., Bay, C., Tilli, F., Bieniek, D., Robinson, N., Stanley, A. P. J., Holt, W., and Ning, A., 2023, "A Comparison of Eight Optimization Methods Applied to a Wind Farm Layout Optimization Problem," Wind Energy Science, **8**(5), pp. 865–891. https://doi.org/10.5194/wes-8-865-2023.

[136] Lei, Z., Gao, S., Wang, Y., Yu, Y., and Guo, L., 2022, "An Adaptive Replacement Strategy-Incorporated Particle Swarm Optimizer for Wind Farm Layout Optimization," Energy Conversion and Management, **269**, p. 116174. https://doi.org/10.1016/j.enconman.2022.116174.

[137] Yang, Q., Li, H., Li, T., and Zhou, X., 2021, "Wind Farm Layout Optimization for Levelized Cost of Energy Minimization with Combined Analytical Wake Model and Hybrid Optimization Strategy," Energy Conversion and Management, **248**, p. 114778. https://doi.org/10.1016/j.enconman.2021.114778.

[138] Martinez, A., and Iglesias, G., 2021, "Multi-Parameter Analysis and Mapping of the Levelised Cost of Energy from Floating Offshore Wind in the Mediterranean Sea," Energy Conversion and Management, **243**, p. 114416. https://doi.org/10.1016/j.enconman.2021.114416.

[139] Ghigo, A., Cottura, L., Caradonna, R., Bracco, G., and Mattiazzo, G., 2020, "Platform Optimization and Cost Analysis in a Floating Offshore Wind Farm," Journal of Marine Science and Engineering., **8**(11), p. 835. https://doi.org/10.3390/jmse8110835.

[140] Lerch, M., De-Prada-Gil, M., Molins, C., and Benveniste, G., 2018, "Sensitivity Analysis on the Levelized Cost of Energy for Floating Offshore Wind Farms," Sustainable Energy Technologies and Assessments, **30**, pp. 77–90. https://doi.org/10.1016/j.seta.2018.09.005.

[141] Lanni, F., Serri, L., Manzini, G., Travaglini, R., Superchi, F., and Bianchini, A., 2025, "Techno-Economic Analysis of Sustainable Hydrogen Production from Offshore Wind Farms: Two Italian Study Cases," Processes, **13**(4), p. 1219. https://doi.org/10.3390/pr13041219.

[142] Jørgensen, B. H., Madsen, P. H., Giebel, G., Martí, I., and Thomsen, K., 2021, *DTU International Energy Report 2021: Perspectives on Wind Energy*, DTU Wind Energy. https://doi.org/10.11581/DTU.00000200.

[143] IRENA, 2024, *Renewable Power Generation Costs in 2023*. [Online]. Available: https://www.irena.org/Publications/2024/Sep/Renewable-Power-Generation-Costs-in-2023. [Accessed: 13-Jan-2025].

[144] IEA Wind, 2020, *IEA Wind TCP Task 37, Definition of the IEA Wind 15-Megawatt Offshore Reference Wind Turbine*. [Online]. Available: https://www.nrel.gov/docs/fy20osti/75698.pdf. [Accessed: 20-Jun-2024].

[145] Zahle, F., Barlas, A., Lønbæk, K., Bortolotti, P., Zalkind, D., Wang, L., Labuschagne, C., Sethuraman, L., and Barter, G., 2024, *Definition of the IEA Wind 22-Megawatt Offshore Reference Wind Turbine*, Technical University of Denmark. https://doi.org/10.11581/DTU.00000317.

[146] Hasager, C. B., Hahmann, A. N., Ahsbahs, T., Karagali, I., Sile, T., Badger, M., and Mann, J., 2020, "Europe's Offshore Winds Assessed with Synthetic Aperture Radar, ASCAT and WRF," Wind Energy Science, **5**(1), pp. 375–390. https://doi.org/10.5194/wes-5-375-2020.

[147] Chirosca, A.-M., and Rusu, L., 2022, "Characteristics of the Wind and Wave Climate along the European Seas Focusing on the Main Maritime Routes," Journal of Marine Science and Engineering, **10**(1), p. 75. https://doi.org/10.3390/jmse10010075.

[148] "Developing the next Generation of Environmentally-Friendly Floating Wind Farms," Floatfarm. [Online]. Available: https://floatfarm-project.eu/. [Accessed: 03-Mar-2025].

[149] Serri, L., Airoldi, D., Lanni, F., Naldi, R., Castorrini, A., Rispoli, F., Soukissian, T., Castro Santos, L., Le Boulluec, M., and Maisondieu, C., 2024, “Technical and Economic Challenges for Floating Offshore Wind Deployment in Italy and in the Mediterranean Sea,” WIREs Energy and Environment, **13**(4), p. e533. https://doi.org/10.1002/wene.533.

[150] Elliott, D., Bell, K. R. W., Finney, S. J., Adapa, R., Brozio, C., Yu, J., and Hussain, K., 2016, “A Comparison of AC and HVDC Options for the Connection of Offshore Wind Generation in Great Britain,” IEEE Transactions on Power Delivery, **31**(2), pp. 798–809. https://doi.org/10.1109/TPWRD.2015.2453233.

[151] Hersbach, H., Bell, B., Berrisford, P., Hirahara, S., Horányi, A., Muñoz-Sabater, J., Nicolas, J., Peubey, C., Radu, R., Schepers, D., Simmons, A., Soci, C., Abdalla, S., Abellan, X., Balsamo, G., Bechtold, P., Biavati, G., Bidlot, J., Bonavita, M., Chiara, G., Dahlgren, P., Dee, D., Diamantakis, M., Dragani, R., Flemming, J., Forbes, R., Fuentes, M., Geer, A., Haimberger, L., Healy, S., Hogan, R. J., Hólm, E., Janisková, M., Keeley, S., Laloyaux, P., Lopez, P., Lupu, C., Radnoti, G., Rosnay, P., Rozum, I., Vamborg, F., Villaume, S., and Thépaut, J., 2020, “The ERA5 Global Reanalysis,” Q.J.R. Meteorol. Soc., **146**(730), pp. 1999–2049. https://doi.org/10.1002/qj.3803.

[152] Yan, B. W., Li, Q. S., Chan, P. W., He, Y. C., and Shu, Z. R., 2022, “Characterising Wind Shear Exponents in the Offshore Area Using Lidar Measurements,” Applied Ocean Research, **127**, p. 103293. https://doi.org/10.1016/j.apor.2022.103293.

[153] International Electrochemical commission, “IEC 61400-1:2019 Wind Energy Generation Systems - Part 1: Design Requirements.” [Online]. Available: https://webstore.iec.ch/en/publication/26423. [Accessed: 14-Feb-2025].

[154] 2022, “General Information Nederwiek,” Offshorewind RVO. [Online]. Available: https://offshorewind.rvo.nl/cms/view/91063764-5eb7-428e-9c6e-e38fcf3adf22/general-information-nederwiek. [Accessed: 19-Jun-2024].

[155] Davis, N. N., Badger, J., Hahmann, A. N., Hansen, B. O., Mortensen, N. G., Kelly, M., Larsén, X. G., Olsen, B. T., Floors, R., Lizcano, G., Casso, P., Lacave, O., Bosch, A., Bauwens, I., Knight, O. J., Loon, A. P. van, Fox, R., Parvanyan, T., Hansen, S. B. K., Heathfield, D., Onninen, M., and Drummond, R., 2023, “The Global Wind Atlas: A High-Resolution Dataset of Climatologies and Associated Web-Based Application.” https://doi.org/10.1175/BAMS-D-21-0075.1.

[156] “Les Éoliennes Flottantes Du Golfe Du Lion - Principle Power, Inc.” [Online]. Available: https://www.principlepower.com/projects/les-eoliennes-flottantes-du-golfe-du-lion. [Accessed: 05-Dec-2024].

[157] Renexia, 2023, “MED WIND An Innovative Floating Offshore Wind Farm in the Heart of the Mediterranean.” [Online]. Available: https://renexia.it/en/med-wind-projects/. [Accessed: 18-Nov-2024].

[158] Severini, L., 2020, *Parco Eolico Flottante Nel Mare Di Sardegna Sud Coccidentale*. [Online]. Available: https://va.mite.gov.it/it-IT/Oggetti/Info/7505. [Accessed: 27-Nov-2022].

[159] Dagher, J. H., Goupee, A. J., and Viselli, A. M., 2024, “Optimized Floating Offshore Wind Turbine Substructure Design Trends for 10–30 MW Turbines in Low-, Medium-, and High-Severity Wave Environments,” Designs, **8**(4), p. 72. https://doi.org/10.3390/designs8040072.

[160] “User Guide — TOPFARM 2.4.0.Post1 Documentation.” [Online]. Available: https://topfarm.pages.windenergy.dtu.dk/TopFarm2/user_guide.html#dtu-cost-model. [Accessed: 26-Nov-2024].

[161] “IEA-15-240-RWT/OpenFAST/IEA-15-240-RWT/Cp_Ct_Cq.IEA15MW.Txt at Master · IEAWindTask37/IEA-15-240-RWT,” GitHub. [Online]. Available: https://github.com/IEAWindTask37/IEA-15-240-RWT/blob/master/OpenFAST/IEA-15-240-RWT/Cp_Ct_Cq.IEA15MW.txt. [Accessed: 16-Jan-2025].

[162] Saint-Drenan, Y.-M., Besseau, R., Jansen, M., Staffell, I., Troccoli, A., Dubus, L., Schmidt, J., Gruber, K., Simões, S. G., and Heier, S., 2020, “A Parametric Model for Wind Turbine Power Curves Incorporating Environmental Conditions,” Renewable Energy, **157**, pp. 754–768. https://doi.org/10.1016/j.renene.2020.04.123.

[163] Sim, S.-K., Peinke, J., and Maass, P., 2023, “Signatures of Geostrophic Turbulence in Power Spectra and Third-Order-Structure Function of Offshore Wind Speed Fluctuation.” https://doi.org/10.48550/arXiv.2203.07685.

[164] Lerch, M., 2019, *Qualification of Innovative Floating Substructures for 10MW Wind Turbines and Water Depths Greater than 50m. | LIFES 50plus Project | Fact Sheet | H2020 | CORDIS | European Commission*. [Online]. Available: https://cordis.europa.eu/project/id/640741. [Accessed: 28-Nov-2022].

[165] Mahfouz, M. Y., Salari, M., Hernández, S., Molins, C., Trubat, P., Bredmose, H., and Pegalajar-Jurado, A., 2020, *Public Design and FAST Models of the Two 15MW Floater-Turbine Concepts*, USTUTT/UPC/COBRA/ESTYCO/DTU. [Online]. Available: https://corewind.eu/wp-content/uploads/files/publications/COREWIND-public-design-and-FAST-models-of-the-two-15mw-floater-turbine-concepts.pdf. [Accessed: 26-Sep-2024].

[166] IEA, 2020, “Turbine-Models/Offshore/IEA_15MW_240_RWT.Csv at Master · NREL/Turbine-Models,” GitHub. [Online]. Available: https://github.com/NREL/turbine-models/blob/master/Offshore/IEA_15MW_240_RWT.csv. [Accessed: 17-Feb-2024].

[167] NREL, 2024, “IEAWindTask37/IEA-22-280-RWT.” [Online]. Available: https://github.com/IEAWindTask37/IEA-22-280-RWT. [Accessed: 26-Nov-2024].

[168] Papi, F., and Bianchini, A., 2022, “Technical Challenges in Floating Offshore Wind Turbine Upscaling: A Critical Analysis Based on the NREL 5 MW and IEA 15 MW Reference Turbines,” Renewable and Sustainable Energy Reviews, **162**, p. 112489. https://doi.org/10.1016/j.rser.2022.112489.

[169] Robertson, A. N., and Jonkman, J. M., 2011, *Loads Analysis of Several Offshore Floating Wind Turbine Concepts*, NREL/CP-5000-50539, National Renewable Energy Lab. (NREL), Golden, CO (United States). [Online]. Available: https://www.osti.gov/biblio/1029026. [Accessed: 17-Jan-2025].

[170] Wu, J., and Kim, M.-H., 2021, “Generic Upscaling Methodology of a Floating Offshore Wind Turbine,” Energies, **14**(24), p. 8490. https://doi.org/10.3390/en14248490.

[171] Roach, K. L., Lackner, M. A., and Manwell, J. F., 2023, “A New Methodology for Upscaling Semi-Submersible Platforms for Floating Offshore Wind Turbines,” Wind Energy Science, **8**(12), pp. 1873–1891. https://doi.org/10.5194/wes-8-1873-2023.

[172] Sergiienko, N. Y., da Silva, L. S. P., Bachynski-Polić, E. E., Cazzolato, B. S., Arjomandi, M., and Ding, B., 2022, “Review of Scaling Laws Applied to Floating Offshore Wind Turbines,” Renewable and Sustainable Energy Reviews, **162**, p. 112477. https://doi.org/10.1016/j.rser.2022.112477.

[173] Liu, Y., Zhang, J.-M., Min, Y.-T., Yu, Y., Lin, C., and Hu, Z.-Z., 2023, “A Digital Twin-Based Framework for Simulation and Monitoring Analysis of Floating Wind Turbine Structures,” Ocean Engineering, **283**, p. 115009. https://doi.org/10.1016/j.oceaneng.2023.115009.

[174] Gaidai, O., Yakimov, V., Wang, F., Zhang, F., and Balakrishna, R., 2023, “Floating Wind Turbines Structural Details Fatigue Life Assessment,” Sci Rep, **13**(1), p. 16312. https://doi.org/10.1038/s41598-023-43554-4.

[175] DNV, *DNV-RP-0286 Coupled Analysis of Floating Wind Turbines*. [Online]. Available: https://www.dnv.com/energy/standards-guidelines/dnv-rp-0286-coupled-analysis-of-floating-wind-turbines/. [Accessed: 28-Nov-2024].

[176] American Bureau of Shipping, *GUIDE FOR BUILDING AND CLASSING, FLOATING OFFSHORE WIND TURBINE INSTALLATIONS*. [Online]. Available: https://ww2.eagle.org/content/dam/eagle/rules-and-guides/archives/offshore/195_floatingoffshorewindturbineinstallations/FOWTI_Guide_e-July14.pdf. [Accessed: 28-Nov-2024].
[177] Zalkind, D., and Bortolotti, P., 2024, “Control Co-Design Studies for a 22 MW Semisubmersible Floating Wind Turbine Platform,” J. Phys.: Conf. Ser., **2767**(8), p. 082020. https://doi.org/10.1088/1742-6596/2767/8/082020.
[178] “Release Fix Nacelle Mass Properties · IEAWindSystems/IEA-15-240-RWT,” GitHub. [Online]. Available: https://github.com/IEAWindSystems/IEA-15-240-RWT/releases/tag/v1.1.11. [Accessed: 05-Mar-2025].
[179] “Release v1.0.1 · IEAWindSystems/IEA-22-280-RWT,” GitHub. [Online]. Available: https://github.com/IEAWindSystems/IEA-22-280-RWT/releases/tag/v1.0.1. [Accessed: 05-Mar-2025].
[180] Maness, M., Smith, A., and Maples, B., 2017, *NREL Offshore Balance-of-System Model*. [Online]. Available: https://research-hub.nrel.gov/en/publications/nrel-offshore-balance-of-system-model. [Accessed: 05-Mar-2025].
[181] Major, D., and Schmitz, S., 2024, “The Optimum Range of Design Axial Induction Factors for Lowest Levelized-Cost of Energy,” Wind Energy Science Discussions, pp. 1–47. https://doi.org/10.5194/wes-2024-109.
[182] Mehta, M., 2023, “Turbine Sizing for Electricity and Hydrogen Production.” https://doi.org/10.5281/zenodo.8380355.
[183] “Welcome to TOPFARM — TOPFARM 2.3.4 Documentation.” [Online]. Available: https://topfarm.pages.windenergy.dtu.dk/TopFarm2/index.html. [Accessed: 19-Jun-2024].
[184] “Welcome to PyWake — PyWake 2.6.3.Dev3+gd6ee25a Documentation.” [Online]. Available: https://topfarm.pages.windenergy.dtu.dk/PyWake/index.html. [Accessed: 19-Jun-2024].
[185] Lundtang Petersen, E., Troen, I., Ejsing Jørgensen, H., and Mann, J., 2014, “The New European Wind Atlas,” Energy Bulletin, (17), pp. 34–39.
[186] “IEC TS 61400-3-2:2019 | IEC Webstore.” [Online]. Available: https://webstore.iec.ch/publication/29244. [Accessed: 03-Jan-2023].
[187] Bastankhah, M., and Porté-Agel, F., 2014, “A New Analytical Model for Wind-Turbine Wakes,” Renewable Energy, **70**, pp. 116–123. https://doi.org/10.1016/j.renene.2014.01.002.
[188] Porté-Agel, F., Bastankhah, M., and Shamsoddin, S., 2020, “Wind-Turbine and Wind-Farm Flows: A Review,” Boundary-Layer Meteorol, **174**(1), pp. 1–59. https://doi.org/10.1007/s10546-019-00473-0.
[189] Katic, I., Højstrup, J., and Jensen, N. O., 1987, “A Simple Model for Cluster Efficiency,” EWEC’86. Proceedings. Vol. 1, pp. 407–410.
[190] “Superposition Models — PyWake 2.6.8.Dev26+g5562afda Documentation.” [Online]. Available: https://topfarm.pages.windenergy.dtu.dk/PyWake/notebooks/SuperpositionModels.html#LinearSum. [Accessed: 10-Feb-2025].
[191] “Rotor Average Models — PyWake Documentation.” [Online]. Available: https://topfarm.pages.windenergy.dtu.dk/PyWake/notebooks/RotorAverageModels.html. [Accessed: 10-Feb-2025].
[192] Pierik, J. T. G., Dekker, J. W. M., Braam, H., Bulder, B. H., Winkelaar, D., Larsen, G. Chr., Morfiadakis, E., Chaviaropoulos, P., Derrick, A., and Molly, J. P., 1999, “European Wind

Turbine Standards II (EWTS-II): 1999 European Wind Energy Conference and Exhibition," Wind energy for the next millennium. Proceedings, pp. 568–571.

[193] Réthoré, P.-E., Fuglsang, P., Larsen, T. J., Buhl, T., and Larsen, G. Chr., 2011, *TOPFARM Wind Farm Optimization Tool*, Risø National Laboratory for Sustainable Energy, Technical University of Denmark.

[194] 2024, "TOPFARM / EDWIN · GitLab," GitLab. [Online]. Available: https://gitlab.windenergy.dtu.dk/TOPFARM/edwin. [Accessed: 06-Feb-2025].

[195] Alencar, M. S. de, 2025, "Mdealencar/Interarray." [Online]. Available: https://github.com/mdealencar/interarray. [Accessed: 06-Feb-2025].

[196] "OpenMDAO," GitHub. [Online]. Available: https://github.com/OpenMDAO. [Accessed: 04-Dec-2024].

[197] Kheirabadi, A. C., and Nagamune, R., 2020, "Real-Time Relocation of Floating Offshore Wind Turbine Platforms for Wind Farm Efficiency Maximization: An Assessment of Feasibility and Steady-State Potential," Ocean Engineering, **208**, p. 107445. https://doi.org/10.1016/j.oceaneng.2020.107445.

[198] Froese, G., Ku, S. Y., Kheirabadi, A. C., and Nagamune, R., 2022, "Optimal Layout Design of Floating Offshore Wind Farms," Renewable Energy, **190**, pp. 94–102. https://doi.org/10.1016/j.renene.2022.03.104.

[199] Rodrigues, S. F., Teixeira Pinto, R., Soleimanzadeh, M., Bosman, P. A. N., and Bauer, P., 2015, "Wake Losses Optimization of Offshore Wind Farms with Moveable Floating Wind Turbines," Energy Conversion and Management, **89**, pp. 933–941. https://doi.org/10.1016/j.enconman.2014.11.005.

[200] *B.3 Mooring System | Guide to a Floating Offshore Wind Farm*. [Online]. Available: https://guidetofloatingoffshorewind.com/guide/b-balance-of-plant/b-3-mooring-system/. [Accessed: 04-Dec-2024].

[201] Allen, C., Viscelli, A., Dagher, H., Goupee, A., Gaertner, E., Abbas, N., Hall, M., and Barter, G., 2020, *Definition of the UMaine VolturnUS-S Reference Platform Developed for the IEA Wind 15-Megawatt Offshore Reference Wind Turbine*, NREL/TP-5000-76773, National Renewable Energy Lab. (NREL), Golden, CO (United States); Univ. of Maine, Orono, ME (United States). https://doi.org/10.2172/1660012.

[202] ESG, 2024, "ESG - Ecology Weighs Most Heavily in Offshore Wind Tenders," ABN AMRO Bank. [Online]. Available: https://www.abnamro.com/research/en/our-research/esg-economist-ecology-weighs-most-heavily-in-offshore-wind-tenders. [Accessed: 06-Mar-2025].

[203] ERM, 2024, "Offshore Wind Tenders: How Developers Can Gain the Edge with Circularity," ERM. [Online]. Available: https://www.erm.com/insights/offshore-wind-tenders-how-developers-can-gain-the-edge-with-circularity/. [Accessed: 06-Mar-2025].

[204] "What Is the Carbon Footprint of Steel?," Sustainable Ships. [Online]. Available: https://www.sustainable-ships.org/stories/2022/carbon-footprint-steel. [Accessed: 04-Mar-2025].

[205] "CO2 Emissions per kWh in Italy - Nowtricity." [Online]. Available: https://www.nowtricity.com/country/italy/. [Accessed: 21-Jan-2025].

[206] "CO2 Emissions per kWh in France - Nowtricity." [Online]. Available: https://www.nowtricity.com/country/france/. [Accessed: 22-Jan-2025].

[207] "Nowtricity." [Online]. Available: https://www.nowtricity.com/. [Accessed: 19-Feb-2025].

[208] Ribnitzky, D., Berger, F., Petrović, V., and Kühn, M., 2024, "Hybrid-Lambda: A Low-Specific-Rating Rotor Concept for Offshore Wind Turbines," Wind Energy Science, **9**(2), pp. 359–383. https://doi.org/10.5194/wes-9-359-2024.

[209] Simpson, J., Loth, E., and Dykes, K., 2020, "Cost of Valued Energy for Design of Renewable Energy Systems," Renewable Energy, **153**, pp. 290–300. https://doi.org/10.1016/j.renene.2020.01.131.

[210] Superchi, F., Mustakis, A., Pechlivanoglou, G., and Bianchini, A., 2023, "Application of the Cost Of Valued Energy (COVE) to a RES-Based Hybrid Energy System on a Mediterranean Island to Evaluate the Potential of Energy Storage Systems," IET Conference Proceedings, **2023**(7), pp. 178–185. https://doi.org/10.1049/icp.2023.1568.

[211] Castro-Santos, L., Filgueira-Vizoso, A., Carral-Couce, L., and Formoso, J. Á. F., 2016, "Economic Feasibility of Floating Offshore Wind Farms," Energy, **112**, pp. 868–882. https://doi.org/10.1016/j.energy.2016.06.135.

[212] European Parliament, 2020, *Offshore Wind Energy in Europe | Think Tank | European Parliament*. [Online]. Available: https://www.europarl.europa.eu/thinktank/en/document/EPRS_BRI(2020)659313. [Accessed: 08-May-2025].

[213] Terna, 2022, "Documento di Descrizione degli Scenari 2022." [Online]. Available: https://www.terna.it/it/sistema-elettrico/rete/piano-sviluppo-rete/scenari. [Accessed: 19-Apr-2023].

[214] Rehman, S., Menesy, A. S., Zayed, M. E., Zaery, M., Al-Shaikhi, A., Mohandes, M. A., Irshad, K., Kassas, M., and Abido, M. A., 2025, "Synergistic Sizing and Energy Management Strategy of Combined Offshore Wind with Solar Floating PV System for Green Hydrogen and Electricity Co-Production Using Multi-Objective Dung Beetle Optimization," Results in Engineering, **25**, p. 104399. https://doi.org/10.1016/j.rineng.2025.104399.

[215] Superchi, F., Moustakis, A., Pechlivanoglou, G., and Bianchini, A., 2025, "On the Importance of Degradation Modeling for the Robust Design of Hybrid Energy Systems Including Renewables and Storage," Applied Energy, **377**, p. 124645. https://doi.org/10.1016/j.apenergy.2024.124645.

[216] Rehman, S., Kotb, K. M., Zayed, M. E., Menesy, A. S., Irshad, K., Alzahrani, A. S., and Mohandes, M. A., 2024, "Techno-Economic Evaluation and Improved Sizing Optimization of Green Hydrogen Production and Storage under Higher Wind Penetration in Aqaba Gulf," Journal of Energy Storage, **99**, p. 113368. https://doi.org/10.1016/j.est.2024.113368.

[217] Superchi, F., Bianchini, A., Moustakis, A., and Pechlivanoglou, G., 2025, "Towards Sustainable Energy Independence: A Case Study of Green Hydrogen as Seasonal Storage Integration in a Small Island," Renewable Energy, **245**, p. 122813. https://doi.org/10.1016/j.renene.2025.122813.

[218] Superchi, F., Mati, A., Pasqui, M., Carcasci, C., and Bianchini, A., 2022, "Techno-Economic Study on Green Hydrogen Production and Use in Hard-to-Abate Industrial Sectors," J. Phys.: Conf. Ser., **2385**(1), p. 012054. https://doi.org/10.1088/1742-6596/2385/1/012054.

[219] Wang, D., Muratori, M., Eichman, J., Wei, M., Saxena, S., and Zhang, C., 2018, "Quantifying the Flexibility of Hydrogen Production Systems to Support Large-Scale Renewable Energy Integration," Journal of Power Sources, **399**, pp. 383–391. https://doi.org/10.1016/j.jpowsour.2018.07.101.

[220] Park, J., Hwan Ryu, K., Kim, C.-H., Chul Cho, W., Kim, M., Hun Lee, J., Cho, H.-S., and Lee, J. H., 2023, "Green Hydrogen to Tackle the Power Curtailment: Meteorological Data-Based Capacity Factor and Techno-Economic Analysis," Applied Energy, **340**, p. 121016. https://doi.org/10.1016/j.apenergy.2023.121016.

[221] McDonagh, S., Ahmed, S., Desmond, C., and Murphy, J. D., 2020, “Hydrogen from Offshore Wind: Investor Perspective on the Profitability of a Hybrid System Including for Curtailment,” Applied Energy, **265**, p. 114732. https://doi.org/10.1016/j.apenergy.2020.114732.

[222] Biggins, F. A. V., Ejeh, J. O., Roberts, D., Yeardley, A. S., and Brown, S. F., 2022, “Optimising a Wind Farm with Energy Storage Considering Curtailment and Uncertainties,” *Computer Aided Chemical Engineering*, L. Montastruc, and S. Negny, eds., Elsevier, pp. 79–84. https://doi.org/10.1016/B978-0-323-95879-0.50014-X.

[223] Yan, X., Zhang, X., Gu, C., and Li, F., 2018, “Power to Gas: Addressing Renewable Curtailment by Converting to Hydrogen,” Front. Energy, **12**(4), pp. 560–568. https://doi.org/10.1007/s11708-018-0588-5.

[224] Gambou, F., Guilbert, D., Zasadzinski, M., and Rafaralahy, H., 2022, “A Comprehensive Survey of Alkaline Electrolyzer Modeling: Electrical Domain and Specific Electrolyte Conductivity,” Energies, **15**(9), p. 3452. https://doi.org/10.3390/en15093452.

[225] Falcão, D. S., and Pinto, A. M. F. R., 2020, “A Review on PEM Electrolyzer Modelling: Guidelines for Beginners,” Journal of Cleaner Production, **261**, p. 121184. https://doi.org/10.1016/j.jclepro.2020.121184.

[226] Travaglini, R., Superchi, F., Lanni, F., Manzini, G., Serri, L., and Bianchini, A., 2024, “Feasibility Study on the Use of Large-Scale Lithium-Ion Batteries to Prevent Energy Wastes Due to Curtailments in Offshore Wind Farms.” https://doi.org/10.52202/077185.

[227] Atif, A., and Khalid, M., 2020, “Saviztky–Golay Filtering for Solar Power Smoothing and Ramp Rate Reduction Based on Controlled Battery Energy Storage,” IEEE Access, **8**, pp. 33806–33817. https://doi.org/10.1109/ACCESS.2020.2973036.

[228] Madhusudanan, G., and Padhmanabhaiyappan, S., 2024, “Solar Power Fluctuation Smoothing through Battery Energy Storage System Using AVOA-SAGAN Approach,” Journal of Energy Storage, **101**, p. 113610. https://doi.org/10.1016/j.est.2024.113610.

[229] Jafari, M., Botterud, A., and Sakti, A., 2020, “Evaluation of Energy- and Capacity-Market Revenues from Lithium-Ion Battery Systems for Offshore Wind Using Advanced Battery Models.” https://doi.org/10.48550/arXiv.2002.00932.

[230] Buhagiar, D., Sant, T., Farrugia, R. N., and Farrugia, D., 2019, “Increasing the Value of Offshore Wind by Integrating On-Board Energy Storage,” J. Phys.: Conf. Ser., **1222**(1), p. 012038. https://doi.org/10.1088/1742-6596/1222/1/012038.

[231] López, A. I., Ramírez-Díaz, A., Castilla-Rodríguez, I., Gurriarán, J., and Mendez-Perez, J. A., 2023, “Wind Farm Energy Surplus Storage Solution with Second-Life Vehicle Batteries in Isolated Grids,” Energy Policy, **173**, p. 113373. https://doi.org/10.1016/j.enpol.2022.113373.

[232] European Commission DG Environment News Alert Service, 2023, “Renewable Energy Storage from Second-Life Batteries Is Viable but May Benefit from Subsidies.” [Online]. Available: https://environment.ec.europa.eu/news/renewable-energy-storage-second-life-batteries-viable-may-benefit-subsidies-2023-09-13_en. [Accessed: 18-Feb-2025].

[233] Ali, H., Khan, H. A., and Pecht, M. G., 2021, “Circular Economy of Li Batteries: Technologies and Trends,” Journal of Energy Storage, **40**, p. 102690. https://doi.org/10.1016/j.est.2021.102690.

[234] Haram, M. H. S. M., Lee, J. W., Ramasamy, G., Ngu, E. E., Thiagarajah, S. P., and Lee, Y. H., 2021, “Feasibility of Utilising Second Life EV Batteries: Applications, Lifespan, Economics, Environmental Impact, Assessment, and Challenges,” Alexandria Engineering Journal, **60**(5), pp. 4517–4536. https://doi.org/10.1016/j.aej.2021.03.021.

[235] Quinteros-Condoretty, A. R., Laukkanen, M., Kainiemi, L., Pinto, S. M., Lourenço, E. J., Oliveira, L., Albareda, L., and Barbiellini, B., 2025, “Conceptual Model for Extending Electric Vehicle Battery Lifetime,” Resources, Conservation and Recycling, **212**, p. 107943. https://doi.org/10.1016/j.resconrec.2024.107943.
[236] Ferrari, L., Bianchini, A., Galli, G., Ferrara, G., and Carnevale, E. A., 2018, “Influence of Actual Component Characteristics on the Optimal Energy Mix of a Photovoltaic-Wind-Diesel Hybrid System for a Remote off-Grid Application,” Journal of Cleaner Production, **178**, pp. 206–219. https://doi.org/10.1016/j.jclepro.2018.01.032.
[237] Directorate-General for Communication (European Commission), 2020, *Circular Economy Action Plan: For a Cleaner and More Competitive Europe*, Publications Office of the European Union. [Online]. Available: https://data.europa.eu/doi/10.2779/05068. [Accessed: 18-Feb-2025].
[238] European Council, 2021, “European Green Deal,” Consilium. [Online]. Available: https://www.consilium.europa.eu/en/policies/green-deal/. [Accessed: 05-Nov-2024].
[239] European Parliamentary Research Service, 2024, “New EU Regulatory Framework for Batteries Setting Sustainability Requirements.” [Online]. Available: https://www.europarl.europa.eu/RegData/etudes/BRIE/2021/689337/EPRS_BRI(2021)689337_EN.pdf. [Accessed: 18-Feb-2025].
[240] Terkes, M., Öztürk, Z., Demirci, A., and Tercan, S. M., 2023, “Optimal Sizing and Feasibility Analysis of Second-Life Battery Energy Storage Systems for Community Microgrids Considering Carbon Reduction,” Journal of Cleaner Production, **421**, p. 138507. https://doi.org/10.1016/j.jclepro.2023.138507.
[241] Piombo, G., Faraji Niri, M., and Marco, J., 2025, “A Novel Application-Aware Retired Lithium-Ion Batteries Regrouping Approach to Enable Improved Second Life,” Journal of Cleaner Production, **489**, p. 144526. https://doi.org/10.1016/j.jclepro.2024.144526.
[242] Gautam, D., and Bolia, N., 2024, “Fostering Second-Life Applications for Electric Vehicle Batteries: A Thorough Exploration of Barriers and Solutions within the Framework of Sustainable Energy and Resource Management,” Journal of Cleaner Production, **456**, p. 142401. https://doi.org/10.1016/j.jclepro.2024.142401.
[243] The Mobility House, 2018, “Energy Storage in Johan Cruijff ArenA Is on the Grid.” [Online]. Available: https://www.mobilityhouse.com/int_en/our-company/newsroom/article/johan-cruijff-arena-3mw-energy-storage-system-launch. [Accessed: 21-Mar-2025].
[244] The Mobility House, 2018, “Stationary Storage: A Second Life for Electric Car Batteries.” [Online]. Available: https://www.mobilityhouse.com/int_en/knowledge-center/article/second-life-storage-projects. [Accessed: 18-Feb-2025].
[245] Toyota, 2015, “2015 Toyota/Yellowstone Lamar Buffalo Ranch Battery Project - Jim Lentz,” Toyota USA Newsroom. [Online]. Available: https://pressroom.toyota.com/2015-yellowstone-lamar-battery-lentz/. [Accessed: 18-Feb-2025].
[246] Mercedes-Benz Energy, 2016, “Il ciclo virtuoso dell’energia dell’impianto di Elverlingsen,” Il ciclo virtuoso dell’energia dell’impianto di Elverlingsen. [Online]. Available: https://media.mercedes-benz.it/il-ciclo-virtuoso-dellenergia-dellimpianto-di-elverlingsen/. [Accessed: 18-Feb-2025].
[247] The Mobility House, 2018, “Coal-Fired Power Plant Built in 1912 Becomes a Milestone in the Energy Transition.” [Online]. Available: https://www.mobilityhouse.com/int_en/our-company/references/article/elverlingsen-spare-part-accumulator-for-vehicle-batteries. [Accessed: 18-Feb-2025].

[248] Song, H., Chen, H., Wang, Y., and Sun, X.-E., 2024, "An Overview About Second-Life Battery Utilization for Energy Storage: Key Challenges and Solutions," Energies, **17**(23), p. 6163. https://doi.org/10.3390/en17236163.

[249] Bai, Y., Muralidharan, N., Sun, Y.-K., Passerini, S., Stanley Whittingham, M., and Belharouak, I., 2020, "Energy and Environmental Aspects in Recycling Lithium-Ion Batteries: Concept of Battery Identity Global Passport," Materials Today, **41**, pp. 304–315. https://doi.org/10.1016/j.mattod.2020.09.001.

[250] Hassini, M., Redondo-Iglesias, E., and Venet, P., 2024, "Battery Passports for Second-Life Batteries: An Experimental Assessment of Suitability for Mobile Applications," Batteries, **10**(5), p. 153. https://doi.org/10.3390/batteries10050153.

[251] Song, Z., Feng, S., Zhang, L., Hu, Z., Hu, X., and Yao, R., 2019, "Economy Analysis of Second-Life Battery in Wind Power Systems Considering Battery Degradation in Dynamic Processes: Real Case Scenarios," Applied Energy, **251**, p. 113411. https://doi.org/10.1016/j.apenergy.2019.113411.

[252] Chen, W.-H., and Hsieh, I.-Y. L., 2023, "Techno-Economic Analysis of Lithium-Ion Battery Price Reduction Considering Carbon Footprint Based on Life Cycle Assessment," Journal of Cleaner Production, **425**, p. 139045. https://doi.org/10.1016/j.jclepro.2023.139045.

[253] Morten Lybech, T., 2021, "Introduction to Wind Turbine Wake Modelling and Wake Generated Turbulence." [Online]. Available: https://help.emd.dk/knowledgebase/content/ReferenceManual/Wake_Model.pdf. [Accessed: 19-Apr-2023].

[254] Sun, S. I., Chipperfield, A. J., Kiaee, M., and Wills, R. G. A., 2018, "Effects of Market Dynamics on the Time-Evolving Price of Second-Life Electric Vehicle Batteries," Journal of Energy Storage, **19**, pp. 41–51. https://doi.org/10.1016/j.est.2018.06.012.

[255] 2022, "IEA Wind TCP Task 42," IEA Wind TCP. [Online]. Available: https://iea-wind.org/task42/. [Accessed: 26-Feb-2024].

[256] Travaglini, R., Superchi, F., Lanni, F., Manzini, G., Serri, L., and Bianchini, A., 2023, "Towards the Development of Offshore Wind Farms in the Mediterranean Sea: A Techno-Economic Analysis on an Italian Case Study," pp. 40–47. https://doi.org/10.1049/icp.2023.1552.

[257] Serri, L., Peviani, M. A., Alborghetti, S., and Milani, S., 2021, *Valutazioni Di Produzione Combinata Di Energia Elettrica Da Onde e Vento Nel Sito Della Boa MOBI Nel Canale Di Sicilia*. [Online]. Available: https://www.rse-web.it/wp-content/uploads/2022/11/21009897.pdf. [Accessed: 02-Nov-2023].

[258] Superchi, F., Papi, F., Mannelli, A., Balduzzi, F., Ferro, F. M., and Bianchini, A., 2023, "Development of a Reliable Simulation Framework for Techno-Economic Analyses on Green Hydrogen Production from Wind Farms Using Alkaline Electrolyzers," Renewable Energy, **207**, pp. 731–742. https://doi.org/10.1016/j.renene.2023.03.077.

[259] Sohoni, V., Gupta, S. C., and Nema, R. K., 2016, "A Critical Review on Wind Turbine Power Curve Modelling Techniques and Their Applications in Wind Based Energy Systems," Journal of Energy, **2016**, p. e8519785. https://doi.org/10.1155/2016/8519785.

[260] EMD International, 2022, *windPRO 3.6 User Manual: Energy*, EMD International, United Kingdom. [Online]. Available: https://help.emd.dk/knowledgebase/content/windPRO3.6/c3-UK_windPRO3.6_ENERGY.pdf. [Accessed: 19-Apr-2023].

[261] Galli, C., Superchi, F., Papi, F., Ferrara, G., and Bianchini, A., 2024, "Innovative Power Smoothing Techniques for Wind Turbines Using Batteries and Adaptive Pitch Regulation," Journal of Energy Storage, **84**, p. 110964. https://doi.org/10.1016/j.est.2024.110964.

[262] Mannelli, A., Papi, F., Pechlivanoglou, G., Ferrara, G., and Bianchini, A., 2021, “Discrete Wavelet Transform for the Real-Time Smoothing of Wind Turbine Power Using Li-Ion Batteries,” Energies. https://doi.org/10.3390/en14082184.

[263] MASE, 2024, “Energia: MASE, Pubblicato Il Decreto FER2 | Ministero Dell’Ambiente e Della Sicurezza Energetica.” [Online]. Available: https://www.mase.gov.it/notizie/energia-mase-pubblicato-il-decreto-fer2. [Accessed: 05-Nov-2024].

[264] Fisher, M., Apt, J., and Whitacre, J. F., 2019, “Can Flow Batteries Scale in the Behind-the-Meter Commercial and Industrial Market? A Techno-Economic Comparison of Storage Technologies in California,” Journal of Power Sources, **420**, pp. 1–8. https://doi.org/10.1016/j.jpowsour.2019.02.051.

[265] “Idrogeno - Un vettore energetico per la decarbonizzazione,” RSE. [Online]. Available: https://www.rse-web.it/prodotti_editoriali/idrogeno_rseview/. [Accessed: 19-Apr-2023].

[266] Han, X., Li, Y., Nie, L., Huang, X., Deng, Y., Yan, J., Kourkoumpas, D.-S., and Karellas, S., 2023, “Comparative Life Cycle Greenhouse Gas Emissions Assessment of Battery Energy Storage Technologies for Grid Applications,” Journal of Cleaner Production, **392**, p. 136251. https://doi.org/10.1016/j.jclepro.2023.136251.

[267] IEA, 2023, *Electricity Grids and Secure Energy Transitions – Analysis*, International Energy Agency. [Online]. Available: https://www.iea.org/reports/electricity-grids-and-secure-energy-transitions. [Accessed: 08-May-2025].

[268] IRENA, 2024, *Floating Offshore Wind Outlook*, International Renewable Energy Agency. [Online]. Available: https://www.irena.org/Publications/2024/Jul/Floating-offshore-wind-outlook. [Accessed: 08-May-2025].

[269] Desalegn, B., Gebeyehu, D., Tamrat, B., Tadiwose, T., and Lata, A., 2023, “Onshore versus Offshore Wind Power Trends and Recent Study Practices in Modeling of Wind Turbines’ Life-Cycle Impact Assessments,” Cleaner Engineering and Technology, **17**, p. 100691. https://doi.org/10.1016/j.clet.2023.100691.

[270] Superchi, F., Mati, A., Carcasci, C., and Bianchini, A., 2023, “Techno-Economic Analysis of Wind-Powered Green Hydrogen Production to Facilitate the Decarbonization of Hard-to-Abate Sectors: A Case Study on Steelmaking,” Applied Energy, **342**, p. 121198. https://doi.org/10.1016/j.apenergy.2023.121198.

[271] Ramakrishnan, S., Delpisheh, M., Convery, C., Niblett, D., Vinothkannan, M., and Mamlouk, M., 2024, “Offshore Green Hydrogen Production from Wind Energy: Critical Review and Perspective,” Renewable and Sustainable Energy Reviews, **195**, p. 114320. https://doi.org/10.1016/j.rser.2024.114320.

[272] Canul-Reyes, D. A., Rodríguez-Hernández, O., Barragán-Peña, M. E., and del Rio, J. A., 2025, “Analysis of Offshore Wind Energy and Solar Photovoltaic Production and Its Relationship with Regional Electricity Demand in the Yucatan Peninsula,” Energy, **314**, p. 134060. https://doi.org/10.1016/j.energy.2024.134060.

[273] Kneebone, J., 2022, “The Mediterranean as a Leader in the Clean Hydrogen Economy: Production, Transmission, End-Use,” Florence School of Regulation. [Online]. Available: https://fsr.eui.eu/the-mediterranean-as-a-leader-in-the-clean-hydrogen-economy-production-transmission-end-use/. [Accessed: 11-Jul-2025].

[274] Canat, A. N., and Özkan, C., 2024, “Supplying Hydrogen for Green Steel through Renewable Energy Sources: A Case Study of Turkiye,” Journal of Cleaner Production, **450**, p. 141961. https://doi.org/10.1016/j.jclepro.2024.141961.

[275] “Fincantieri | Fincantieri and Viking Announce the World’s First Hydrogen-Powered Cruise Ship and Sign Contracts for Two New Units.” [Online]. Available: https://www.fincantieri.com/en/media/press-releases/2025/fincantieri-and-viking-

announce-the-world-s-first-hydrogen-powered-cruise-ship-and-sign-contracts-for-two-new-units/. [Accessed: 11-Jul-2025].

[276] Sebbahi, S., Assila, A., Alaoui Belghiti, A., Laasri, S., Kaya, S., Hlil, E. K., Rachidi, S., and Hajjaji, A., 2024, "A Comprehensive Review of Recent Advances in Alkaline Water Electrolysis for Hydrogen Production," International Journal of Hydrogen Energy, **82**, pp. 583–599. https://doi.org/10.1016/j.ijhydene.2024.07.428.

[277] Singlitico, A., Østergaard, J., and Chatzivasileiadis, S., 2021, "Onshore, Offshore or in-Turbine Electrolysis? Techno-Economic Overview of Alternative Integration Designs for Green Hydrogen Production into Offshore Wind Power Hubs," Renewable and Sustainable Energy Transition, **1**, p. 100005. https://doi.org/10.1016/j.rset.2021.100005.

[278] Niblett, D., Delpisheh, M., Ramakrishnan, S., and Mamlouk, M., 2024, "Review of next Generation Hydrogen Production from Offshore Wind Using Water Electrolysis," Journal of Power Sources, **592**, p. 233904. https://doi.org/10.1016/j.jpowsour.2023.233904.

[279] Bernat, R., Milewski, J., Dybinski, O., Martsinchyk, A., and Shuhayeu, P., 2024, "Review of AEM Electrolysis Research from the Perspective of Developing a Reliable Model," Energies, **17**(20), p. 5030. https://doi.org/10.3390/en17205030.

[280] Gul, E., Baldinelli, G., Farooqui, A., Bartocci, P., and Shamim, T., 2023, "AEM-Electrolyzer Based Hydrogen Integrated Renewable Energy System Optimisation Model for Distributed Communities," Energy Conversion and Management, **285**, p. 117025. https://doi.org/10.1016/j.enconman.2023.117025.

[281] Yang, B., Zhang, R., Shao, Z., and Zhang, C., 2023, "The Economic Analysis for Hydrogen Production Cost towards Electrolyzer Technologies: Current and Future Competitiveness," International Journal of Hydrogen Energy, **48**(37), pp. 13767–13779. https://doi.org/10.1016/j.ijhydene.2022.12.204.

[282] Wang, J., Yang, J., Feng, Y., Hua, J., Chen, Z., Liao, M., Zhang, J., and Qin, J., 2025, "Comparative Experimental Study of Alkaline and Proton Exchange Membrane Water Electrolysis for Green Hydrogen Production," Applied Energy, **379**, p. 124936. https://doi.org/10.1016/j.apenergy.2024.124936.

[283] Danish, M., "Hydrogen Production by Water Electrolysis: A Review of Alkaline Water Electrolysis, PEM Water Electrolysis and High Temperature Water Electrolysis." [Online]. Available: https://www.academia.edu/67369858/Hydrogen_Production_by_Water_Electrolysis_A_Review_of_Alkaline_Water_Electrolysis_PEM_Water_Electrolysis_and_High_Temperature_Water_Electrolysis. [Accessed: 27-May-2025].

[284] Tofighi–Milani, M., Fattaheian–Dehkordi, S., and Lehtonen, M., 2024, "Dynamic Response Analysis of Alkaline and PEM Electrolyzers in Low-Inertia Power Systems: A Comparative Study," *2024 IEEE International Conference on Environment and Electrical Engineering and 2024 IEEE Industrial and Commercial Power Systems Europe (EEEIC / I&CPS Europe)*, pp. 01–06. https://doi.org/10.1109/EEEIC/ICPSEurope61470.2024.10750998.

[285] Schmidt, O., Gambhir, A., Staffell, I., Hawkes, A., Nelson, J., and Few, S., 2017, "Future Cost and Performance of Water Electrolysis: An Expert Elicitation Study," International Journal of Hydrogen Energy, **42**(52), pp. 30470–30492. https://doi.org/10.1016/j.ijhydene.2017.10.045.

[286] Reksten, A. H., Thomassen, M. S., Møller-Holst, S., and Sundseth, K., 2022, "Projecting the Future Cost of PEM and Alkaline Water Electrolysers; a CAPEX Model Including Electrolyser Plant Size and Technology Development," International Journal of Hydrogen Energy, **47**(90), pp. 38106–38113. https://doi.org/10.1016/j.ijhydene.2022.08.306.

[287] Benghanem, M., Almohamadi, H., Haddad, S., Mellit, A., and Chettibi, N., 2024, "The Effect of Voltage and Electrode Types on Hydrogen Production Powered by Photovoltaic System Using Alkaline and PEM Electrolyzers," International Journal of Hydrogen Energy, **57**, pp. 625–636. https://doi.org/10.1016/j.ijhydene.2023.12.232.

[288] Calado, G., Castro, R., Pires, A. J., and Marques, M. J., 2024, "Assessment of Hydrogen-Based Solutions Associated to Offshore Wind Farms," Renewable and Sustainable Energy Reviews, **192**. https://doi.org/10.1016/j.rser.2023.114268.

[289] Komorowska, A., Benalcazar, P., and Kamiński, J., 2023, "Evaluating the Competitiveness and Uncertainty of Offshore Wind-to-Hydrogen Production: A Case Study of Poland," International Journal of Hydrogen Energy, **48**(39), pp. 14577–14590. https://doi.org/10.1016/j.ijhydene.2023.01.015.

[290] Jang, D., Kim, J., Kim, D., Han, W.-B., and Kang, S., 2022, "Techno-Economic Analysis and Monte Carlo Simulation of Green Hydrogen Production Technology through Various Water Electrolysis Technologies," Energy Conversion and Management, **258**, p. 115499. https://doi.org/10.1016/j.enconman.2022.115499.

[291] Egeland-Eriksen, T., and Sartori, S., 2024, "Techno-Economic Analysis of the Effect of a Novel Price-Based Control System on the Hydrogen Production for an Offshore 1.5 GW Wind-Hydrogen System," Energy Reports, **11**, pp. 2633–2655. https://doi.org/10.1016/j.egyr.2024.02.016.

[292] Hill, S. J. P., Bamisile, O., Hatton, L., Staffell, I., and Jansen, M., 2024, "The Cost of Clean Hydrogen from Offshore Wind and Electrolysis," Journal of Cleaner Production, **445**. https://doi.org/10.1016/j.jclepro.2024.141162.

[293] Mehta, M., Zaaijer, M., and Terzi, D. von, 2022, "Optimum Turbine Design for Hydrogen Production from Offshore Wind," J. Phys.: Conf. Ser., **2265**(4), p. 042061. https://doi.org/10.1088/1742-6596/2265/4/042061.

[294] Rogeau, A., Vieubled, J., de Coatpont, M., Affonso Nobrega, P., Erbs, G., and Girard, R., 2023, "Techno-Economic Evaluation and Resource Assessment of Hydrogen Production through Offshore Wind Farms: A European Perspective," Renewable and Sustainable Energy Reviews, **187**, p. 113699. https://doi.org/10.1016/j.rser.2023.113699.

[295] Rezaei, M., Akimov, A., and Gray, E. M. A., 2024, "Techno-Economics of Offshore Wind-Based Dynamic Hydrogen Production," Applied Energy, **374**, p. 124030. https://doi.org/10.1016/j.apenergy.2024.124030.

[296] Santana, L., Santos, G. dos, Santos, A., Marinho, C., Bispo, A., Villardi, H., and Pessoa, F., 2024, "Evaluating the Economic Influence of Water Sources on Green Hydrogen Production: A Cost Analysis Approach," International Journal of Hydrogen Energy, **89**, pp. 353–363. https://doi.org/10.1016/j.ijhydene.2024.09.274.

[297] Travaglini, R., Papi, F., and Bianchini, A., 2025, "Floating Wind Farms in Sea Basins with Moderate Wind Speeds: A Critical Assessment of the Potential of Low-Specific-Power Turbines in Reducing the LCoE," Renewable and Sustainable Energy Reviews, **222**, p. 115990. https://doi.org/10.1016/j.rser.2025.115990.

[298] Abdel Haleem, A., Huyan, J., Nagasawa, K., Kuroda, Y., Nishiki, Y., Kato, A., Nakai, T., Araki, T., and Mitsushima, S., 2022, "Effects of Operation and Shutdown Parameters and Electrode Materials on the Reverse Current Phenomenon in Alkaline Water Analyzers," Journal of Power Sources, **535**, p. 231454. https://doi.org/10.1016/j.jpowsour.2022.231454.

[299] Wallnöfer-Ogris, E., Grimmer, I., Ranz, M., Höglinger, M., Kartusch, S., Rauh, J., Macherhammer, M.-G., Grabner, B., and Trattner, A., 2024, "A Review on Understanding and Identifying Degradation Mechanisms in PEM Water Electrolysis Cells: Insights for Stack

Application, Development, and Research," International Journal of Hydrogen Energy, **65**, pp. 381–397. https://doi.org/10.1016/j.ijhydene.2024.04.017.

[300] Martinez Lopez, V. A., Ziar, H., Haverkort, J. W., Zeman, M., and Isabella, O., 2023, "Dynamic Operation of Water Electrolyzers: A Review for Applications in Photovoltaic Systems Integration," Renewable and Sustainable Energy Reviews, **182**, p. 113407. https://doi.org/10.1016/j.rser.2023.113407.

[301] Xu, Y., Li, G., Gui, Y., and Li, Z., 2024, "Generation of Input Spectrum for Electrolysis Stack Degradation Test Applied to Wind Power PEM Hydrogen Production," Global Energy Interconnection, **7**(4), pp. 462–474. https://doi.org/10.1016/j.gloei.2024.08.006.

[302] Tiktak, J., 2019, "Heat Management of PEM Electrolysis: A Study on the Potential of Excess Heat from Medium- to Large-Scale PEM Electrolysis and the Performance Analysis of a Dedicated Cooling System." [Online]. Available: https://repository.tudelft.nl/islandora/object/uuid%3Ac046820a-72bc-4f05-b72d-e60a3ecb8c89. [Accessed: 20-Jun-2024].

[303] Wind Europe, 2017, "Repowering and Lifetime Extension: Making the Most of Europe's Wind Resource." [Online]. Available: https://windeurope.org/wp-content/uploads/files/policy/position-papers/WindEurope-Repowering-and-Lifetime-Extension.pdf. [Accessed: 19-Apr-2023].

[304] "Maritime Spatial Planning - Shipping Deputy Ministry - Gov.Cy." [Online]. Available: https://www.gov.cy/dms/en/documents/maritime-spatial-planning-2/. [Accessed: 29-May-2025].

[305] Papi, F., Bianchini, A., and Travaglini, R., 2025, "Floating Wind Farms in Sea Basins with Moderate Wind Speeds: A Critical Assessment of the Potential of Low-Specific-Power Turbines in Reducing the LCoE - Supplementary Data." https://doi.org/10.5281/zenodo.14981730.

[306] Acaroğlu, H., and García Márquez, F. P., 2022, "High Voltage Direct Current Systems through Submarine Cables for Offshore Wind Farms: A Life-Cycle Cost Analysis with Voltage Source Converters for Bulk Power Transmission," Energy, **249**, p. 123713. https://doi.org/10.1016/j.energy.2022.123713.

[307] Gorenstein Dedecca, J., and Hakvoort, R. A., 2016, "A Review of the North Seas Offshore Grid Modeling: Current and Future Research," Renewable and Sustainable Energy Reviews, **60**, pp. 129–143. https://doi.org/10.1016/j.rser.2016.01.112.

[308] Noor Azam, A. M. I., Ragunathan, T., Zulkefli, N. N., Masdar, M. S., Majlan, E. H., Mohamad Yunus, R., Shamsul, N. S., Husaini, T., and Shaffee, S. N. A., 2023, "Investigation of Performance of Anion Exchange Membrane (AEM) Electrolysis with Different Operating Conditions," Polymers, **15**(5), p. 1301. https://doi.org/10.3390/polym15051301.

[309] Campbell-Stanway, C., Becerra, V., and Prabhu, S., 2025, "Techno-Economic Analysis with Electrolyser Degradation Modelling in Green Hydrogen Production Scenarios," International Journal of Hydrogen Energy, **106**, pp. 80–95. https://doi.org/10.1016/j.ijhydene.2025.01.359.

[310] "SunGreenH2." [Online]. Available: https://www.sungreenh2.com/product/200---500-nm3-hr-aem-electrolyzer. [Accessed: 09-Jun-2025].

[311] Roberta, B., 2021, "Experimental Characterization of a Pre-Commercial Anion Exchange Membrane Electrolyzer and Its Techno-Economic Prospects for Industrial-Scale Hydrogen Production," Politecnico di Torino. [Online]. Available: https://webthesis.biblio.polito.it/19981/1/tesi.pdf. [Accessed: 15-Apr-2025].

[312] Titheridge, L. J., and Marshall, A. T., 2024, “Techno-Economic Modelling of AEM Electrolysis Systems to Identify Ideal Current Density and Aspects Requiring Further Research,” International Journal of Hydrogen Energy, **49**, pp. 518–532. https://doi.org/10.1016/j.ijhydene.2023.08.181.
[313] Kim, M., Lee, D., Qi, M., and Kim, J., 2024, “Techno-Economic Analysis of Anion Exchange Membrane Electrolysis Process for Green Hydrogen Production under Uncertainty,” Energy Conversion and Management, **302**, p. 118134. https://doi.org/10.1016/j.enconman.2024.118134.
[314] Travaglini, R., Superchi, F., and Bianchini, A., 2025, “Mitigating Curtailments in Offshore Wind Energy: A Comparative Analysis of New and Second-Life Battery Storage Solutions,” Journal of Cleaner Production, **519**, p. 146055. https://doi.org/10.1016/j.jclepro.2025.146055.
[315] “Wind Resource Data for Wind Farm Developments | Vortex FDC,” VORTEX. [Online]. Available: https://vortexfdc.com/. [Accessed: 19-Jun-2025].

La borsa di dottorato cofinanziata con risorse dell'Unione europea-*NextGeneration EU*
Piano Nazionale di Ripresa e Resilienza Missione 4 – Componente 2 "Dalla Ricerca all'Impresa" – Investimento 3.3
"Introduzione di dottorati innovativi che rispondono ai fabbisogni di innovazione delle imprese e promuovono l'assunzione dei ricercatori dalle imprese" _ CUP B12B22000580007